LA-UR- 97-1698

Title: A STUDY OF THE INTERACTION OF X-RAYS AND ACOUSTIC, STRESS AND SHOCK WAVES IN SOLIDS

Author(s): Allan Hauer, P-24

Submitted to:

MASTER

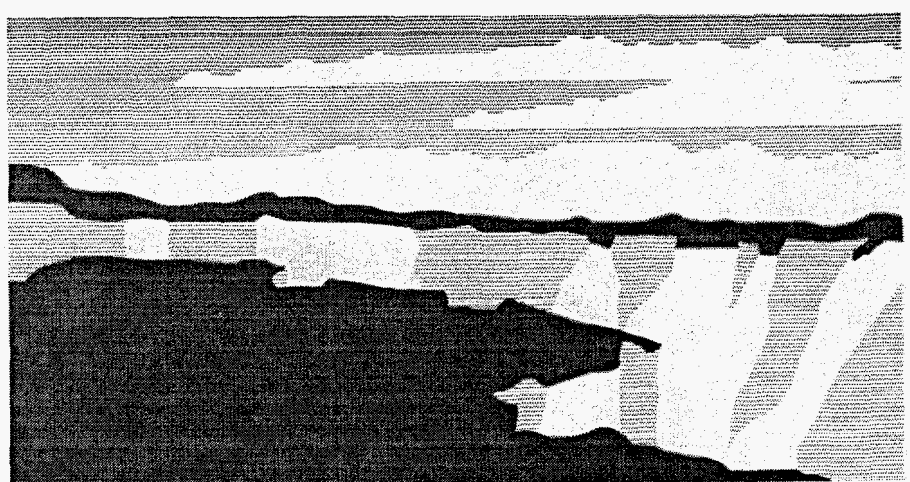

Los Alamos
NATIONAL LABORATORY

Form No. 836 R5
ST2629 10/91

HH

DISTRIBUTION OF THIS DOCUMENT IS UNLIMITED

A Study of the Interaction of X-rays and Acoustic, Stress and Shock Waves in Solids

Allan A. Hauer

ACKNOWLEDGEMENTS

The author would like to gratefully acknowledge the help and support of numerous individuals.

I would like to express gratitude to my advisor, Dr. James Forsyth, for guidance and support in the preparation of this thesis.

I would like to thank Dr. Stephen Burns for instruction in the use of x-ray diffraction equipment and for an introduction to some special techniques of diffractometry.

Dr. E.H. Jacobsen generously contributed his time on numerous occasions. The discussions that I had with him on the subject of crystal lattice dynamics were invaluable.

A debt of gratitude is due Dr. William Bassett for generously allowing the author to use his x-ray diffraction equipment. Without his generosity, the present work would not have been possible.

Douglas Smith of the Institute of Optics shop patiently aided the author on numerous occasions in the final stages of polishing crystals.

Norman Howe of the Materials Science Program gave invaluable assistance on several occasions when major equipment repairs were needed.

Finally, in the areas of non-technical support, special thanks are due to Mrs. Shirley Steinberg for her expert typing of this manuscript, and to my mother for her unfailing moral support and encouragement.

DISCLAIMER

ABSTRACT

The primary emphasis of this thesis involves an investigation of techniques for the control and modulation of x-ray radiation through acoustic perturbation of solids. The use of x-ray diffraction and x-ray optical techniques for the study of acoustic fields and atomic motion was also investigated.

Analysis of the basic properties of x-ray propagation in solids reveals that practical methods for x-ray control or modulation must involve changes in the spatial configuration of x-ray scatterers.

Numerical methods for the study of x-ray propagation in acoustically perturbed crystals are formulated. In developing these methods special emphasis has been placed on Borrmann transmission in thick crystals.

Modulation and shuttering (on a micro-second timescale) of x-rays are experimentally demonstrated. A quantitative investigation of the basic interactions used to produce modulation and shuttering is presented. Agreement between the experimental observations and the theoretical predictions is within experimental error.

An analytical investigation of the basic potential and limitations of x-ray modulation shuttering and control devices is presented. Basic design criteria for x-ray modulation devices is formulated and applied to practical configurations.

Nov. 1976

TABLE OF CONTENTS

LIST OF TABLES

LIST OF FIGURES

PUBLICATIONS AND PATENT

The following publications and patent related to this study have appeared during the course of this work.

Hauer A.,Burns S.J. , "Observation of an X-ray Shuttering Mechanism Utilizing Acoustic Interruption of the Borrmann Effect ", Appl. Phys. Lett.27(10) p.524 (1975).

Hauer A.," Fast X-ray Shutters",Proc. SPIE. Conf. on Optical Methods in Energy Conversion , Rochester July ,1975.

Hauer A. , U.S. Patent , "Methods for the Control and Measuement of X-rays", Serial No.594846, issued 11/19/76.

CHAPTER 1

INTRODUCTION TO X-RAY OPTICAL PHENOMENA

1.1 General Introduction.

1.2 X-Ray Dispersion Characteristics.

1.3 Basic Properties of Crystal Diffraction of X-Rays.

1.4 Interaction of X-Rays and Acoustic Perturbations in Solids (X-Ray Acoustooptic Effects).

1.5 Summary.

1.1 GENERAL INTRODUCTION

As the region of coherent electromagnetic generation has been extended from the microwave into the optical regime, the need for control and detection devices in these regions of the spectrum has greatly increased. This need has produced a variety of electro- and acoustooptic devices that can modulate, shutter, filter, or redirect the radiation, usually on a fast time scale. In addition, these control devices, in conjunction with appropriate feedback mechanisms, in many cases form the basis for the coherent signal generation itself. The possibility of generation of coherent x-rays and the correlative need to better understand x-ray control and detection forms the inspiration for the present study.

One prominently mentioned possibility for the generation of stimulated x-ray emission is the use of a laser produced plasma. Large fluxes of incoherent x-ray emission are routinely produced in laser plasma experiments. In many cases these x-ray pulses are subnanosecond in duration. The temporal structure of these pulses cannot thus be studied by conventional detector-oscilloscope measurement systems. Traditionally very fast pulses (<1nsec) in the optical regime have been studied by the use of either streak camera systems or sampling (shuttering or framing) devices. Recently streak photography techniques have been extended to x-ray wavelengths. Thus far, however, switching or shuttering methods for x-rays have not been demonstrated (even on microsecond timescales). It would be very useful to know the basic potential for devices that are capable of

sampling the temporal characteristics of a fast x-ray pulse.

Conversely, the very fast, intense burst of x-rays produced by a laser plasma provides intriguing possibilities for the study of fast processes in solids. For example, lasers can be used to produce very intense shock waves in solids [1]. These shocks, in turn, can produce solid-solid phase changes. The temporal character of such phase changes might be studied with the use of fast x-ray bursts synchronized to the main shock inducing laser pulse. In order to evaluate such possibilities a study of the basic nature of x-ray scattering in the presence of transient solid perturbations has been undertaken.

Typically fast (subnanosecond) switching or shuttering devices, in the optical regime, operate through use of some form of the electrooptic effect. As discussed below, electrooptic effects at x-ray wavelengths (changing the x-ray polarizability of a material) would be quite difficult to observe. On the other hand, x-ray wave propagation in a solid can be markedly affected by changing the relative positions of atomic scatterers within the material. A simple example of this can be obtained by considering ordinary Bragg reflection from a crystal. When a collimated monochromatic beam of x-rays falls on a crystal, "reflection" occurs when the beam makes a certain angle with internal planes of atoms (i.e. satisfies Bragg's Law). If the spacing of atomic planes is disrupted, the reflection of x-rays will be reduced or eliminated.

It is found that changes in the spatial configuration of x-ray scatterers is the most effective way of controlling x-ray propagation.

The primary thrust of the present study is an investigation of methods for the control of the propagation of x-rays. It should be mentioned, however, that many of the results obtained here also have been applied to the converse situation: the use of x-rays to study atomic movements in solids.

Theoretical models have been developed to describe x-ray scattering in perturbed structures. These techniques are described in Chapter 2 and applied to the description of experimental results in Chapter 3. The comparison of theoretical and experimental results provides the foundation for a basic understanding of the interaction of x-rays and acoustic waves. Chapter 3 also describes demonstration of several practical applications for both the control of x-rays and the use of x-rays to study acoustic fields.

An analytical evaluation of methods for producing acoustic perturbations is given in Chapter 4. In Chapter 4, the theoretical and experimental framework laid in Chapters 2 and 3 is employed to investigate the fundamental limitations on x-ray control device parameters.

1.2 X-RAY DISPERSION CHARACTERISTICS

The description of elastic scattering of x-rays by atoms follows the classical Lorentz harmonic oscillator model[2] (which is also used in the optical regime). The shift to the higher energies of x-rays involves deeper resonances of the atoms until all of the electronic resonances are exhausted. The calculation of the x-ray dispersion characteristics of atoms can generally be made to fit the Lorentz model, but the suppression of more of the resonances of the electronic system (than in the optical regime) dictates modifications to the picture that lead to drastically different values of refractive index.

The dispersion calculation proceeds as in the optical case (such as appears in detail in many classical references[3][4]). Only a brief outline of the procedure will be given here. The equation of motion of the atomic electrons is written as a differential equation for a damped harmonic oscillator (the damping being due to radiation reaction). The solution of the equation of motion yields an expression for the polarizability of an atom. Once the polarizability of an individual atomic species has been determined, a calculation of the scattering from an ensemble of atoms yields an expression for the index of refraction of the material. This model yields the familiar picture for the behavior of the real part of the refractive index, as illustrated in Figure 1-1. In calculating the dispersion characteristics according to the Lorentz model, one finds that in the x-ray regime,the index of refraction falls

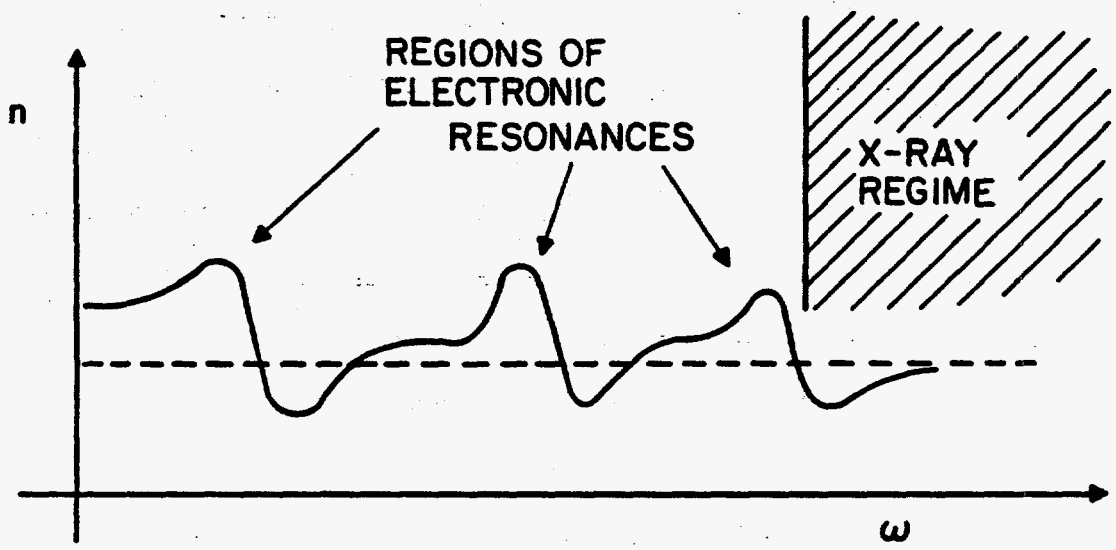

Figure 1-1. Real part of the refractive index as a function of frequency.

below unity. This is the natural outcome of the classical dispersion equations for frequencies that are higher than all or most of the system resonances.

The simple Lorentz model is adequate to predict the general behavior of the refractive index in the x-ray regime. When more detailed information (such as the angular distribution of x-ray scattering) is needed, a departure from conventional optical scattering theory is required. In the present study, we are principally concerned with x-ray wavelengths between .5 $\mathring{A}$ and 50 $\mathring{A}$. In the x-ray regime wavelengths become comparable to atomic dimensions. This requires that interference effects between the scattered waves from various electrons within an atom must be taken into account in calculating the total scattering due to an atomic species. In most cases the scattering process is taken to be Thompson free electron scattering. The distribution of electron density within the atom is, however, obtained from quantum mechanical calculations (Thomas-Fermi or Hartree-Fock).

Tabulations of atomic scattering factors (or "form factors", as they are sometimes referred to) vs. wavelength and scattering angle are found in almost all books on x-ray diffraction theory[5][6]. In the vicinity of atomic resonances, such as the energy necessary to remove a K-shell electron, (referred to as the K edge), it is necessary to add correction factors. These corrections have both a real and an imaginary part.The imaginary part of the atomic scattering factor contains the description of the absorption processes.

More will be said about atomic scattering factors in the next chapter.

The implications for reflection and refraction of an index slightly less than unity are clear. Substantial Fresnel reflections from surfaces can only occur at large angles of incidence (typically grazing angles of a few degrees). In addition, at very large incidence angles, it is possible to have total external reflection (since the index of a solid medium will be less that of vacuum). The small departure of the index from unity also implies that no lenses of significant power can be constructed. Thus, in considering possible x-ray switching, modulation and control devices, we must remember that substantial refractive effects (in the usual sense) cannot be produced.

The fact that x-ray frequencies are large compared to most electronic resonances has other important consequences. At x-ray frequencies, most of the electrons appear free, i.e. the energy of x-ray quanta approaches the binding energy of most of the electrons. This implies that the electrons start to participate more or less equally in the scattering of x-ray radiation. In fact, detailed calculations of the scattering of x-rays by atomic electrons show the cross sections to be more heavily weighted toward the inner electrons. Thus, in order to produce electro-optic effects, externally applied fields must perturb the whole electronic cloud. This requires electric field strengths of the order that would ionize most or all of the electrons.

As an example, consider the difference in x-ray index for Be ($1 - n = 5.3 \times 10^{-6}$) and Ge ($1-n = 1.5 \times 10^{-5}$). The difference is directly due to the difference in local electron density. Changing the local (total) electron density on a fast scale would probably be quite difficult. A typical example of this limitation would be the formation of a plasma from a solid target by a fast,pulsed laser. The time for absorptive processes and ionization to occur can be quite fast[7]. The expansion phase (which would be the mechanism for affecting the total electron density), however, due to basic inertial considerations always occurs on nanosecond and longer time scales.

In essence, the previous analysis has shown that it would be very difficult to affect the real part of the x-ray index. It might be somewhat easier, however, to change the imaginary part of the index. The imaginary part is due to absorption which, in the wavelength region of interest, is almost entirely due to the photoelectric effect. With presently existing laser technology, it is possible to rapidly produce high ionization states of small portions of solid materials. For example, calculations[7] indicate that the time needed to create a high density of these higher ionization states could be less than .1 nanosecond. It, thus, would be possible to strip absorbing atoms down to a shell that could no longer be ionized by incoming x-rays.

Suppose, for example, 44 Å radiation (carbon Kα) were being used to probe a laser produced aluminum plasma. If the initial

target consisted of a one micron foil, it would transmit only $e^{-8.1}$ (at 44 Å). When the aluminum is heated with a flux density of 10^{14} watts/cm^2, helium and hydrogen-like states are easily produced. Once these ionization states have been reached, a significant change in the (44 Å) transmission of the foil should take place. Such a process could be used in probing the instantaneous ionization state of a plasma.

The angular characteristics of x-ray reflection from solid surfaces provides a further possibility for the control of x-ray propagation. Total external reflection of x-rays can be described by the classical analysis used in the optical regime. We know[4][2] that when total reflection occurs, that the damped evanescent wave penetrates into the less dense medium a distance of the order of one wavelength. Thus, the process of total reflection of x-rays involves only a very small portion of the material (near the surface). Such thin layers can be very rapidly heated by a laser.

Systematic (experimental) studies of x-ray reflection properties in the 1-10 Å range are described in Compton and Allison[2]. Studies in the 20-100 Å range have been performed by Lukirski[8]. These studies show that the general behavior of the x-ray reflection coefficients are adequately predicted by ordinary classical dispersion theory. Certain details such as behavior near absorption edges require a quantum mechanical treatment[2]. In the present analysis, we will rely on the classical predictions.

The complex index of refraction is usually written as

$$n = n_r + i\, n_i$$

$$= 1 - \delta - i\beta$$

where $n_r = 1 - \delta$ = real part of index

$n_i = -\beta$ = imaginary part of index.

Two important relations involving δ and β are easily derived[2] from classical dispersion theory.

$$\delta = \theta c^2/2$$

where θc = critical angle (1-1)

$$\beta = \frac{\lambda \mu_e}{4\pi} \quad (1\text{-}2)$$

where μ_e = linear absorption coefficient.

By substituting the complex form of the index into the usual Fresnel formulae, an expression for the reflection coefficient R in terms of the critical angle and absorption coefficient can be obtained.

Figure 1-2 shows a plot of R vs. the ratio $\theta/\theta c$ for various values of absorption (β). Such relationships provide valuable information for evaluating methods of control of x-ray propagation.

First, we note that reflectivity is a strong function of angle. For example, the reflectivity of Be at 23 Å will change from 17% at 3^{o} (grazing angle) to .25% at 4^{o}. At 4 Å the reflectivity of aluminum will change from 70% at 40' to 5% at $1^{o}30'$. Thus, rather sharp changes in reflectivity can be produced by changing the angle of incidence. In the next section, methods for producing such changes will be discussed.

We note also from Figure 1-2 that the reflectivity depends strongly on the imaginary part (governed by absorption) of the index for angles of incidence near the critical angle. A change in the absorption, such as by production of high ionization states (as described earlier), could, thus, measurably alter the reflectivity. Changing the absorption coefficient by an order of magnitude would, however, be quite difficult. For lower atomic number elements ($Z<20$), the change in passing through the K shell edge is about one order of magnitude. Thus, in order to produce a change in absorption coefficient by as much as 10, it would be necessary to remove enough electrons so that the remaining ionization potential was greater than the x-ray photon energy.

In conclusion, it would be very difficult to control x-ray propagation by perturbing the electronic configuration (in analogy with electrooptic effects) of x-ray scattering materials.

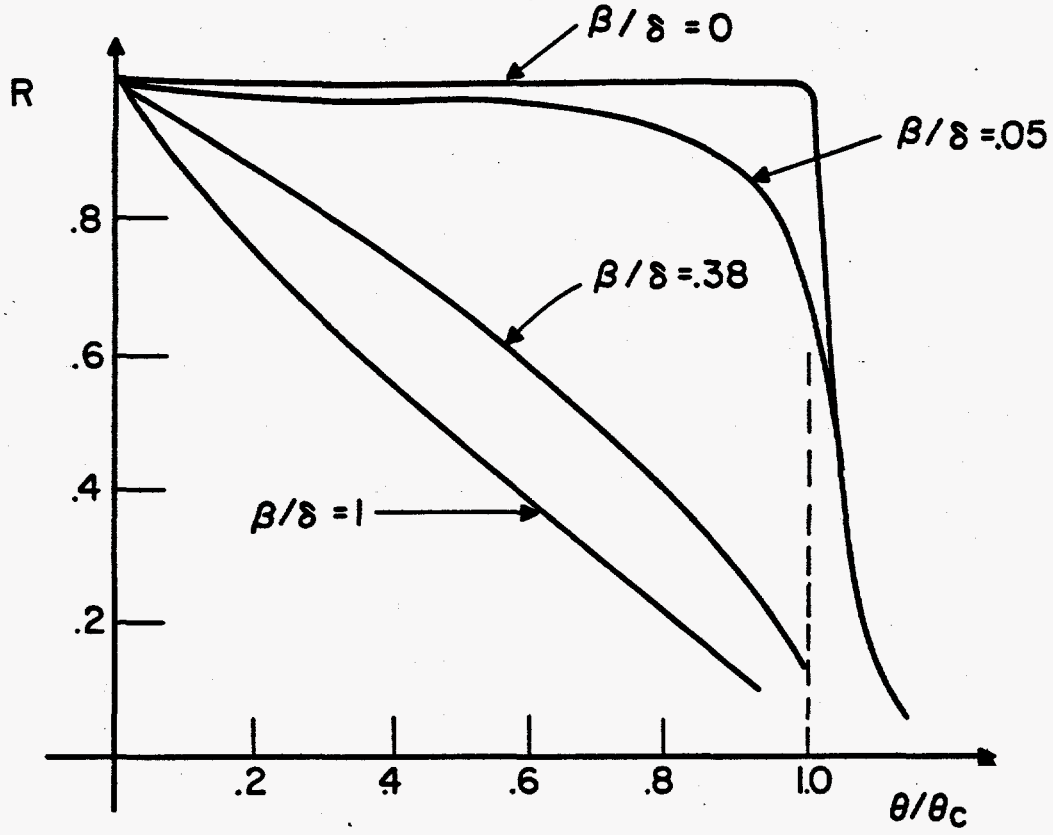

Figure 1-2. X-ray reflection coefficient as a function of departure from critical angle for various values of absorption.

1.3 BASIC PROPERTIES OF CRYSTAL DIFFRACTION OF X-RAYS

In the x-ray region of the spectrum, the dispersion characteristics of solids take on unique properties because of the periodic regular arrangement of atoms. The periodic array of atoms in a crystalline structure resembles a microscopic interferometer. This periodic structure can lead to coherent three-dimensional scattering analogous to the diffraction of optical radiation by two-dimensional structures. The simplest picture of such a process is the well-known phenomenon of Bragg reflection from planes of atoms parallel to the surface of a crystal.

The present section provides an introduction to the basic principles of x-ray diffraction that are pertinent to switching, modulation, and control of x-rays. In addition, a brief review is given of some of the special diffraction theory terminology that will be used in Chapter 2.

The detailed theory of x-ray diffraction for the Bragg case will be discussed in Chapter 2. It is, however, useful to recall that the earliest complete theory of x-ray diffraction used a model in which the crystal was treated as an atomic scale interferometer.[9] A series of difference equations was written describing the coherent addition of x-ray reflections from the various atomic planes (in the Bragg geometry). A very interesting conclusion of this theory is that a monochromatic ray incident on a crystal is diffracted (or reflected) only for incident angles within a few seconds of arc of the Bragg angle.

We recall Bragg's law relating the angle of incidence, x-ray wavelength, and atomic plane spacing:

$$2d \sin \theta = \lambda \qquad (1\text{-}3)$$

Differentiating, we obtain

$$\frac{\lambda\, \delta(2d)}{(2d)^2} = \cos \theta\, d\theta$$

or,

$$d\theta = \frac{\delta(2d)}{(2d)} \tan \theta \qquad (1\text{-}4)$$

The quantity $\delta(2d)/2d$ in Equation 1-4 corresponds to a strain. Since a significant change in diffraction occurs only for values of $\Delta\theta > 10^{-5}$, a strain induced change in the 2d spacing of about 10^{-5} would be required to significantly reduce the diffracted intensity. One of the primary purposes of this investigation is to study the reduction in diffracted intensity when strains are introduced by acoustic waves.

Figure 1-3 illustrates a crystal diffraction geometry that is less familiar than the Bragg case but equally important: the Laue geometry. In this case, the diffracting atomic planes are perpendicular to the faces of the crystal.

The more detailed theories of x-ray diffraction (to be discussed in Chapter 2) reveal several unique properties of x-ray wavefields

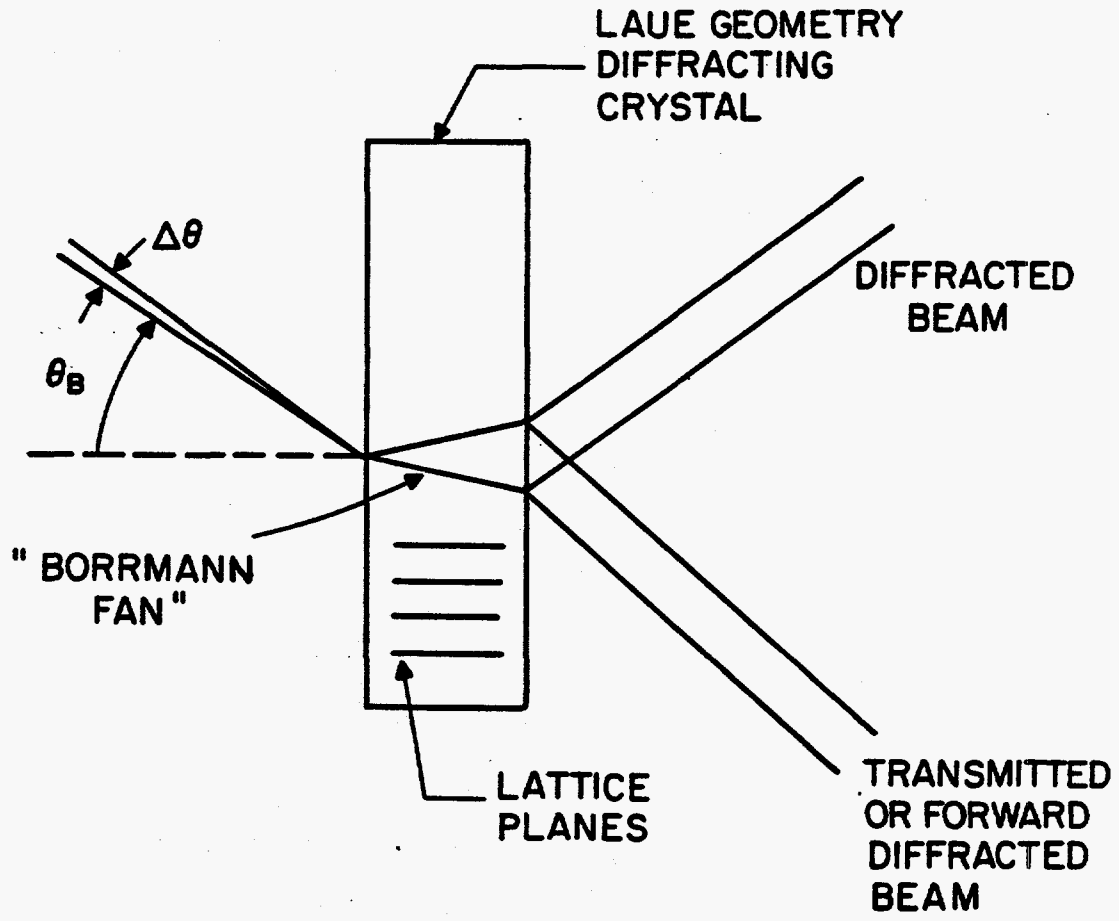

LAUE GEOMETRY

Figure 1-3. Laue Diffraction geometry (used for observation of the Borrmann effect).

in solids in both the Laue and Bragg cases. One interesting property that becomes evident is the fact that the absorptive character of the field can be highly directionally dependent. A striking manifestation of this behavior is the Borrmann effect.[12]

The Borrmann effect is observed when a crystal is diffracting in the Laue geometry, as shown in Figure 1-3. X-ray reflection from the Bragg planes sets up a wavefield in the crystal that results in energy transmission roughly parallel to the lattice planes. A standing wave is set up in the crystal with nodes at the lattice planes. The presence of field nodes at the lattice planes results in reduced photoelectric absorption. A highly perfect single crystal oriented for Laue geometry diffraction can have an absorption which is orders of magnitude lower than normal photoelectric absorption (as, for example, for a ray not incident at the Bragg angle). When the geometry of Figure 1-3 is disturbed by distortion of the crystal, atoms move into high field regions and strong absorption occurs. In the present study, reduction in Borrmann transmission was investigated in the case where the strains and distortions are introduced by acoustic waves[10]. In addition to reduction in transmission, several other interesting effects, such as refraction of the x-rays, also occur in the acoustically perturbed Borrmann case.[13] These effects are discussed in detail in Chapters 2 and 3.

The phenomenon of x-ray crystal diffraction is the result of constructive interference of the beams reflected from atomic lattice planes. The characteristic distance over which this multiple reflec-

tion phenomenon builds up is referred to as an extinction distance. An example of the meaning of an extinction distance, in the particular case of the Bragg diffraction geometry, is shown in Figure 1-4. The diffraction process in a highly perfect crystal will be very effective in removing energy from the incident beam (wavevector $\underline{K}_0$) and transferring it to the diffracted beam (wavevector $\underline{K}_H$). The x-ray field penetrates only a small distance into the crystal and the diffraction results from contributions from a very thin layer near the surface.

The extinction distance has a quantitative meaning that will be developed in Chapter 2, but its qualitative implications are clear. The extinction distance (in the Bragg geometry) typically varies from about .5 to 10 microns. This characteristic distance is very important. If acoustic propagation times were the limiting factor, these regions can be "addressed" in times ranging from 50 p.s. to 10 n.s.

The process of x-ray diffraction from crystal lattice planes is highly angle dependent. In order to characterize the efficiency of diffraction (a quantity analogous to a reflection coefficient) for a quasi-collimated, non-monochromatic beam, the principle of integrated intensity is introduced[11]. The basic concept of integrated intensity is illustrated in Figure 1-5(a).A diffracting crystal is rotated (angular rate ω) while diffracting the uncollimated non-monochromatic input beam. The entrance aperture is assumed large enough to collect all of the diffracted x-rays at all times.

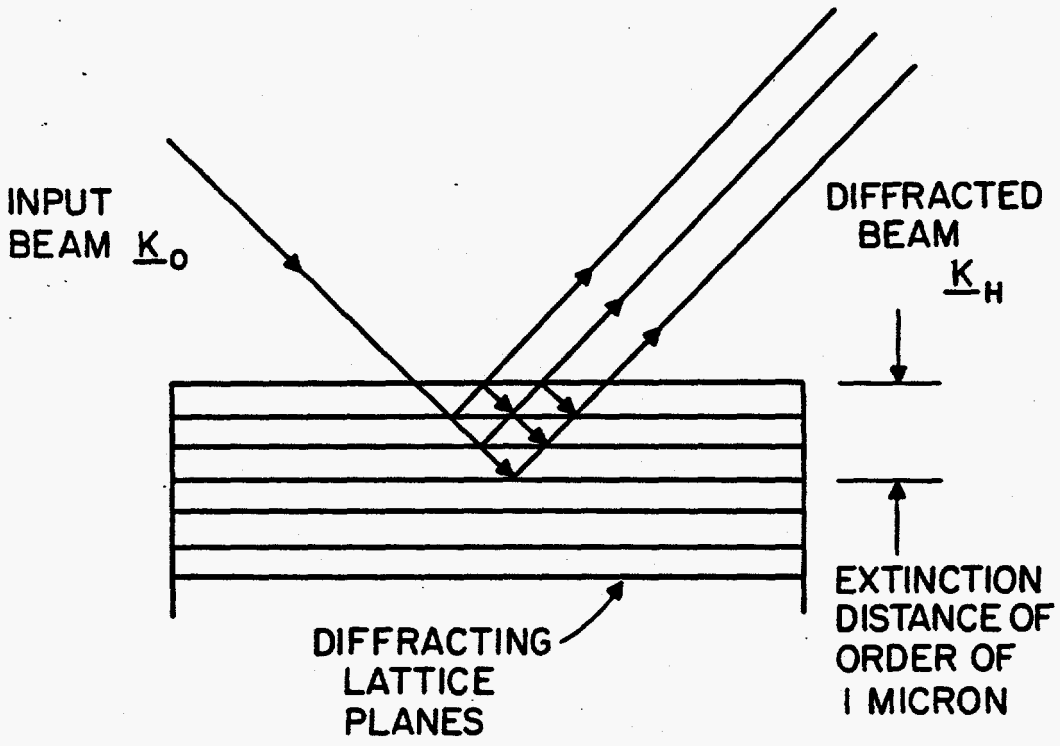

Figure 1-4. Illustration of the phenomena of extinction.

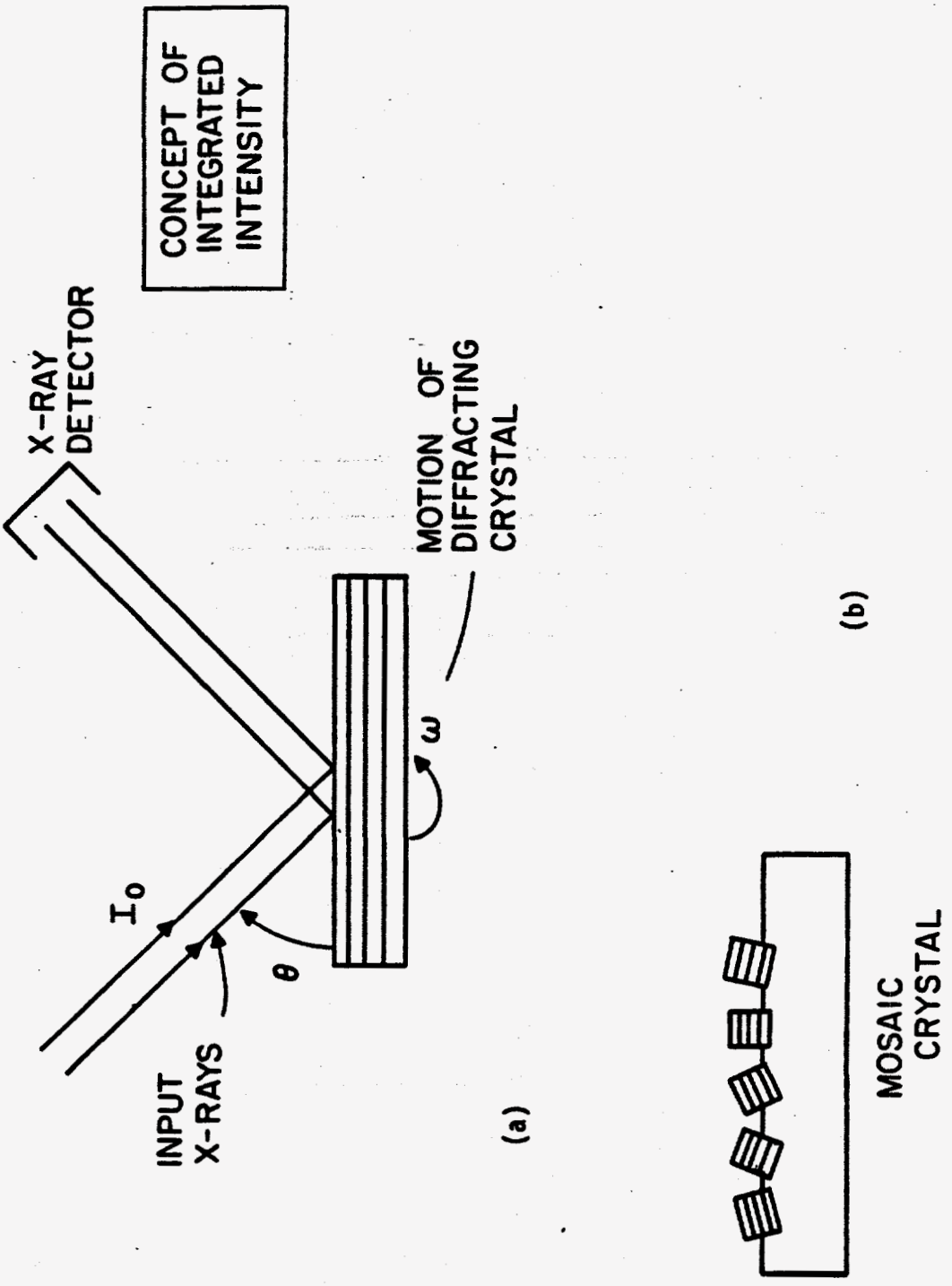

Figure 1-5. Illustration of the concept of integrated intensity and the elementary model of a mosaic crystal.

Each monochromatic component in the input will at some time during the rotation satisfy Bragg's law for some ray striking the crystal surface. The total energy reaching the detector is an integration of the diffracted intensity over the area of the beam and over time. Let us define:

$$dt = d\theta/d\omega$$

where θ = angle of incidence of a ray striking the crystal.

$$\text{Then } E = \frac{1}{\omega} \iint I dA d\theta$$

$$= \frac{1}{\omega} \int P d\theta \qquad (1\text{-}5)$$

where E = total energy reaching the detector

P = diffracted power.

At the crystal face, we assume that the area of the incident and diffracted beams are equal. Therefore:

$$P/P_o = IA/I_o A_o = I/I_o$$

$$\text{and } E = \frac{P_o}{\omega} \int \frac{I}{I_o} d\theta \qquad (1\text{-}6)$$

The quantity $E\omega/P_o$ is sometimes referred to as the "integrated reflectivity" and is used in the sense of an effective reflection

coefficient to be associated with the x-ray diffraction process.

The concept of integrated reflectivity can be used to explain one very interesting aspect of x-ray diffraction by slightly imperfect crystals. Shown in Figure 1-5(b) is a simple model of a slightly imperfect crystal. Each small block contains a domain of perfect crystalline material. The domains are, however, slightly misaligned with respect to one another. Such a picture is referred to in diffraction literature as a mosaic crystal.

Now, suppose a ray is incident on one of the mosaic blocks but (because of angle or λ), does not satisfy Bragg's law. Because of the small size of the block, the ray can penetrate it without suffering much absorption and intercept a block beneath that does satisfy Bragg's law. Thus, a slightly imperfect crystal can, under some circumstances, present a larger effective angular collection aperture than a perfect crystal and, thus, have a greater integrated reflectivity. It is possible to introduce imperfections that resemble the mosaic picture through the use of acoustic waves. This situation will be discussed in Chapter 2.

1.4 INTERACTION OF X-RAYS AND ACOUSTIC PERTURBATIONS IN SOLIDS (X-RAY ACOUSTOOPTIC EFFECTS)

In contrast to electronic perturbations, physical motion of the atomic scattering centers in a solid can easily produce observable effects. A simple example of such an effect is the well-known temperature dependence of Bragg x-ray diffraction[6]. At elevated temperatures, the atoms in a solid execute large deviations from their equilibrium lattice positions. This process smears out the atomic lattice planes and leads to a cancellation of the coherent x-ray interference. In most of the cases to be considered in the present study, the atomic vibrations will have a spectrum closer to the monochromatic single frequency case than the distribution produced by random motion induced at elevated temperatures.

The multiple reflection processes that occur when Bragg's law is satisfied exhibit significant sensitivity to lattice perturbations. (A specific example is provided by the Borrmann effect.) In contrast, an x-ray passing through the solid at an arbitrary angle (not at a Bragg angle with respect to any set of atomic lattice planes) would be negligibly affected by the small perturbation in x-ray index caused by an imposed acoustic wave.

Perturbation of the x-ray diffraction process, thus, provides one method for modulation and shuttering of x-rays. This process is investigated theoretically and experimentally in the following chapters.

The second situation where acoustic control of x-rays can be

performed involves solid surface perturbations. As was seen earlier, x-ray dispersion characteristics of solids are such that reflection only occurs at very large angles of incidence. As the x-ray photon energy increases, the x-ray index comes closer to unity and the grazing angle at which any substantial reflection occurs becomes smaller.

Consider the case of reflection of 5 $\mathring{A}$ radiation from a flat highly polished aluminum surface. If 5 $\mathring{A}$ x-rays are incident on the surface at a grazing angle of $.68^{o}$, they are 70% reflected. Now, suppose, as illustrated in Figure 1-6, that a sine wave perturbation of the surface is introduced. If the amplitude of the wave were about 200 $\mathring{A}$ with a wavelength of 1 micron, a ray incident at a node would have its angle of incidence changed by 7.2^{o} (with respect to the initial condition of a flat surface). The reflectivity for 5 $\mathring{A}$ incident on aluminum at 7^{o} (grazing angle) is less than 1%. The surface acoustic perturbations will, thus, act like a diffracting grating. Methods for production of acoustic waves of this type, as well as a detailed analysis of their application, are discussed in Chapter 4.

In Chapter 4, we give a basic analysis of the use of changes in bulk and surface solid structure for the control and measurement of x-rays. The effects are referred to under the general heading of acoustooptic interactions. X-ray acoustooptic effects for the purpose of control, modulation, and shuttering have not been previously studied.

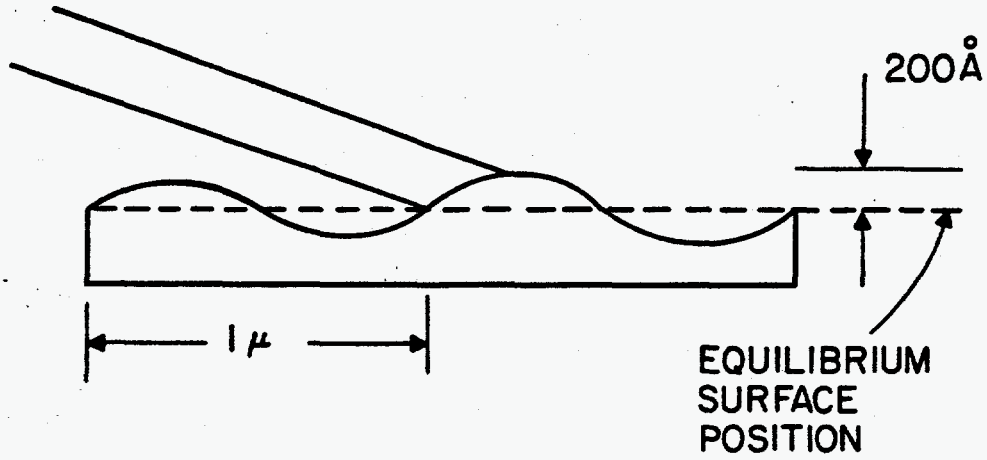

Figure 1-6. Diffraction of x-rays by acoustic surface perturbations.

It should be pointed out that the word acoustic is occasionally used here in a broader sense than is usually associated with that word. For example, certain types (modes) of atomic vibration in a crystal lattice could be very useful in altering x-ray propagation but cannot in a strict sense be described as acoustic.

1.5 SUMMARY

In the theoretical portion of this thesis, basic models have been developed for the study of x-ray scattering in dynamically perturbed structures. In one case (Bragg diffraction geometry), an entirely new technique has been developed for the solution of the basic propagation equations. Numerical (computer) methods have been developed for analyzing acoustic interruption of Borrmann transmission. These methods have been used for specific quanti-

tative comparison with experiment. A phenomenological description of the effect of vibrational spectrum on acoustic perturbation of diffraction is presented.

In Chapter 3, various techniques for modulation and shuttering of x-rays are experimentally investigated. In addition, the phenomena of interruption of x-ray diffraction has been used to study properties of acoustic fields in solids. For example, a portion of the work described in Chapter 3 represents the first use of the Borrmann effect for the study of acoustic waves in solids. The technique developed here has very recently been employed by another author[14] to study important properties of acoustoelectric amplification. Several other applications of this sort are described in the ensuing chapters.

In Chapter 4, a fundamental analysis of the potential and limitations of x-ray modulation, shuttering and control devices is given. The basic design criteria for modulating devices is formulated, and specific numerical examples are given.

CHAPTER 1 REFERENCES

1. Peercy, P.S., Jones, E.D., Bushnell, J.C., and Gobeli, G.W., "Ultrafast Rise Time Laser Induced Stress Waves in Solids", Appl. Phys. Lett., 16, (3), p. 120, (1970).

2. Compton, A.H., and Allison, S.K., X-Rays in Theory and Experiment, D. Van Nostrand, p. 263, (1935).

3. Stone, J.M., Radiation and Optics, p. 376, McGraw-Hill, (1963).

4. Born, M., and Wolf, E., Principles of Optics, p. 84, Pergamon, 4th ed., (1964).

5. Warren, B.E., X-Ray Diffraction, Wiley, p. 372, (1968).

6. James, R.W., Optical Principles of the Diffraction of X-Rays, p. 93, Cornell University Press, (1948).

7. Whitney, K.G., "Stimulated VUV Emission from Carbon-Like Ions in Laser Produced Plasmas." Laboratory for Laser Energetics Internal Report.

8. Lukirski, A.P., et al., Soviet Optics and Spectroscopy, 16, p. 168, (1964).

9. Darwin, C.G., "Theory of X-Ray Reflection", Phil. Mag., 27, p. 315, (1914).

10. Hauer, A., and Burns, S.J., "Observation of an X-Ray Mechanism Utilizing Acoustic Interruption of the Borrmann Effect", Appl. Phys. Lett., 27, (10), p. 524, (1975).

11. Warren, B.E., Loc. Cit., p. 324.

12. Meieran, E.S., "Application of X-Ray Topographical Techniques to the Study of Semiconductor Crystals and Devices," Siemans Review XXXVII, (1970).

13. Authier, A., "Contrast of Dislocation Images in X-Ray Transmisson Topography," Advances in X-Ray Analysis, 10, (46), p. 9, (1967).

14. LeRoux, S.D., Colella, R., and Bray, R., "Effect of Acousto-electric Phonons on Anomalous Transmission of X-Rays", Phys. Rev. Lett., 37, (16), p. 1056, (1976).

CHAPTER 2

THEORY OF THE INTERACTION OF X-RAYS AND ACOUSTIC WAVES IN CRYSTALS

2.1 Introduction to the Theory of X-ray Diffraction in Crystals.

2.2 Darwin or Multiple Reflection Picture of X-ray Diffraction.

2.3 Application of Darwin-Matrix Picture to Calculation of Characteristics of Interest in Acoustic Perturbation Studies.

2.4 Comparison Between the Analytical and Matrix Solution of Darwin's Equations.

2.5 Ewald-von Laue Formulation of Dynamical Theory.

2.6 Propagation in Imperfect Crystals.

- 2.6-1 General Outline
- 2.6-2 Simple Absorption Theory - Description and Application
- 2.6-3 Refractive Theory of X-ray Propagation - Description and Application
- 2.6-4 Limits of Refractive Theory and Introduction to Generalized Diffraction Theory

2.7 General Theory of X-ray Scattering in the Presence of Lattice Vibrations.

2.1 INTRODUCTION TO THE THEORY OF X-RAY DIFFRACTION IN CRYSTALS

For the majority of x-ray diffraction work such as materials' structure analysis, a simplified approach known as kinematical theory is used. In general, it can be said that this theory predicts to a good approximation the directional characteristics of the x-ray field and gives a rough approximation of the intensity. Kinematical theory does not take into proper account the effects of multiple x-ray reflections or of absorption. For example, in the well-known picture of Bragg reflection it is assumed that there is no multiple scattering and that the process of diffraction negligibly perturbs the propagation of the input beam. Ironically, this approximate theory works best when the crystals under consideration have a large degree of perturbation of the regular lattice structure. In such a case multiple reflections do not build up over a significant number of atomic planes and absorption can be dealt with by simple exponential factors.

When a crystal has a high degree of regularity and starts to approximate the ideal lattice structure, multiple reflections (scattering) become important and significantly affect the propagation of the input beam. The situation begins to approximate the operation of an interferometer. In fact, the simplest development of the multiple reflection phenomena (Darwin)[1,2] is closely analogous to the analysis of multilayer optical thin films.

As in the case of optical interferometers when the number of effective reflections (or interfering beams) increases, the resolution, or resonant selectivity, also increases. Viewed from a different

perspective, the high resolving power also implies that for a monochromatic beam, there is a high degree of sensitivity to changes in the periodic structure of the interferometer. In the case of a diffracting crystal, a change in the characteristic spacing of lattice planes sharply changes its angular and wavelength reflection characteristics.

When the lattice structure of a perfect crystal is perturbed, a variety of effects can occur, and the integrated intensity might increase or decrease. We are primarily concerned here with dynamic, or time dependent perturbations introduced by acoustic waves and lattice vibrations. In this chapter we will first present the formal derivation of the complete equations of dynamical diffraction theory. The case of Bragg diffraction (lattice planes parallel to the entrance face) will be treated primarily from the Darwin point of view. The formulation of the Darwin picture will emphasize a matrix technique developed for the present study using analogies from thin film theory.

The Laue geometry problem (diffracting planes perpendicular to the crystal entrance face) will be developed using the more rigorous Ewald-von Laue picture. In using both of the major theoretical approaches, we develop the full range of techniques needed to deal with all of the interesting cases that will arise later when dealing with imperfect crystals. In addition, we are able to state the Laue and Bragg problems in the simplest and most physically intuitive forms.

The Darwin matrix and Ewald-von Laue theories are next extended to describe distorted crystals. In the case of slightly distorted crystals, two theories have been developed. A computer ray trace

program based on a lamellar model of the crystal is described. This is referred to as the simple absorption model. A second computer ray trace program was developed that is based on the classical model of x-ray propagation in slightly distorted crystals developed by Penning and Polder.[15] This picture takes into account refraction of x-rays and has many similarities to Eikonal theory in ordinary optical propagation theory.

When very large strain gradients are present, both of the above-mentioned theories fail and more sophisticated techniques are required. This regime is described theoretically and related to experimental observations in Chapter 3.

Finally, at the end of the present chapter, we describe the effects of various types of crystal lattice vibrations (including the always present thermally induced spectrum) on x-ray diffraction.

2.2 DARWIN OR MULTIPLE REFLECTION PICTURE OF X-RAY DIFFRACTION

In order to give a quantitative description of the effect of acoustic perturbations on x-ray diffraction, it is necessary to employ one of the formulations of dynamical diffraction theory.

The simplest, and historically the earliest, treatment of dynamical x-ray diffraction theory was given by Darwin[1,2] in 1914. He dealt with the simple picture of Bragg diffracting planes parallel to the face of a crystal.

Darwin's solution of the problem involves three basic steps.

1) First, the Fresnel diffraction problem for a plane studded with discrete scattering centers (atoms) is solved. This gives an effective (complex) reflection and transmission coefficient for x-rays incident on the atomic planes at a particular scattering angle θ. This is illustrated in Figure 2-1. The reflection coefficient is iq where

$$q = \frac{e^2}{mc^2} M \frac{\lambda f(2\theta)}{(\sin\theta)}$$

The quantity e^2/mc^2 is simply the classical electron radius,

while M = number of atoms/unit area in the plane.

f = atomic scattering factor at angle θ for the particular atoms involved.

The transmission coefficient through the plane of atoms is $(1-h+iq_o)$. The quantity h is a phenomenological absorption term representing the loss a ray suffers in passing through a plane of atoms. The quantity $1+iq_o$ represents the primary beam plus the forward scattered component

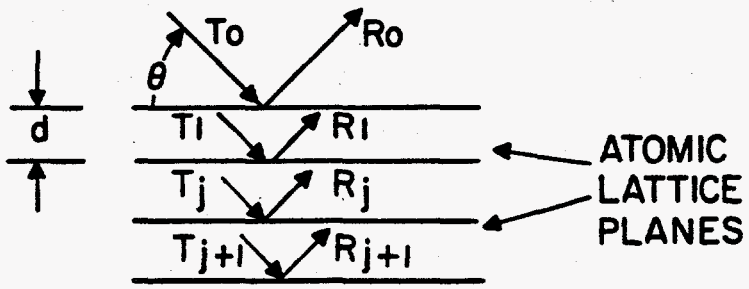

$$R_j = T_j(iq) + (1-h+iq_o)R_{j+1}e^{-i\phi}$$

$$T_{j+1} = (1-h+iq_o)T_j e^{-i\phi} + iq\,R_{j+1}e^{-2i\phi}$$

DARWIN DIFFERENCE EQUATIONS

$$\phi = \frac{2\pi d \sin\theta}{\lambda} \qquad q = \frac{e^2}{mc^2}\frac{M\lambda f(2\theta)}{(\sin\theta)}$$

MULTIPLE REFLECTION PICTURE OF BRAGG GEOMETRY CRYSTAL DIFFRACTION

Figure 2-1. Illustration of the Darwin difference equation formulation of the Bragg reflection problem.

(at scattering angle θ=o).

2) The reflection coefficients obtained in part (1) are then used to write a series of difference equations that relate the electric field at a particular atomic plane to the fields one plane above and one below. The situation is indicated in Figure 2-1.

3) Finally, in the original Darwin formulation, an approximate analytical solution to these difference equations is found.

One of the purposes of the present study is to exploit and develop analogies between interferometric and acousto-optic techniques (in the optical regime) and similar techniques at x-ray wavelengths. In this vein, it is very interesting to compare the Darwin approach to general theories of wave propagation periodically stratified media[3,4,5] such as are applied to problems in multilayer coating work. In order to emphasize these relationships, a derivation of the Darwin results using a matrix approach is presented.

We make the following identifications of coefficients in the Darwin equations.

$$A \equiv iq$$

$$B \equiv (1-h+iq_o)\, e^{-i\phi}$$

$$C \equiv (iq)\, e^{-2i\phi}$$

The Darwin equations are now written as

$$R_j = AT_j + B\, R_{j+1} \qquad (2\text{-}1)\,a$$

$$T_{j+1} = BT_j + C\,R_{j+1} \qquad (2\text{-}1)\,b$$

Solving for T_j in 2-1(a) and substituting into 2-1(b),

$$R_j = A\left[\frac{T_{j+1} - CR_{j+1}}{B}\right] + BR_{j+1}$$

or,

$$\boxed{R_j = \frac{A}{B}T_{j+1} + \left[B - \frac{AC}{B}\right]R_{j+1}} \qquad (2\text{-}2)$$

Substituting this expression for R_j back into 2-1(a)

$$\frac{A}{B}T_{j+1} + \left[B - \frac{AC}{B}\right]R_{j+1} = AT_j + BR_{j+1}$$

from which

$$\boxed{T_j = \frac{1}{B}T_{j+1} - \frac{C}{B}R_{j+1}} \qquad (2\text{-}3)$$

Using 2-2 and 2-3, we may write the following matrix equation.

$$\begin{bmatrix} T_j \\ R_j \end{bmatrix} = \underbrace{\begin{bmatrix} \frac{1}{B} & -\frac{C}{B} \\ \frac{A}{B} & \frac{B^2-AC}{B} \end{bmatrix}}_{\underline{\underline{M}}} \begin{bmatrix} T_{j+1} \\ R_{j+1} \end{bmatrix} \qquad (2\text{-}4)$$

The matrix $\underline{\underline{M}}$ expresses the relationship between the reflected and

transmitted waves at one plane in terms of R and T at the next adjacent plane.

It is helpful at this point to introduce a new variable

$$v = \frac{2\pi d}{\lambda} (\sin\theta - \sin\theta_B) \qquad (2\text{-}4)a$$

which is essentially a deviation parameter indicating the departure of the incidence angle from the nominal Bragg angle. As shown by Warren[2], Bragg's law may now be written:

$$\frac{2d\pi \sin\theta}{\lambda} = m\pi + q_o + v \qquad (2\text{-}5)$$

Equation (2-5) incorporates the usual form of Bragg's law plus a correction for the average index of refraction of the crystal. Using the parameter v the elements of matrix $\underline{\underline{M}}$ may now be written:

$$A = iq$$

$$B = (1-h+iq_o)e^{-i(m\pi+q_o+v)}$$

$$C = (iq)\, e^{-2i(m\pi+q_o+v)} \qquad (2\text{-}6)$$

The quantities q_o and q represent the scattering at the angles 0 and θ respectively, of a single plane of atoms. They are small quantities of the order of 10^{-4} - 10^{-5}. The deviation parameter, v, in typical situations is

also of the order of 10^{-4}. We, thus, make approximations for the phase factors,

$$(e^{-2\pi})\, e^{-i2(q_o+v)} \simeq (1-2q-2iv).$$

The quantity B may, thus, be written

$$B = (1+iq_o)\,(1-iq_o-iv)$$

$$\simeq 1-iv-h$$

ignoring higher powers of small quantities as compared to unity. Likewise, we may express the quantities:

$$B^2-AC \simeq$$

$$(1-h-iv)^2 - (iq)^2\,(1-2iq_o-2iv)$$

$$\simeq 1-h-i(2v)$$

Matrix $\underline{\underline{M}}$ may now be written as:

$$\underline{\underline{M}} = \frac{1}{1-h-iv}\begin{bmatrix} 1 & -[2(qq_o+qv)+iq] \\ (iq) & 1-h-i(2v) \end{bmatrix} \qquad (2\text{-}7)$$

The usual quantity that is of interest in thin film and crystal problems is the ratio of incident to reflected field amplitude at the boundary of the material, i.e., the effective reflection coefficient of the structure. In order to obtain this information, boundary conditions must be imposed on the equations. Normally, one assumes that there is a finite extent to the layered medium with no reflected wave coming from the substrate. Thus, at some layer, $j=f$, $R_f=0$, and T_f is totally transmitted into the substrate. If n is defined as the number of layers in the structure, we may write

$$\begin{bmatrix} T_1 \\ R_1 \end{bmatrix} = (\underline{\underline{M}})^n \begin{bmatrix} T_f \\ 0 \end{bmatrix}$$

where $(\underline{\underline{M}})^n$ is the nth power of the matrix in Equation 2-4. Letting

$$(\underline{\underline{M}})^n = \begin{bmatrix} I & II \\ III & IV \end{bmatrix}$$

$$\frac{R_1}{T_1} = \frac{III}{I} = r \qquad (2\text{-}8)$$

r is an effective amplitude reflection coefficient for the crystal. The fundamental difference between the multilayer film problem and x-ray diffraction is that in the former case the number of layers involved is a definite, fixed, known quantity. In this case the reflection

coefficient of the stack is obtained by exponentiation of the matrix $\underline{\underline{M}}$. In the x-ray case, however, the usual assumption (as in Darwin's solution) is that, the crystal has in infinite number of layers. As will be shown below, the reflection process itself effectively confines the interaction to a finite number of atomic layers. Thus, in order to treat the x-ray problem by the matrix method, one must assume a fixed number of layers as a starting point. The resulting transmission through such a structure can then be used to choose a new number of layers in a self-consistent process.

2.3 APPLICATION OF DARWIN-MATRIX PICTURE TO CALCULATION OF CHARACTERISTICS OF INTEREST IN ACOUSTIC PERTURBATION STUDIES

In order to obtain the reflection coefficient for a crystal, the matrix $\underline{\underline{M}}$ must be raised to the appropriate power n where n = the number of atomic layers involved. A computer program has been written to numerically evaluate the exponentiation of the matrix $\underline{\underline{M}}$. This routine can efficiently calculate powers of $\underline{\underline{M}}$ as high as 3×10^4. The intensity reflection coefficient R is then obtained from the following formula.

$$R = \frac{III^* \; III}{I^* \quad I} \qquad (2\text{-}9)$$

Let us consider a typical example of the 200 reflection in NaCl. For this reflection $q \simeq 2\times10^{-4}$ and h (the loss in passing through a single plane of atoms) is $\simeq 8\times10^{-6}$. We will first calculate the reflection coefficient for a ray incident exactly at the Bragg angle (that is v=o). Figure 2-2 shows a plot of the computer calculations of reflection coefficient as a function of the number of atomic planes in the crystal. Two very important characteristics of x-ray diffraction can be discerned from this plot. First we see that as the number of atomic lattice planes becomes larger, the reflection coefficient asymptotically approaches unity. We, thus, can see that under perfect satisfaction of the Bragg condition, that the process of x-ray diffraction can be quite efficient. Of course, in most practical cases, there is a deviation from the Bragg condition. (An uncollimated non-monochromatic beam will, of course, show less reflection.)

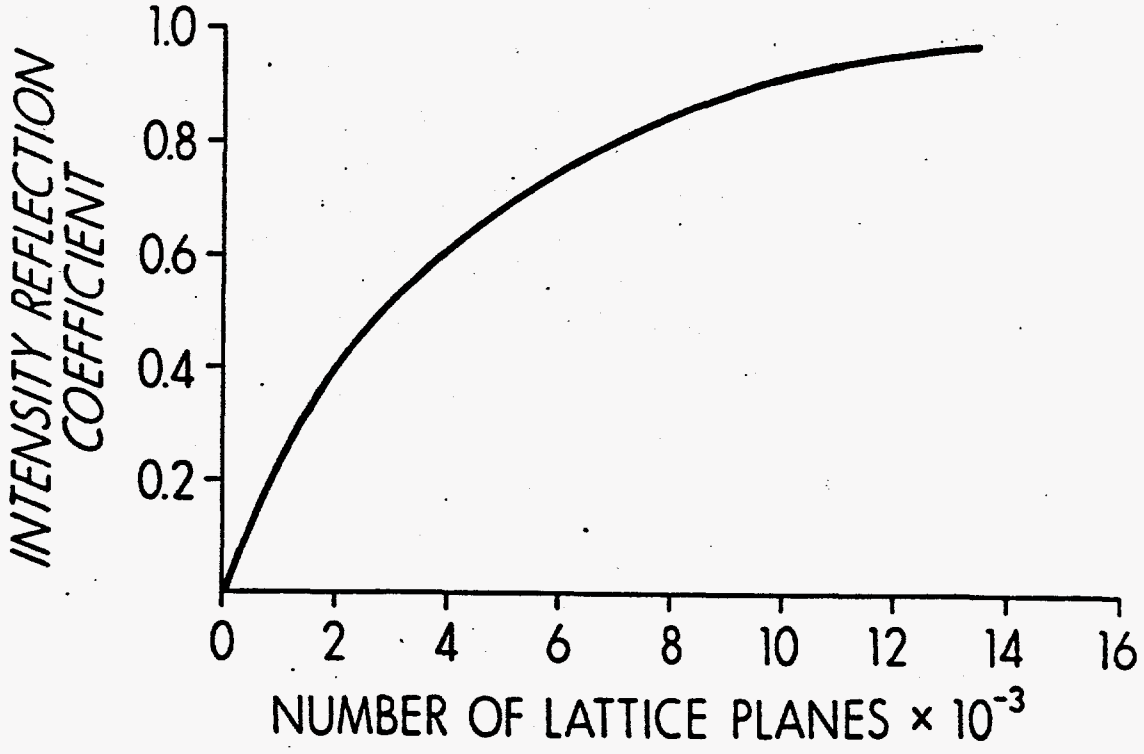

Figure 2-2 . Numerical (matrix) calculation of the x-ray intensity reflection coefficient as a function of the number of lattice planes in the crystal.

The second important characteristic of Figure 2-2 is that the reflection coefficient asymptotically approaches unity. This is a manifestation of the phenomenon of extinction. The diffraction process efficiently reflects energy out of the incident beam thus limiting its penetration into the crystal. We see from Figure 2-2 , that after about 14×10^3 lattice planes, almost all of the energy has been transferred from the incident to the reflected wave. Thus, the matrix approach easily lends itself to a numerical calculation of the extinction distance once the quantities q and h are known.

An analytical expression for the extinction distance can be obtained by using the original method (Darwin) of solution of the basic Equations 2-1. Darwin assumed an analytic solution of the form:

$$T_j = X^j \qquad (2\text{-}10)$$

where X is a polynomial.

Darwin found that X can be adequately approximated by:

$$X + 1/X = 2 + q^2 + (h+iv)^2$$

The typical convention for defining the extinction distance is to calculate the distance for the primary beam to fall to 1/e of the input and to use the approximation that v=0.[2][18]

Using this convention and the solution given by 2-10, the following expression for the extinction distance may be obtained.

$$d_{ext} = \frac{1}{\frac{\pi}{2}\left[\frac{e^2}{mc^2}\right] M^*\lambda F} \qquad (2\text{-}11)$$

where $M^* = M/d$ = atomic density of the crystal

d = spacing of atomic lattice planes.

Using Equation 2-11, we calculate the extinction distance for the (200) planes in salt (for $\lambda = 1\text{A}^{\circ}$) to be 0.91 microns. As may be seen from Figure 2-2, the 1/e point as calculated by the matrix technique is approximately 1.08 microns (recalling that the 2d spacing is 2.8 A°). There is, thus, good agreement between the matrix and analytical techniques for solving the Darwin equations. The matrix numerical routine and Equation 2-11 now provide the analytical tools necessary to calculate the region of a crystal that must be perturbed in order to significantly affect the diffracted fields.

One relationship that is of particular interest is the ratio of the extinction distance to the absorption distance. The absorption distance is taken to be the distance traversed by a beam while suffering a 1/e reduction in intensity due to normal (photoelectric) absorption. For NaCl ($\lambda = 1.1\ \text{A}^{\circ}$), the absorption coefficient is[2] about 26 cm^{-1}. The 1/e distance is, thus, 380 microns.We, thus, see that under certain circumstances, extinction can be a much stronger effect than ordinary absorption. In Chapter 4, typical values for both extinction and absorption distances will be calculated and discussed in relation to potential device parameters.

The second property of crystal diffraction that is of vital interest is the angular width of the reflection or,in other words,the diffracted

intensity as a function of deviation from the exact Bragg angle (corrected for the average refractive index). In order to calculate the angular behavior using the Matrix technique, we must return to Equation 2-7 and include the parameter v which is a measure of deviation from the Bragg angle. The input data to the computer matrix exponentiation routine is now updated to include the parameter v.

As a numerical example, we will once again base our calculation on the (200) reflection in NaCl. Figure 2-3 displays a plot of diffracted intensity vs. angular deviation from the Bragg condition. We find that to reduce the diffracted intensity by 1/2 of the peak (v=o) requires an angular deviation $\Delta\theta \simeq 1.52 \times 10^{-5}$ rad. Such a sensitivity is typical of the crystal diffraction process where angular deviations of only a few seconds of arc significantly reduce the x-ray diffraction.

Darwin's solution of the fundamental equations yields an analytical expression for diffracted intensity as a function of the deviation parameter v. Using the solution given in 2-10, Darwin finds the relationship to be:

$$r = \frac{R_o}{T_o} = \frac{iq}{iv + \sqrt{q^2 + (iv)^2}} \qquad (2\text{-}12)$$

Using this formulation (with $R = \left(\frac{R_o}{T_o}\right)\left(\frac{R_o}{T_o}\right)^*$), we find that to reduce the diffracted intensity by 1/2, $\Delta\theta \simeq 1.8 \times 10^{-5}$. The agreement between the matrix and analytical solutions to the fundamental Equations (2-7) is thus once again quite satisfactory. For reference, we also note

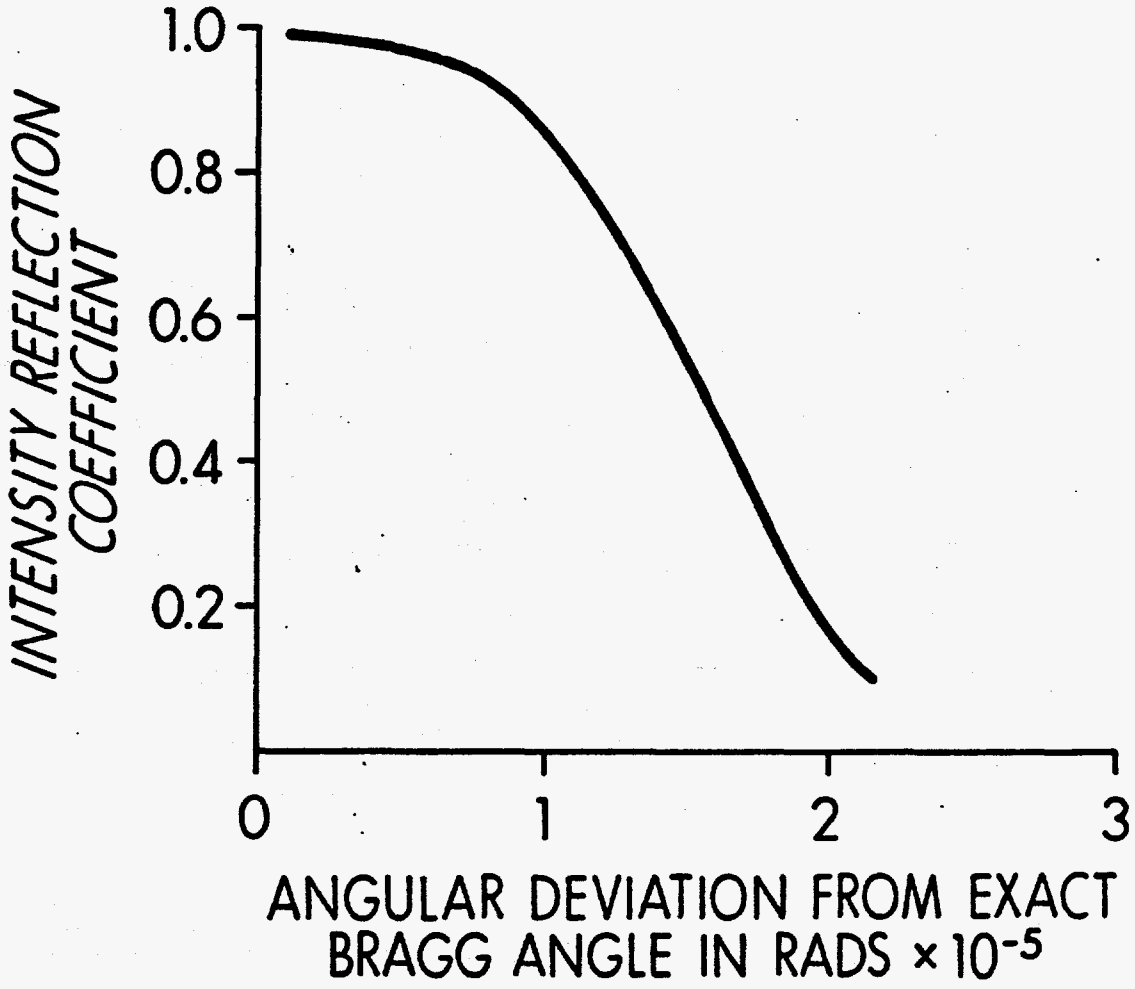

Figure 2-3 . Numerical (matrix) calculation of the x-ray intensity reflection coefficient as a function of angular deviation from the exact Bragg angle.

the following useful approximation for the angular width of the diffraction curve as derived by Warren[2] from the analytical solution of the fundamental equations,

$$\Delta\theta \simeq \lambda^2 \frac{e^2}{mc^2} \frac{|F|M^*}{\pi \sin(2\theta)} \qquad (2\text{-}13)$$

where F = crystalline structure factor.

From the point of view of modulation and control of x-rays, strains on the order of 10^{-5} in the crystal lattice will be required to significantly affect the diffraction. Of course, a simple change in the 2d spacing is not the only possible type of lattice perturbation that could be introduced. A net bending of the lattice planes can also be introduced by an acoustic wave. The effect of such a perturbation is not, however, easily treated by the Darwin or Matrix formulations. When such effects occur, one must resort to "refractive" theories that are described later in this chapter.

2.4 COMPARISON BETWEEN ANALYTICAL AND MATRIX SOLUTION OF DARWIN'S EQUATIONS

A new approach (Matrix) to the solution of the Darwin equations has been presented here primarily in order to emphasize the analogies between the phenomena of x-ray diffraction and interferometry in the optical regime. The method, however, has an inherent value in its own right. Darwin's original analytical solution yields the two convenient

approximate formulas for extinction distance (2-11) and the form of the diffraction curve (2-12). These two expressions can be derived through the use of the matrix formulation, but the process is quite a bit more cumbersome. Darwin's analytical solution is, however, based on the assumption of an infinitely thick crystal (thickness >> extinction distance) and cannot be easily modified to treat thinner crystals. The matrix approach, however, is well suited to such a problem since a desired thickness can be studied simply by changing the number of exponentiations of the matrix. In addition, when the matrix must be raised to large powers, techniques from thin film work can be utilized in order to save computer time.

An even more important application of the matrix technique involves the analysis of slightly distorted crystals. In this case, the analytical solution is of no value. The matrix approach can, for example, accommodate perturbations in the $2d$ spacing by changing the local value (at any particular depth into the crystal) of the parameter v. To the author's knowledge, a perturbation technique of this sort based on Darwin's equations has never been used before in the treatment of x-ray propagation in distorted crystals. In fact, only one other general treatment of distortions in the Bragg geometry has been given[30] (none in the English literature). This treatment, by Bonse, is based on the Ewald-von Laue formulation of dynamical theory (to be discussed in the next section).

2.5 EWALD-VON LAUE FORMULATION OF DYNAMICAL THEORY

Although the Darwin-Matrix formulation has an engaging simplicity and lends itself to very useful analogies with optical interferometry, it is not of sufficient generality to treat all of the problems of interest in x-ray diffraction. For example, the picture of multiple reflections is very difficult to apply to the Laue geometry where the diffracting planes are perpendicular to the entrance face of the crystal. In addition, when the crystal lattice is slightly perturbed, a much more general picture is needed. The matrix variation of Darwin theory presented in the previous sections is, to the author's knowledge, the first suggestion for the use of the multiple reflection picture in the case of perturbed crystals.

In order to obtain a more general theoretical picture, we use a formulation due primarily to Ewald[6] and von Laue[7] (EVL). This theoretical picture closely follows other generalized descriptions of wave propagation in periodically stratified media[3,4,5]. Indeed, the phenomena of Bragg reflection or forbidden bands of propagation is very general, applying in slightly modified forms to electrons, phonons, and neutrons as well as to the present case of photons.

As Von Laue has pointed out, the problem set by dynamical diffraction theory is the solution of Maxwell's equations in a medium with a periodically varying complex dielectric constant. In solid state physics, the implications of the periodic distribution of crystal parameters in the lattice are usually stated in terms of a very general picture known as Bloch's theorem[8]. A well known consequence of

Bloch's theorem[9] is that crystalline properties such as electron density, $\rho(r)$, may be expressed as a fourier series with the reciprocal lattice vectors as the basis. We write

$$\rho(r) = \frac{1}{V} \sum_H F_H \exp(-2\pi i \underline{H} \cdot \underline{r}) \qquad (2\text{-}14)$$

where:

$F_{\underline{H}}$ is the crystalline structure factor for the reflection corresponding to reciprocal vector $\underline{H}$.

V = volume of the unit cell of the crystal lattice.

In addition, one can write field quantities in the crystal in the general form

$$\underline{A} = e^{i\omega t} \sum_H \underline{A}_H \exp(-2\pi i \underline{K}_H \cdot r) \qquad (2\text{-}15)$$

From elementary dispersion analysis, we know that the dielectric constant may be written as

$$\varepsilon(r) = 1 - \left[\frac{e^2}{mc^2}\right] \frac{\lambda^2}{\pi} \rho(r) \qquad (2\text{-}16)$$

where the quantity in brackets is the classical electron radius. Using Equations 2-14 and 2-16, the following expression for the dielectric constant is obtained.

$$\varepsilon = 1 - \left[\frac{e^2}{mc^2}\right] \frac{\lambda^2}{\pi V} \sum_H F_{\underline{H}} \exp\left[-2\pi i (\underline{H} \cdot \underline{r})\right] \qquad (2\text{-}17)$$

The Ewald-von Laue (EVL) exposition of dynamical diffraction theory is presented in a number of excellent references[10,11,12]. The purpose of the brief summary that will be given here is to formulate the theory in such a way that it will be easily applicable to the case of primary interest here, that of x-ray propagation in slightly distorted crystals. Absorption is taken into account be defining a complex dielectric constant. This is done through the crystalline structure factor, which is usually written:

$$F_H = \sum_n (f+\Delta f'+i\Delta f'') \exp(2\pi i \underline{H}\cdot\underline{r}_n) \qquad (2\text{-}18)$$

(We use prime notation for the real part and double prime for the imaginary part of a complex quantity.) The details of the atomic scattering process (including absorption) are contained in the lower case f's, which are referred to as form factors or atomic scattering factors.

We define Ψ_H as:

$$\Psi_H = -\left[\frac{e^2}{mc^2}\right]\frac{\lambda^2}{\pi V} F_H \qquad (2\text{-}19)$$

where Ψ_H is written in terms of real and imaginary parts as:

$$\Psi_H = \Psi_H' + i\Psi_H''$$

As would be expected, the imaginary part of the structure factor can be related directly to the linear absorption coefficient

$$\mu = \frac{2\pi}{\lambda_o} \Psi_o'' \qquad (2\text{-}20)$$

Using Maxwell's equations, we derive a form of the wave equation convenient for the present problem. The x-ray diffracting medium is assumed to have zero conductivity and permeability $\mu=\mu_o$. Maxwell's equations in cgs units are:

$$\nabla\cdot\underline{E} = 0 \qquad \nabla\cdot\underline{B} = 0$$

$$\nabla x\underline{E} = \frac{1}{c}\frac{d\underline{B}}{dt} \qquad \nabla x\underline{B} = \frac{1}{c}\frac{d\underline{E}}{dt} \qquad (2\text{-}21)$$

In the following, upper case K's are taken to be wavevectors inside the crystal (such as $\underline{K}_o$ and $\underline{K}_H$) and lower case k is the vacuum wavevector outside the crystal.

Writing the wave equation, we obtain

$$\nabla x\nabla x(\tfrac{1}{\epsilon})D = \frac{-1}{c^2}\frac{d^2D}{dt^2} \qquad (2\text{-}22)$$

Substituting Equations2-18and2-19 into Equation 2-17,an expression for the dielectric constant is obtained. We now substitute this expression for ϵ and the expansion for the displacement field $\underline{D}$ (as given by 2-15) into the wave equation

$$\underline{D}\,(1-\Psi) = e^{i\omega t}\left\{\sum_H D_H\, e^{-2\pi i\underline{K}_H\cdot\underline{r}} \sum_G \sum_L \Psi_G\, D_L \exp\left[-2\pi i x\,(\underline{G}+\underline{K}_L)\cdot r\right]\right\} \qquad (2\text{-}23)$$

where $\underline{G} \equiv$ any reciprocal lattice vector other than $\underline{H}$.

Recalling Bragg's law

$$\underline{K}_H = \underline{K}_o + \underline{H}$$

and letting H-L=G, Equation 2-23 becomes

$$(1-\Psi)\,\underline{D} = e^{i\omega t} \sum_H (D_H - \sum_L \Psi_{H-L}\, D_L) \left[\exp(-2\pi i\, \underline{K}_H \cdot \underline{r})\right] \quad (2\text{-}24)$$

Inserting this expression in 2-23

$$\nabla x \nabla x \left[e^{i\omega t} \sum_H (D_H - \sum_L \Psi_{H-L}\, D_L) \exp(-2\pi i(\underline{K}_H \cdot \underline{r})\right] =$$

$$\frac{-1}{c^2} \frac{d^2}{dt^2} \sum_H D_H \exp 2\pi i(\underline{K}_H \cdot \underline{r}) \quad (2\text{-}25)$$

Recalling the following equivalence for operators,

$$\partial/\partial t \rightarrow \omega x$$

and

$$\nabla x \nabla x \rightarrow \underline{K}_H x \underline{K}_H x$$

and using these in Equation (2-25)

$$\underline{K}_H (\underline{K}_H \cdot \underline{D}_H) - \underline{D}_H (K_H - \underline{K}_H) - \sum_L \Psi_{H-L} \left[\underline{K}_H (\underline{K}_H \cdot \underline{D}_L) - \underline{D}_L (\underline{K}_H \cdot \underline{K}_H)\right] = \underline{D}_H\, k^2 \quad (2\text{-}26)$$

We recall that for transverse fields

$$\left.\begin{aligned} \underline{K}_H \cdot \underline{D}_H &= 0 \\ \text{and } \underline{K}_0 \cdot \underline{D}_0 &= 0 \end{aligned}\right\} \qquad (2\text{-}27)$$

Using 2-27 in 2-26 gives

$$\sum_L \Psi_{H-L} \left[\underline{K}_H(\underline{K}_H \cdot \underline{D}_L) - \underline{K}_H^2 \, \underline{D}_L\right] = (k^2 - \underline{K}_H^2)\, \underline{D}_H \qquad (2\text{-}28)$$

Expression (2-28) is a set of equations that represents the fundamental laws of propagation for x-rays in anisotropic media. In general, they could represent a large number of modes $\underline{K}_H$ propagating in the crystal. Practically speaking, however, there are usually only two modes of importance for any particular set of boundary conditions. The two modes can be thought of as the incident, $\underline{K}_0$, and diffracted, $\underline{K}_H$, although, in fact, inside the crystal, they are a coupled set and the terms lose specific meaning.

In the case of two propagating modes, a very useful geometrical construction can be used to visualize the behavior of the x-ray wavefield. This picture is a slight modification of the familiar Ewald reciprocal space construction[2], illustrated in Figure 2-4(a).In the case of two propagating modes, two points in reciprocal space are in contact with the sphere. Full use of these geometrical models will be made below, but first a modified form of the basic two mode equations is needed.

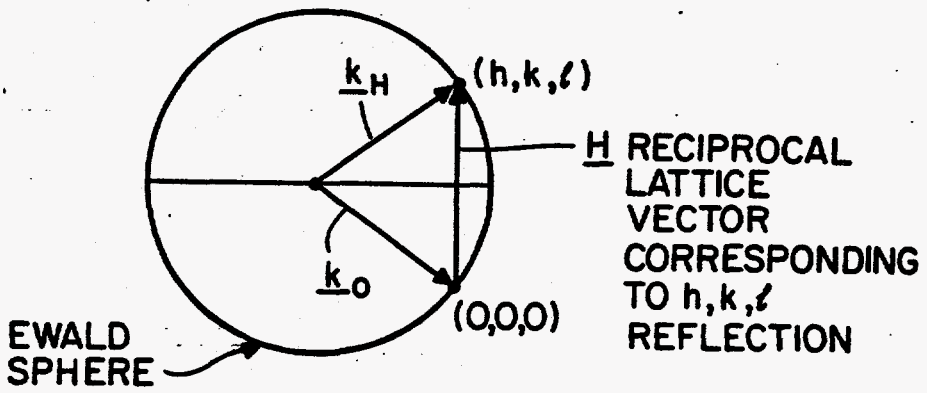

Figure 2-4a Kinematical Ewald construction in reciprocal space.

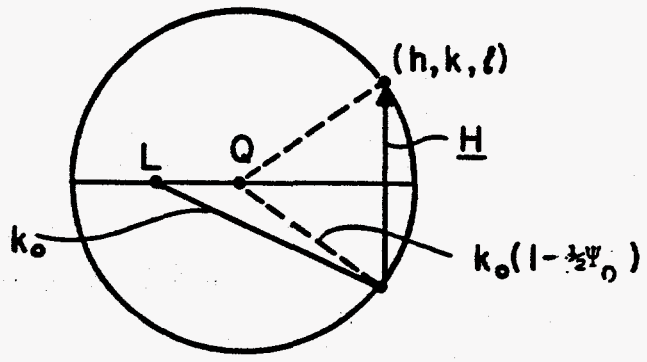

Figure 2-4b Ewald construction modified for average x-ray refractive index.

For the two mode case, the Equation 2-28 reduces to two equations. Equation 2-28 is a complex expression representing equations for the real and imaginary parts, respectively. Our first expression is obtained by the summation of terms for L=0 and L=H.

$$\Psi_H (\underline{K}_H \cdot \underline{D}_o) \underline{K}_H - \Psi_H \underline{K}_H^2 \underline{D}_o + \Psi_o (\underline{K}_H \cdot \underline{D}_H) \underline{K}_H - \Psi_o \underline{K}_H^2 \underline{D}_H = (\underline{k}^2 - \underline{K}_H^2) \underline{D}_H$$

Using 2-27, this expression becomes:

$$\Psi_H (\underline{K}_H \cdot \underline{D}_o) \underline{K}_H - \Psi_H \underline{K}_H^2 \underline{D}_o = \left[k^2 - \underline{K}_H^2 (1-\Psi_o)\right] \underline{D}_H \qquad (2\text{-}29)$$

The other equation is obtained for the symmetrical case with exchange of indices o and H. The fundamental system of equations for the two beam case thus becomes

$$\Psi_H (\underline{K}_o \cdot \underline{D}_H) \underline{K}_o - \Psi_H \underline{K}_o^2 \underline{D}_H = \left[k^2 - \underline{K}_o^2 (1-\Psi_o)\right] \underline{D}_o \qquad (2\text{-}30a)$$

$$\Psi_H (\underline{K}_H \cdot \underline{D}_o) \underline{K}_H - \Psi_H \underline{K}_H^2 \underline{D}_o = \left[k^2 - \underline{K}_H^2 (1-\Psi_o)\right] \underline{D}_H \qquad (2\text{-}30b)$$

Each of the two equations 2-30 itself represents two equations, one for each state of polarization. To see this behavior, we take the dot product of 2-30a with $\underline{D}_o$ and 2-30b with $\underline{D}_H$. Using Equation 2-27 in 2-30 and letting:

$\gamma \equiv$ angle between $\underline{D}_o$ and $\underline{K}_H$, we obtain

$$\underline{D}_H \cdot \underline{D}_o = |D_H| \; |D_o| \sin\gamma$$

We thus have:

$$\left[-\underline{K}_o^{\,2} + k^2 (1-\Psi_o)\right] \underline{D}_o - \left[k^2 \Psi_o \sin\gamma\right] \underline{D}_H = 0$$

$$\left[-\Psi_H \, k_o^{\,2} \sin\gamma\right] \underline{D}_o - \left[\underline{K}_H^{\,2} - k^2 (1-\Psi_o)\right] \underline{D}_H = 0 \qquad (2\text{-}31)$$

Equations 2-31 have been specifically written so as to be compatible with the well-known expositions of dynamical diffraction theory[10,11,12,15] and can be easily transformed into the notation used by these authors.

The basic equations 2-31 can be transformed into a very compact and useful form by defining the following quantities:

$$\alpha_o = (\underline{K}_o \cdot \underline{K}_o)^{\frac{1}{2}} - k(1-\tfrac{1}{2}\Psi_o)$$

$$\alpha_H = (\underline{K}_H \cdot \underline{K}_H)^{\frac{1}{2}} - k(1-\tfrac{1}{2}\Psi_o) \qquad (2\text{-}32)$$

These quantities represent the difference between the magnitude of the wavevector in the crystal and the vacuum value corrected for the average index of refraction.

In order for a solution to exist for Equations 2-31, the determinant of the coefficients must vanish. The fundamental equation resulting can be written using the product of the parameters in 2-32 as:

$$\alpha_0 \alpha_H = \frac{1}{4} k^2 (\sin \gamma)^2 \left[\frac{e^2\lambda^2}{mc^2\pi v}\right]^2 F_H F_H \qquad (2\text{-}33)$$

This is a convenient form to utilize in constructing the geometrical picture of x-ray wave propagation. As mentioned before, the construction is an alteration of the familiar Ewald sphere, shown in 2-4a. The average index of refraction in the crystal differs from the vacuum value and is given by $k(1-1/2\Psi_0)$. This shifts the center of the Ewald sphere, as shown in Figure 2-4b.

We recall that dynamical diffraction theory deals with the coupled interaction or interference of incident and diffracted x-rays. Accordingly, we note that Equation 2-33 predicts the behavior of $\underline{K}_0$ and $\underline{K}_H$ perturbed from their kinematical values, shown in the simple Ewald construction of Figure 2-4a. The product of the deviation of the magnitude of $\underline{K}_0$ and $\underline{K}_H$ from their average values inside the crystal is a constant.

The locus of points is a two sheet hyperbolic surface known as the dispersion surface. Figure 2-5 shows the nature of the surface. The two sheets are usually referred to as branches. The left hand sheet in Figure 2-5b is called the α branch and the right hand is referred to as the β branch.

The radii of the sections of spheres represented by the dotted lines are the magnitudes of $\underline{K}_0$ and $\underline{K}_H$ in the kinematical case. At any point where there is an allowed solution for the x-ray wavefield, such as the point T, the α's are shown to be the difference in magnitude

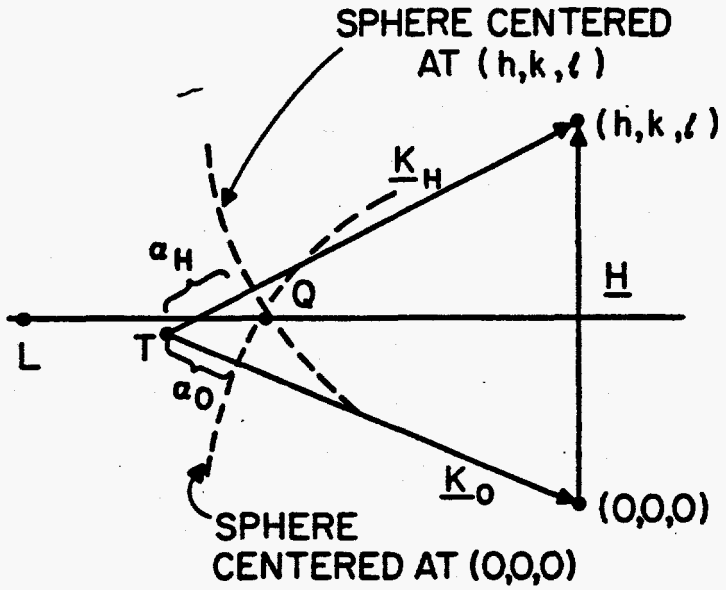

Figure 2-5(a). Geometrical construction displaying behavior of dispersion equation.

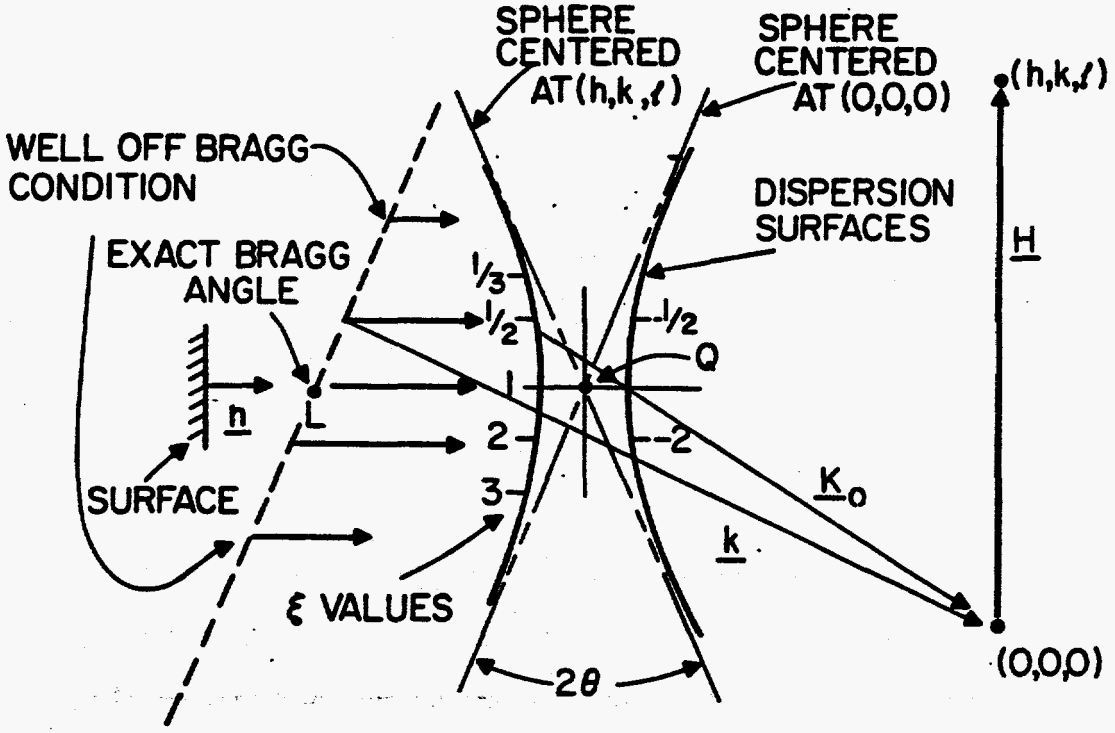

Figure 2-5(b). Enlarged view of the dispersion surfaces in the vicinity of point Q.

between the vacuum values and the actual values taking into account all of the interference effects. Figure 2-5b shows an enlarged view of the dispersion surfaces themselves, which are the locus of points such as T in 2-5a, satisfying Equation 2-30.

Remembering that dispersion surfaces are drawn in reciprocal space (or spatial frequency space), the surfaces are locii of constant x-ray frequency ω or $\omega(K)$ = const.

To follow the propagation of a ray, one now applies the boundary conditions where the rays enter and exit the crystal. Fortunately, in the x-ray case, these conditions are rather simple. We first note that we are ignoring true (Fresnel) reflection by dealing only with large angles with respect to the crystal surface.Some fascinating effects can occur when true reflection and diffraction are present simultaneously[13], but we shall deal here only with diffractive effects. The absence of true reflection implies that the field vectors (E, D, H, etc.) are continuous across the boundary. The wavevectors $\underline{K}$ are chosen so as to match phase fronts across the boundary. This results in the conclusion[10,14] that the change in wavevector across the surface occurs only along the normal to the surface.

The implications of this are easy to see in Figure 2-4(b). $\underline{k}$ is a wavevector in vacuum outside the crystal, while $\underline{K}_o$ is the wavevector inside the crystal; the difference must occur along the surface normal. The dotted line in Figure 2-5(b) is a section of a sphere centered at (0,0,0) and having radius equal to the vacuum magnitude of the wavevector. A vector in direction from L (usually referred to as the Laue point) to (0,0,0) is exactly at the Bragg angle (for free space conditions). The distance, from L along the dotted line, of the intersection of the input $\underline{k}$ is proportional to the deviation of the input vector from the Bragg angle. The choice of the direction of vacuum wavevector $\underline{k}$ selects an operating point T on the dispersion surface. The point T is usually

referred to as the tie point. Once this point has been selected by the input conditions, it determines all of the directional and absorptive properties of the x-ray wavefield. $\underline{k}$ in Figure 2-5b has been chosen to illustrate the condition for a ray incident slightly off the Bragg angle. A ray incident exactly at the Bragg angle would extend from L to (0,0,0).

It should be noted here that the surface geometry illustrated in Figure 2-5 with the normal pointing along the line LQ represents the Laue diffraction geometry with the diffracting planes normal to the entrance surface. The Bragg geometry would have the dispersion surface rotated by 90^{o}.

We will state one bit of information without proof that will be valuable in the derivations to follow. It has been shown[10,16] that the direction of net energy flow (poynting vector) for any operating point on the dispersion surface is along the normal to the surface at that point. In other words, the group velocity $v_g = \nabla_K \omega$, where ω is the constant frequency parametric form of the dispersion surface equations.

At this point, it is important to note an interesting characteristic of the selection of tie points in the Laue case. Because of the sharp curvature of the dispersion surfaces, a spread in input angle of only a few seconds of arc fills the region of crystal between $\underline{K}_o$ and $\underline{K}_H$ with energy. This phenomena is sometimes referred to as angular amplification. Authier[35] has rigorously shown that energy fills the region between $\underline{K}_o$ and $\underline{K}_H$, which is sometimes referred

to as the Borrmann triangle.

Space does not permit a full derivation of all of the diffraction properties that are of interest to acousto optic effects. The framework of dynamical diffraction theory has, however, been presented fully enough so that the statements made below follow naturally.

A very important parameter that is associated with a tie point on the dispersion surface is the ratio of diffracted to incident field strengths D_H/D_o. We define

$$D_H/D_o \equiv \xi$$

For convenience in the present discussion, we will refer only to the Laue geometry with diffracting planes perpendicular to the crystal entrance face. From Equations 2-31 and 2-32, we see that:

$$\xi = D_H/D_o = \frac{-2\alpha_o \sin\gamma}{k\Psi_H} = \frac{-k\,\Psi_H \sin\gamma}{2\alpha_H} \qquad (2\text{-}34)$$

ξ is a very important quantity since it expresses the ratio of incident to diffracted field. Since we know that the product $\alpha_o\alpha_H$ is a constant on the dispersion surface, the ratio ξ changes as we select different input angles corresponding to movement along the dispersion surface. The basic behavior is shown in Figure 2-5b.

For the α branch of the dispersion surface at angles larger than the Bragg angle, $\xi<1$, for angles smaller than θ_B, $\xi>1$. For the β branch of the dispersion surface, the ratios are the exact inverse.

The ratio ξ is of fundamental importance since at any point in the crystal, it represents the diffraction efficiency or reflection coefficient, the same quantity that was calculated earlier from the Darwin picture. Rather than rederive the formulas obtained earlier by the Darwin-Matrix method, we will emphasize other properties of the wave field that will aid in understanding propagation in acoustically perturbed crystals.

We first consider the absorptive properties of the x-ray wave field and the specific characteristics of the Borrmann effect. In the EVL picture, absorption is taken into account by expressing the propagation wavevector as a complex quantity. The intensity absorption factor is, thus, expressed using the imaginary part and is proportional to the quantity $(\underline{K}_0'' \cdot r)$. In all practical x-ray diffraction problems, the ratio of K''/K' is quite small (of the order of 10^{-5}). The directional information is thus, to a good approximation, carried by the real part of the wavevector and the imaginary part is used only in the absorption calculations. The boundary condition on K, which requires matching of phase fronts at the surface, implies that the imaginary part of K will be along the surface normal.

Before we proceed with a formal derivation of the equations for absorption, a few general properties will be discussed. The planes of constant amplitude (perpendicular to $\underline{K}''$) are parallel to the crystal surface. Thus, in considering absorption along any particular direction associated with a tie point on the dispersion surface, we must use an effective absorption coefficient:

$$\mu = K_0'' \cos(\underline{n},\underline{s}) \qquad (2\text{-}35)$$

where $\underline{n} \equiv$ unit vector along the surface normal

$\underline{s} \equiv$ unit vector in propagation direction.

The quantity μ is thus, the component of the imaginary part of the wavevector along the direction of energy flow. Intuitively, we can see that this is correct since this quantity represents the degree to which a ray cuts the atomic lattice planes where the (photoelectric) absorptive processes are localized. In other words, flow parallel to the lattice planes would represent minimum absorption. Thus, as we look at Figure 2-5, we recognize that modes with ξ much different than 1 (well off the Bragg angle) represent large angles with respect to the Bragg planes and thus, large absorption.

We now obtain an analytic expression for the absorption coefficient associated with a particular operating point on the dispersion surface. We will identify a point by the parameter ξ which can be directly related back to the input deviation from the Bragg angle. We need to write expressions for K_0'' and $\cos(\underline{n}, \underline{s})$ in terms of ξ and the crystal constants Ψ_0 and Ψ_1 (structure factors).

To find an expression for K_0'', we substitute the complex form for $\underline{K}_0$, $\underline{K}_H$, Ψ_0, Ψ_1,

$$\underline{K}_0 = \underline{K}_0' + i\,\underline{K}_0''$$

$$\underline{K}_H = \underline{K}_H' + i\,\underline{K}''$$

$$\Psi_o = \Psi_o' + i\,\Psi_o''$$

$$\Psi_H = \Psi_H' + i\,\Psi_H''$$

into Equations 2-31.

We recall that $|K_H''| = |K_o''|$ and that the real parts of the K vectors are greater than the imaginary by about 10^5. The real and imaginary parts of each of the equations are then set equal to zero and $\underline{K}_H'$ and $\underline{K}_o'$ eliminated. We can now express the absorption coefficient in terms of the field amplitudes

$$\mu = \frac{\mu_o}{\cos\alpha}\left[1 - \frac{2(F_H''/F_o'')D_H}{D_o^2 + D_H^2}\right] \qquad (2\text{-}36)$$

where α is the angle of propagation with respect to the bisector of $\underline{K}_o$ and $\underline{K}_H$, i.e. angle with respect to the lattice planes.

Equation 2-36 is more conveniently expressed in terms of the mode parameter ξ as:

$$\mu = \mu_o\left\{1 - \frac{2\xi\ F_H''/F_o''}{1+\xi^2}\right\} \qquad (2\text{-}37)$$

Batterman and Cole[10] have written this formula in a slightly different form by relating ξ directly to the input conditions.

$$\mu = \mu_o\left\{1 \pm \frac{F_H''/F_o''}{\sqrt{1 + \frac{\Delta\theta\ \sin\theta}{\Gamma\ |F_H|}}}\right\} \qquad (2\text{-}38)$$

$$\Gamma = (e^2/mc^2)(\lambda^2/\pi V)$$

where the choice of sign in (2-38) is governed by the choice of the branch of the dispersion surface: negative for the α branch and positive for the β branch.

The angle of propagation with respect to the lattice planes is obtained through the fact that the poynting vector is normal to the dispersion surface. Thus, the angle is an explicit function of ξ. Wagner[16,17] has shown that for a unit vector, $\hat{j}$, in the direction of the poynting vector,

$$\hat{j} = \frac{1}{\sqrt{\left[1+\xi^4+2\xi^2\cos(2\theta_B)\right]}}\left[(1+\xi^2)\cos\theta_B\,\hat{Z} - (1-\xi^2)\sin\theta_B\,\hat{X}\right]. \quad (2\text{-}39)$$

where $\hat{X}$ is a unit vector parallel to the lattice planes and $\hat{Z}$ is a unit vector perpendicular to the lattice planes.

The angle that the wavevector of any mode makes with respect to the lattice planes is thus,

$$\operatorname{Tan}\alpha = \frac{\xi^2-1}{\xi^2+1}\operatorname{Tan}\theta_B \quad . \quad (2\text{-}40)$$

Formulas 2-37 and 2-38 constitute a theoretical explanation of the Borrmann effect. The quantity F_H''/F_o'' is always close to unity. Thus, when ξ is positive and close to one, the absorption coefficient is greatly reduced from the normal value μ_o. These formulae point up another very important characteristic of the Borrmann effect. For the other branch of the dispersion surface $\xi<1$ (positive sign taken in 2-38), and thus, is characterized by a

greater than normal attenuation. In the introductory chapter, the Borrmann effect was explained in terms of an x-ray standing wave pattern inside the crystal. The high absorption case associated with the β branch of the dispersion surface thus corresponds to the case where the standing wave pattern is located with high field regions occurring at the lattice planes.

Another interesting characterisitc of the Borrmann effect is contained in the factor $F_H"/F_o"$. The closer this quantity is to unity, the smaller the effective absorption (in the low absorption case). The quantity $F_H"/F_o"$ is an indicator of the spatial distribution of absorbing power of the atom and is sometimes referred to as the effective atomic size. If the atoms were truely confined to infinitesimal point, lattice sites $F_H"/F_o"$ would equal unity exactly.

We can also see from(2-38)the effect of lattice perturbations on the absorption. As a ray begins to violate the Bragg condition, the absorption increases. This, of course, leads to a rocking curve of transmitted or diffracted intensity versus deviation from the Bragg angle (or change in the 2d lattice spacing). This is analogous to the Bragg case derived earlier from the Darwin point of view. However, in the case of Borrmann transmission, the absorption plays a somewhat more important role than in the Bragg reflection case.

SUMMARY OF EWALD-VON LAUE (EVL) FORMULATION OF DYNAMICAL THEORY

(1) The EVL picture was used to derive results primarily for the case of Laue geometry diffraction, which is the situation encountered in Borrmann transmission. The dispersion surface geometry was introduced as a compact visualization of the fundamental equation for x-ray propagation, 2-33.

Input boundary conditions select a tie point (or operating point) on the dispersion surface. This tie point then determines both the directional and absorptive properties of the x-ray propagation. The tie point is usually indentified by its mode parameter ξ.

(2) As the angle of input rays deviates from the Bragg angle, energy propagates at increasing angles with respect to the lattice planes. The angle of propagation with respect to the lattice planes, in terms of the mode parameter ξ, is given by Equation 2-40.

(3) An effective absorption coefficient as a function of the mode parameter ξ is given by Equation 2-37. This allows one to calculate the absorption associated with any particular ray direction.

(4) Equations 2-37 and 2-38 are the essential relations necessary in order to calculate diffracted intensity vs. deviation from the Bragg condition. The same type of information is contained in the "Darwin curve" calculated earlier for the Bragg case. A graph of the variation of diffracted intensity as a function of deviation from the Bragg angle is referred to (in both the Bragg and Laue cases) as the diffraction curve.

2.6 PROPAGATION IN IMPERFECT CRYSTALS

2.6-1 General Outline

Interest in x-ray propagation in imperfect crystals was historically generated by a desire to study intrinsic lattice defects, such as dislocations. When x-ray topographs of crystals are taken, various mechanisms lead to contrast (either an increase or a decrease in diffracted x-ray intensity) giving a type of "image" of the defect regions.

Numerous theories have been proposed to deal with x-ray propagation in perturbed lattice structures. They can, however, be placed in one of three general categories:

(1) Refractive theories, usually associated with the original developers, Penning and Polder[15].

(2) Diffractive theories, which are a more exact calculation of the x-ray wave field and generally referred to under the heading of Takagis' equations[19].

(3) More exact theories, based on a quantum-mechanical formulation of the x-ray scattering[20,29]. Although these models are quite rigorous, they are also quite cumbersome and have yet to be applied to any practical distorted crystal problem.

In addition to these three theoretical approaches, another model has been proposed as part of this study exclusively for the case of Borrmann propagation in acoustically distorted crystals. It will be referred to as the simple absorption model.

We have applied the first two categories of theory and the simple absorption model to the case of acoustically perturbed Borrmann trans-

mission in both the one and two crystal cases. Quantitative comparisons between these theories and experimental results are described in Chapter 3. Each of the theoretical approaches is now described in detail. In addition, the quantitative methods of calculation are described and typical calculations are presented. To begin with, we will discuss the simple absorption picture.

2.6-2 SIMPLE ABSORPTION THEORY - DESCRIPTION AND APPLICATION

When an acoustic wave is introduced into a crystal, a sinusoidal strain variation results. This situation is illustrated in Figure 2-6. Rays entering the crystal spread out into the Borrmann fan (or triangle). A typical scale for the actual extent of the Borrmann fan when high absorption is present is shown (labeled "actual path of rays"). Because of the acoustic strain, rays which satisfy the Bragg angle at the entrance face may pass into regions where the Bragg law is no longer satisfied.

As explained in section 2-5, energy flow fills the Borrmann triangle when there is a variation of input angle (on the order of a few seconds). As shown in formulas 2-37 and 2-38, rays which propagate the furthest off axis suffer the greatest attenuation. Thus, in the case of a thick perfect crystal which exhibits a strong Borrmann effect, the effective angular spread of rays is limited to somewhat less than the full Borrmann triangle, as illustrated in Figure 2-6. It is sometimes said that the Borrmann effect results from energy transmission parallel to the lattice planes. We now see from the more accurate calculations of dynamical theory that this is true only

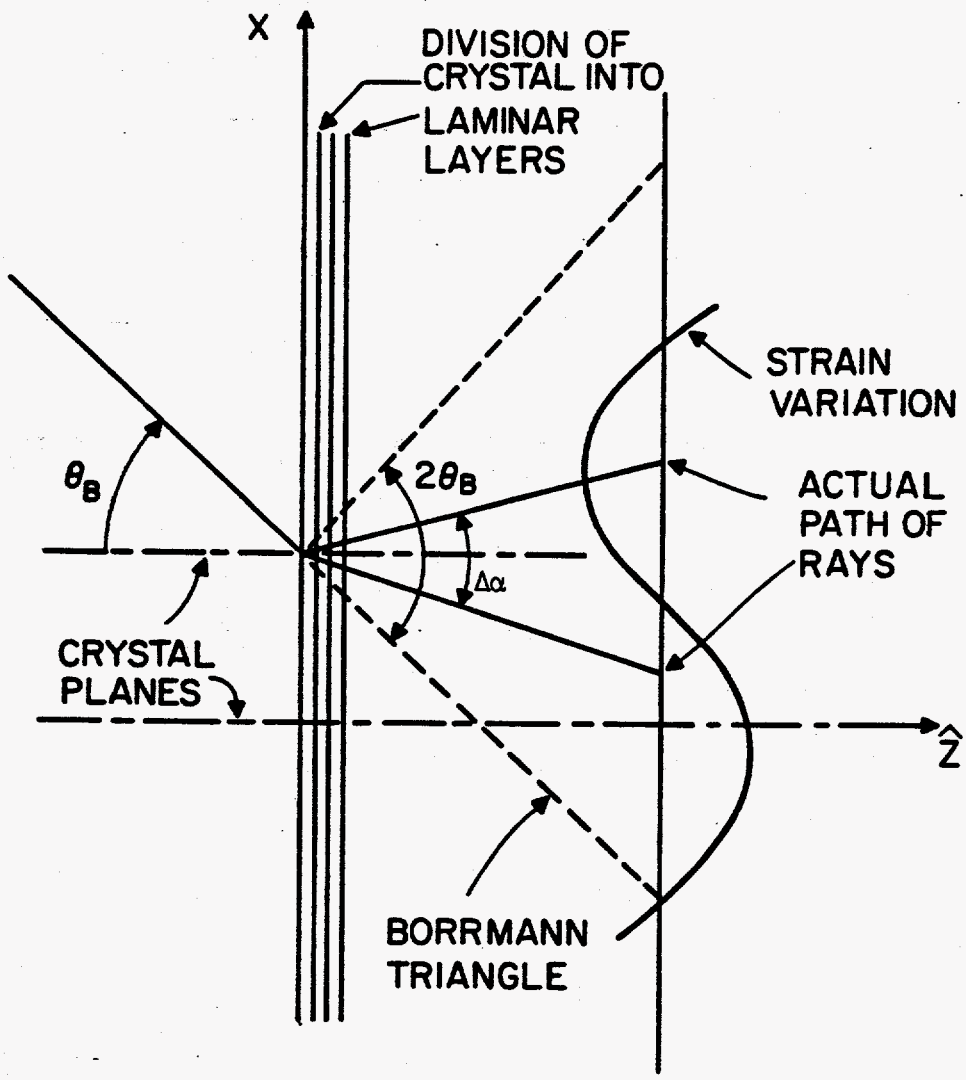

Figure 2-6. Geometrical representation of simple absorption calculation.

in an average sense. Gerward,[31] using variations of formulas 2-37 and 2-38, has made detailed calculations of the energy flow in silicon crystals. He has developed a useful formula (based on 2-37) for the effective angular spread of rays in the Borrmann fan. He defines the fan by the rays that have been attenuated to 1/e of the intensity of the central ray (see Figure 2-6). The following formula for the Borrmann fan angle $\Delta\alpha$ (see Figure 2-6) results:

$$\Delta\alpha \cong \tan^{-1}\left[\left(\frac{2\ln 2}{\mu_o \varepsilon t - 1}\right)^{\frac{1}{2}} \tan(2\theta_B)\right] \qquad (2\text{-}41)$$

where $\varepsilon = F_H''/F_o''$

t = crystal thickness

μ_o = linear absorption coefficient.

We now assume a sinusoidally varying strain is acoustically introduced along the X axis, as shown in Figure 2-6. Assume that x-rays are incident on the crystal in an uncollimated, non-monochromatic beam (quantitative values for the parameters will be considered later). At any particular point on the entrance surface, assume that there is incident a packet of rays (with central ray exactly at the Bragg angle) with angular width greater than the (Darwin curve) width of the reflection. A fan of rays will spread out filling the effective Borrmann triangle. A ray that spreads off axis will no longer satisfy the Bragg condition and start to suffer a greater absorption then would be implied by the mode parameter ξ of the ray through Equation 2-37.

In order to calculate the overall attenuating effect of the acoustic strain, we trace an ensemble of rays within the Borrmann fan and

estimate the effective absorption of each ray. To perform this calculation, we divide the crystal into thin lamina (parallel to the X axis and the crystal faces). At the boundary of each lamina along the path of a ray, we calculate the strain (or deviation from the Bragg law) by subtracting the local value of the 2d spacing from that at the entrance point of the ray on the front surface of the crystal. The local strain is defined by the following relation.

σ = local strain at X referenced with respect to a ray entering the crystal at X_o.

$$\sigma = \sigma_o \sin\left(\frac{2\pi X}{\Lambda}\right) - \sigma_o \sin\left(\frac{2\pi}{\Lambda} X_o\right) \qquad (2\text{-}42)$$

Using this value for the strain, we calculate the attenuation of a ray in passing through one of the lamina by using formulas 2-37 and 2-38.

A computer ray trace program has been written that traces an ensemble of rays within the Borrmann fan, calculating the cumulative absorption in passing through many lamina. An ensemble of rays is traced for many different entrance points on the crystal face. The number of points on the entrance face is always chosen so that a large number (typically ≈ 20) occur within an acoustic wavelength.

A number of other features are included in the ray trace program in order to make it as realistic as possible. The choice of the number of rays in any particular case is governed by the calculation of the effective Borrmann fan angle from Equation 2-41. The number of lamina

is chosen so that the lamina thickness is very small compared to the acoustic wavelength, but larger than an extinction distance. If significant strain variations were to occur within an extinction distance, "diffractive" effects would start to occur, which are not predicted by the simple absorption theory. This problem will be discussed in detail later.

In addition, the mode parameter ξ of each individual ray is recorded, and used to calculate the relative contribution of the ray to the diffracted intensity.

Examples of results from the simple absorption theory are given in Figures 2-7 and 2-8 (for the case of uncollimated radiation incident on a sinusoidal strain variation, as shown in Figure 2-6). These graphs show the fall off in diffracted intensity as a function of the coordinate X along the exit face of the crystal.

For illustrative purposes, we trace rays for only one particular entrance point on the front face. In the practical cases described in Chapter 3 (in conjunction with experiment), many points were used. In Figure 2-7, the entrance point is aligned so that the central ray passes through a node of the acoustic pattern. Off axis rays in this case will thus encounter the greatest deviation from the input conditions. In 2-8, the entrance point is opposite an antinode and shows the much slower drop off of diffracted intensity as a function of angular deviation from the central ray. The diagram in the upper right hand corner of Figures 2-7 and 2-8 shows the relative relationship of the effective spread of the Borrmann fan (1/e points in intensity) and the acoustic wavelength. In Chapter 3, an extensive series of computer curves will

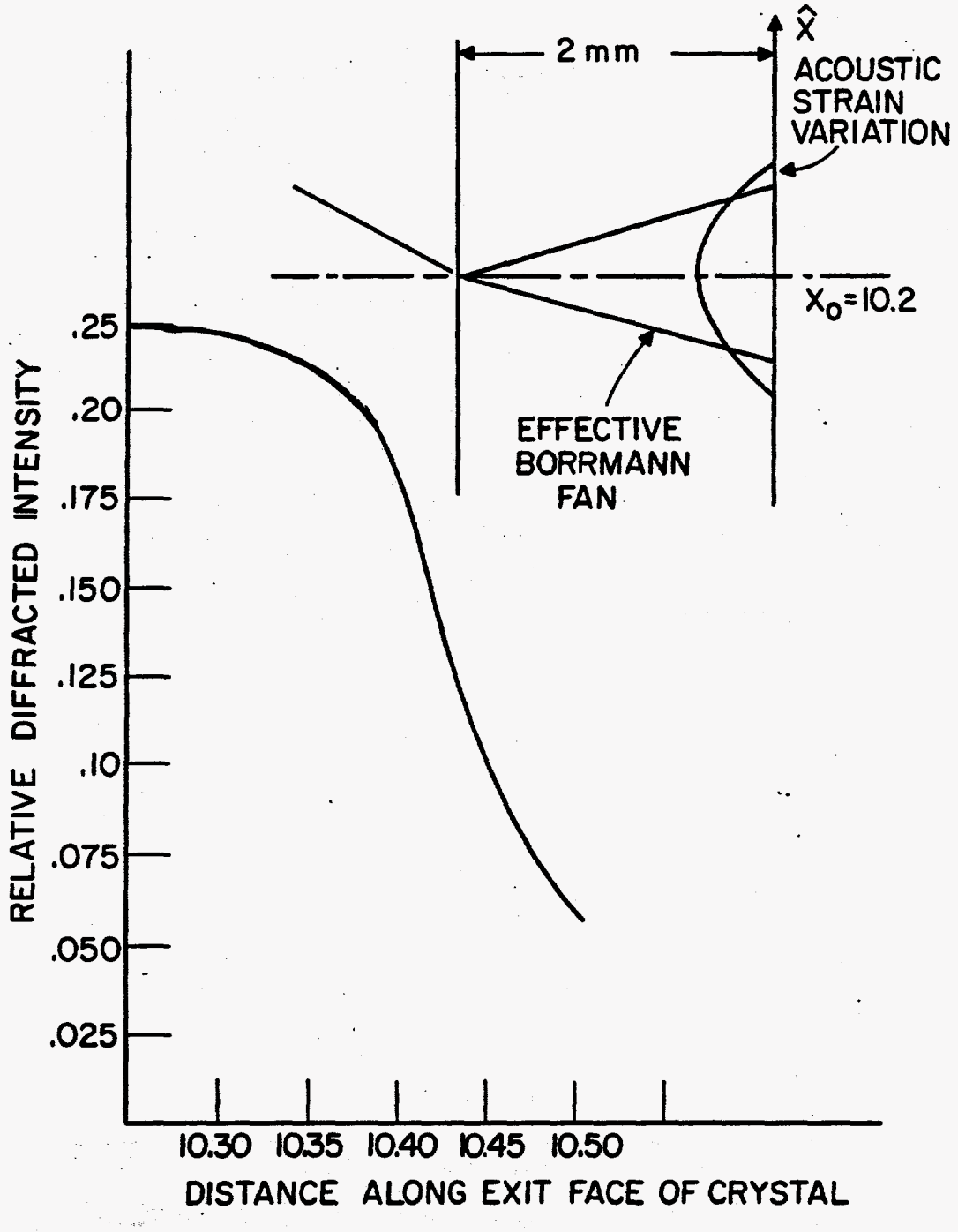

Figure 2-8. Simple absorption calculation for a ray entering the crystal at the anti node of the acoustic pattern.

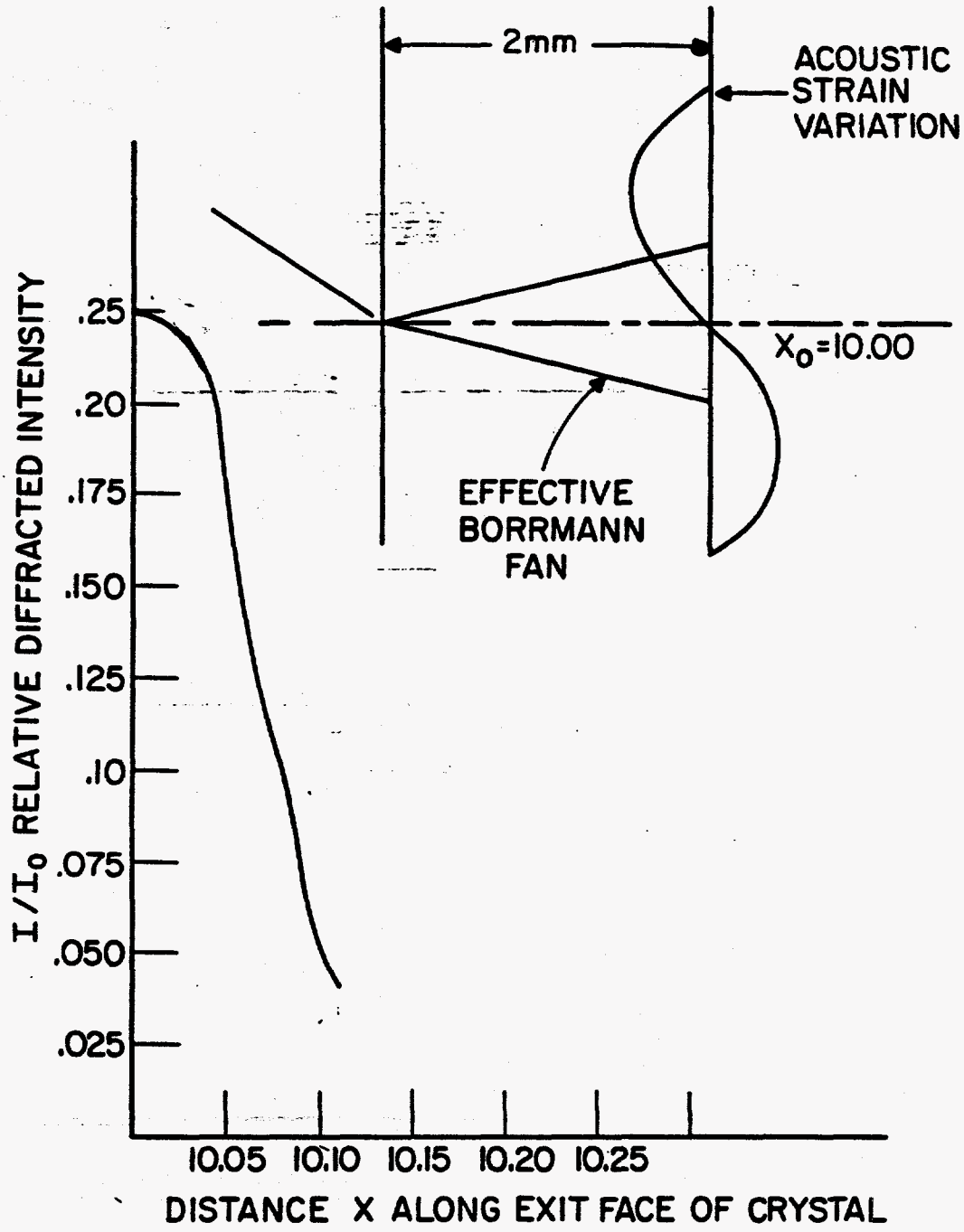

Figure 2-7. Simple absorption calculation for ray entering the crystal at a node of the acoustic pattern.

be compared with experimental measurements of acoustic attenuation of Borrmann transmission.

Since the acoustically induced strain is varying in time, proper account must be taken of the time averaged attenuation of the x-rays. In the simple absorption model, the attenuation in passing through a single lamina depends only on the magnitude of deviation from the Bragg condition and not on the sign. Thus, in comparing results of the simple absorption model with experiment, we take the rms strain level as an indication of the average deviation of the lattice from perfection.

2.6-3 REFRACTIVE THEORY OF X-RAY PROPAGATION - DESCRIPTION AND APPLICATION

The simple absorption theory described in the previous section ignores some details of x-ray propagation in perfect crystals. A detailed analysis of the energy propagation shows that x-rays passing through strained regions of a crystal suffer refraction much the same as an optical beam passing through a medium of varying index. There is, however, a clear distinction between the x-ray and optical cases. An x-ray passing through a strained crystal at an arbitrary angle will suffer no detectable refractive effects. Only when an x-ray is incident at certain unique angles (a Bragg angle with respect to some crystalline plane) can refractive effects be observed. Only when multiple reflection effects are present is there any sensitivity of x-ray transmission to strains in the solid. From these considerations, we deduce that the regular lattice structure acts as an intermediary in the interaction of sound and x-rays. The multiple reflection phenomena that are set up when Bragg's law is satisfied perturbs the normal x-ray index. This perturbed value of the index is, in turn, changed by the acoustic distortion of the lattice.

In 1961, Penning and Polder[15] proposed a theory of x-ray propagation in distorted crystals which utilized the concept of a slowly varying reciprocal lattice vector. In a local sense, all of the laws of dynamical theory apply for the particular local value of $\underline{H}$. The propagation from point to point was handled by a ray-optic theory. That is, the spread in wavevector $\underline{K}$ was small enough that the beam could be considered a plane wave; and the lateral extent of the ray small enough that it could be characterized by a single reciprocal vector $\underline{H}$. The

conditions will be noticed to be quite similar to those employed in the Eikonal theory of light propagation in inhomogeneous media. In fact, most of the assumptions are quite similar.

One important difference concerns absorption effects.In the optical case, the refractive ray bending affects only the directional characteristics. We have shown that the absorptive properties of x-ray propagation are quite directionally dependent. When refractive effects are present and directional changes take place, the operating or tie point on the dispersion surface changes (see Figure 2-5b). With a change in tie point, the local value of the mode parameter changes and thus, the effective absorption coefficient through Equation 2-37. In somewhat simpler terms, the directional changes lead to a varying angle of propagation with respect to the lattice planes (larger angles leading to a greater effective cross section for absorption).

In order to better understand the mechanism by which refraction occurs, the following phenomenological picture has been constructed. This picture is specifically based on the sinusoidal strain variation encountered in acoustic fields, even though other types of lattice distortion can also lead to refractive effects[22].

In Figure 2-9(a), we summarize some results that were derived in the section on EVL formulation. A ray incident on a crystal at greater than the Bragg angle(dashed line)selects a tie point such that $\xi<1$ and,thus,propagates in the upper portion of the Borrmann fan.(We will assume in this discussion that the crystal exhibits a strong Borrmann effect and,thus, only one branch of the dispersion surface is excited). Rays incident

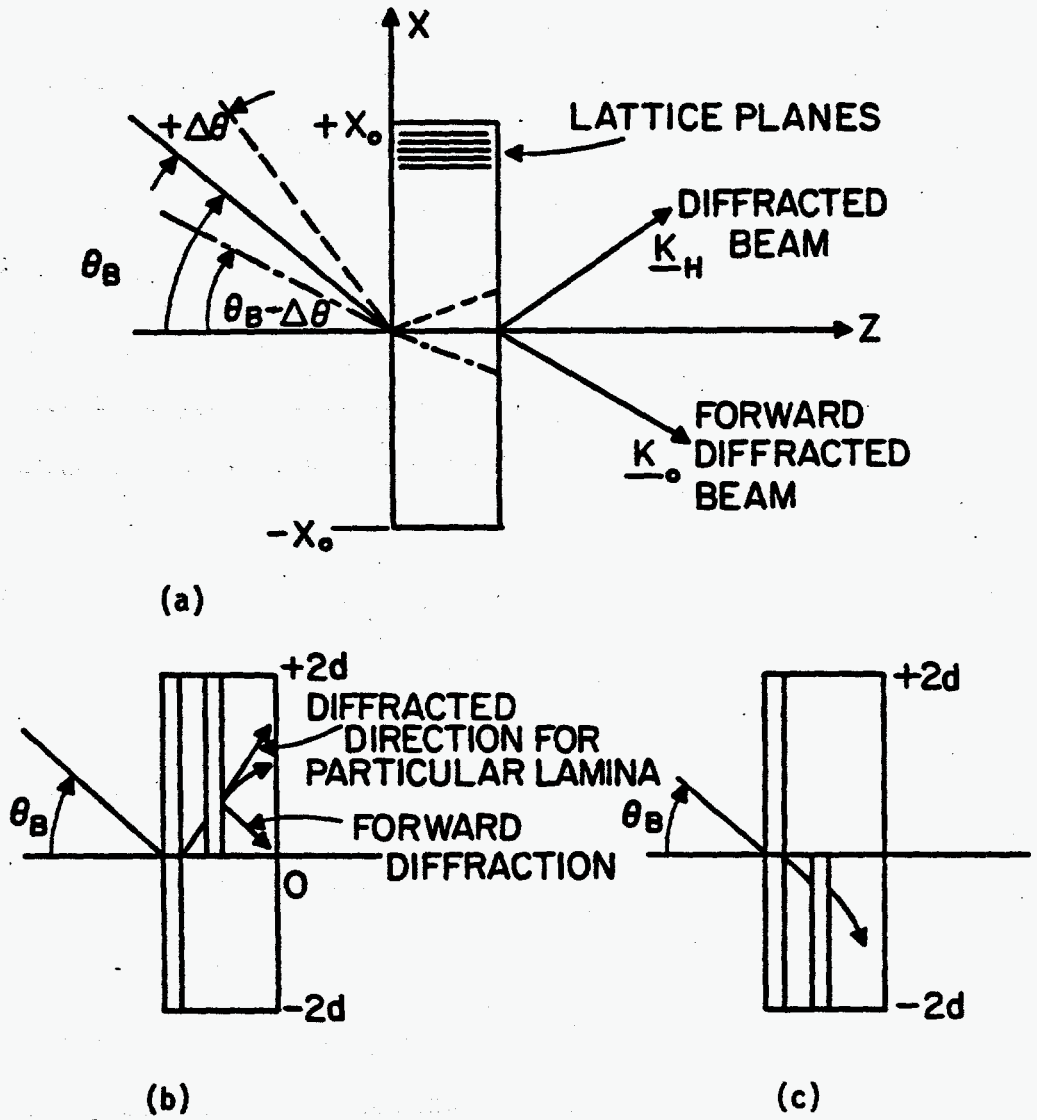

Figure 2-9. Illustration of x-ray refraction.

at angles smaller than the exact Bragg angle (broken line) select a tie point with $\xi>1$ and propagate in the lower half of the Borrmann fan.

Suppose now that a strain gradient is introduced into the crystal such that the portion of crystal at X=o has the quiescent value of 2d spacing, while portions at $+X_o$ have a larger than normal spacing, and those at $-X_o$ a smaller spacing. Consider the ray traces in Figure 2-9(b) and 2-9(c). A ray propagating in the upper portion of the Borrmann fan encounters a portion of the crystal with larger than normal 2d spacing. As was demonstrated in the upper part of the figure, for a ray incident on a region with an angle greater than the Bragg angle (which is equivalent to greater than normal 2d spacing) a mode is excited that emphasizes the diffracted radiation. As the ray propagates through the strained region, the energy flow continues to bend toward the diffracted direction, thus giving the ray trajectory shown in Figure 2-9(b). Rays in the bottom half of the fan encounter smaller than normal 2d spacing and accordingly, are bent downward, as shown in Figure 2-9(c). Thus, all rays are bent in the direction of the density or refractive index gradient (smaller than normal 2d spacing, implying higher than normal density), as is the normal condition for optical refractive effects. The limits of refractive or Penning and Polder theory will be considered later, but we will say here that the approach is valid as long as significant changes in the reciprocal vector (such as changes in the lattice parameter) do not occur within an extinction distance.

We will now consider the refractive theory in a more quantitative manner and apply it to the specific case of acoustic perturbations. As

was pointed out earlier in this chapter, the group velocity for x-ray propagation inside the crystal is normal to the dispersion surface.It should be remembered that this velocity characterizes the total field. Inside the crystal, the field is not resolved into incident and diffracted components, but propagates as one mode characteristic of a particular branch of the dispersion surface.

The fundamental assumption of Penning and Polder theory[15,17] is that the change in direction of one component of the x-ray wavefield, e.g. $\underline{K}_0$, can be written in analogy with the optical Eikonal equation

$$d\,\underline{K}_0 = a\nabla(\underline{H}\cdot\hat{j}) \qquad (2\text{-}43)$$

$$\text{where } a = 1/|\underline{v}_g|$$

$$\underline{v}_g = |v_g|\hat{j}$$

Thus, the change in the wavevector $\underline{K}_0$ is governed by the component of ∇H along the ray direction.

Recalling the expression for $\hat{j}$ given in 2-39, it is easy to show[17] that:

$$d\,\underline{K}_0 = \frac{-\xi^2}{\sqrt{\left[1+\xi^4+2\xi^2\cos(2\theta_B)\right]}}\,\nabla(\underline{H}\cdot\underline{K}_H)\cdot dl \qquad (2\text{-}44)$$

where dl = unit length along the ray path.

We now must write the change in $\underline{H}$ as a function of a given lattice perturbation. Let $\underline{r}_0$ and $\underline{r}$ represent the quiescent and perturbed positions respectively of the lattice points within the crystal.

$$\underline{r} = \underline{r}_0 + \underline{u} \qquad (2\text{-}45)$$

We are only interested, however, in a strain component in the direction of $\underline{H}_0$, the original value of $\underline{H}$. We can now write:

$$\frac{d\underline{H}}{dl} = \nabla\left[\hat{j}\cdot\nabla(\underline{u}\cdot\underline{H}_0)\right] \qquad (2\text{-}46)$$

Using this relation in Equation 2-44, Penning and Polder[15] have written what is probably the most useful form of the refractive equation which gives the variation of the mode parameter ξ along the refracted ray path. A slight rearrangement of their formula gives:

$$\frac{d\xi}{dl} = -\frac{(2\xi^2)/\chi_H}{K^3\sqrt{\left[1+\xi^4+2\xi^2\cos(2\theta_B)\right]}}(\underline{K}_H\cdot\nabla)(\underline{K}_0\cdot\nabla)(\underline{H}\cdot\underline{u}) \qquad (2\text{-}47)$$

where χ_H = x-ray susceptibility for H reflection

$$\chi_H = \frac{R}{\pi}\frac{\lambda^2}{V}F_H \qquad (2\text{-}47a)$$

R = classical electron radius

V = volume of unit cell.

Using the coordinate system shown in Figure 2-9, we can rewrite (2-47) in a different form.

$|u|$ = magnitude of lattice displacement,

then

$$\underline{H}\cdot\underline{u} = \frac{1}{d}|u| = \frac{2u\sin\theta}{\lambda}$$

Equation 2-47 now becomes:

$$\frac{d\xi}{dl} = \frac{(4\xi^2 \sin\theta_B)/\chi_H}{\sqrt{\left[(1+\xi^4+2\xi^2\cos(2\theta_B)\right]}}\left[\cos^2\theta_B \frac{\partial u^2}{\partial Z^2} - \sin^2\theta_B \frac{\partial^2 u}{\partial X^2}\right] \qquad (2\text{-}48)$$

It is interesting to consider the effect of the two terms within the brackets in Equation 2-48. As Kato[23] has pointed out, a nonvanishing value of $\partial u/\partial Z$ represents a tilt of the lattice planes and $\partial^2 u/\partial Z^2$ a bending. $\partial u/\partial X$ represents a change in the 2d lattice spacing, while $\partial^2 u/\partial X^2$ is a spatial rate of change of lattice expansion or contraction. The relative importance of the two terms is governed by the magnitude of the Bragg angle, θ_B.

As a practical case, consider the (220) planes in silicon (which will be considered experimentally in Chapter 3). We calculate the quantities $\cos^2\theta_B$ and $\sin^2\theta_B$ for various wavelength x-rays.

Table 2-1. Diffraction data for (220) planes in silicon.

	λ Å	θ_B(°)	$\sin^2\theta_B$	$\cos^2\theta_B$
MoK_α	.71	10.7	.034	.96
CuK_α	1.54	23.6	.16	.84
CrK_α	2.3	36.8	.36	.64
CaK_α	3.3	59.2	.74	.26

We see from Table 2-2 that if refractive effects are to be used to control or modulate x-rays, that expansion and contraction of the lattice becomes increasingly important as the radiation becomes softer.

In the experimental work in the present study, acoustic waves were propagated perpendicular to the lattice planes, thus primarily causing expansion and contraction. This was done for simplicity and ease of comparison with theory. Other types of lattice deformation could, of course, be produced by acoustic disturbances. More will be said about potential device design procedures in Chapter 4.

We now consider the application of refractive theory to specific acoustic perturbation problems. We consider a sinusoidal perturbation along the $\hat{X}$ axis (along the reciprocal vector). This, of course, is the geometry often encountered in acousto optic effects in the optical regime.

The strain du/dX is thus written:

$$\frac{du}{dX} = u_o \sin\left(\frac{2\pi}{\Lambda}X\right) \qquad (2\text{-}49)$$

where Λ = acoustic wavelength.

In order to calculate the x-ray transmission in an acoustically perturbed Borrmann transmitting crystal, a complete x-ray refractive ray trace computer program has been written.

Rearranging 2-39, we can obtain an equation for the 'slope' of a ray:

$$\frac{dX}{dZ} = \frac{\xi^2-1}{\xi^2+1} \tan\theta_B \qquad (2\text{-}50)$$

In the ray trace program, the crystal is once again divided into a large number of lamina parallel to the faces (perpendicular to the lattice planes). At any particular point on the entrance face of the crystal, an ensemble of rays having different initial mode parameters is chosen.

Using Equation 2-49 in 2-50, we obtain:

$$\frac{d\xi}{dl} = \frac{(4\xi^2 \sin^3\theta_B \quad u_o)/\chi_H}{\sqrt{\left[(1+\xi^4+2\xi^2 \cos(2\theta_B)\right]\Lambda}} \cos\left[\frac{2\pi X}{\Lambda}\right] \qquad (2\text{-}51)$$

The change in mode parameter in passing through a lamina is calculated using Equation 2-51 with $\underline{dl} = \underline{dX} + \underline{dZ}$ within each lamina. The trajectory of a ray within each lamina is governed by Equation 2-50 with the value of ξ being taken to be the value at the entry point of the ray into the lamina.

The absorption of a ray, of course, depends on its path with respect to the lattice planes. The effective absorption coefficient for a ray is calculated using Equation 2-37, which expresses the absorption as a function of ξ. As before, the value taken for ξ is the value at the entry to each lamina.

Figures 2-10 and 2-11 show typical examples of ray traces for a strain amplitude of 10^{-5}.

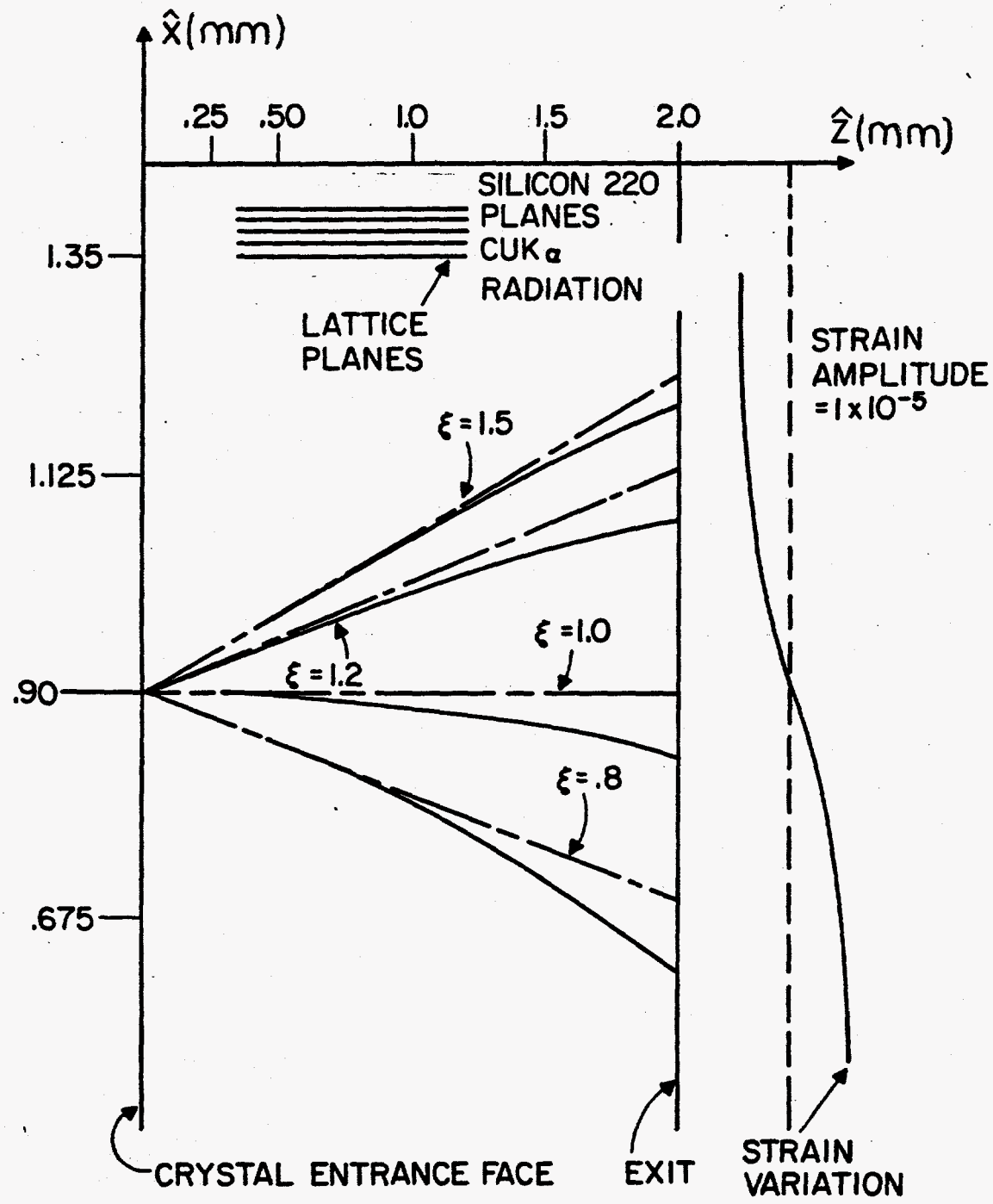

Figure 2-10 Refractive ray trace entrance point opposite node, negative strain gradient.

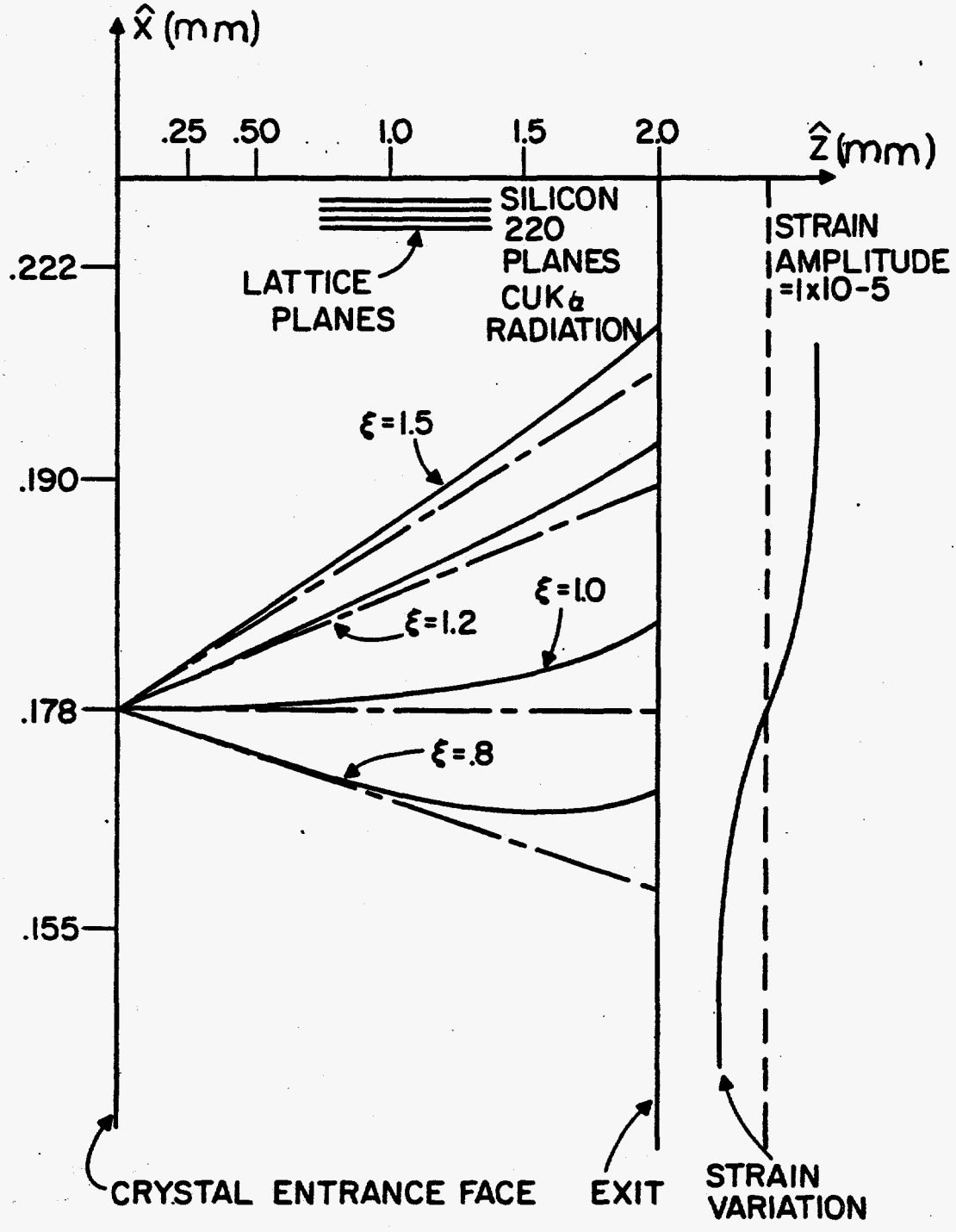

Figure 2-11 Refractive ray trace entrance point opposite node, positive strain gradient.

The sign of the strain gradient in 2-$\bar{1}$0 is reversed from that in 2-$\bar{1}$1, while in both cases, the entrance point is directly opposite the node of the acoustic pattern. The cross hatched lines show the unrefracted paths that the rays would take in the absence of a strain gradient. We can see from these plots new details of the acoustic interruption not contained in the simple absorption model. We recall that rays with $\xi>1$ contribute more to the diffracted beam. We, thus, see that the attenuation of the diffracted beam due to acoustic perturbation will change when the sign of the strain gradient changes. In certain cases, the transmission of a ray might be slightly enhanced (refracted so as to propagate more closely parallel to the lattice planes). Since the sign of the strain gradient reverses once every acoustic cycle, the difference between 2-10 and 2-$\bar{1}$1 is averaged out. This situation does point up, however, the need to carefully consider the time averaging when making numerical calculations using the refractive model.

When calculating the x-ray transmission vs. acoustic strain level, complete ray traces (including the full array of points on entrance surface) are numerically computed for one complete acoustic cycle (2 traces with the strain gradient reversed and amplitude taken equal to rms value). The resulting transmission is then taken to be the average of these values.

In Figures 2-12 and 13 are shown ray traces for entry points opposite the antinode, but with twice the strain level as that indicated in Figures 2-10 and 11. The strain level of 10^{-5} in Figures 2-10

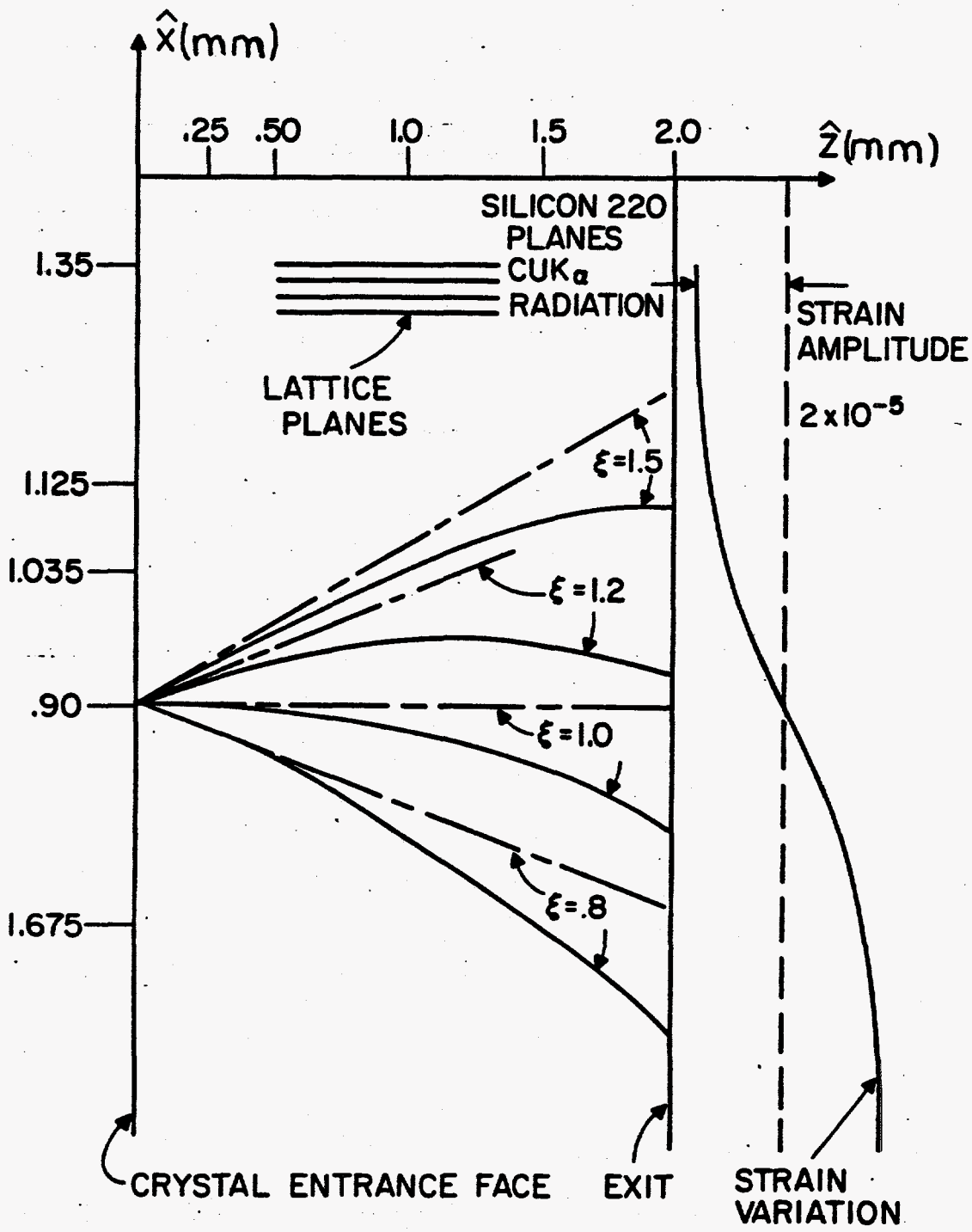

Figure 2-12 . Refractive ray trace entrance point opposite node, negative strain gradient.

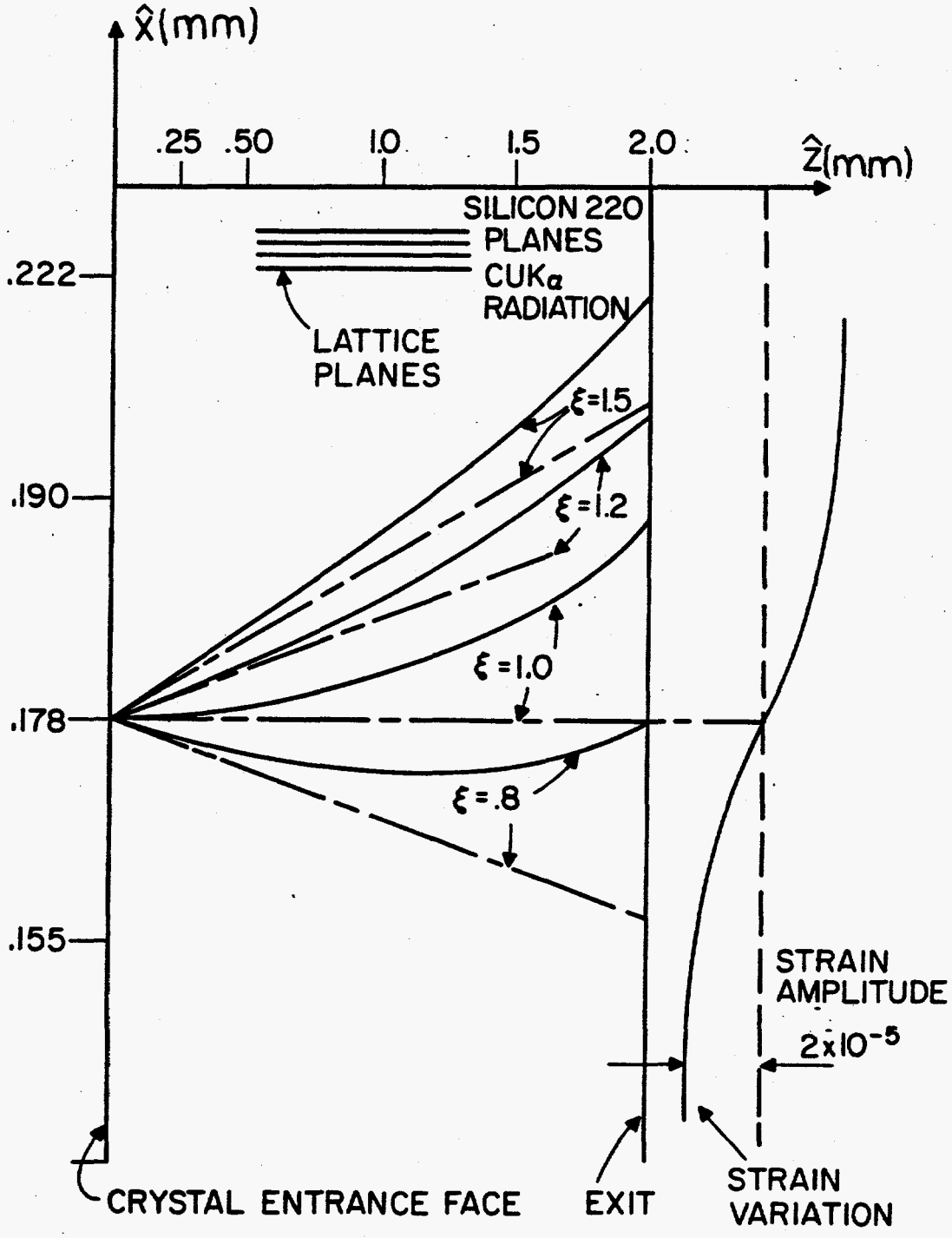

Figure 2-13 . Refractive ray trace entrance point opposite node, positive strain gradient.

was near the threshold for significant attenuation effects to appear for this particular case (220 planes of silicon and CuK_{α} radiation). In Figures 2-12 and 2-13, the refractive effects are much more pronounced.

In Figure 2-14, we see ray traces identical to those in 2-13, except that the entry point of the fan of rays is now opposite an antinode instead of a node. The strain gradient being weaker, the refractive effects are also weaker. The rays suffer less deviation from their normal trajectories and, thus, less attenuation. The distribution of x-ray intensity at the exit face of the crystal will, thus, be a fringe pattern with high intensity at an antinode and low intensity at a node. This pattern can be used to visualize the complete acoustic field inside a crystal, as will be discussed in detail in the next chapter.

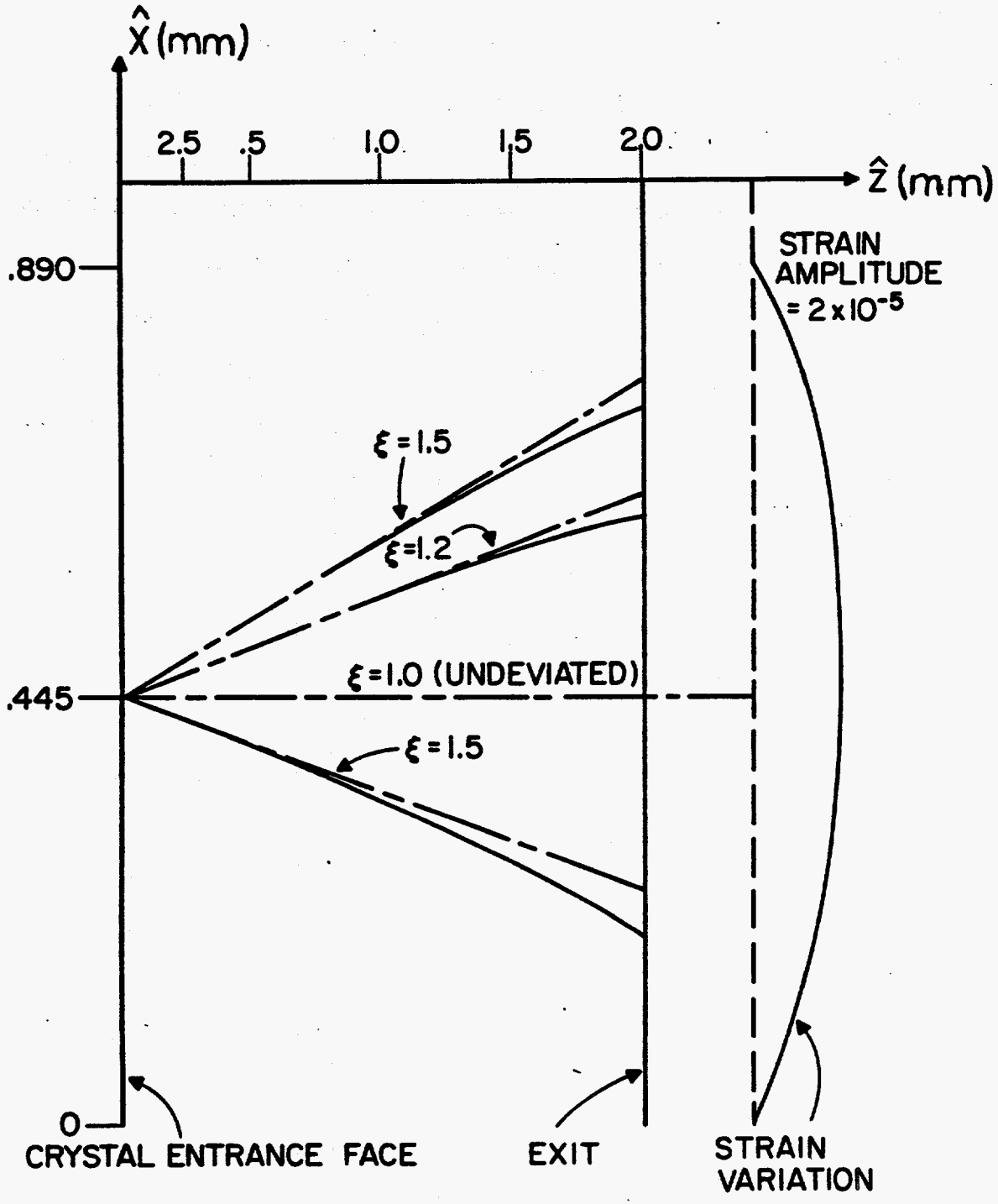

Figure 2-14. Refractive ray trace entrance point opposite antinode.

2.6-4 LIMITS OF REFRACTIVE THEORY AND INTRODUCTION TO GENERALIZED DIFFRACTION THEORY

When large strain gradients are present in a crystal (such as might be induced by high power, high frequency acoustic waves), the rayoptic approximation of the refractive and simple absorption models becomes increasingly invalid. The situation is quite similar to the case of optical propagation in a medium whose refractive index is varying so rapidly that diffraction effects can no longer be ignored. As Kato[23] has pointed out, the situation amounts to a breakdown of the WKBJ approximation. When the strain gradient becomes large, significant changes in the lattice parameter (and, thus, in the reciprocal vector) take place within an extinction distance. The propagation can no longer be pictured in terms of migration of the tie point along one branch of the dispersion surface. In fact, there starts to be a significant transfer of energy from one branch of the dispersion surface to the other[14]. The phenomena is usually referred to as interbranch scattering and was first observed experimentally by Lang[24].

One can understand the basic nature of interbranch scattering by recalling the form of the boundary conditions imposed in the case of x-ray diffraction. A ray encountering a highly distorted region in the crystal will behave in a manner similar to a ray encountering the boundary of the crystal with vacuum. The ray will be resolved into its diffracted and direct (forward diffracted) components. On encountering, once again, regions of perfection, tie

points will be excited on both branches of the dispersion surface, (as is always the case at an entrance surface). In the case of Borrmann transmission, this is highly important since the second branch of the dispersion surface represents a higher than normal absorption (i.e. inverse Borrmann effect). Kato[23] has also noted that rapid strain variation transverse to the ray path can also lead to diffractive effects. In this case, a region of highly distorted, (poorly diffracting) crystal acts like a diffracting aperture.

At first, one might think that ordinary diffraction by an aperture would not be significant because of the very small wavelength. We must remember, however, that the crystal diffraction process is sensitive to angular deflections on the order of seconds of arc. One second of arc would be the angular position of the first order of a single slit diffraction pattern with the slit width = 21 microns (for $\lambda = 1\text{Å}$). This can lead to what is known as a broadening of the tie point on the dispersion surface. In other words, a single tie point on the dispersion surface is no longer adequate to describe the propagation of a single input mode (unique value of ξ).

In order to deal with questions of this sort, a complete re-examination of the foundations of dynamical diffraction theory must be made. The most widely recognized method (and, thus far, the only method to be applied to practical calculations) for dealing with this situation has been proposed by Takagi[32].

In Takagi's theory, the concept of a local reciprocal lattice

vector is retained, but now its variation is explicitly included in the fourier expansion of the field quantities and the dielectric constant.

To begin with, the expansion of field quantities (analogous to Equation 2-14) is now written as a sum over all possible diffracted components $\underline{H}$:

$$\underline{A} = e^{i\omega t} \sum_{H} A_H (\underline{r}) \exp(-2\pi i \underline{K}_H \cdot \underline{r}) \qquad (2\text{-}52)$$

($\underline{A}$ = E,D,etc.)

In contrast to Equation 2-14, the fourier coefficient is now a function of position within the crystal. The primary restriction on the expansion in Equation 2-52 is that the spatial variation of $\underline{A}_H(r)$ must be slow compared to the x-ray wavelength.

The modified form of the Bloch waves (2-43) cannot be interpreted in terms of a dispersion surface.[35] In addition, there is an ambiguity in the definition of the incident field $\underline{K}_o$. In most treatments, it is taken equal in magnitude to $n|k|$ (where n is the average index of refraction). The expansion expression for the index of refraction is written as before (2-16) except that the reciprocal lattice vector $\underline{H}$ is shown to explicitly depend on position.[32] The rest of the derivation of Takagi theory parallels quite closely the development of the EVL formulation in this chapter. In the Takagi case, however, the final system of propagation equations are differential equations, as opposed to the system of algebraic equations given

in 2-27. In the two beam case, these equations have the following form.

$$\frac{\partial A_o}{\partial S_o} = -i\pi kc\ \chi_H\ A_H$$

$$\frac{\partial A_H}{\partial S_H} = -i\pi kc\ \chi_H\ A_o + i2\pi k\ \beta_H\ A_H \qquad (2\text{-}53)$$

where

S_H, S_o are unit vectors in the kinematically determined directions $\underline{K}_o$ and $\underline{K}_H$.

$c \equiv$ polarization factor

$$= \begin{cases} 1, & K_o \text{ perpendicular to plane of incidence} \\ \cos(2\theta_B), & K_o \text{ parallel to plane of incidence.} \end{cases}$$

$\beta = \frac{1}{k} \frac{\partial}{\partial S_H} (\underline{H} \cdot \underline{u})$ (Proportional to local deviation from Bragg condition.)

In order to include absorption effects, both the real and imaginary parts of the x-ray susceptibility must be included.

$$\chi = \chi' + i\chi''$$

Using this in Equation 2-53, the following set of equations is obtained:

$$\frac{\partial}{\partial S_o}(B) = \pi kc \left[-\chi' F + \chi'' G\right] \qquad (2\text{-}54a)$$

$$\frac{\partial}{\partial S_o}(A) = \pi kc \left[\chi' G + \chi'' F\right] \qquad (2\text{-}54b)$$

$$\frac{\partial}{\partial S_H}(F) = \pi kc \left[\chi'' A + \chi' B\right] - 2\pi k\beta G \qquad (2\text{-}54c)$$

$$\frac{\partial}{\partial S_H}(G) = \pi kc \left[-A\chi' + \chi'' B\right] + 2\pi k\beta F \qquad (2\text{-}54d)$$

where $\underline{D}_o = \underline{A} + i\underline{B}$

$\underline{D}_H = \underline{F} + i\underline{G}$

Once a local value of β due to distortion of the lattice has been determined, the system of Equations 2-54 can be solved to determine the complete field distribution inside the crystal. Unfortunately, Equations 2-54 have analytical solutions only in a very restricted number of special cases[13]. Most of the practical applications[33,34] thus far, (all of which involve contrast effects caused by natural crystal dislocations), have employed numerical solution of 2-54.The computer routines utilized in these numerical routines are quite large and time consuming to run.

Some useful characteristics of the "diffractive" region of x-ray propagation (large strain gradients) can, however, be obtained from Takagi theory without a complete solution of the equations. One useful property that may be determined in this way is a general criterion for the magnitude of strain gradient for which diffractive

effects become important. As in the optical regime, there is no sharp boundary between the "refractive" and "diffractive" regions.

The last two terms in Equations 2-54(c) and 2-54(d) are the perturbation terms due to departure from crystalline perfection. Authier, Balibar and Epelboin[36] have established the following criterion for neglecting these terms.

$$\frac{\partial \beta}{\partial S_o} << \frac{\pi}{2} \frac{\lambda}{(d_{ext})^2} \qquad (2\text{-}55)$$

where

d_{ext} = extinction distance.

It is a mathematical statement of the fact that for large values of $|\partial\beta/\partial S_o|$, significant departures from the Bragg condition occur within an extinction distance.

2.7 GENERAL THEORY OF X-RAY SCATTERING IN PRESENCE OF LATTICE VIBRATIONS

Historically, only the effect of thermally excited lattice vibrations on x-ray diffraction has been considered.[2,18] The effect of these vibrations on the intensity of Bragg peaks is usually lumped into a quantity known as the Debye-Waller factor. We will derive this formula, as well as the effect of monochromatic vibrations, in a way that is a slight alteration of the classical derivation. To emphasize the analogies with optical regime effects, we will couch the derivation in terms that are used in ordinary optical diffraction problems.

The problem of x-ray diffraction from lattice planes is quite similar to the optical diffraction by an array of many slits (diffraction grating). When a plane wave is incident on the structure, the location of principle maxima is given by the Bragg law. The width of diffraction peaks is proportional to the number of slits (in the x-ray case, the number of participating lattice planes). Even the finite extent of the lattice planes (which determines the exact form of the structure factor) has an analogy with the finite width of the slits which, in turn, determines the envelope function. The double crystal rocking process has its analogy in the situation of one diffraction grating being illuminated by the diffraction pattern of another identical grating. Our present concern is analogous to that of the effect of perturbations (both random and coherent) in the spacing of slits (lattice planes).

The diffracted amplitude from an array of N slits is written[26] as the following.

$$A = \sum_{j=1}^{N} e^{-iK(\underline{S}-\underline{S}_0)} \cdot \underline{R}_j \qquad (2\text{-}56)$$

where $\underline{S}$ and $\underline{S}_0$ are vectors representing incident and diffracted directions.

$\underline{R}_j$ = position jth slit

The equivalent expression for the x-ray case is written (in the kinematical approximation(2)) as

$$A = \sum_{j=1}^{N} f_j e^{-i(\underline{K}-\underline{K}_0) \cdot \underline{R}_j} \qquad (2\text{-}57)$$

where $\underline{R}_j$ = position of jth atom.

We now introduce the quantity Δ, which represents the instantaneous perturbation of the position of the jth atom (or slit).

I = diffracted intensity = AA*

$$= \sum_j f_j e^{-i(\underline{K}-\underline{K}_0)\cdot(R_j+\Delta_j)} \sum_i f_i e^{-i(\underline{K}-\underline{K}_0)\cdot(R_i+\Delta_i)}$$

$$= \left(\sum_i \sum_j f_i f_j e^{i(\underline{K}-\underline{K}_0)\cdot(\underline{R}_j-\underline{R}_i)} \right) \left\langle e^{i(\underline{K}-\underline{K}_0)\cdot(\Delta_i-\Delta_j)} \right\rangle \qquad (2\text{-}58)$$

where <> = denotes time averaging.

The term in parentheses is the normal summation leading to Bragg peaks in the x-ray case and to various diffracted orders in case of a slit array. The quantity of primary interest here is the term in time average brackets. We first rewrite the quantity:

$$\left\langle e^{i(\underline{K}-\underline{K}_o)\cdot(\Delta_i-\Delta_j)} \right\rangle = \left\langle e^{i|K|(w_i-w_j)} \right\rangle$$

where w = component of vibration or displacement along $\underline{K}-\underline{K}_o$ • and $|K| = \frac{2\pi}{\lambda}$

$$\left\langle e^{i|K|(w_i-w_j)} \right\rangle = (1+i\langle w_i-w_j\rangle - 1/2\ \langle (w_i-w_j)^2\rangle + \ldots\ldots)e^{|K|} \quad (2\text{-}59)$$

Since the atomic displacement is always small, we keep only second order terms and lower.

In the usual analysis of thermal vibrations,[2] the second term in Equation 2-59 is dropped, since it is assumed that the motion is random and, thus, no correlation exists between w_i and w_j. In order to understand the effect of correlated motion of the atomic planes, we must retain this term.

We can now rewrite Equation 2-58.

$$I = \sum_i \sum_j f_i\ f_j\ \exp(-1/2|K|^2\langle w_i^2\rangle)\ \exp(-1/2|K|^2\langle w_j^2\rangle)$$

$$x\ \exp\left[|K|\ (\underline{K}-\underline{K}_o)\cdot(R_i-R_j)\right]\ x\ \exp(-|K|\langle w_i-w_j\rangle)$$

$$+ \sum_i \sum_j f_i\ f_j\ \exp\left[i|K|\ (\underline{K}-\underline{K}_o)\cdot(R_i-R_j)\right]\ x$$

$$[\exp(|K|^2\langle w_i\ w_j\rangle)-1] \quad (2\text{-}60)$$

We identify individual terms:

$$A = \exp\left(-1/2|K|^2\langle w_i^2\rangle\right)$$

$$B = \exp\left(-1/2|K|^2\langle w_j^2\rangle\right)$$

$$C = \exp\left(-|K|\langle w_i - w_j\rangle\right)$$

The terms A and B are the familiar Debye-Waller factors which lead to a weak decrease in the Bragg peaks as the temperature (and, thus, w_i^2) is elevated. The elevation of the temperature of a diffracting crystal is, thus, one method for controlling the diffracted intensity. Typical magnitudes for this effect will be discussed in Chapter 4.

The second summation term in 2-60 is usually referred to as the diffuse scattering component. In the thermal case, when w_i and w_j are poorly correlated, there are no contributions from large values of $R_i - R_j$, and, thus, no sharp Bragg peaks. This term, thus, leads to a broad diffuse scattering. When the atomic motion becomes correlated, however, the diffuse scattering is gathered into a peak that represents the doppler shifted component of the x-rays. Only recently has it become possible to observe such a sharp peak, since in order for it to be significant[27], the monochromatic vibrations must become comparable to the average thermal excitation of the mode involved. Nevertheless, a few experiments with acoustoelectric amplification[28] have produced vibration-amplitudes of this magnitude and peaks are observed.

The next term of interest is that labeled C. In the case of

random motion it averages to zero. As the motion starts to be more coherent, the term increases. It represents a deviation from the Bragg condition. A complete analysis of the term would, of course, employ the exact displacement behavior of the vibration mode involved (pure compression, etc.) and the acoustic wavelength, as well as the autocorrelation function of the vibration. A complete analysis would also have to include multiple reflection dynamical effects. The foregoing analysis is kinematical (as is the classical derivation of the Debye-Waller factor). Only very recently has a complete theory been proposed that includes[20] all these factors. It is, however, of such complexity that it has only been applied to the special case of thermal vibrations[29].

We can,however,understand the general phenomenological behavior of term C. We first recognize that the term corresponds to a strain, i.e. it is only non zero when there is a variation in Δ as a function of position within the crystal. Thus, as we saw earlier in the chapter, only atomic motion that corresponds to a lattice strain will lead to a deviation from the Bragg condition. In addition, there must be a correlation in the atomic motions u_i and u_j. In the thermal case (when a large number of modes of the solid are excited), the atomic motion is quasi random and term C is approximately zero. When a narrow bandwidth acoustic wave is present, the correlated motion will lead to a strain and, thus, a contribution from term C.

It should be pointed out here that one theory has been proposed

to describe dynamical x-ray diffraction in the presence of monochromatic lattice vibrations[37]. Unfortunately, it deals only with the relatively trivial case of an increase in integrated intensity when an uncollimated beam falls on a vibrating crystal. In addition, it is applicable only at low frequencies where the acoustic wavelength is much greater than an extinction distance. In such a case, the vibrating crystal presents a semi continuum of 2d lattice spacings to the input beam. Therefore, the integrated intensity will increase in a manner analogous to the case of a mosaic crystal described in Chapter 1.

CHAPTER 2 REFERENCES

1. Darwin, C.G., "Theory of X-Ray Reflection", Phil. Mag. 27, p. 315 and p. 675, (1914), 43, 800, (1922).

2. Warren, B.W., X-Ray Diffraction, Wiley, (1968).

3. Brillouin, L., Wave Propagation in Periodic Structures, Dover, (1946).

4. Slater, J.C., "Interaction of Waves in Crystals", Rev. Mod. Physics, 30, (1), p. 197, (1958).

5. Jacobsson, R., "Wave Propagation in Periodically Stratified Media", Progress in Optics, vol. 5., North-Holland, (1965).

6. Ewald, P.P., "Crystal Optics and X-Ray Diffraction", Rev. Mod. Phys., 37, (1), 46, (1965).

7. von Laue, M., Rontgen Stralinterferenzen, Leipzig Verlag, (1960).

8. Kittel, C., Introduction to Solid State Physics, 3rd ed., Wiley, (1966).

9. Ziman, J., Principles of the Theory of Solids, 2nd ed., Cambridge, (1972).

10. Batterman, B.W., and Cole, H., "Dynamical Diffraction of X-rays by Perfect Crystals", Rev. Mod. Phys., 36, (3), (July 1964).

11. Zacrarisen, W.H., Theory of X-Ray Diffraction in Crystals, Dover, (1967).

12. James, R.W., Solid State Physics, vol. 15, (Ed Seitz and Turnbull), Academic Press, (1963).

13. Indenbom, V.L., and Chukhovski, F.N., "Problem of Image Formation in X-Ray Optics", Sov. Phys. Uspek., 15, (3), p. 298, (1972).

14. Hart, M., "Dynamical X-Ray Diffraction in the Strainfields of Individual Dislocations", Thesis Univ. of Bristol, (1963).

15. Penning, P., and Polder, D., "Anomalous Transmission of X-Rays in Elastically Deformed Crystals", Phillips Research Reports, 16, p. 419, (1961).

16. Wagner, E.H., "Energy Flow in Dynamical X-Ray Diffraction", Z. Phys., 154, p. 352, (1959).

17. Hart, M., and Milne, A.D., "Ray Tracing with X-Rays in Crystals", Acta. Cryst., A27, p. 430, (1971).

18. James, R.W., Optical Principles of the Diffraction of X-Rays, Cornell Univ. Press, (1946).

19. Takagi, S., "Dynamical Theory of Diffraction Applicable to Crystals with Any Kind of Small Distortion", Acta. Cryst., 15, p. 1311, (1962).

20. Afanasev, A.M., and Kohn, V.G., "Dynamical Theory of X-Ray Diffraction in Crystals with Defects", Acta. Cryst., A27, p. 421, (1971).

21. Kuriyama, M., "The Dynamical Scattering Amplitude of an Imperfect Crystal", Acta. Cryst., A28, p. 588, (1972).

22. Cole, N., and Brock, G.E., "Self-Adjustment of Internal Radiation Fields to Compensate for Linearly Varying 2d Spacing in X-Ray Diffraction", Phys. Rev., 116, (4), (1958).

23. Kato, N., X-Ray Diffraction, (Ed. L. Azaroff), McGraw-Hill, (1974).

24. Lang, A., Z. Naturfor., "X-Ray Topographic Determination of the Sense of a Pure Screw Dislocation", 20, p. 636, (1965).

25. Tucker, I.W., and Rampton, V.W., Microwave Ultrasonics in Solid State Physics, North-Holland, (1972).

26. Stone, J.M., Radiation and Optics, McGraw-Hill, (1963).

27. Carlson, D.G., et al., Appl Phys. Lett., 18, (8), p. 330, (1971).

28. LeRoux, S.D., et al., "Effect of Acoustoelectric Phonons on Anomalous Transmission of X-Rays", Phys. Rev. Lett.,37, (16), p. 1056, (1976).

29. Afanasev, A.M., and Kagen, Y., "The Role of Lattice Vibrations in Dynamical Theory of X-Rays", Acta. Cryst., A24, p. 163, (1967).

30. Bonse, V., Z. Phys., 177, p. 385 and p. 529, (1964).

31. Gerward, L., "Energy Flow of X-Rays in Silicon Single Crystals", Acta. Cryst., A27, p. 18, (1971).

32. Takagi, S., "A Dynamical Theory of Diffraction for a Distorted Crystal", J. of Phys. Soc. Jap., 26, (5), p. 1239, (1969).

33. Authier, A., "Contrast of Dislocation Images in X-Ray Transmission Topography", Advances in X-Ray Analysis, 10, (46), p. 9, (1967).

34. Chukovski, F.N., Shtolberg, A.A., "On the Dynamical Theory of X-Ray Images in Real Crystals", Phys. Stat., Sol. 41, p. 815, (1970).

35. Authier, A., "Ewald Waves in Theory and Experiment", in Advances in Structure Research by Diffraction, vol. 3, (Ed. Brill, H., and Mason, M.), p. 24, Pergamon, (1970).

36. Authier, A., Balibar, F., and Epelboin, Y., "Theoretical and Experimental Study of Interbranch Scattering Near a Dislocation Line in X-Ray Topography", Phys. Stat. Sol., 44, p. 225, (1970).

37. Kohler R,Mohling W, Peibst H.,"Intensity Relations in Laue Case Reflections of Perfect Crystals Containing Nearly Monochromatic Lattice Vibrations " ,Phys.Stat. Sol.41 p.75 (1970).

CHAPTER 3

EXPERIMENT AND COMPARISON WITH THEORY

3.1 Introduction

3.2 Single crystal Borrmann experiments

3.2-1 Description of experimental equipment and techniques

3.2-2 Demonstration of acoustic interruption of x-ray diffraction

3.2-3 Visualization of acoustic standing wave patterns

3.2-4 Measurements of acoustically induced high frequency strain

3.2-5 Quantitative comparisons between theory and experiment for acoustic modulation of Borrmann transmission

3.3 Experiments with x-ray interferometers

3.4 X-ray topography of acoustic fields in solids

3.5 X-ray modulation experiments

3.1 INTRODUCTION

In this chapter experiments are described in which modulation and shuttering of x-rays has been demonstrated. This represents the first use of Borrmann transmission or the techniques of x-ray interferometry for the modulation and control of x-ray propagation [1]. The emphasis in the experiments has, however, been on obtaining a basic understanding of the interaction of x-rays and acoustic waves in crystals.

The most extensive measurements have been made in the single crystal Borrmann configuration. Experiments have also been performed with a two crystal x-ray interferometer. The theoretical analyses developed in Chapter 2 are applied to the experimental situations in order to predict such characteristics as contrast ratio (or modulation depth) and total transmitted integrated intensity. The comparison between the theoretically predicted and experimentally measured parameters agree to within experimental error.

The converse application, that of x-ray diffraction investigation of acoustic field properties has also been pursued experimentally. A detailed description is given of x-ray topographic mapping of acoustic standing waves. Quantitative measurements of some acoustic field properties are made using x-ray topography.

The topographic method is also applied to the confirmation of certain aspects of the theoretical picture of acoustic Borrmann interruption.

An important feature of our work is that the various descriptions ("diffractive", "refractive", etc.) of the x-ray propagation in distorted crystals can be directly investigated by systematically changing the acoustic frequency and amplitude. The diffracted intensity distribution predicted by the various models are of great interest when using x-rays to study intrinsic defects in solids.

The purpose of the present study was to establish the orders of magnitude that would be involved in producing practical x-ray modulating, shuttering and control devices.

3.2 SINGLE CRYSTAL BORRMANN EXPERIMENTS

3.2-1 DESCRIPTION OF EXPERIMENTAL EQUIPMENT AND TECHNIQUES

Borrmann or anomalous transmission of x-rays (in the Laue geometry) is particularly sensitive to perturbations in the crystal lattice. In the following experiments the perturbations were produced by acoustic waves. The acoustic waves were excited by bonding a piezoelectric transducer to the edge of the crystal, as indicated in Fig. 3-1. As described in Chapter 2, the perturbed behavior of the x-ray wavefield in the crystal is particularly dependent on the gradient of strain. This was controlled by changing both the strain amplitude and the acoustic frequency. Experiments were performed at 5, 10, 20 and 60 MhZ.

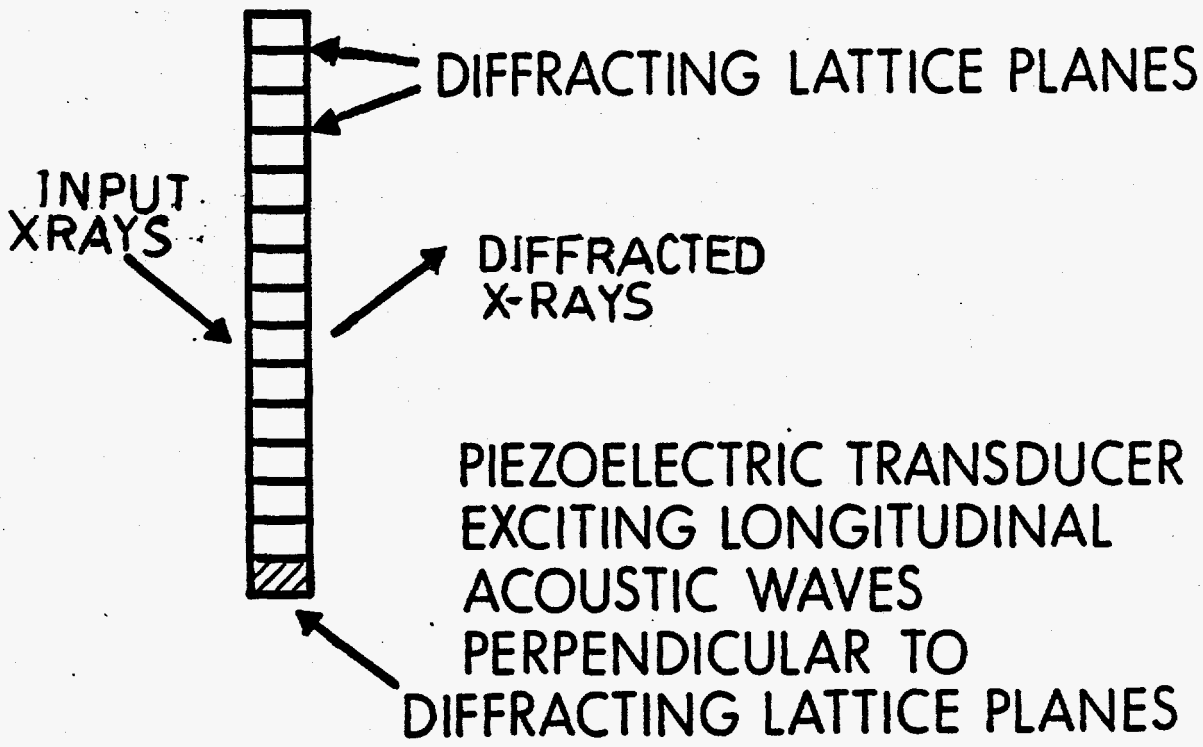

Figure 3-1 . Configuration used for the excitation of acoustic waves in Borrmann interruption experiments.

Most of the crystal experiments described in this chapter were performed with highly perfect samples of Czolchalski grown silicon. For all Borrmann work, the(220)planes of the diamond cubic silicon structure were used. The silicon samples were oriented using the Laue back reflection technique. [2] Using this technique, it was possible to orient the lattice planes with respect to an external (cut)face to about 1^{o}.

Once the samples were oriented, they were cut on a high speed crystal wafering machine. This produced a much smoother and more accurately cut surface than either a low speed saw or string abrasion saw.

The x-ray entrance and exit faces of the crystal were fine ground and then polished with a very fine optical polish. The samples were then acid polished to remove surface damage left by the grinding and polishing processes. At first, the well known CP4 chemical polish [3] was used, but it was later found that a simple solution of three parts nitric acid to one part hydrofluoric acid produced a better quality surface. The literature on work with the Borrmann effect [3,4] indicated that acid polishing was definitely necessary because mechanical polishing damage could extend up to 25 microns below the surface. Tests showed, however, that only about 15% difference in x-ray transmission was present between two initially identical samples where only one was acid polished prior to testing.

The crystal surface on which the acoustic transducer was bonded and the opposite face (where acoustic reflection occurred) were polished

with very fine optical polish. These faces were made parallel to tolerances on the order of 10 arc seconds. These surfaces were specified so that the lack of parallelism and surface roughness were always less than 1/10 the acoustic wavelength for that particular crystal.

Two types of acoustic transducer were used, lead zirconate titanate (PZT) and lithium niobate, both cut for a primary thickness expansion vibration mode. PZT is available with hard silver coatings for electrodes and thus was convenient to use at 5 and 10 MhZ. Because of its lower acoustic loss at high frequencies, the lithium niobate was used at 20 and 60 MhZ. Electrodes were applied to the lithium niobate by evaporating indium onto the surfaces.

Several types of bonding were investigated. Indium itself can be used by evaporating onto the active surface. The transducer is then pressed against the crystal and held firmly in place while the crystal is heated to slightly above the melting point of indium(156^{o}) The bond that is formed is not very rugged and tends to rupture easily. The best general purpose bond was found to be a special low viscosity epoxy. The epoxy (ISO-Chem. 212)forms a thin,strong bond with acceptable acoustic losses when cured for about 3 hours at 130^{o}C.

At low frequencies (5, 10 MhZ), electrical connections were made with silver epoxy, as shown in Fig. 3.2(a) At higher frequencies, the silver epoxy tends to be somewhat lossy and the special connection shown in Fig. 3.2(b) was used.

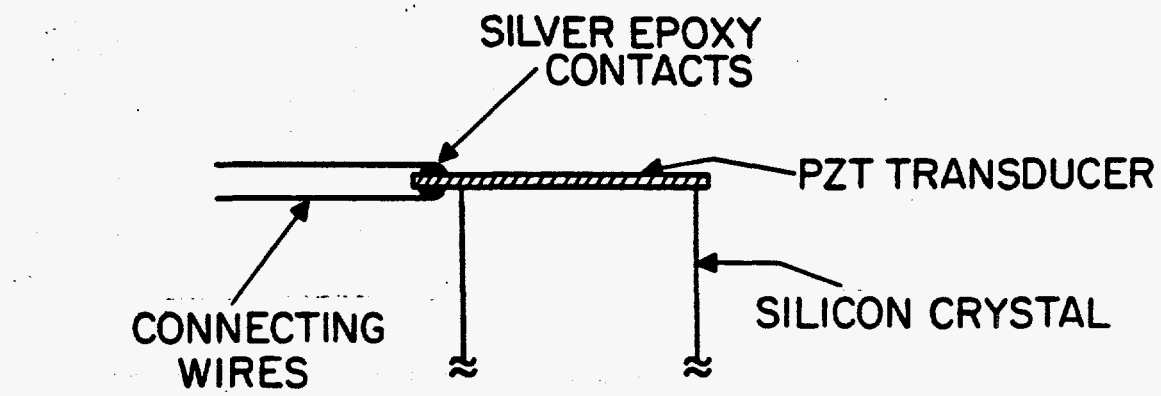

(a) LOW FREQUENCY TRANSDUCER CONNECTION

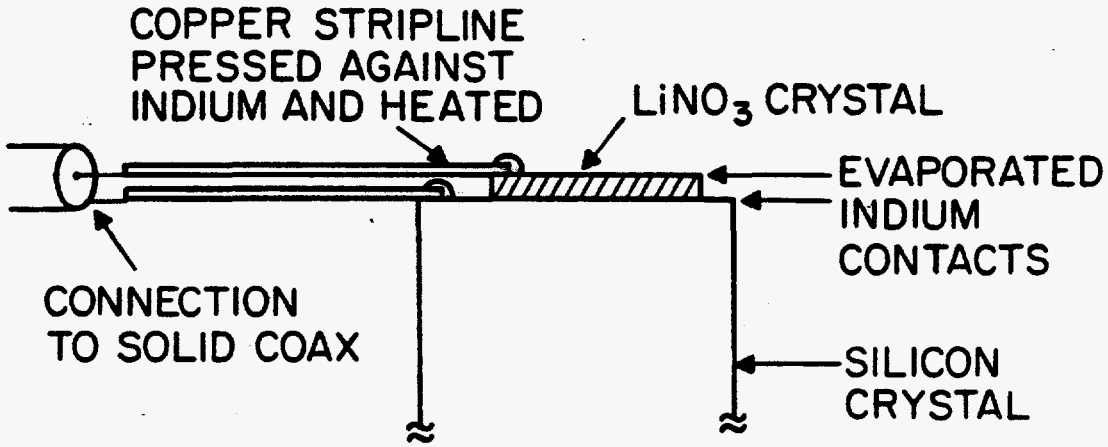

(b) HIGH FREQUENCY TRANSDUCER CONNECTION

Figure 3-2. Procedures for electrical connection to to acoustic transducers.

3.2-2 DEMONSTRATION OF ACOUSTIC INTERRUPTION OF X-RAY DIFFRACTION

The initial experiment that was performed to demonstrate acoustic interruption is illustrated in Fig. 3-3.

The transducer excites bulk longitudinal acoustic waves perpendicular to the(220)diffracting planes. The input beam came from an effectively broad x-ray source (spot focus on the x-ray tube) so that the transmission was an integrated intensity.

One possible criticism of this experiment is that reduction in transmitted x-rays may be due to simple gross motion of the crystal wavering in and out of the Bragg angle.This question was very carefully investigated. First, the experimental configuration shown in Fig. 3-3 does not have a great sensitivity to angular misalignment. The input beam is only crudely collimated and small vibrations of the crystal will only cause a different part of the crystal to diffract. The entrance slits on the detector are very wide (≈1cm) so that all of the x-ray flux would still be collected. The macroscopic motion of the crystal was investigated by taking holographic interferograms with power on the transducer. These revealed that there was no out of plane motion (perpendicular to the entrance face) greater than one micron. Overall motion of the crystal was thus negligible.

3.2-3 VISUALIZATION OF ACOUSTIC STANDING WAVE PATTERNS

The acoustic wave in the crystal has both standing and travelling wave components.The static portion of the pattern of absorption in the strained crystal can be readily visualized by taking a Borrmann topograph of the crystal. There are many types of x-ray topography [6] through

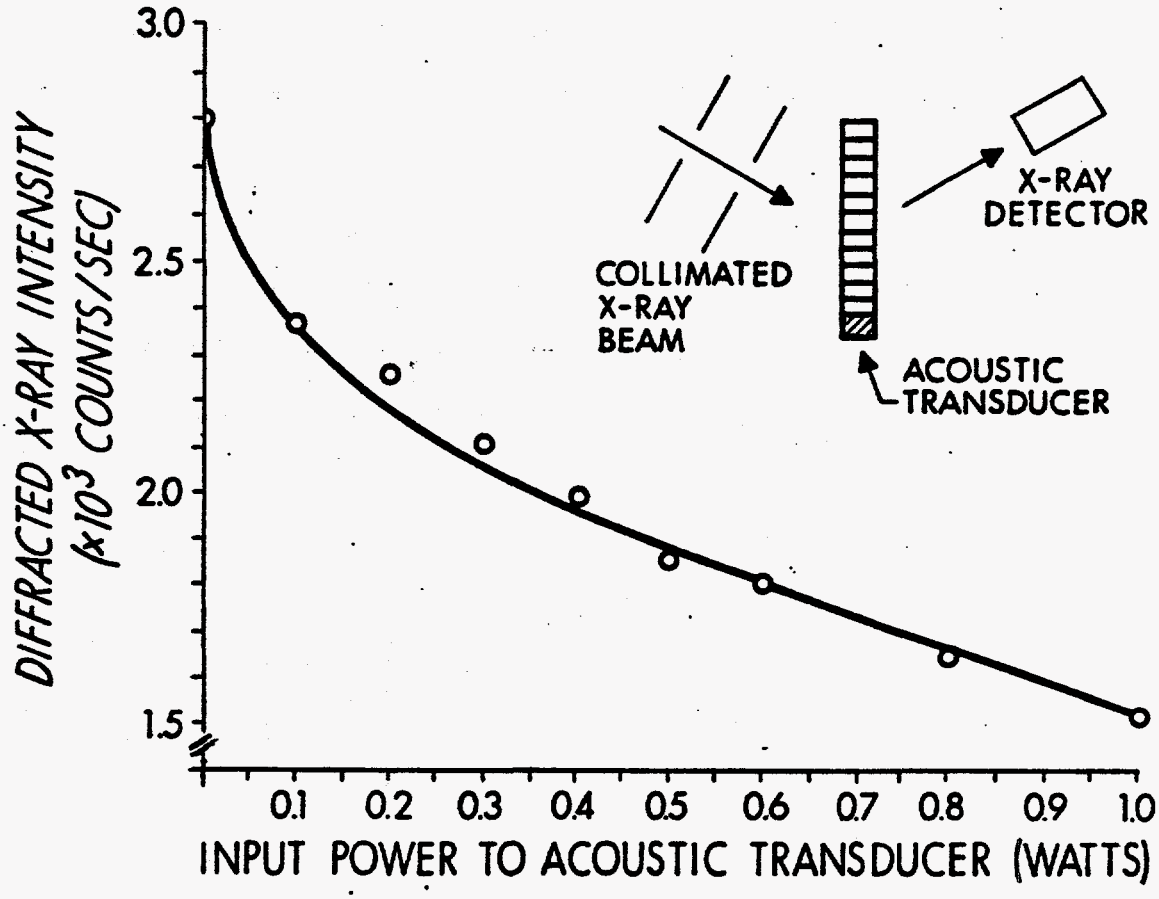

Figure 3-3. Acoustic interruption of Borrmann x-ray transmission through a silicon crystal.

which an image-like visualization of the internal structure of a crystal may be obtained.

In forming a Borrmann topograph, a distributed source of x-rays is used. In most of the present experiments, a line source of x-rays was used. The configuration for taking Borrmann topographs is given in Fig. 3-4 Each point on the source will emit a ray that satisfies Bragg's law at the crystal. For ray directions other than those in the plane of incidence, the beam is freely diverging.

A type of x-ray shadowgraph (or projection) of the crystal is thus formed. When defect structure (such as dislocations) is present in the crystal, the Borrmann transmission is disrupted and absorption occurs. A shadow-like image of the defect region is thus formed. The topograph can also be used to visualize the acoustic standing wave pattern. An extensive experimental program was undertaken with the purpose of producing better resolution and definition in Borrmann topographs.

The excitation potential of the x-ray tube must be carefully selected. The continuum radiation surrounding the Kα line is also diffracted and produces a background on the topograph. One would thus like to choose an x-ray tube potential that gives the maximum ratio of Kα line radiation to continuum. This requirement must, however, be balanced against the need to reduce background due to scattering and fluorescence (crystal and mount). When the excitation potential is quite high, hard components of the continuum can penetrate the crystal causing a background and loss of resolution.

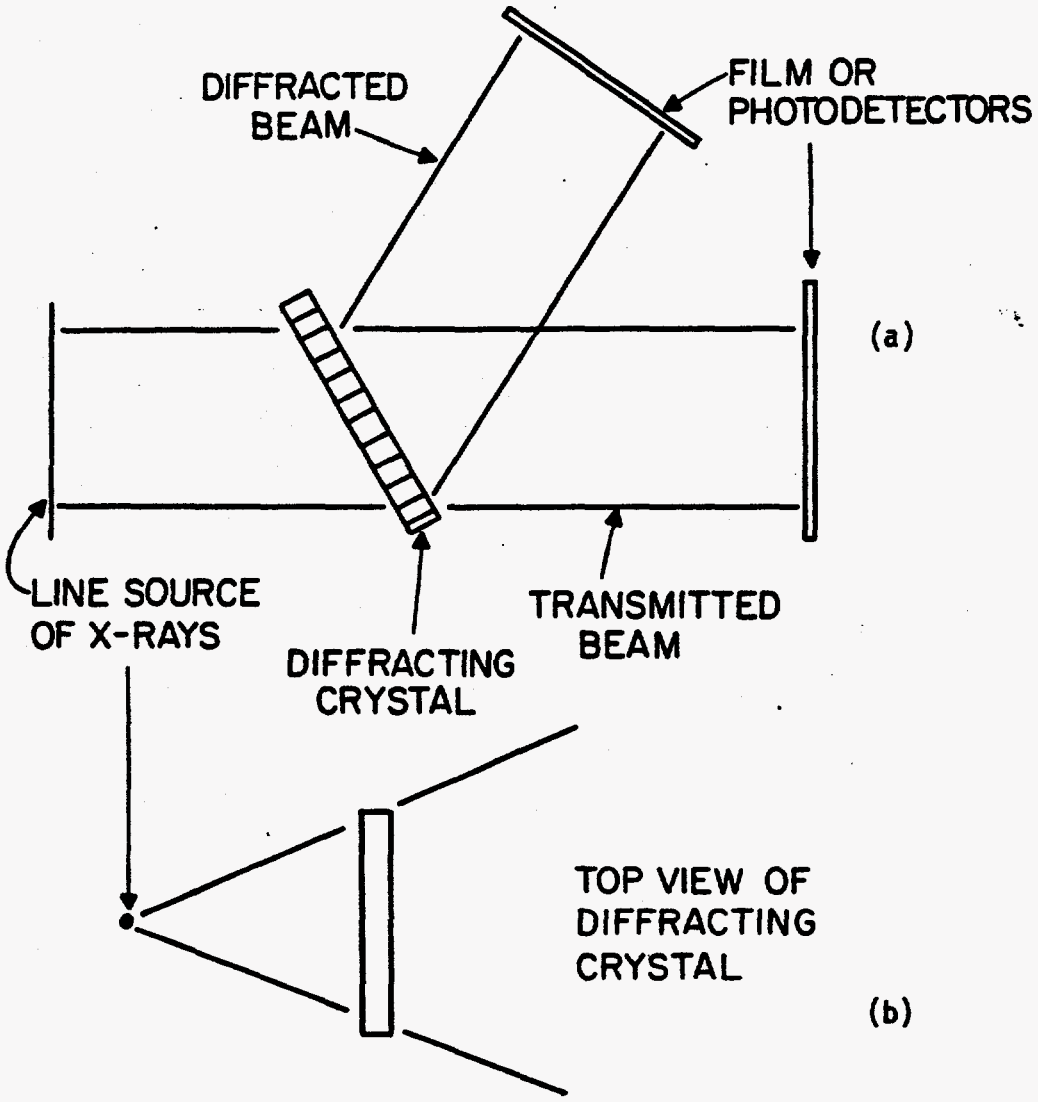

Figure 3-4 . Geometry used in obtaining Borrmann x-ray topographs. (a) side view
(b) top view.

In addition to considerations like those in the previous paragraph, there is one fundamental limitation to Borrmann topograph resolution. At each point on the entrance surface of the crystal, a cone of rays centered around the Bragg angle is diffracted. As was shown in Chapter 2, the energy flow for this cone of rays spreads out into the "Borrmann fan".The resolution is,thus,no better than the total spread at the exit face of the crystal. The shadow or projection-like image of a small defect localized near the entrance surface of the crystal will thus be smeared out by this divergence. The disturbance caused by bulk longitudinal waves extends all the way across the crystal from entrance to exit face.Thus, when the acoustic wavelength becomes comparable to or smaller than the Borrmann fan angle,the contributions to high contrast from regions near the entrance face are ultimately smeared out. When the acoustic wavelength becomes very small, the diffracted intensity distribution becomes uniform (contrast washes out completely). There remains an attenuation of the overall total diffracted flux (integrated intensity).

Figure 3-5 shows an x-ray topograph of a 10 MhZ acoustic standing wave pattern in a silicon single crystal. The acoustic wave is pure longitudinal(in the 220 direction)and has a wavelength of about .9mm .

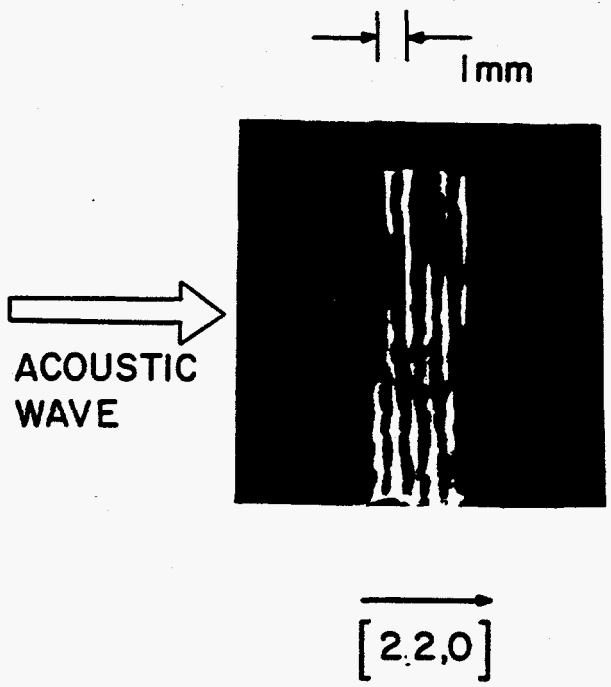

Figure 3-5 Borrmann x-ray topograph showing an acoustic standing wave pattern in a low dislocation density silicon crystal.

3.2-4 MEASUREMENTS OF ACOUSTICALLY INDUCED HIGH FREQUENCY STRAIN

In order to quantitatively understand the x-ray interruption phenomena described in previous sections, measurements of the acoustically induced strain levels must be made.

Measurement of absolute acoustic strain levels has always been a difficult task in physical ultrasonics [7]. For the present study,

measurement of the time average strain level, as well as the standing wave ratio, was desired. Ideally, one would like a direct measurement technique that does not depend on information about acoustical and electrical impedance matching. Acousto-optic diffraction offers such a possibility if the elasto-optic coefficient for the materials of interest are known. Silicon is transparent to both CO_2 (10.6μ) and YAG (1.06μ) laser wavelengths. The elasto-optic coefficient for the (220) planes in Si has not been accurately measured. Using information on structurally similar materials like Ge, GaAS, and InSb, one can probably estimate the value of the coefficient to within 20%. The acousto-optic effects are, unfortunately, too weak (in silicon, the primary material of interest) to be of much value in the present study. As an alternative to direct acousto-optic measurements, three other techniques have been employed.

(i) Replicas of the silicon crystals are constructed out of dense flint glass. Dense flint has approximately the same acoustic impedance as silicon, so that the acoustic matching characteristics of the two materials should be nearly identical. The dense flint has a large elasto-optic coefficient and is transparent to the convenient HeNe 6328Å line. Acousto-optic measurements of strain are easily obtained with dense flint.

Acousto-optic measurements of strain in dense flint glass samples were made at 5,10,20 and 60MhZ. The samples were cut to the same geometrical dimensions as the silicon crystals.

Theoretical developments of acousto-optic diffraction [9] show that the time average intensity of light diffracted into the first order is given by:

$$I_1 = \sum_r J_r^2(v') J_{r-1}^2(v'/a) \qquad (3\text{-}1)$$

$$\text{where } v' = \frac{\pi n^3 p}{2} \frac{L}{\lambda} \varepsilon \qquad (3\text{-}2)$$

with L = thickness of material traversed by light wave (perpendicular to acoustic propagation vector.)

λ = optical wavelength

p = elasto-optic coefficient

ε = time average strain

a = acoustic standing wave ratio.

A pure standing wave has a = 1 and a pure travelling wave has a = ∞.

Cook and Hiedemann [9] have made convenient plots of the relationship given in (3-1). Optical measurement of the SWR is made by comparing the ratio of light intensity modulated at twice the acoustic frequency to the unmodulated light. This measurement can then be compared to SWR determinations made by the acoustic pulse echo method.

(ii) Strain Gauges micro-miniature strain gauges are bonded to the surface of both the silicon crystals and their dense flint glass replicas. These gauges are connected to an A-C bridge that senses

only the deviation from equilbrium resistance. (The actual RF time varying strain cannot be measured directly because of the pickup of RF radiated by the transducer.) The bridge circuit filters out the RF pickup and gives a signal proportional to the time average strain. An elaborate test procedure was set up to ensure that RF pickup did not affect the time average strain measurement.

(iii) Bond Transmission A method was devised for measuring the relative value of the transmission coefficient of the bond between the transducer and the crystal (and the relative SWR of the crystal transducer system). The basic principle of the method is illustrated in Fig. 3-6 . A second transducer was bonded to the face opposite the usual power driving transducer (#1). Instead of using the usual epoxy, the second transducer was attached with phenyl salicylate. This material melts at low temperature ($80^{o}C$) and recrystallizes at room temperature forming an acoustically efficient bond. The advantage of this method is that the latter transducer can easily be removed without distrubing the other transducer (or the quality of the face to which the second transducer is attached). We let t_1 = the transmission coefficient of the first bond and t_2 for the second. If an acoustic pulse is applied to the first transducer, a series of pulses will be observed at the oscilloscope outputs S_1 and S_2. A pulse traversing a single pass and observed at S_2 suffers an attenuation $t_1\ t_2$. A double pass observed at S_1 is attenuated by $t_1^{\,2}\ (1-t_2)$. With these two

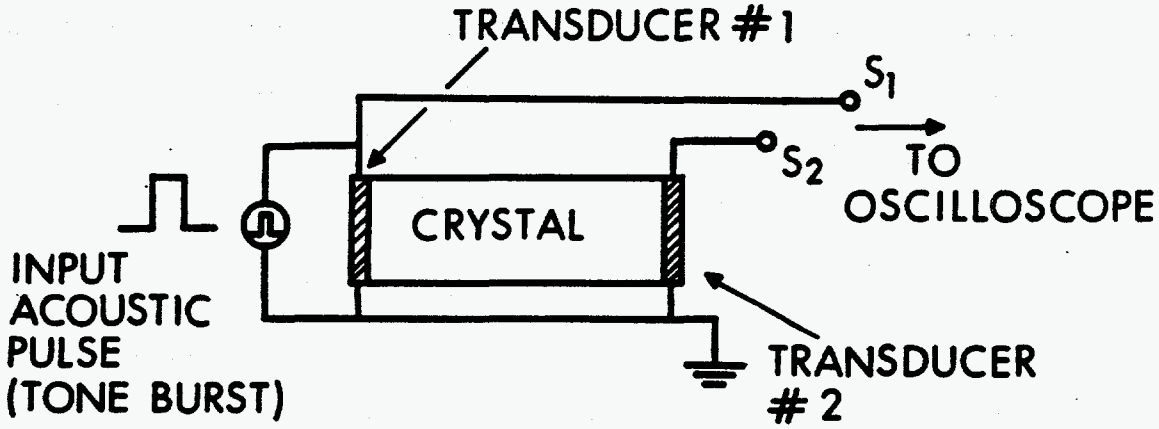

(a)

SINGLE PASS: $t_1 t_2$

DOUBLE PASS: $t_1^2(1-t_2)$

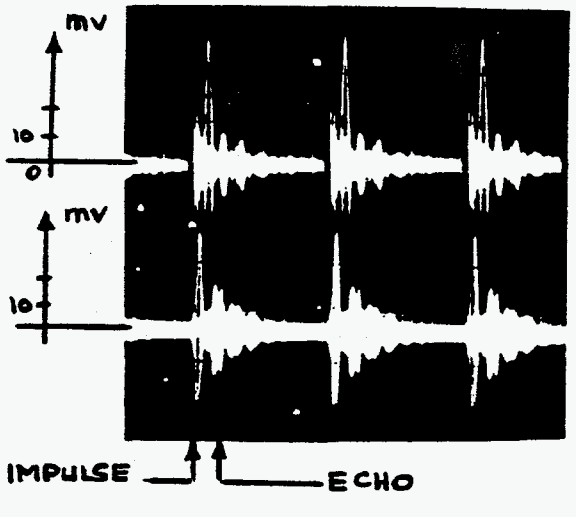

DOUBLE PASS SIGNAL (S_1) FROM TRANSDUCER #1 (EPOXY BONDED)

SINGLE PASS SIGNAL (S_2) FROM TRANSDUCER #2 (PHENYL SALICILATE BONDED)

(b)

Figure 3-6. Configuration used for experimental measurements of acoustic bond transmissions. (a) schematic diagram (b) typical signals

relationships, the value of the transmission for both bonds can be solved for.

In this study, only the relative values of bond transmission between the crystal samples and the flint replicas were desired. For this application, the double pass measurement alone was found to be adequate (while assuming that reflection from the second face with no transducer bonded was = 100%). The two transducer technique seems to be, however, a useful new method [8] for the measurement of bond transmissions that could also be applied to absolute measurements.

By comparing measurements made with all three methods (acousto-optic, strain gauge, and bond transmission), a quantitative picture of the acoustic field inside the crystals or glass replicas can be obtained.

Since different combinations of the three techniques were used at the various frequencies, the descriptions of the actual measurements will be categorized by frequency.

5MhZ At 5MhZ strain measurements were made using each of the three techniques(strain gauge , replicas,and bond transmission).

Several samples of dense flint and silicon were prepared and bonded to 5 MhZ transducers. Optical measurements of the strain in the dense flint samples were performed as described above. Strain gauges were then bonded to both the flint glass and silicon samples. Optical measurements on the glass samples were repeated after bonding the strain gauges and it was determined that the application of the gauge had not altered the acoustic pattern. Optical measurements of the SWR were also made. Knowing the SWR, the position of the strain gauge within the standing pattern is taken into account in correcting the strain gauge reading. Fig. 3-7 gives a plot which compares the total time average strain measurement as made by acousto-optic diffraction with the strain gauge measurements. The data in Fig. 3-7 was taken at only one of several resonant frequencies (around 5 MHz) and for one of two samples of dense flint glass.

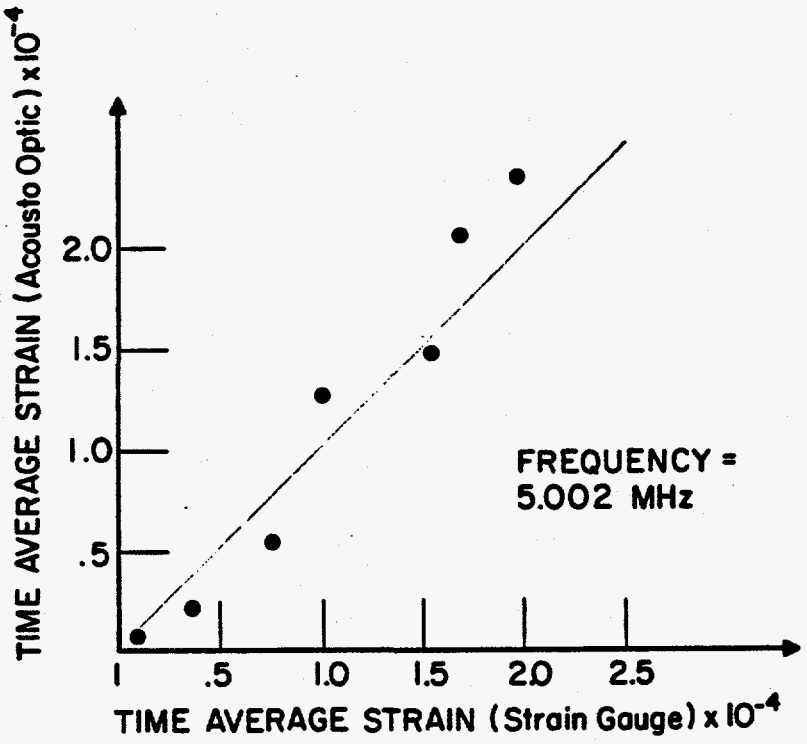

Figure 3-7 . Comparison of measurements of time average strain as made by strain gauges and by acousto-optic light diffraction.

Strain gauge measurements were also made on the silicon crystals. The results for one of the crystals is presented in Table 3-1. The quantity in the final column is the ratio of the strains in the two materials (silicon and glass) corrected for individual sample differences in bond transmission.

Table 3-1. Strain gauge measurements

Input Power (electrical) (watts)	Strain in Dense Flint Glass	Strain in Silicon	Ratio of Silicon and Glass Strains Corrected for Bond Transmission
.10	7.5×10^{-5}	$.68 \times 10^{-5}$	7.8
.20	1×10^{-4}	1.3×10^{-5}	7.7
.30	1.4×10^{-4}	2.0×10^{-5}	7.0
.40	1.6×10^{-4}	3.5×10^{-5}	6.5

The ratio is close to the value one would predict from the differences in elastic constants between the glass and silicon (6.5).

The strain gauge measurements were thus shown to give accurate results when compared to the well established acousto-optic technique. Since the strain gauge permitted a direct measurement of the acoustically induced strain in silicon, it was used as the primary standard at 5MhZ.

The position of the strain gauge within the standing wave pattern was accurately measured by a travelling microscope. This was also confirmed by taking a Borrmann topograph with the gauge in view. This is shown in Fig. 3-8. The grill of the gauge, being very thin, does not show well in the photograph, but the solder dots and connecting wires are clearly visible.

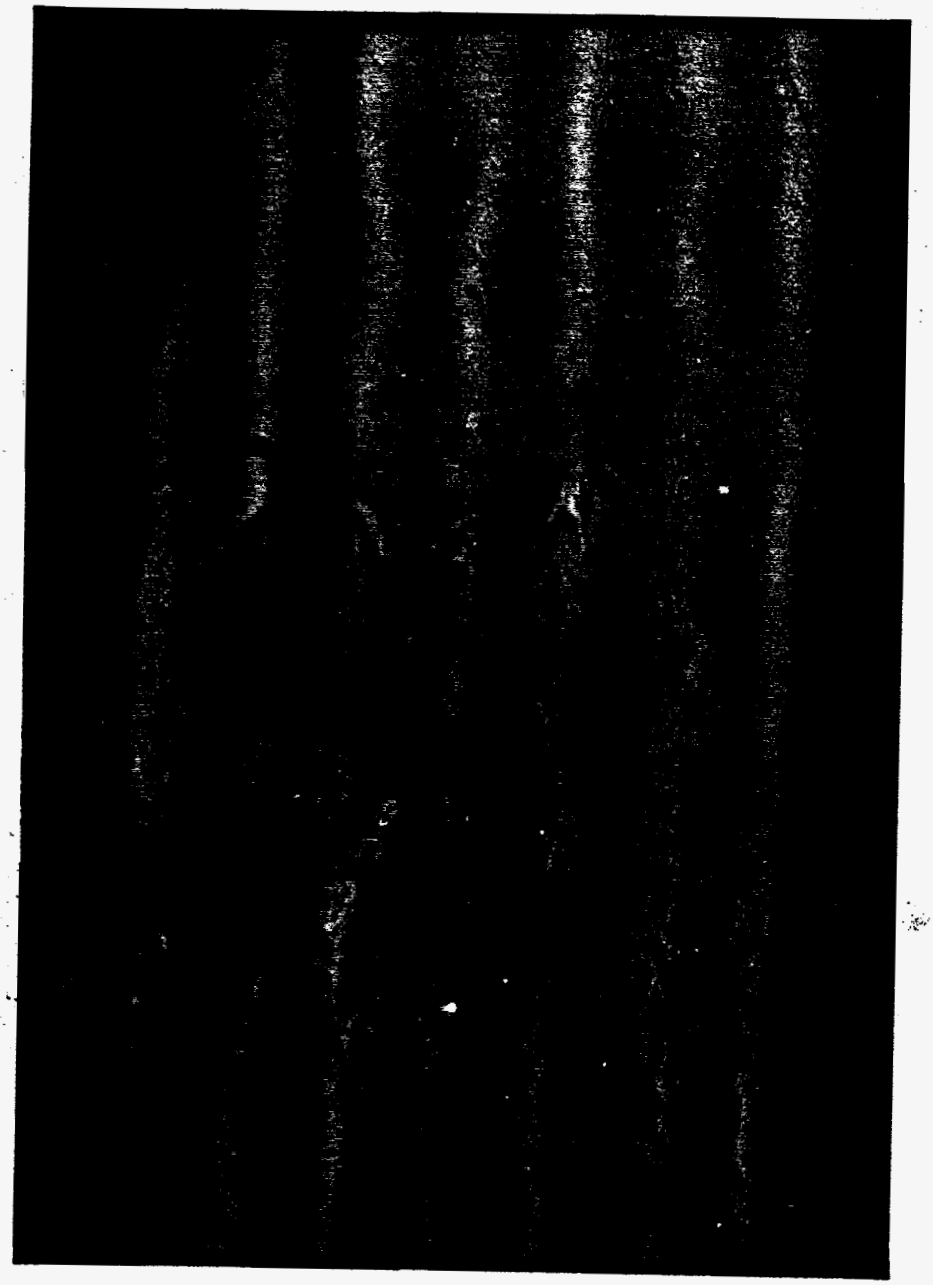

Figure 3-8 . Borrmann x-ray topograph of a silicon crystal with a bonded strain gauge in the field of view.

Such photos also confirm the qualitative nature of the acoustic Borrmann interruption process. The strain gauge location provides an accurate reference with respect to the standing wave pattern and the edge of the crystal. The regions of low x-ray transmission are found to be at nodes of the standing wave pattern.

10, 20, 60 MhZ

At 10 MhZ the acoustic wavelength in flint is too small for accurate strain gauge measurements to be made. The acoustic wavelength in silicon is somewhat larger but accurate positioning of the gauge is still difficult. For higher frequency acoustic strains, the acousto-optic measurements on dense flint were thus used as the standard. The silicon strain was then determined using the relative bond transmission (silicon vs. dense flint) measurements.

3.2-5 QUANTITATIVE COMPARISONS BETWEEN THEORY AND EXPERIMENT FOR ACOUSTIC MODULATION OF BORRMANN TRANSMISSION

In order to make a quantitative evaluation of the contrast ratio in the diffracted x-ray fringe pattern and of the reduction in total integrated intensity, one could take densitometer traces of the topographs such as that in Fig. 3-8. It proved somewhat difficult, however, to obtain accurate results this way because of uncertainties in film calibration.

A more accurate method would be to traverse the crystal parallel to the diffraction vector (reciprocal lattice vector) while using a collimated input beam. Devices for producing such a traverse while

accurately maintaining the Bragg angle alignment are used in topograph cameras of the Lang type. Such a device was not available for the present study, so a slightly different method of scanning was devised. The method is illustrated in Fig. 3-9.

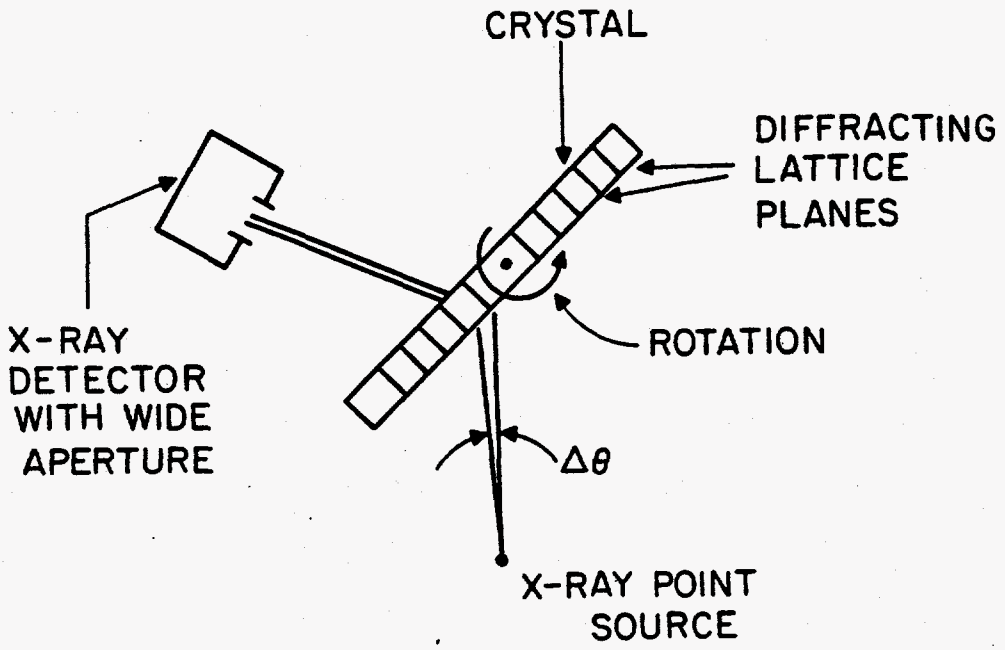

$$\frac{\Delta\theta}{\theta} \simeq \frac{\Delta\lambda}{\lambda}$$

Figure 3-9 . Configuration used to obtain x-ray scans of acoustic standing wave patterns in crystals.

Essentially uncollimated x-ray radiation (3^0 divergence) is incident on the crystal from a point source. The crystal is then rotated. At any instant of time, the cone of rays accepted by the crystal has a divergence of about 10^{-3} radians, as governed by the spectral width of the source (usually CuK_α x-ray line). The region intercepted at the crystal by this cone is narrow compared to the acoustic wavelength. As the crystal is scanned, the narrow x-ray beam will traverse the acoustic standing wave pattern. Examples of such scans are given in Fig. 3-10. As mentioned before, there are two important parameters associated with such curves.

(a) CONTRAST RATIO, defined as the average ratio of maxima to minima in the transmitted fringe pattern.

(b) INTEGRATED INTENSITY - a measure of the total x-ray transmission during the scan as indicated by the area under the curve. The integrated intensity was evaluated in two different ways. The total photon count during the scan was often taken. This required anticipating the shape of the curve and where to cut off the count. Integrated intensity measurements were also taken by graphically and numerically integrating the finished curve using a programable calculator and curve digitizer. The latter proved to be the more reliable and accurate method.

Figures 3-11 and 3-12 give plots of measured contrast ratio vs. rms strain level for two silicon crystals with 5 MhZ PZT transducers exciting the acoustic waves. Also included are the contrast ratios as predicted by the simple absorption theory and the refractive (Penning and Polder) theory.

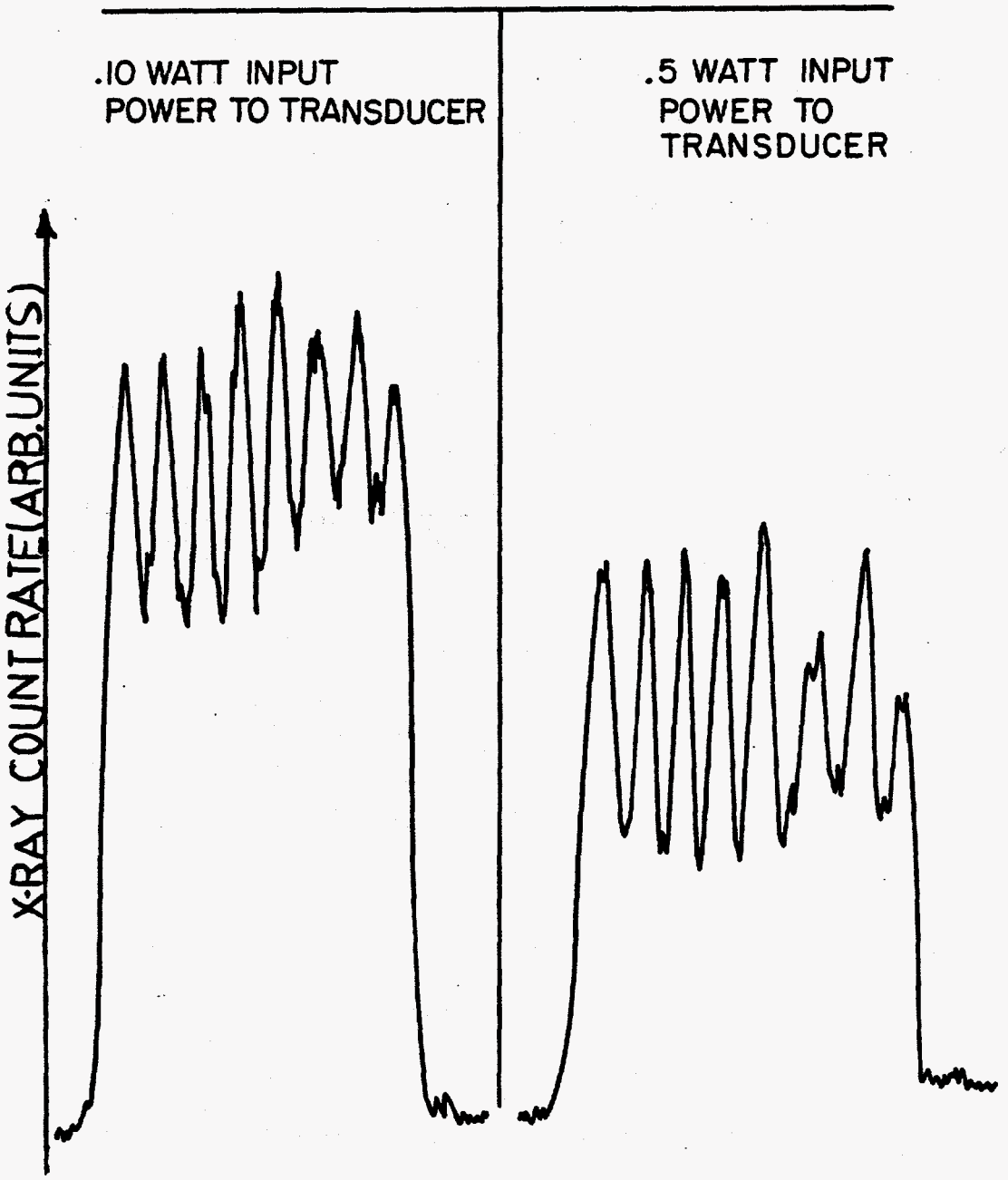

Figure 3-10. X-ray scans of 5 MhZ acoustic standing wave patterns in a silicon crystal.

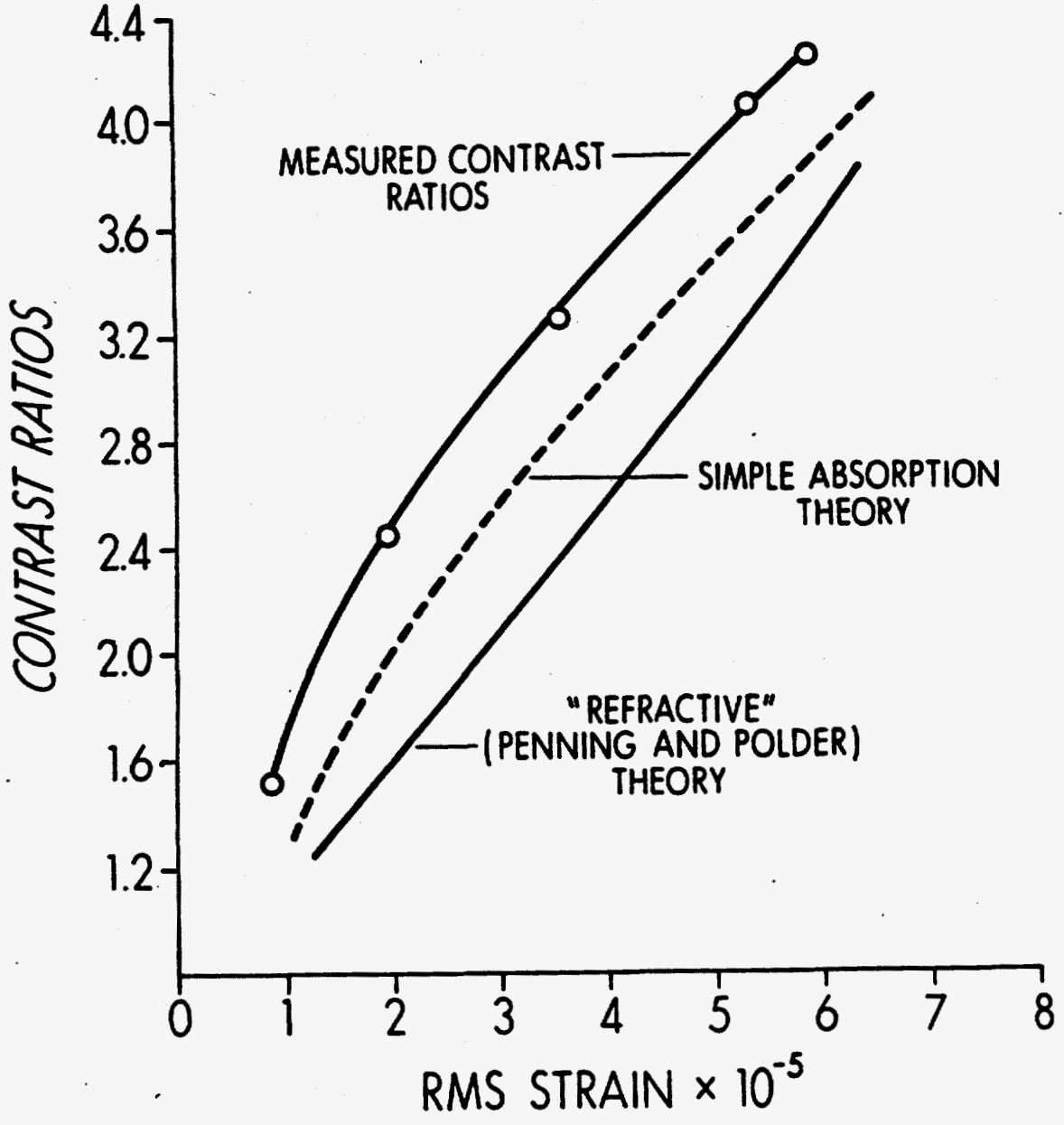

Figure 3-11. Comparison between measured and theoretically predicted contrast ratios in x-ray scans of acoustic standing wave (5MhZ) in silicon crystal #1 (CuK_{α} x-rays).

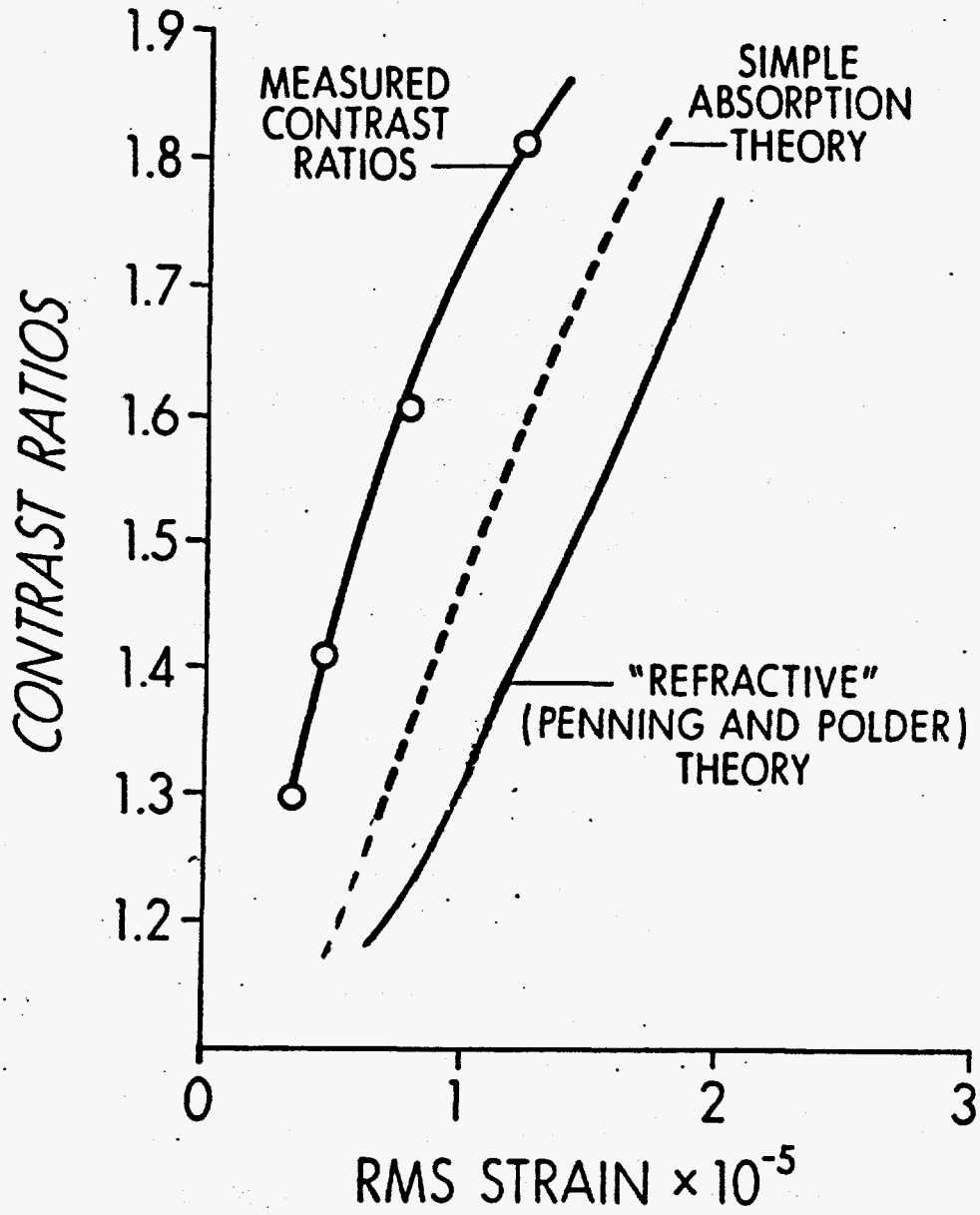

Figure 3-12. Comparison between measured and theoretically predicted contrast ratios in x-ray scan of acoustic standing waves (5MhZ) in silicon crystal #2 (CuK_α x-rays).

The theoretical and experimental values for integrated intensities are plotted in Figures 3-13 and 3-14.Integrated intensities are calculated by summing the contributions (for all rays in the Borrmann fan) from all entrance points. The agreement between theory and experiment for these two particular parameters is within the expected error in the strain measurements of $\pm .5 \times 10^{-5}$. There is also, however, a systematic trend of higher measured than theoretically predicted values for both contrast ratio and integrated intensity. This might indicate that the measurements of strain were consistently low.

The theories themselves are approximate. There are a limited number of rays traced for each point on the entrance surface of the crystal.For a pure longitudinal (sinusoidal) acoustic wave one would expect a smooth sinusoidal x-ray intensity distribution (at the exit face).The scatter(around a sine wave distribution) in intensity for various rays traced indicate that the limited number of rays could cause as much as 10% error in the calculated values for contrast ratio.

In terms of potential applications the contrast ratio would be of interest in such areas as acoustic mapping, while integrated intensity would relate to modulation and shuttering. For example , in a modulation application, one would want to minimize the insertion loss while at the same time keeping a high modulation depth.

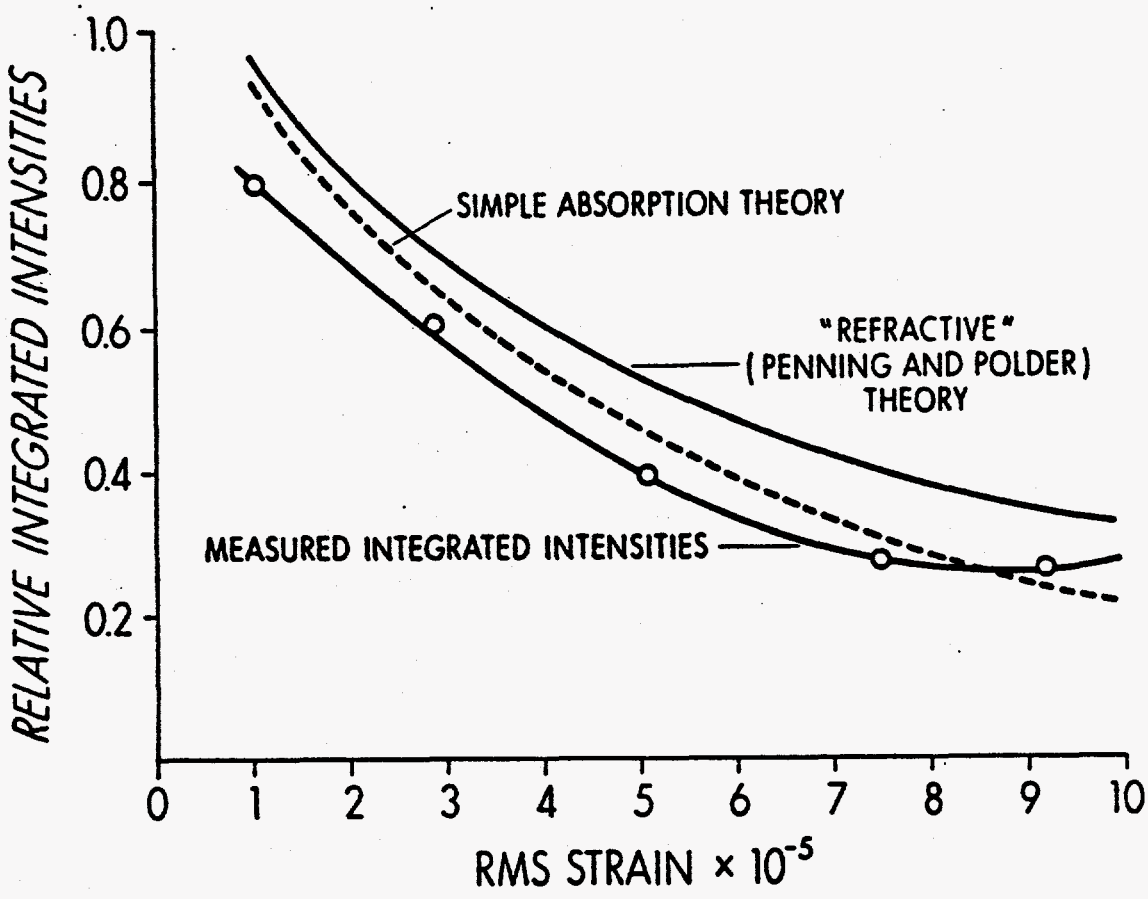

Figure 3-13. Comparison of theoretical and experimental values for integrated intensities in x-ray scans of acoustically perturbed silicon crystal #1 (at 5MhZ).

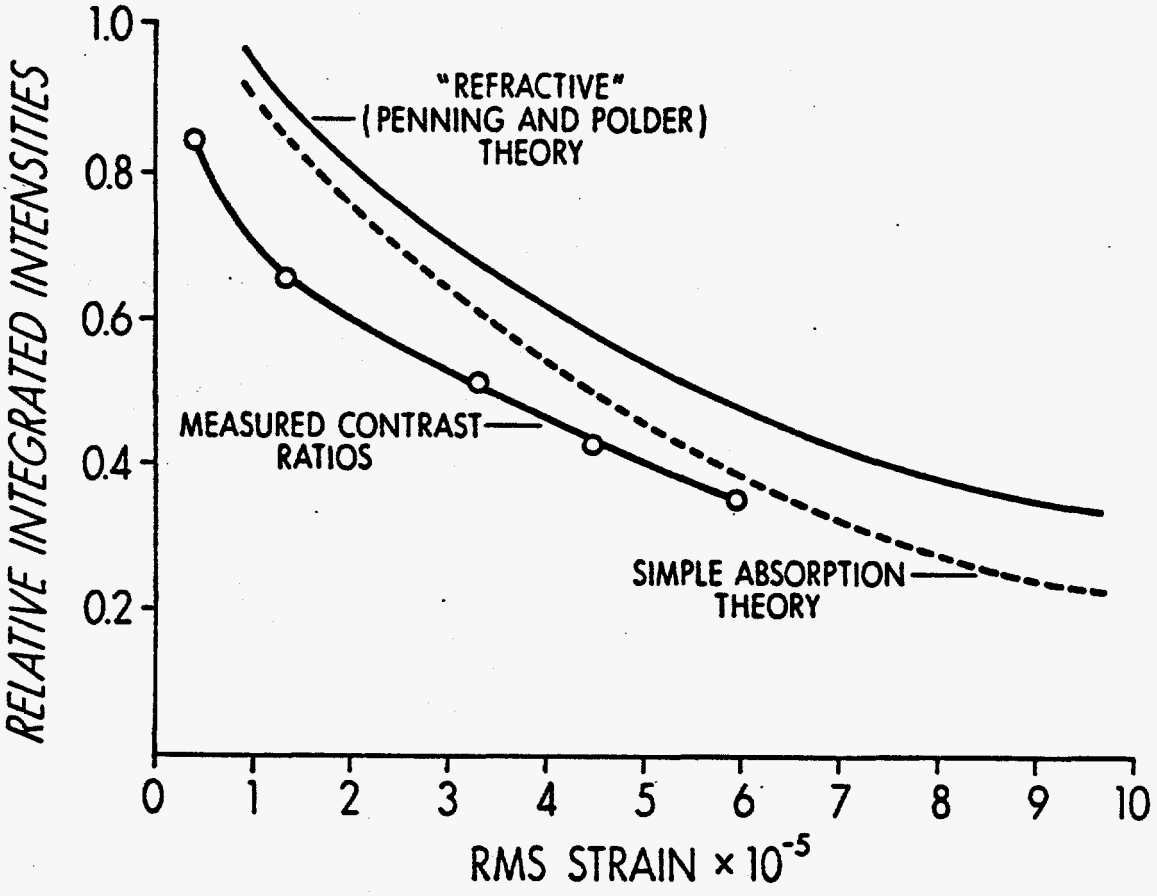

Figure 3-14. Comparison of experimental and theoretical values for integrated intensities in x-ray scans of acoustically perturbed (5MhZ) silicon crystal # 2

Acoustic scans were performed with different wavelength x-rays in order to investigate the variation in interruption with absorption coefficient. Figure 3-15shows two acoustic scans of crystal #1 (5MhZ acoustic wave) with chromium K_α radiation (λ =2.3 A). With chromium radiation the μt (product of absorption coefficient and crystal thickness) increases from 25 to 78.

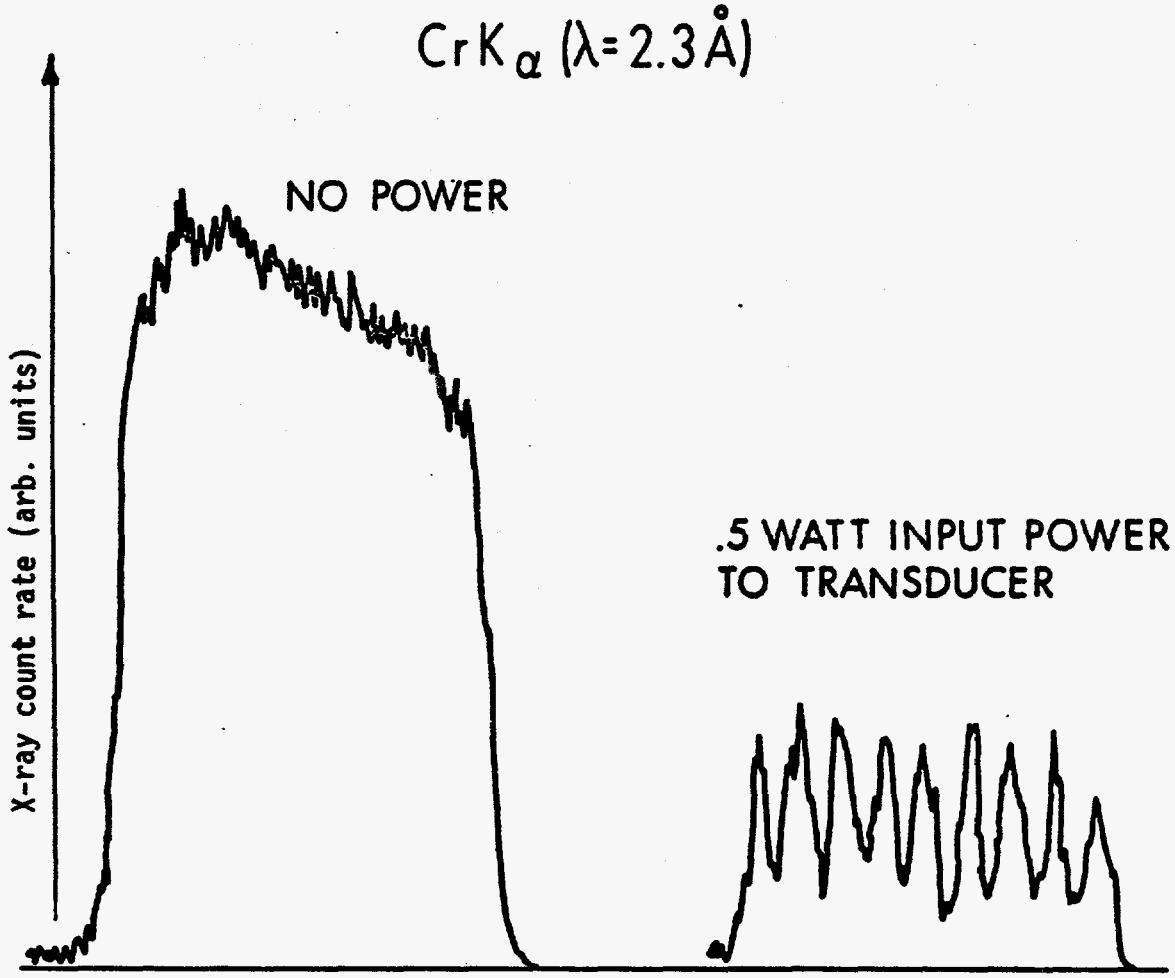

Figure 3-15. Chromium K_α x-ray scans of a 5MhZ acoustic standing wave pattern in a silicon crystal.

As shown in Chapter 2, the directional character of energy flow within the Borrmann fan (1/2 angle of effective Borrmann fan) is only weakly dependent on the x-ray wavelength. Thus, the effective divergence of rays passing through an acoustic pattern remains about the same, and the primary effect is the increased absorption coefficient.

Data from chart recorder traces such as Fig. 3-15 do indeed show a greater percentage attenuation for a given acoustic strain level (than with CuK_α). In addition to the absorption coefficient, the "refractive" effects are also slightly changed by using softer radiation. As seen from Eq. 2-51, Chapter 2, the refraction is inversely dependent on χ_H and directly proportional to $\sin^3\theta_B$ χ_H is roughly proportional to the square of the wavelength. Thus, as the Bragg angle becomes larger for softer radiation, the refraction of the rays increases approximately as $\sin \theta_B$

Fig. 3-16 gives experimental and theoretical results for the dependence of Borrmann interruption on x-ray wavelength.

The wavelength dependence is also illustrated in Fig. 3-17, where x-ray scans of the same crystal with strain level held constant are given for various wavelengths. The x-ray count rate for the unperturbed crystal was adjusted to be the same in all cases by changing the emission current level on the x-ray tubes.

Such results are a useful guide when choosing the crystal type and thickness for a particular application. For example, one might wish to maximuze modulation depth while at the same time, minimizing the

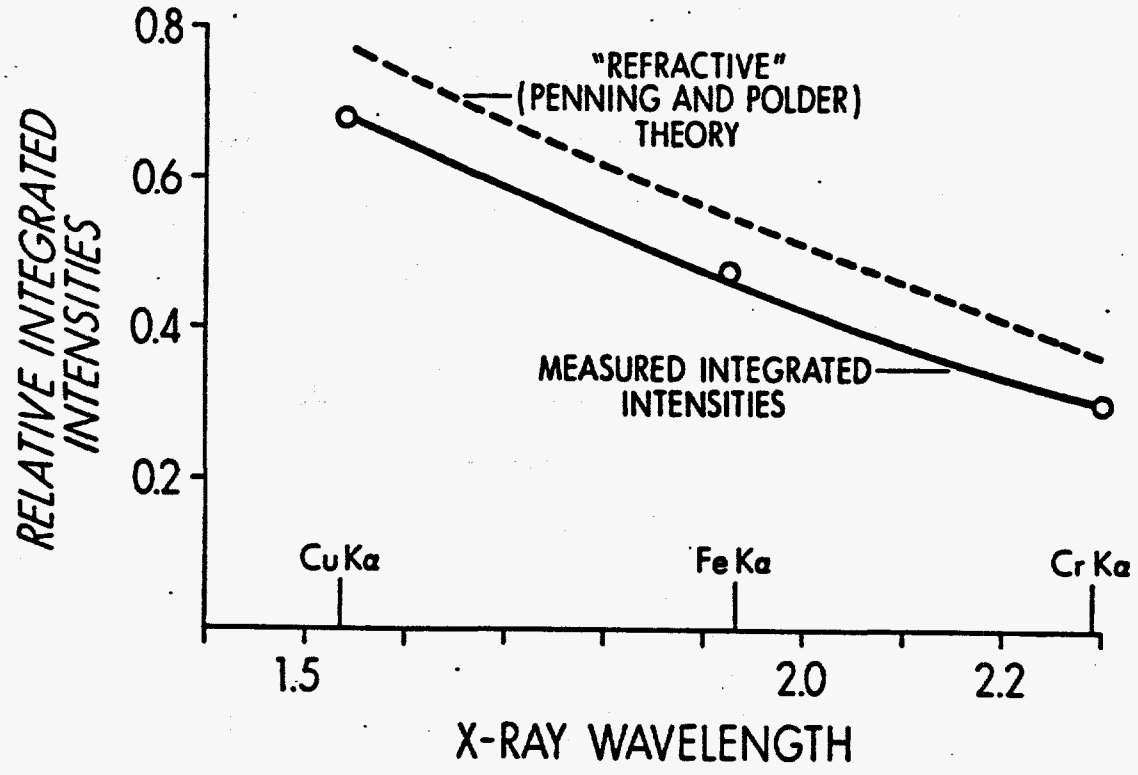

Figure 3-16. Integrated intensity as a function of x-ray wavelength with acoustic strain amplitude held constant.

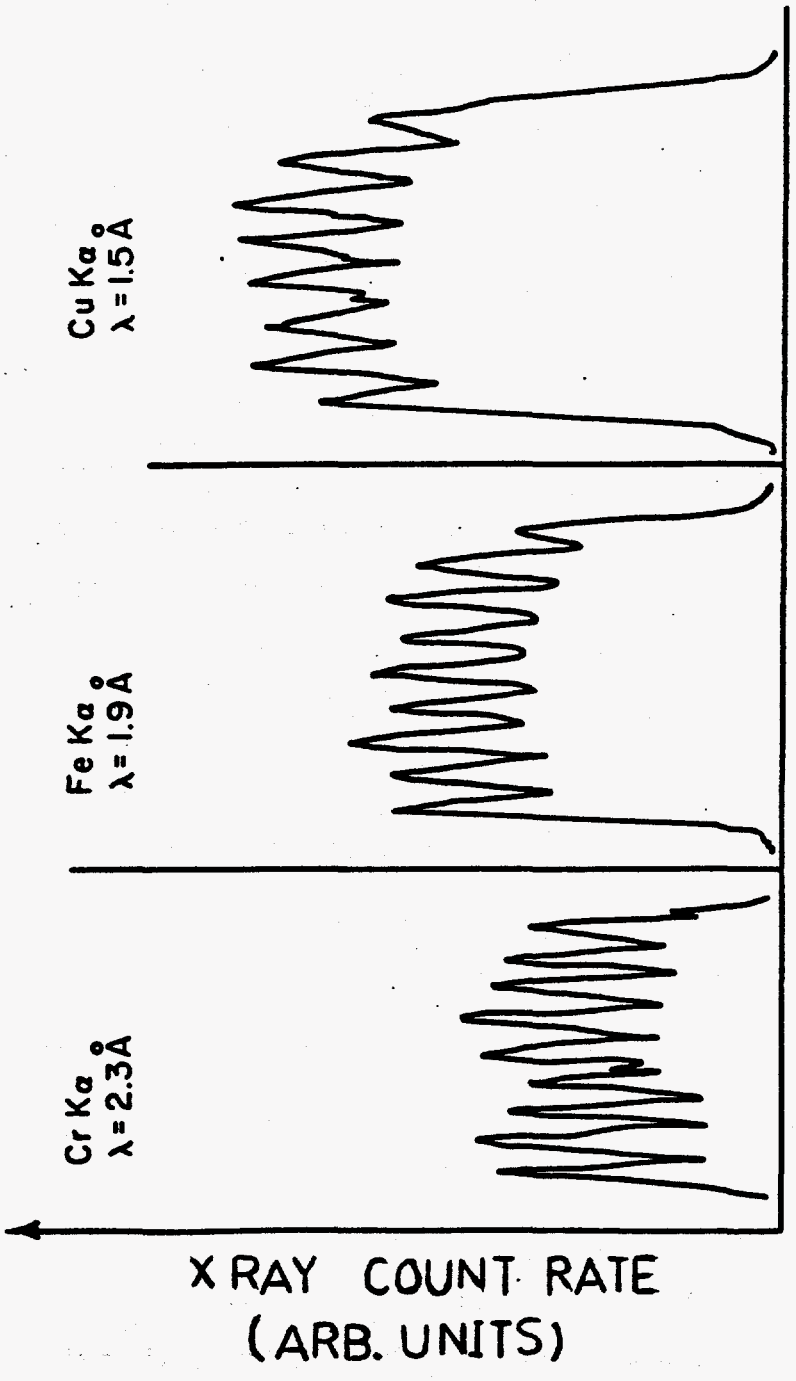

Figure 3-17. X-ray scans of a 5MhZ acoustic standing wave pattern in silicon crystal #1 for various x-ray wavelengths at constant acoustic strain amplitude.

absorption (or insertion loss) of the unperturbed crystal.

The resolution of the scan system is limited by three factors: a) the finite size of the x-ray source, b) the spectral width of the x-rays, which determines the cone angle of rays accepted by the crystal, c) the spread of rays within the Borrmann fan.

Since the entrance slits on the detector must be kept wide open in order to accommodate the movement of the x-ray beam along the entrance face of the crystal. the acoustic wavelength becomes small enough that both factors (a) and (c) start limiting the resolution. These effects can be seen in Fig. 3-18, where a typical x-ray scan of a 10 MhZ acoustic standing wave pattern is presented. The fringe structure due to the acoustic pattern is beginning to be lost in the noise. This scanning method remains, of course, a perfectly valid method for measuring integrated intensity.

The best method for performing scans of this sort would be to monochromate the input beam with another crystal and limit its spatial extent with a slit. In this way, one could limit the cone of rays accepted on the entrance face to around 50 microns. This distance would be small compared to the acoustic wavelength (in silicon (220)) for frequencies around 20-25 MhZ. In addition, such a system could limit the divergence of rays to less than the normal Borrmann fan by exciting a limited region of the dispersion surface.

The contrast formation in the x-ray topographs is slightly

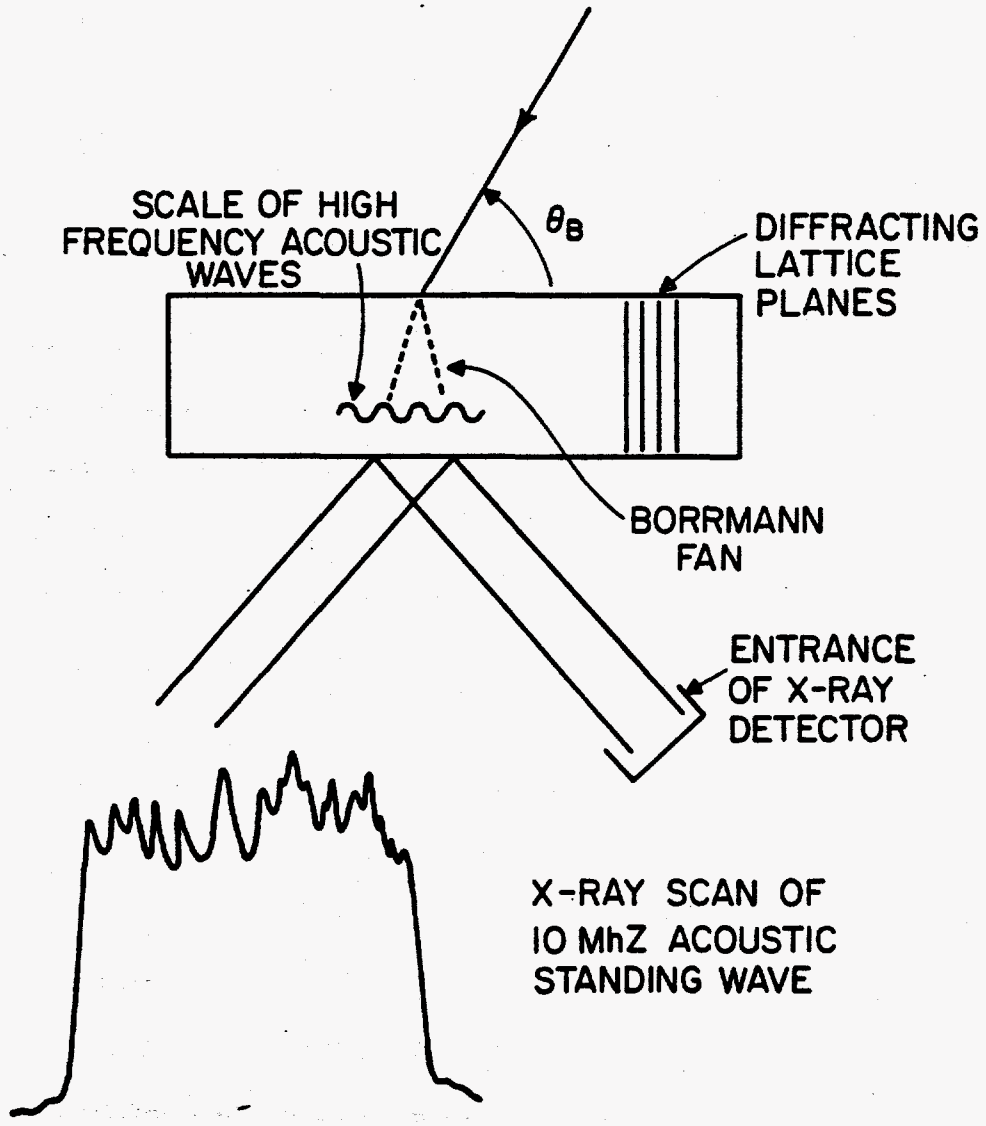

Figure 3-18. Illustration of the limitation of resolution in acoustic scan system due to energy spread in the Borrmann fan.

different than with the scan system and fringe structure can be observed at much higher acoustic frequencies. For the reasons mentioned previously, it is more difficult to obtain quantitative information with the topographs. They are still useful for qualitative evaluation of the contrast formation at higher acoustic frequencies. Fig. 3-19 shows densitometer traces of Borrmann topographs taken(@10MhZ) with silicon crystal #3 with different acoustic power levels in the crystal. The measured reduction in integrated intensity agrees to within about 15% with the results obtained from the scan system.

Results for integrated intensity reduction at 10 MhZ using the scan system are presented in Fig. 3-20. As expected, they are quite similar to the 5 MhZ data. This is to be expected since the strain gradient has not yet reached levels where geometrical optics does not apply. In other words, there is no transfer of energy to the other branch of the dispersion surface.

The slight tendency for a greater reduction in integrated intensities in the 10 MhZ case than 5 MhZ is due to the simple process of rays within the Borrmann fan penetrating into regions with greater deviation from Bragg angle. The larger gradient (for equal strain amplitude) in the 10 MhZ case leads to more refraction and thus, greater reduction in integrated intensity. Going to higher modulation frequencies, while maintaining the same rms strain level, will thus gradually lead to greater reduction in x-ray transmission.

One limitation on going to high frequencies is that in general, the acoustic loss will increase as the frequency is elevated. Below

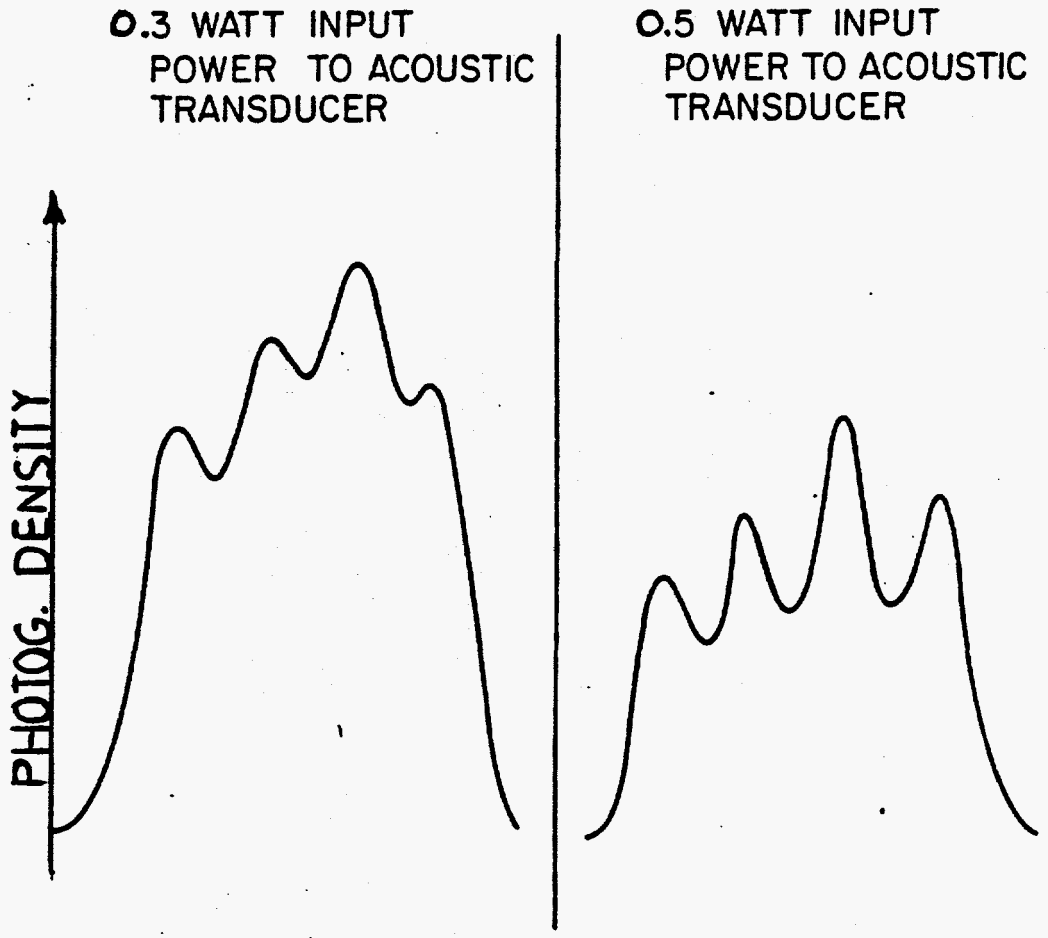

Figure 3-19. Densitometer traces of Borrmann x-ray topographs of 10 MhZ acoustic standing wave patterns in a silicon single crystal.

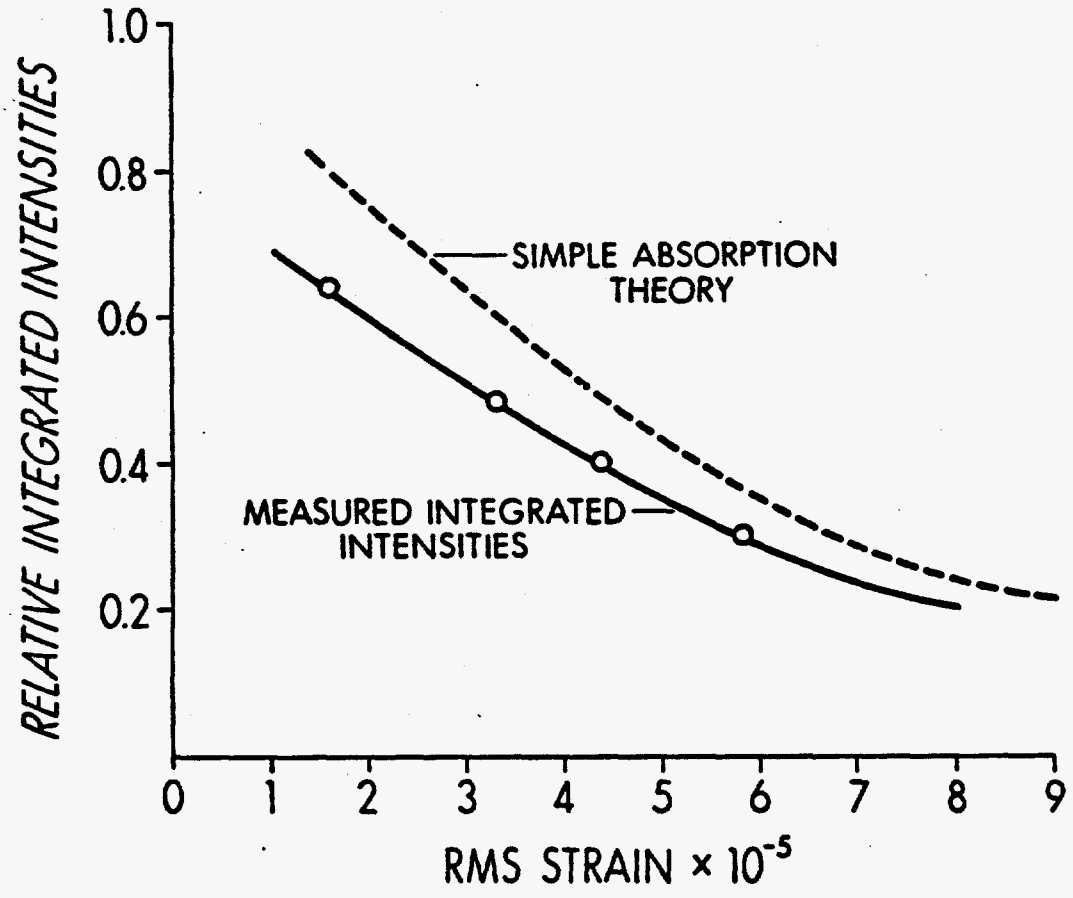

Figure 3-20. Comparison of theoretical and experimental values for integrated intensities in x-ray scans of a 10 MhZ acoustic perturbation in silicon crystal #3.

100 MhZ, however, there are many useful materials that have a very small acoustic loss. Silicon, in particular, has very small loss below 200 MhZ.

As the strain gradient becomes larger, a point is reached where the simple pictures of x-ray diffraction, such as given in the Penning and Polder model, are clearly inadequate. Important changes in the lattice (such as changes in the 2d spacing or bending of the lattice planes) start to occur within an extinction distance (the characteristic distance over which diffraction effects are set up). The transition is quite similar to the optical case where rapid changes in refractive index lead to a transition from refractive to diffractive effects.

It was found that the more convenient and interesting way of investigating higher strain gradient regimes (from the point of view of probing fine details of acoustic structure) was to go to higher frequencies. As described earlier, a $LiNbO_3$ transducer was used at higher frequencies because of its low acoustic loss. It could also be operated at higher harmonics (which was not possible with PZT) so that a range of frequencies could be produced with a single transducer.

On exciting acoustic waves at the primary resonance of one transducer (22 MhZ), a dramatic reduction in x-ray transmission was immediately noticed. An input electrical power of only about one watt would reduce the x-ray count rate to near the noise level. (It might be noted here that the noise level is taken to be the count rate registered when

the crystal is well off the Bragg peak.) Fig. 3-21 shows a typical result for one of the 22 MhZ experiments. The integrated intensity has been reduced to less than 20% of the uninterrupted x-ray transmission.

The simple absorption and the Penning and Polder models were used to calculate the expected reduction in transmission.

The comparison between the analytical model and measured values for reduction in integrated intensity (at 20 MhZ) is given in Fig. 3-22. There is a trend toward divergence between the measured and theoretical curves as the strain gradient becomes larger. This behavior can be explained in terms of the phenomena of interbranch scattering. There begins to be a transfer of energy to the other branch of the dispersion surface. In the Borrmann thick-crystal case, this branch is characterized by very high absorption and thus leads to an additional reduction in the transmitted x-ray intensity.

The approximate criterion for judging the importance of interbranch scattering is given by Formula 2-55, which for reference, is repeated here.

$$\frac{\partial \beta}{\partial S_o} << \frac{\pi}{2} \frac{\lambda}{(d_{ext})^2} \qquad (3\text{-}3)$$

The extinction distance (dext) for the 220 silicon planes is approximately 20 microns[6]. The right hand side of Eq. 3-3 is thus (for CuK_α) about 3.9×10^{-3}. For an rms strain level of 4×10^{-5} and acoustic frequency of 20 MhZ, the strain gradient component along S_o is about 7×10^{-4}. Observable effects due to interbranch scattering can be seen when the left

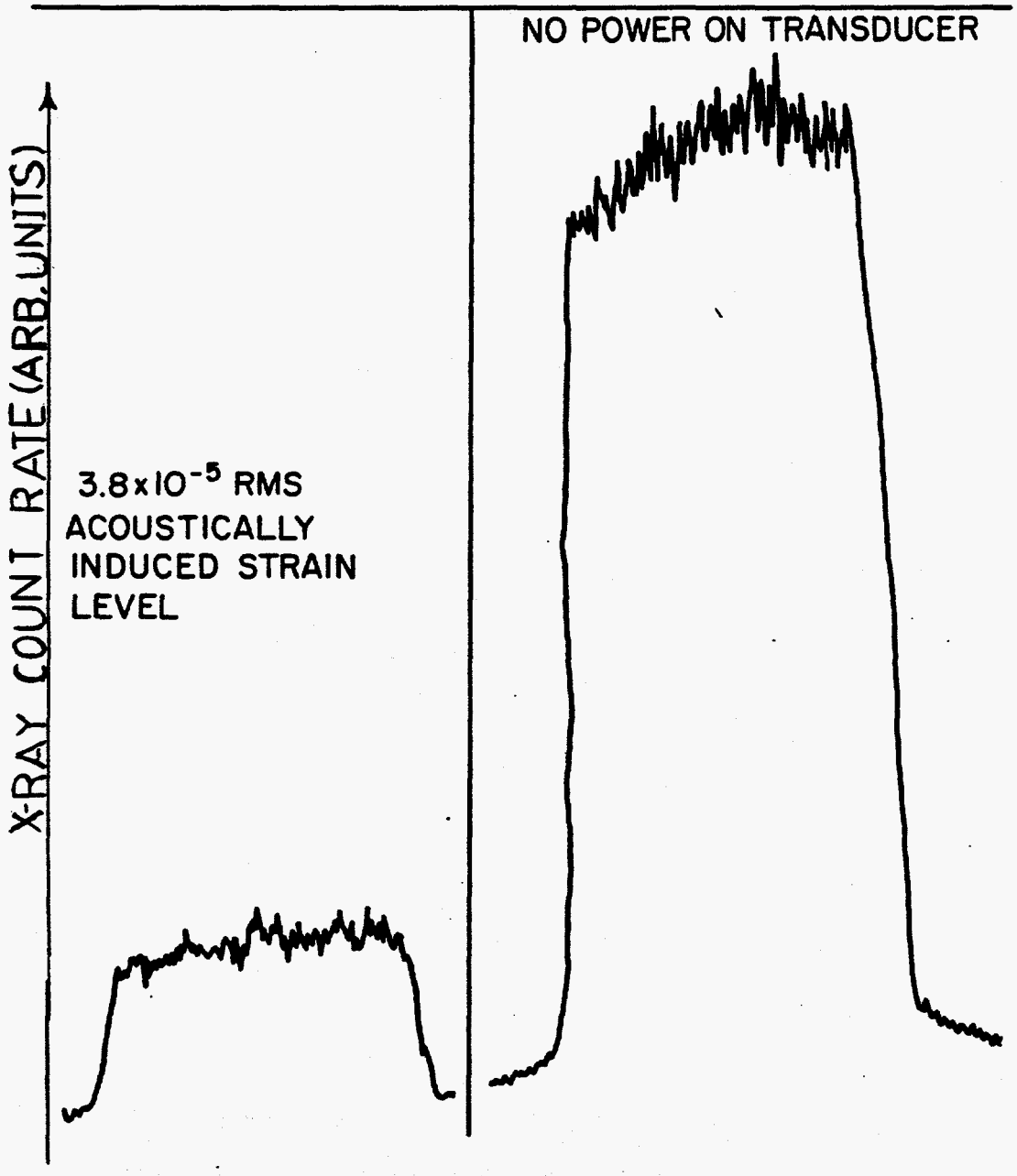

Figure 3-21. High frequency acoustic (22 MhZ) interruption of x-ray transmission through silicon crystal #4 (CuK_{α} radiation).

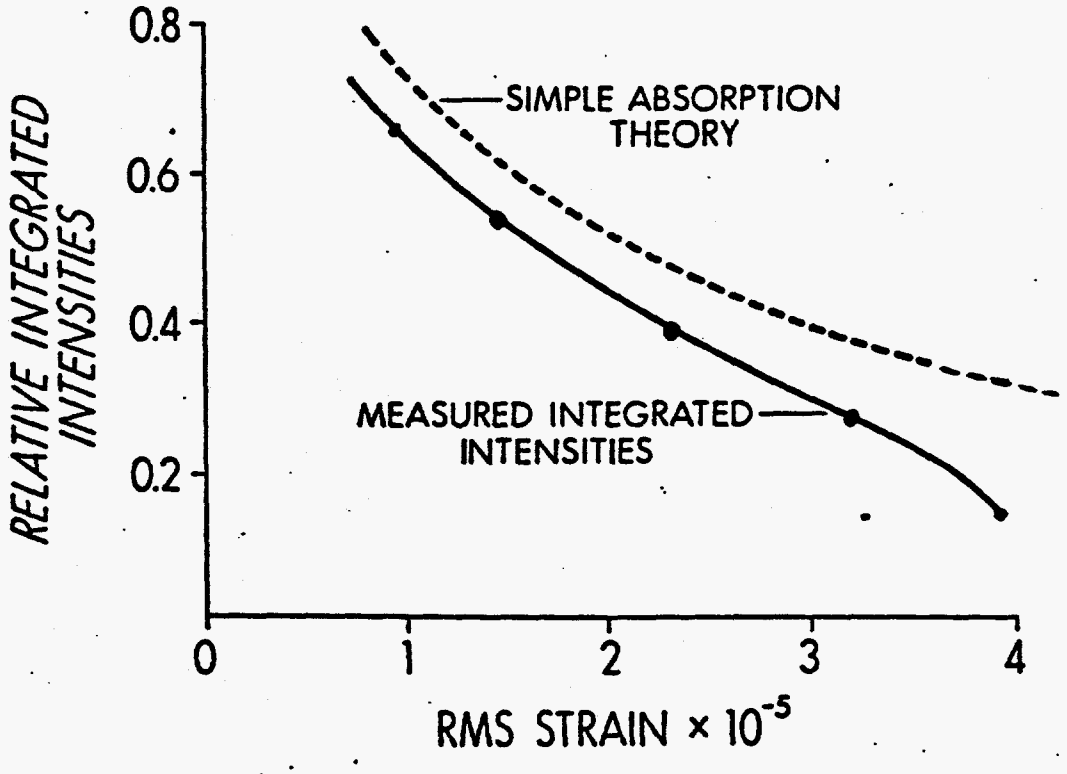

Figure 3-22. Comparison of theoretical and experimental values for integrated intensities in x-ray scans of a high frequency (22MhZ) acoustic perturbation in a silicon crystal.

side of (3-3) is more than 10 times greater[11]. The enhanced reduction in diffracted x-ray intensity seen in Fig. 3-22 can thus be explained in terms of the phenomenon of interbranch scattering. A rigorous quantitative prediction of the exact amount of interbranch scattering requires the generalized dynamical diffraction theory given by Takagi (and reviewed in Chapter 2).

The definition in Borrmann topographs remains quite good at 22 MhZ, as shown in Fig. 3-23. The spatial frequency of the fringes is quite similar to that found in many high resolution topograph studies of naturally occurring crystal defects, such as dislocations. This points up the fact that the techniques developed in the present work are appropriate for the study of both the micro-structure of acoustic fields in solids and also the basic topographic contrast mechanisms (in the case of rapid spatial variation of lattice parameters). This will be discussed in more detail below in the section on topography.

Before concluding the present section on single crystal Borrmann work, remarks concerning the general character of the results in relation to measurement error are in order. The difficulty in making absolute acoustic strain measurements provided the major source of error. In the low frequency case the magnitude of error was estimated from the scatter in the comparison of strain gauge and acousto-optic techniques (see for example figure 3-7). The error was seen to be about $\pm.5\times10^{-5}$. Although the analytical predictions are within the expected error, there also seems to be a systematic tendency (which actually applies at all frequencies) for the interruption of the x-ray

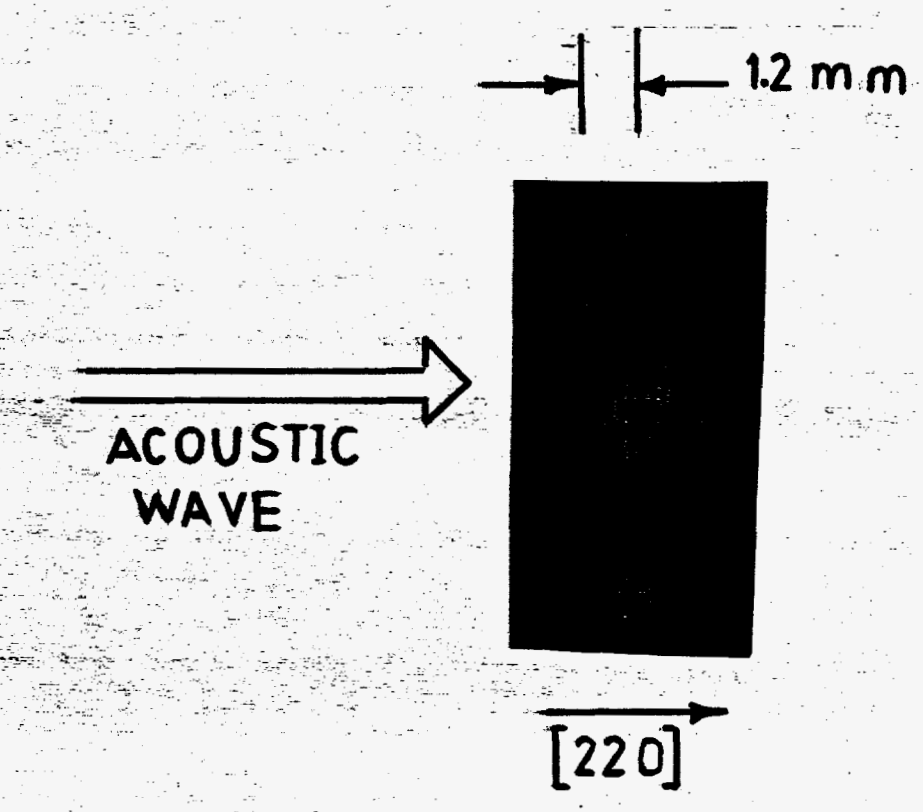

Figure 3-23. Borrmann topograph of high frequency (22 MhZ) acoustic wave in a silicon single crystal.

transmission to be greater than predicted by theory.

An interesting comparison between theory and experiment is shown in Fig. 3-24. Here, instead of using values of strain measured in the conventional way, a different method is used according to the following scheme. A threshold level for any noticeable effect on the integrated intensity (approximately 1% reduction) is observed experimentally and predicted with the simple absorption theory. By taking the value of strain at this point to be that predicted by the theory, all higher strain levels are calculated by multiplying by the square root of the ratio of electrical input powers. Since we are certainly in the region of elastic behavior of the crystal, the strain level should be proportional to the squareroot of the electrical power input. Although the agreement between the measurement and theory improves, the systematic tendency for the measured values to give lower integrated intensity seems to remain.

Another possible source of error is the assumption of a pure longitudinal acoustic wave. This picture is used in all the theoretical calculations. One has only to consult the x-ray topographs taken to realize that this is only an approximation. This will be discussed in more detail later, but it can be said here that densitometer traces of many topographs at 5 and 10 MhZ show about 1.8% rms deviation in the acoustic wavelength across the transverse extent of the crystal.

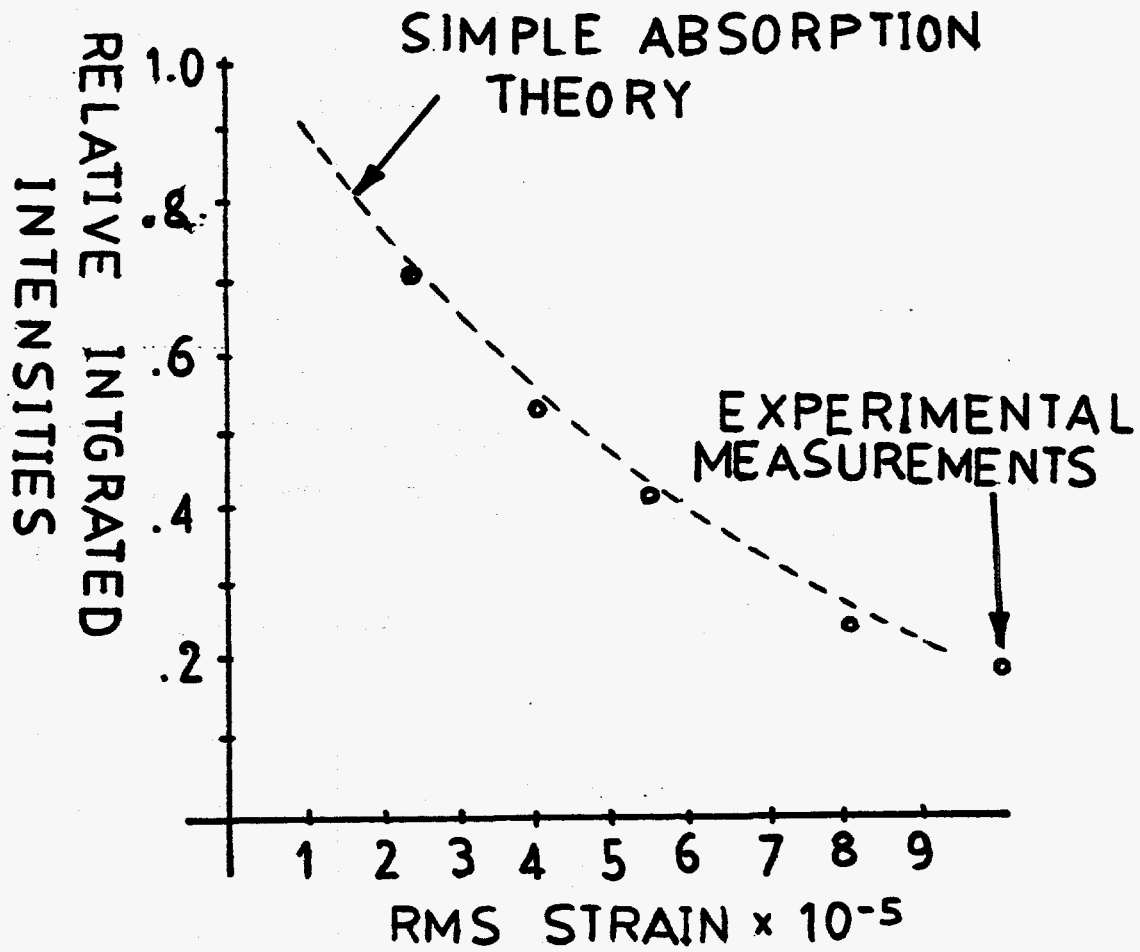

Figure 3-24. Reduction of integrated intensity in silicon crystal #1 (with strain levels normalized to theoretically predicted threshold).

The purpose of the present study was, however, to establish the orders of magnitude that would be involved in producing practical x-ray modulating, shuttering, and control devices. Within the context of this viewpoint, the accuracy of the present experiments is adequate.

3.3 EXPERIMENTS WITH X-RAY INTERFEROMETERS

Although the present experiments have shown that the x-ray transmission can be quite sensitive to acoustic perturbation, in certain possible applications, it would be desirable to have even greater sensitivity. It would be desirable to have a larger gradient of strain along the direction of ray propagation in the Borrmann fan. In many naturally occurring crystal defects, curvature of planes, and other complicated distortions, occur in addition to simple compression or dilation of the lattice planes. If, for example, the acoustic wave could be confined to certain portions of the cross section of the crystal (in the plane of incidence), much more abrupt changes in lattice parameter could be produced. This would, of course, lead to curvature of the lattice planes, since discontinuous changes in lattice parameter cannot be produced.

One way that a more abrupt change in lattice parameter can be realized is shown in Fig. 3-25, where use is made of one type of x-ray interferometer. The design of the interferometer is a slight modification of one of several suggested by Bonse and Hart[10]. The

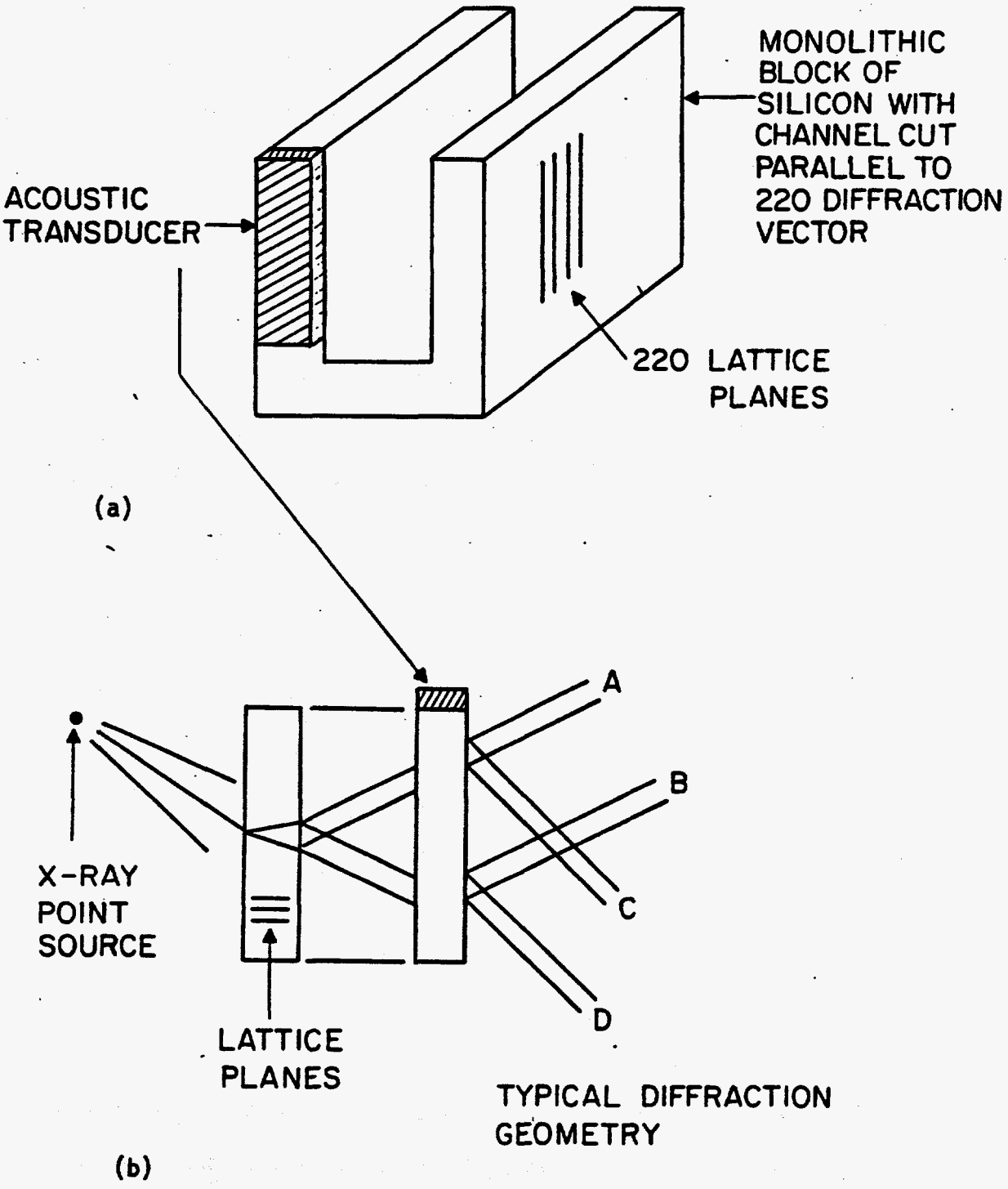

Figure 3-25. Configuration used in the experimentation with x-ray interferometers. (a) crystal geometry (b) diffraction geometry

entire structure was cut out of a monolithic block of silicon.

The device used in the present experiments was manufactured from a 1 cm. slab of Czolchalski grown silicon. The sample was oriented as previously described. The channel was machined in the block by taking repeated cuts with a high speed diamond crystal milling (wafering) machine. The entire unit was then chemically polished with the nitric HF mixture described before. The polishing was performed by looping a length of teflon tape through the channel and tying it firmly. With this, one could provide vigorous agitation that uniformly polished all the surfaces. The edges of the upright arms of the interferometer were optically polished to provide the surfaces for bonding the transducer and for acoustic reflection. In order to prevent undue stress being placed on the arms during the polishing process, a special polishing block was constructed. The acoustic transducers were bonded in the manner previously described.

More care had to be taken in mounting the sample than was necessary in the single crystal experiments. If a strain was introduced in one arm relative to the other, significant changes in the transmission were observed. This actually was used to advantage in an experiment described below, where a prestressed condition was used to select the operating point on the diffraction curve (input deviation from Bragg condition). During the majority of experiments, however, any nonacoustic strain was removed by using a special mount and soft silicone rubber bonding.

Although the phenomena of interruption of Bormann transmission is basically the same in the two crystal case, the specific details of the processes are different. As in the case of double crystal spectrometers, the first crystal acts like a monochrometer and collimator. Although it represents common terminology in x-ray diffraction theory, one must be careful to understand the sense in which the term collimation is used here. A broad non-monochromatic beam is incident on the first crystal. At any point on the first crystal, a ray is selected for transmission only if its wavelength and angle satisfy Bragg's law. Radiation falling on the second crystal is thus filtered so that at each point, only radiation of the right wavelength and corresponding angle (satisfying Bragg's law) is incident. Thus, any change in lattice geometry in one of the arms, such as compression or dilation of the lattice planes or a tilting of the arm, reduces the transmission according to the diffraction curve (diffracted intensity vs. departure from Bragg condition), and is not a function of the collimation and spectrum of the input radiation.

The basic geometry used in the acoustic perturbation experiments is shown in Fig. 3-26. In the single crystal case, radiation accepted at each point on the entrance surface satisfied Bragg's law. Now, consider radiation incident on the second arm of the interferometer. A ray incident at the node of the acoustic field sees the undistorted lattice, and Bragg's law is satisfied. The spread of energy flow in the Borrmann fan causes radiation to enter regions where Bragg's law is

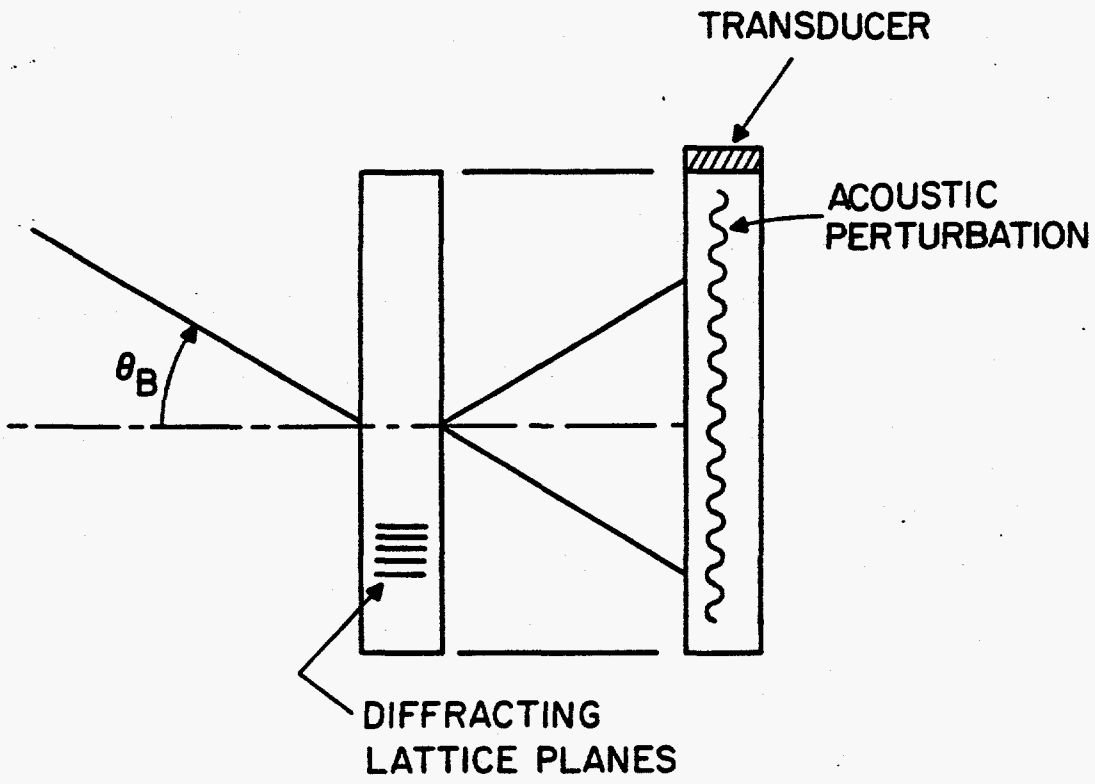

Figure 3-26. Acoustic perturbation of x-ray propagation in an interferometer.

not satisfied. This is the same situation that prevailed in the single crystal case. A ray entering at the peak of the acoustic field does not satisfy Bragg's law and starts to be attenuated. As it spreads out, there is a tendency toward satisfaction of the Bragg condition. Qualitatively speaking, in the two crystal case, the peaks of the acoustic pattern, as well as the nodes, are involved in the attenuation process. Rays entering the crystal at the acoustic peak see much less strain gradient than at the nodes, and thus spread much less rapidly into regions of differing 2nd spacing. This implies that the fringe contrast in the double crystal Borrmann case that is set up by an acoustic standing wave is reversed (with respect to the single crystal Borrmann case) with minimum x-ray transmission occurring at the acoustic peaks. Also, for lower acoustic frequencies (below the region where interbranch scattering is important), the magnitude of the strain gradient is somewhat less important, since the whole acoustic pattern is contributing to the interruption.

In order to form a more quantitative picture, a slight alteration to the simple absorption ray trace program was made corresponding to the change in the boundary conditions at the entrance face of the second crystal. Now, rays enter the crystal at a fixed angle (taken to be the Bragg angle for undistorted case), regardless of the acoustic perturbation present at that point.

In order to compare with previous single crystal results, the same (220) diffracting planes and Borrmann (thick crystal) mode were

used. Several other diffracting configurations are possible with interferometers of this type and will be discussed later. In the measurements presented below, both beams a and b (Fig. 3-25) were simultaneously collected by the detector. In the thick crystal case, these two beams should have the same diffracted intensity and thus, behave the same in response to perturbations. Fig. 3-27 shows chart recorder traces (θ-2θ scans) for the case of 10 MhZ acoustic wave perturbation. In addition to the sharp reduction in integrated intensity, there seems also to be a very slight change in the shape of the trace. This is probably due to residual stresses in the mounting that introduce a slight nonuniform misalignment of the two arms of the interferometer. Fig. 3-28 gives a plot of the measured reduction in integrated intensity vs. strain for a 10 MhZ acoustic wave. The theoretical calculation, using the simple absorption model, is also included. For reference, the measured values for x-ray interruption in the single crystal case are included in the same plot. Similarly, 3-29 displays the same information in the case of 5 MhZ acoustic frequency.

In both cases, there seems to be a rather strong departure from theory at very low values of strain. A trend in this direction was noticed in the single crystal case, but the tendency seems stronger in the double crystal case. The error in strain measurements is greater in this region, but the difference between the double and single crystal cases seems explicable only in terms of an inadequacy of the theoretical model.

ACOUSTIC INTERRUPTION OF X-RAY TRANSMISSION THROUGH A TWO CRYSTAL BORRMANN MODE X-RAY INTERFEROMETER

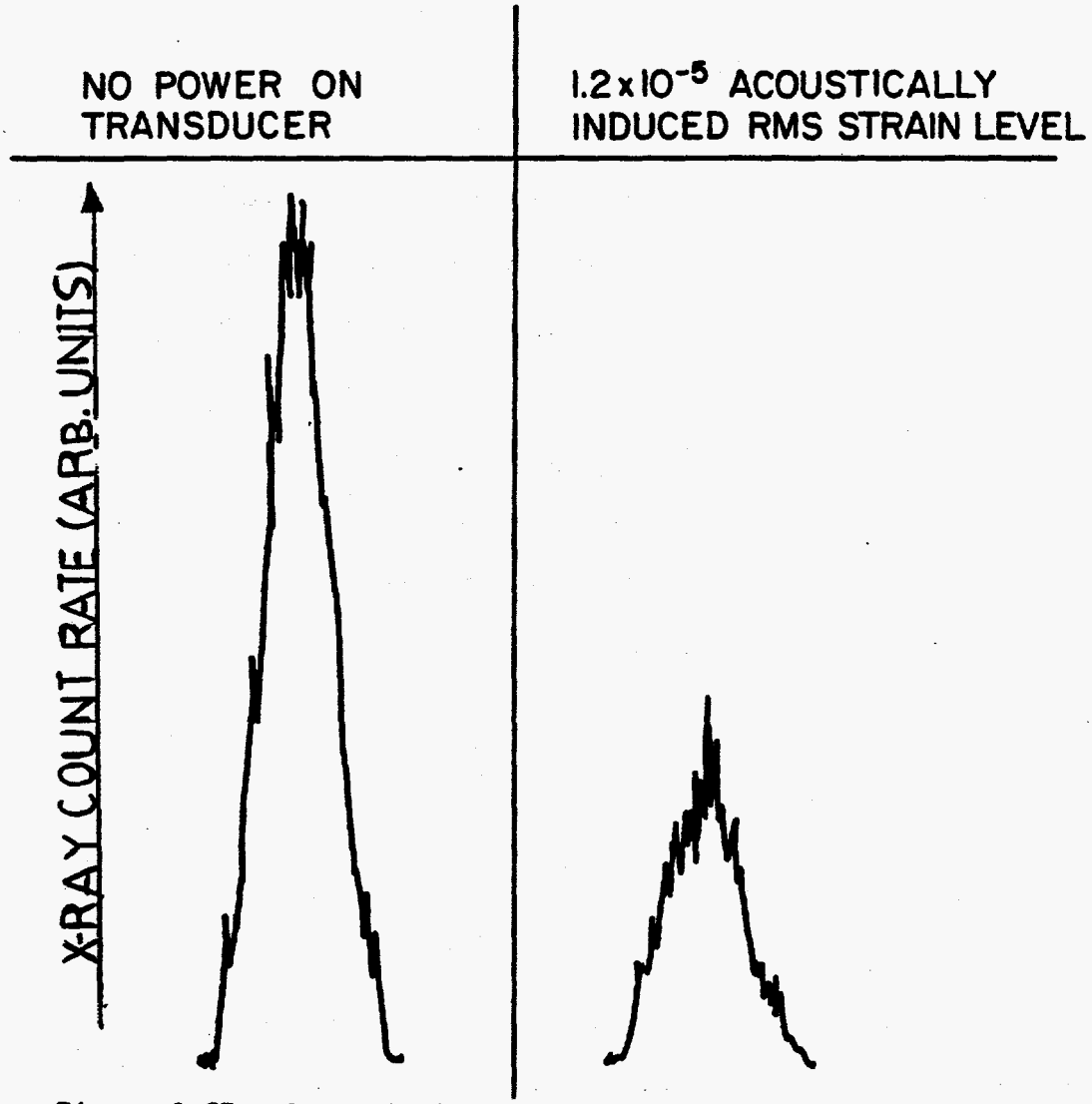

Figure 3-27. Acoustic interruption of x-ray transmission through a two crystal Borrmann mode x-ray interferometer.

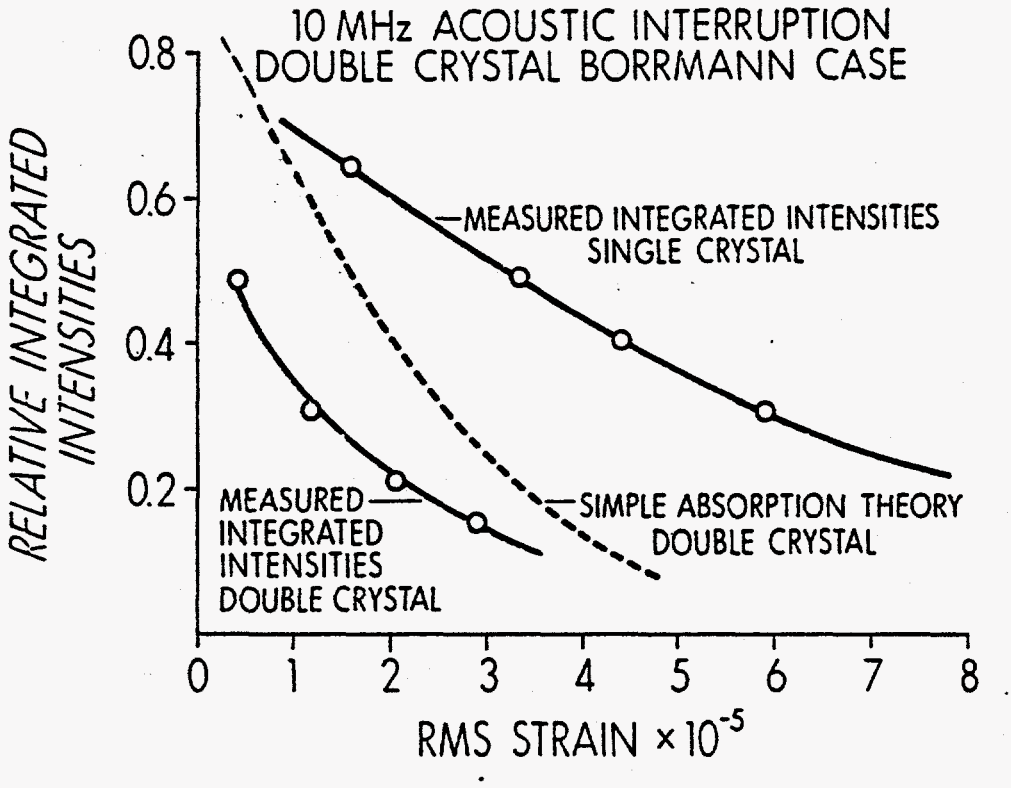

Figure 3-28 . Experimentally measured and theoretically predicted values for integrated intensity in the double crystal Borrmann case (10 MhZ).

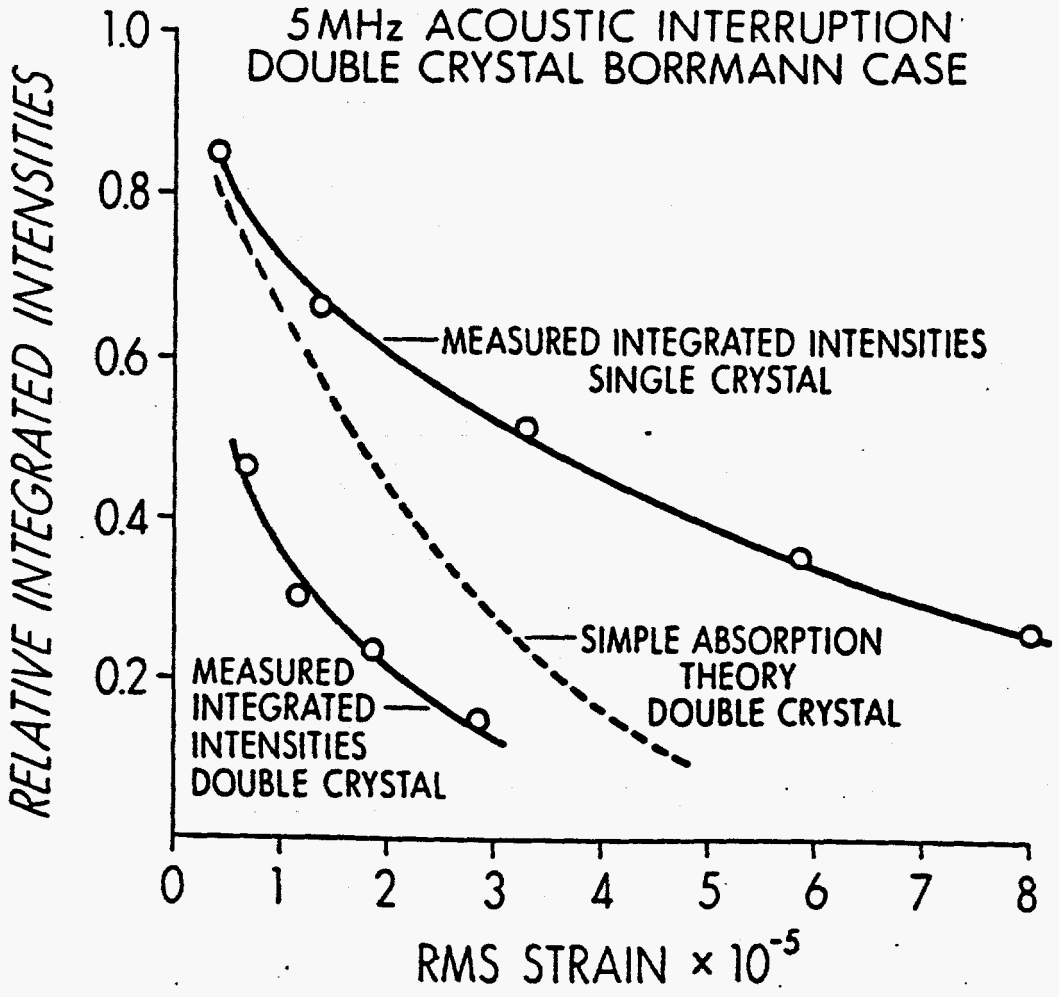

Figure 3-29. Theoretical and experimental values for integrated intensity, for 5MhZ acoustic interruption double crystal Borrmann case.

In the double crystal experiments, the important consideration to note is the substantial difference in sensitivity of x-ray transmission to acoustic interruption. The qualitative description of this behavior is based once again on the interferometer model of x-ray diffraction. When a large number of effective reflections are involved, a great sensitivity of transmission vs. wavelength is achieved. The greatest value of x-ray interferometers arises when many passes (corresponding to more than two arms or multiple reflections from the same arms) or effective reflections are involved. These situations will be considered in more detail in Chapter 4.

In the present experimental situation with two effective reflections per beam, the primary advantage is obtained by being able to introduce a discontinuous change in lattice spacing between the two elements or arms of the interferometer. A single crystal case (with a thickness equal to the sum of the thickness of the two arms) would involve the same number of effective reflections from atomic lattice planes. The single crystal case with uncollimated input radiation, however, essentially allows for a self-adjustment of the radiation field, selecting those portions that satisfy the Bragg relation at the entrance surface.

The foregoing experiments, with introducing an acoustic perturbation into one arm of an interferometer, essentially constitute a new way of performing a double crystal rocking measurement. The change in 2d spacing is, of course, transient, but the instantaneous effect is still the same. One could conceive of introducing DC changes in the

2d spacing (or orientation of the two arms) in order to select a particular operating point for the interferometer. Possible applications will be discussed in more detail later.

In order to demonstrate some of the concepts behind possible applications, the following experiment was performed. The interferometer was mounted with epoxy in such a way that stress was placed on one arm of the interferometer. This process was difficult to perform accurately and was done essentially by trial and error with an epoxy that was discovered to be partially soluble in hot trichloroethelyene. After bonding, the transmission of the interferometer was then measured relative to the unstrained case. Fig. 3-30 shows a θ-2θ x-ray scan of the interferometer with stress applied. The right side of Fig. 3-30 shows the scan with the interferometer in the same condition of stress but with the addition of an acoustic wave excited in one of the arms. As can be seen, there is now a dramatic increase rather than decrease in x-ray transmission. Since the epoxy stress could not be applied accurately, the arm was strained rather far into the wings of the diffraction (rocking) curve. Thus, a greater acoustic power (and thus, strain) was needed to bring the transmission back to that of the totally unstrained condition than would be expected from the previous non-prestressed measurements. There seems in this case to be a pronounced change in the shape of the θ-2θ scan. We expect this because the zero power condition definitely has a large stress applied in a way that is likely to be nonuniform. Using methods of this sort, one can "tune" the interferometer to a desired

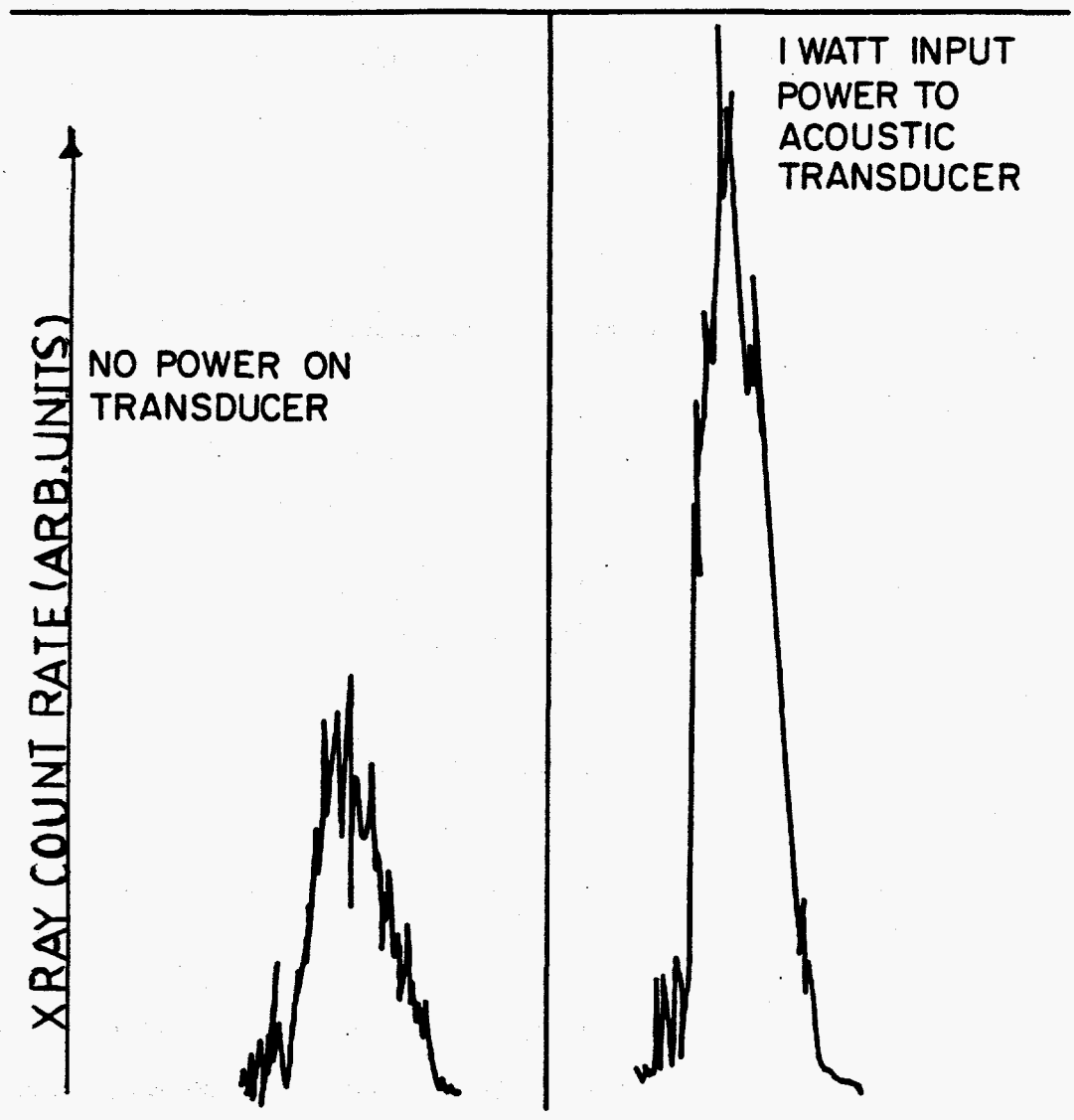

Figure 3-30. Increase in X-ray transmission caused by acoustic perturbation of prestressed (misaligned) X-ray interferometer.

portion of the rocking curve. For example, an operating point on the steep edges of the curve would show a great sensitivity to further perturbations and produce a greater contrast ratio in switching and shuttering experiments. In addition, such a tuning capability could be useful in producing a desired radiation input condition for x-ray topograph investigations. With respect to modulation and shuttering concepts, these experiments demonstrate that "turn on" as well as "turn off" processes are feasible.

3.4 X-RAY TOPOGRAPHY OF ACOUSTIC FIELDS IN SOLIDS

One application that is an outgrowth of the present work is the use of x-ray diffraction in general and topography, specifically to map the microstructure of acoustic fields in solids. This information could, in turn, be used in studies of a variety of acoustic interactions in solids (e.g., acoustoelectric amplification experiments). Conversely, on introducing various configurations of carefully controlled acoustic perturbations, x-ray contrast formation mechanisms can themselves be studied. In particular, the transition from refractive to diffractive regions of x-ray image formation can be studied. These concepts are applicable to the thick crystal Borrmann case, as well as to thin, double crystal, and Bragg geometry cases.

One of the first applications of topography in the present study was an investigation of the fundamental nature of contrast formation in the single crystal Borrmann case. Our basic model of contrast

formation that is proposed in this study involves the concept of rays entering the crystal at the Bragg angle and spreading into regions where the Bragg condition is no longer satisfied. This picture is described in detail in Chapter 2 (in the subsection on simple absorption theory). This model immediately suggests that the minimum x-ray transmission will occur at the nodes of the acoustic pattern. Since the edge (opposite the transducer) of the crystal imposes a minimum on the acoustic standing wave, the presence of a light or dark fringe in the x-ray pattern at the edge should confirm the model. It proved, however, difficult to distinguish the edge of the crystal by simply placing it in the projected field (see Fig. 3-4(a) of the line source. In all topographs taken, the edge was very blurred and it was impossible to determine the fringe structure.

To circumvent this problem, a sharp edge razor blade was positioned parallel to the edges under a microscope and then glued to the surface. X-ray topographs of the crystal showed the edge in sharp detail. The position of the blade edge with respect to the crystal edge was accurately measured with a travelling microscope. The final fringe at the edge of the crystal was determined to be a white fringe (i.e., minima in x-ray intensity), confirming the model of contrast formation.

This picture is additionally confirmed by several topographs, such as shown in Fig. 3-8, which were taken with a strain gauge in view. The structure of the gauge being clearly visible in the topograph could then be easily referenced with respect to the standing wave pattern and the edges of the crystal.

Other aspects of the contrast formation can also be investigated by topography. The analytical model of contrast that is proposed in this study assumes that the basic mechanism is an increase in absorption due to an interruption of the Borrmann effect. Thus, regions of lattice perturbation cast "shadows" in both the diffracted and direct (forward diffracted) beams. Moreover, in the thick crystal case, dynamical diffraction theory predicts symmetrical energy distribution in the diffracted and forward beams. With the symmetric time varying nature of the acoustic perturbation, one also expects the same contrast behavior in the forward and diffracted beams. This means, of course, that nodes in the acoustic field should represent minima of x-ray transmission in both of the beams.

In the thin crystal case, a variety of interference effects (some involving the other branch of the dispersion surface) are possible that could cause complementary contrast in the two beams. In the thick crystal case, there are also subtle details. If the standing acoustic wave were frozen in time, the strain gradient would spatially alternate sign. At one particular node, rays in the top half of the Borrman fan (contributing more to the diffracted beam) might be refracted away from the lattice planes, causing increased absorption, while rays in the bottom of the fan (contributing more to the forward beam) would be refracted closer to the lattice planes. When there is, however, strong Borrmann transmission, the fan of rays tends to converge around the central ray (parallel to lattice planes), making the distinction between the top and bottom half of the Borrmann fan less

important.

In order to check the relative contrast in the two beams, one could check the position of fringes in the two beams relative to a fiducial mark, such as the razor blade used earlier. An even more accurate method was discovered that utilizes a naturally occurring defect in the crystal, which itself served as a fiducial mark

The direct beam, in addition to forward diffraction, also contains hard components that penetrate the crystal. In order to expose the forward and diffracted beams on the same plate, this hard component must be reduced. This was done by reducing the excitation potential on the x-ray tube. This, unfortunately, also reduces the efficiency of excitation of the Kα line and thus the line to continuum ratio. This, in turn, results in poorer quality topographs with reduction in contrast and a slight blurring of once sharp detail. Numerous topographs of the crystal were taken in order to determine the optimum value for tube potential to maximize contrast in both the forward and diffracted beam simultaneously. For CuKα, this was determined to be 13KV. In order to provide good resolution, exposures were taken on electron-microscope image plates. These provide much better resolution than no screen film at a sacrifice of about 10 times in sensitivity. 649 spectroscopic plates would provide the best possible resolution, but the extremely long exposures necessitated by this emulsion (about 3 times longer than em plates) were deemed prohibitive.

Fig. 3-31 shows a CuKα topograph of a silicon crystal with an acoustic standing wave present. The images of both the direct

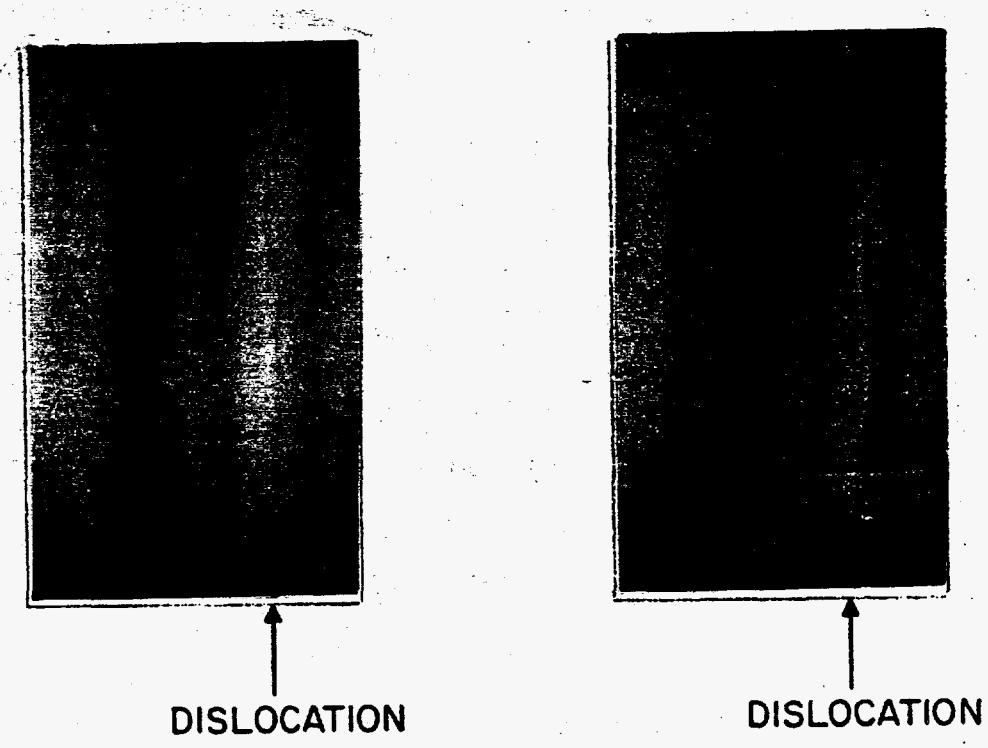

Figure 3-31. X-ray topograph of a silicon crystal with an acoustic standing wave pattern applied. Dislocation in the field of view acts as a fiducial mark. (both diffracted and forward diffracted images are shown).

(forward diffracted) and diffracted beams are shown. Since the two exposures are taken on the same plate, the forward beam is approximately normal to the plate, while the diffracted beam is incident at the Bragg angle. This causes the slight difference in the apparent spacing of the fringes and size of the dislocation. As can be seen from the figure, the position of the dislocation with respect to the acoustic pattern is exactly the same in both the diffracted and direct beams. This confirms that the contrast formation is the same in both the diffracted and direct (forward diffracted) beams.

In addition to the study of contrast formation, this method of topography also lends itself to study of the acoustic field itself and its interaction with defects such as dislocations. Fig. 3-32 shows an x-ray topograph of a region where a dislocation is present. The two views show the diffracted image with and without an acoustic standing wave perturbation present. The right hand photo shows what seemed to be a standard feature of the acoustic field in the vicinity of defects. The nodal lines bulge slightly and seem to cause a broadening of the adjacent fringe. More will be said about applications of x-ray acousto-optic effects in Chapter 4.

In all the experiments performed in this study, longitudinal waves were propagated perpendicular to the 220 planes used for diffraction. The geometry is illustrated in Fig. 3-33. Silicon has a diamond cubic lattice structure and acoustic velocities can be expressed simply in terms of three elastic constants [12].

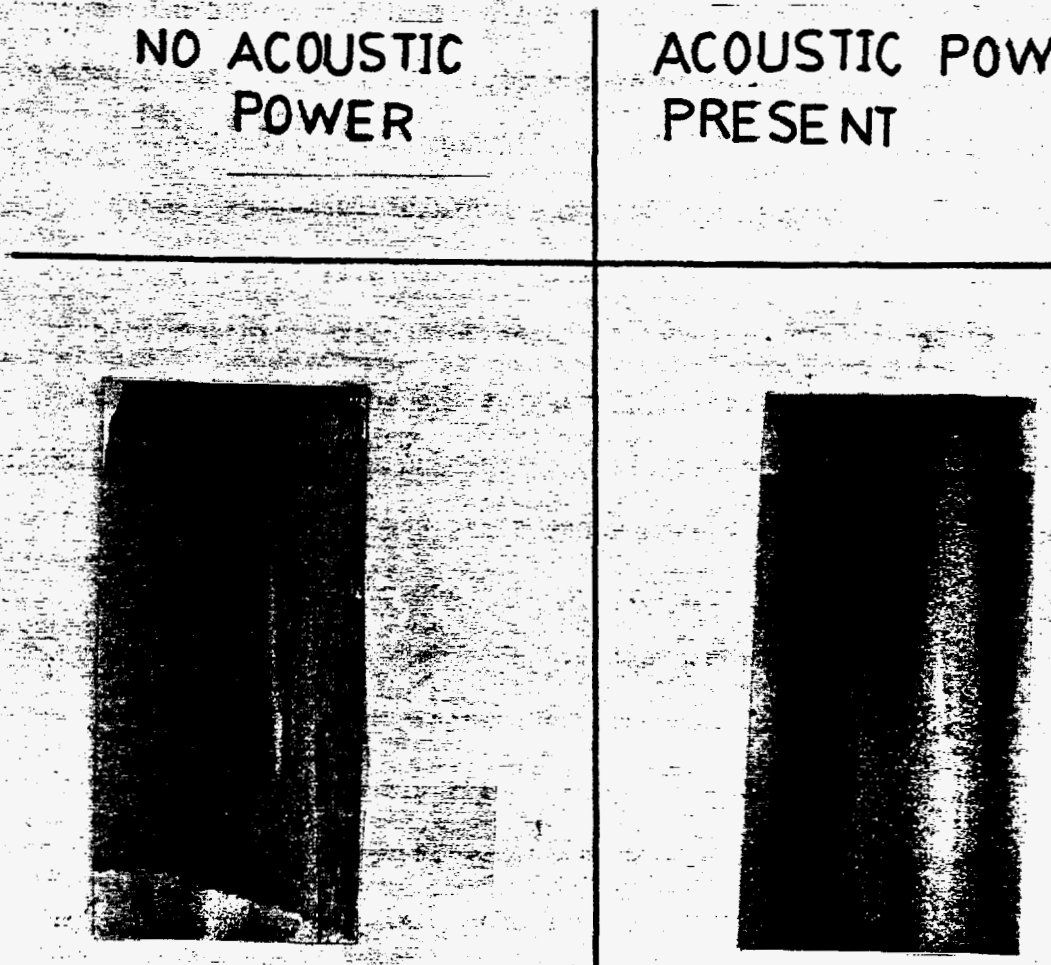

Figure 3-32. Borrmann x-ray topograph of a silicon single crystal (containing a dislocation) with and without acoustic standing wave.

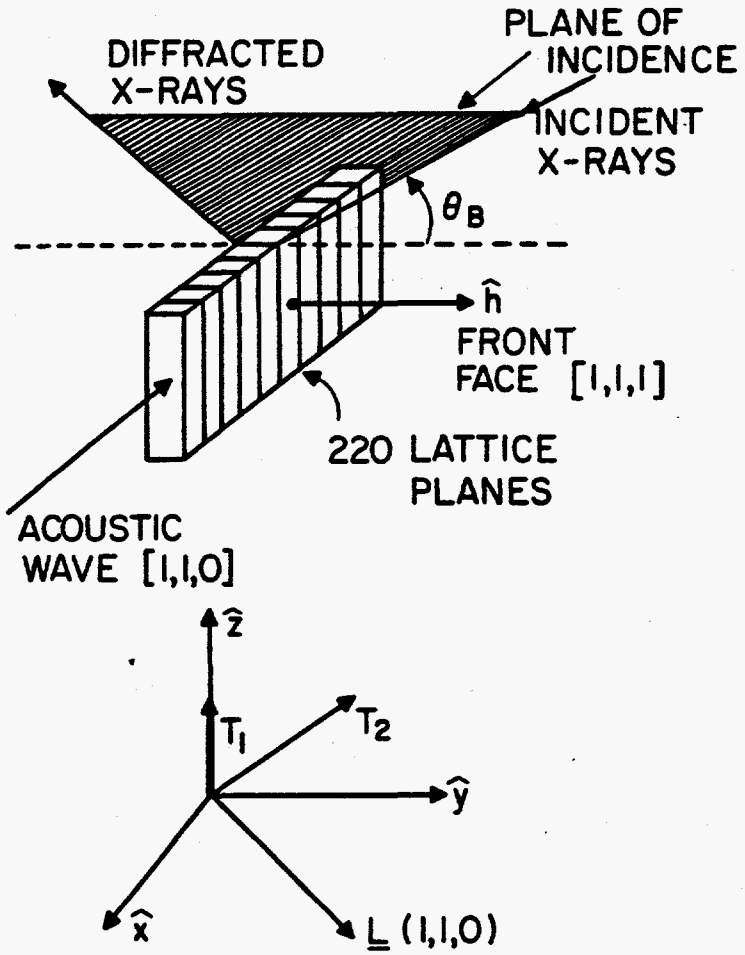

Figure 3-33. Acoustic propagation in a silicon single crystal slab.

$$\left.\begin{aligned} C_{11} &= 1.66 \\ C_{12} &= .639 \\ C_{44} &= .769 \end{aligned}\right\} \times 10^{12} \ \frac{\text{dyne}}{\text{cm}^2}$$

For waves propagating in the 110 direction, there are three possible modes of the lattice, one longitudinal and two transverse, whose polarizations are as shown in Fig. 3-33. The effective elastic constants for these modes are:

$$L: \ 1/2 \ (C_{11} + C_{12} + 2C_{44})$$

$$T_1: \ C_{44}$$

$$T_2: \ 1/2 \ (C_{11} - C_{12})$$

The transverse directions do not fall along the edge of the samples used in the present study so that the velocity of shear waves would be some average of v_{T_1} and v_{T_2}.

Most of the Borrmann topographs show an acoustic pattern that is more complicated than would be produced by a simple longitudinal mode. In particular, many of the nodal lines have small perturbations and waves in them. One possible explanation for this behavior would be local variation in the microscopic compressibility of the materials. This, however, seems unlikely in the case of the silicon samples used in the present study. They are carefully grown single crystal samples with a very low dislocation density. Certain individual perturbations

in the acoustic pattern might be due to dislocations, but on an overall basis, the small scale perturbations seem to occur too frequently (in a spatial sense) to be explained this way. Another explanation might be the weak excitation of modes other than the primary longitudinal one. In addition to the characteristic modes of the silicon lattice, each individual sample, of course, has its own overall acoustic modes characteristic of its macroscopic dimensions. All of the samples used in the present study were in the form of thin slabs. The problem of acoustic wave propagation in a slab is analytically soluble if the width of the cross section is large compared with the thickness.[13] This is approximately satisfied in most of the samples used. We note here that at the frequencies used in the present study, there might be a tendency to excite surface or Rayleigh wave modes.

In order to experimentally determine the nature of the acoustic field, a large number of topographs (@ 10 MhZ) were taken showing different views of the same crystal with the same acoustic field conditions. Each topograph showed about .5 cm^2 of the crystal. The photographic plate was aligned accurately normal to the diffracted beam. The acoustic fringe pattern on the plate thus represents a projection at the Bragg angle of the pattern in the crystal onto the plate. The excitation frequency was very accurately measured (±.01%) with a digital frequency counter.

Several densitometer traces were taken of each topograph. In taking some traces, the exit slit height was opened to average (over

the whole width of the pattern). In others, the slit height was reduced in order to study any localized behavior that might be present. The traces, however, produced nearly identical results with respect to both the average value and the statistical variation. Table 3-2 displays the results at 10 MhZ and at 22 MhZ, (where fewer topographs were taken). The calculated and measured values agree to well within the standard deviation of the measurement. This is strong evidence that the primary acoustic mode was pure longitudinal compression. This provides a justification for the model used in the theoretical calculations. It also suggests that if other modes of propagation are responsible for the detail in the acoustic pattern, that they are rather weakly excited.

f (MhZ)	Λ (mm) Measured From Topographs	Standard Deviation in Measurements	Calculated From Known Elastic Constants	Two Possible Values Calculated For Transverse Λ_{T_1}	Λ_{T_2}
10	.884	1.8%	.866	.549	.693
21	.429	2.3%	.415	.275	.335

f= frequency

Λ= acoustic wavelength

Table 3-2. Analysis of an acoustic standing wave pattern.

3.5 MODULATION EXPERIMENTS

This section describes experiments which directly demonstrate modulation and shuttering of x-rays by acoustic waves. Because of the low x-ray power available from the standard Coolidge type x-ray diffraction tubes, count rates from the phototube detector are typically on the order of a few KhZ. In addition, the standard pulse counting and discriminator circuits associated with diffractometry equipment respond very slowly to changes in x-ray count level. The diffractometry equipment available for the present work was limited to count rate changes (slew rate) of no faster than 100 hZ. In order to demonstrate fast interruption processes, special sampling circuitry

had to be constructed.

In order to demonstrate low frequency modulation of x-rays, the basic diffraction geometry shown in Fig. 3-3 was used. Fig. 3-34 shows the abrupt "turn on" and "turn off" of the acoustic perturbation. As the transducer was energized and de-energized, monitoring was both by a strain gauge bonded to the surface and by the x-ray transmission through the crystal. Likewise, Fig.3-35 shows sine wave modulation of the x-ray transmission through the crystal. The RF power driving the acoustic transducer was amplitude modulated at a rate of a few hertz. The left side of Fig. 3-35 shows the sin wave modulation of the acoustic strain as monitored by the strain gauge.

To observe transient (shutter-like) interruption on a reasonably fast time scale (of order of microseconds), the slow discriminator circuit used above was completely inadequate. Instead, a new sampling type measurement system was devised. A block diagram of the circuitry is given in Fig. 3-36. In typical experiments utilizing this circuit the transducer was excited with 10-20 micro second bursts of 10MhZ carrier frequency. The leading edge of each burst triggers the time to amplitude convertor (TAC). The next pulse from the x-ray detector "stops" the TAC which,in turn,outputs a pulse whose amplitude is proportional to the interval between start and stop pulses. By tuning the pulse height filter, one thus obtains a plot of the probability of an x-ray photon passing through the crystal vs. phase of the interrupting acoustic signal. (A multi-channel analyzer could perform the tuning process automatically and immediately provide a histogram of

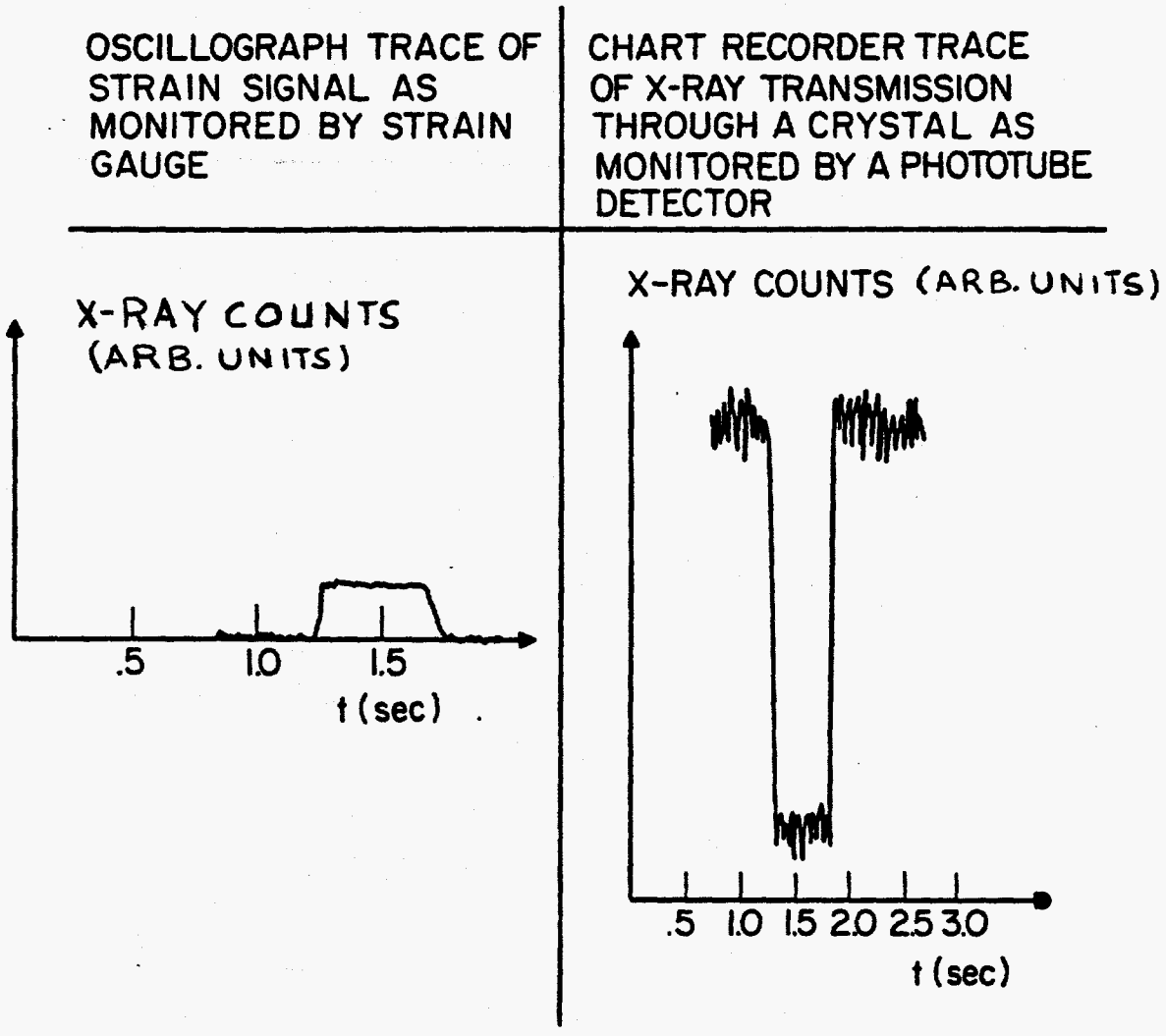

Figure 3-34. Strain and x-ray transmission signal responses to a burst of RF power applied to acoustic transducer.

OSCILLOSCOPE TRACE OF ACOUSTICALLY INDUCED STRAIN AS MONITORED BY A STRAIN GAUGE

CHART RECORDER TRACE OF THE X-RAY TRANSMISSION THROUGH A CRYSTAL AS MONITORED BY PHOTOTUBE SIGNAL

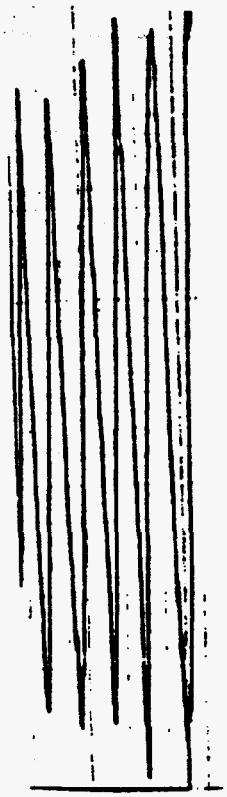

Figure 3-35. Sine wave modulation of x-ray transmission (Borrmann mode). AM modulated RF power is applied to the acoustic transducer.

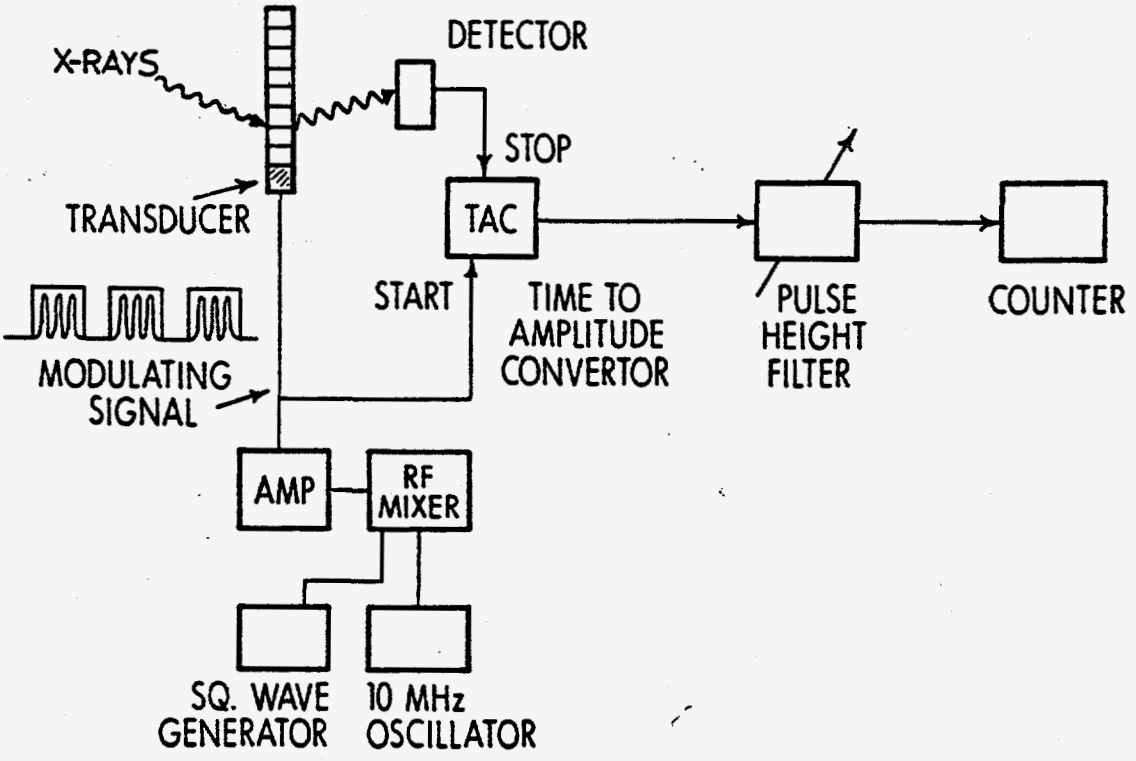

Figure 3-36. Electronic configuration used to observe transient interruption of Borrmann x-ray transmission.

number of pulses vs. pulse height and thus delay with respect to the exciting signal).

Fig.3-37 shows a typical trace obtained with the sampling system. The duration of interruption of x-ray transmission is slightly more than that of the acoustic burst, since one acoustic reflection passes back through the x-ray transmitting region. This also explains the somewhat slower fall time than rise time. Only one acoustic reflection was important, as was later confirmed by acoustic reflection pictures like those presented in the strain measurement section.

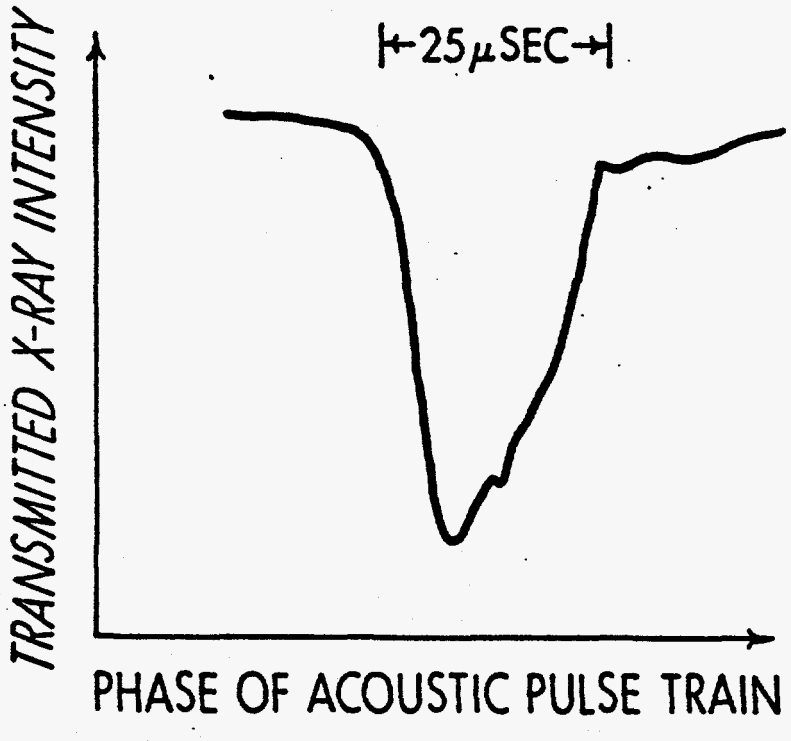

Figure 3-37. Borrmann x-ray transmission through a silicon crystal as a function of the phase of an acoustic pulse train.

CHAPTER 3 REFERENCES AND FOOTNOTES

1. Hauer, A., "Methods for the Control and Measurements of X-rays", U.S. Patent Serial No. 594846 (issued 11/19/76)

2. Barrett, C.S., Structure of Metals, McGraw Hill (1943)

3. Smithells, C.J., Metals Reference Book, Butterworths (1945)

4. Batterman, B.W., "Effect of Thermal Vibrations on Diffraction From Perfect Crystals," Phys. Rev. 126 p. 1461 (1962).

5. Hunter, L., "X-ray Measurements of Microstrain in Germanium Single Crystals," J. App. Phys. 30(6), p.874 (1958).

6. Meiren, E.S., "Application of X-ray Topographical Technigues to the Study of Semiconductor Crystals and Devices", Siemans Rev. XXXVII (1970).

7. Beyer, R.T., Letcher S.V., Physical Ultrasonics, Academic Press (1969).

8. After completion of the work described in this chapter, it was discovered that a slightly similar method for measuring bond transmissions has been published by Redwood and Lamb Proc IEE. (Pt. B) 103 P773 (1955). Their method does not involve the use of phenyl salicylate.

9. Cook, B.D., Hiedemann, E.A., "Diffraction of Light by Ultrasonic Waves of Various Standing Wave Ratios", J. Acoustical Soc. Am. 33 (7) p. 945 (1961).

10. Bonse, U., Hart, M., "Tailless X-ray Single Crystal Reflection Curves Obtained by Multiple Reflection", Appl. Phys. Lett., p.238 (1965).

11. Authier, A., "Contrast of Dislocation Images in X-ray Transmission Topography", Advances in X-ray Analysis, 10 (46), p.9. (1967)

12. Kittel, C., Introduction to Solid State Physics (3rd.ed.), p.120 Wiley (1966)

13. Morse, R.W., "Dispersion of Compressional Waves in Isotropic Rods of Rectangular Cross Section", J. Acous. Soc. Am. 20(6) p.833, (1948)

CHAPTER 4

DEVICE APPLICATIONS AND POTENTIAL DEVICE PARAMETERS

4.1 Methods of Excitation of Crystal Perturbations.

- 4.1-1 Typical Frequencies and Bandwidths of Lattice Vibrations
- 4.1-2 Optically Induced Solid Perturbations
  - 4.1-2(a) Stimulated Brillouin and Raman Scattering
  - 4.2-2(b) Piezoelectric Effects
  - 4.1-2(c) Thermal Heating of Diffracting Lattice Structures
  - 4.1-2(d) Laser Induced Shock Waves and Shock Induced Surface Effects
- 4.1-3 Microwave Ultrasonics

4.2 X-Ray Diffraction Constraints on Device Parameters.

- 4.2-1 Crystalline Parameters and Their Relation to Device Design
  - 4.2-1(a) Fast Shuttering
  - 4.2-1(b) High Frequency Modulation
- 4.2-2 Control of Diffraction Sensitivity

4.3 Typical Modulator Design

4.1 METHODS OF EXCITATION OF CRYSTAL PERTURBATIONS

The theme of the present work has been an investigation of changes in x-ray propagation induced through perturbation of the structure of the x-ray scattering material or, in other words, changes in the spatial configuration of x-ray scatterers. Ideally, such a study could encompass molecular structure changes that can cause significant x-ray diffraction effects in liquids or gases[1][2]. We will, however, limit the discussion to perturbations of crystal lattice structure in the case of bulk x-ray diffraction and to simple to macroscopic surface perturbation in the case of surface scattering of x-rays.

Certainly, one of the characteristics of x-ray modulating and shuttering devices that is of particular interest is their ultimate speed. We have demonstrated shuttering and modulation in the microsecond regime experimentally in the present study. This speed can certainly be improved upon, and calculations will be presented in this chapter indicating the fundamental limitations on temporal characteristics that x-ray shuttering and modulation devices might be expected to have.

Going to higher frequencies offers the possibility of achieving a higher strain gradient, which, as we have seen in Chapters 2 and 3, is the primary parameter of interest for controlling x-ray diffraction.

With these objectives in mind, in the present section we present an analysis of the basic vibrational properties of crystalline solids.

This analysis deals with the typical frequencies (bearing on potential strain gradients) and bandwidths (relating to potential speed of excitation) which characterize lattice vibrations.

With the basic framework for the study of lattice vibrations having been laid, the question of methods of excitation (and their limitations) is then addressed.

4.1-1 TYPICAL FREQUENCIES AND BANDWIDTHS OF LATTICE VIBRATIONS

In analyzing the vibrational properties of solids, we are dealing with a broader class of phenomena than is implied by the word acoustic. We are treating the general case of the relative motion of the atomic x-ray scattering centers in the solid.

Any solid has two types of vibrational resonances associated with it. First are vibrational modes associated with the macroscopic dimensions of the solid. (This characteristic is primarily applicable to x-ray modulating devices using steady state or quasi steady state ultrasonic waves and will be discussed in the next section.) In this section, we will be primarily concerned with the microscopic perturbations to the lattice structure.

The atomic lattice structure of a solid possesses a large number of vibrational modes (the number of modes being equal to number of atoms composing the lattice[2][3]. The frequency spectrum involved extends from 0 HZ to around 10^{13} HZ, and in many cases, well above 10^{13} HZ. The complete description of the vibrational spectrum of complex solids constitutes a very complex problem, many aspects of

which are still areas of active research.[3] Many of the general characteristics of the vibrations can, however, be predicted by rather simple models. We find these models adequate to characterize the general constraints on speed of excitation that would be present in x-ray shuttering devices.

The two simplest forms of a lattice are monoatomic (with one atom per unit cell) and diatomic (with two atoms per unit cell) models. These idealized models are discussed in all text books on solid state physics.[4][5] One usually assumes interatomic forces to act only between nearest neighbors and only along the lines between atomic centers. The problem of the vibrational spectrum reduces to that of an ensemble of coupled harmonic oscillators to which plane wave solutions are sought. Figure 4-1(a) shows examples of typical dispersion curves that result for monoatomic and diatomic lattice structures. A distinct feature of these curves is that the diatomic dispersion characteristic has an additional branch not present in the monoatomic case. This additional branch is referred to as the optical branch. This terminology arises from the fact that adjacent atoms vibrate in an opposite sense, so that if the binding is such that charge separation is caused by this mode, an electromagnetic wave could couple energy in directly. The frequencies involved generally correspond to the far infrared.[6]

The type of motion implied by these lattice modes is illustrated in Figures 4-1(b)and 4-1(c). An example of a typical scale that would be assigned to dispersion curves, such as those in Fig.4-1 is shown

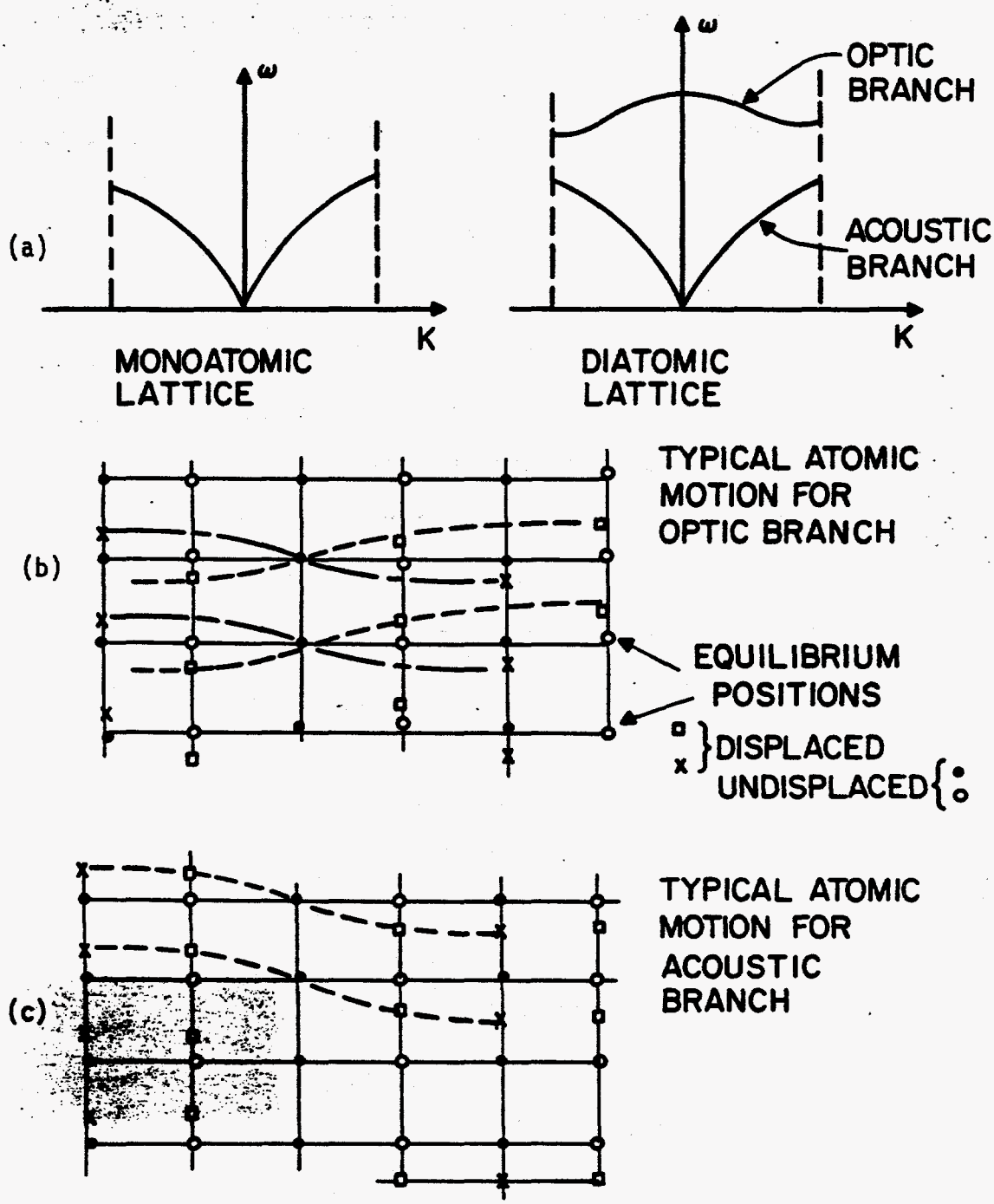

Figure 4-1. Dispersion characteristics and typical atomic motion for crystal lattice vibrations.

Figure 4-2. These values were experimentally determined[7] for a simple cubic (salt) lattice structure. Resonant frequencies are on the order of $2x10^{12}$ HZ for the acoustic modes and about $4x10^{12}$ for the optical modes. In some other solids, there can be as much as an order of magnitude difference in the frequencies of acoustic and optical modes.[3]

The frequency of vibrational modes depends on the type of interatomic binding (and, thus, the energy level structure of the solid) which affects the force constants to be used in the simple model described above,[4] on the mass of the atomic species, and on the characteristic spacing of the atoms.

A limited amount of detailed information is available on the bandwidths of individual vibrational modes. Experimentally, these quantities are usually determined by Raman scattering. In addition, the simple lattice models have proved adequate to make rough estimates of vibrational bandwidths.[8] Eckhardt has estimated that bandwidths will usually lie between $6x10^{10}$ and $2x10^{12}$ sec^{-1}.

An interesting example of the vibrational bandwidth of an optical mode is the so-called A_1 mode of calcite (which is composed of an in plane expansion and contraction of the carbonate $(CO_3)^{2-}$ radical). This is of particular interest because a very detailed experiment[9] has been performed on the optical excitation (by stimulated Raman scattering) of this mode of calcite. Krishnon[10] has studied this mode and concluded that the vibrational frequency is about $3x10^{13}$ HZ and a bandwidth of 10^{12} HZ.

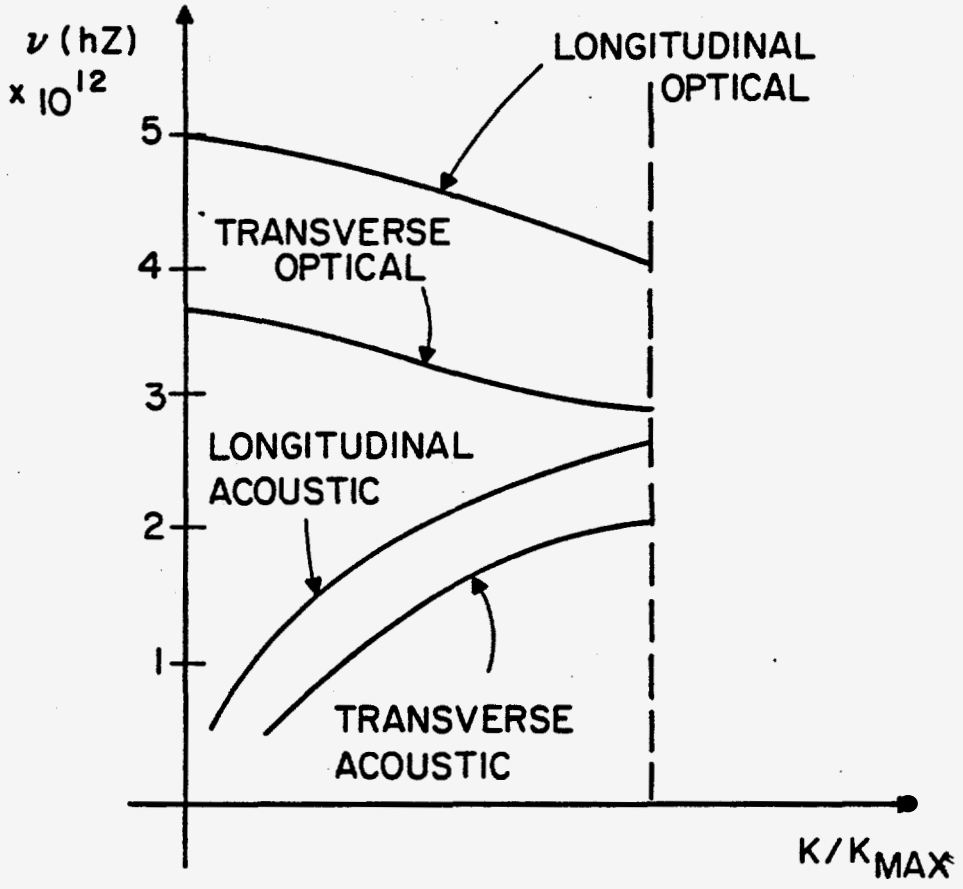

Figure 4-2. Experimentally determined dispersion curves for simple cubic lattice structure.

In a solid one is, thus, usually dealing with vibrational modes that range in frequency from about 10^{12}HZ to few times 10^{13}HZ and bandwidths between 10^{10} and $3x10^{12}$ HZ. Thus, it would seem that the lattice could potentially be excited with rise times ranging from 1 to 100 picoseconds. This is, of course, critically dependent on the method of excitation.

The complete lattice spectrum extends over many modes and a very large frequency bandwidth. The thermally excited spectrum of solids has been studied experimentally with the use of x-rays and neutrons[10] and usually extends from OHZ to well over 10^{13}HZ. If we excite a large number of modes in the solid (such as by raising the temperature), a broad vibrational spectrum will be involved and, thus, the processes can probably be excited rapidly. On the other hand, the atomic motion produced by such a process is quasi random. In this case, the only reduction in x-ray diffraction will be due to the Debye-Waller factor, as outlined in Chapter 2 (section 2.7).

4.1-2 OPTICALLY INDUCED SOLID PERTURBATIONS

If fast rise time switching and shuttering were the primary consideration, optical excitation methods would probably be the only practical ones. Sub-nanosecond pulse technology is well developed in the optical regime, where laser mode locking, in conjunction with other electrooptic technology, can be utilized. Since the most likely applications for fast x-ray switching would be associated with laser systems, the logical control mechanism would be ultra

fast laser pulses. Probably, the best known methods of optical excitation are the stimulated scattering processes and laser induced shock waves.

4.1-2(a) STIMULATED BRILLOUIN AND RAMAN SCATTERING

Lattice vibrations in solids may be excited optically through the processes of stimulated Brillouin (SBS) and stimulated Raman scattering (SRS). In solids, the distinction between Raman and Brillouin scattering is that the former occurs when optical modes are excited, while the latter involves the excitation of acoustic modes.

Brillouin[12] first suggested that one could observe an optical frequency shift from thermally excited acoustic modes. With the advent of lasers and the very high power densities they can produce, stimulated scattering processes have become possible. When stimulated effects occur, particular vibrational modes are excited by the input light field. A parametric process is, thus, established where energy is fed from the input light into a shifted electromagnetic mode whose frequency differs from the input by the vibrational frequency.

The coupling of the optical field to the lattice in the case of SBS is different than SRS and the two processes will be discussed separately.

With stimulated Brillouin scattering, the coupling of the field to the lattice is accomplished via the phenomena of electro-

striction. An electromagnetic wave propagating in a medium can create an acoustic wave through the phenomena of electrostriction.[13][14] Electrostriction is a second order effect in electric field strength and occurs in all dielectric media, regardless of crystal symmetry. The electrostrictive pressure can be expressed as

$$p = \gamma E^2 \qquad (4\text{-}1)$$

where $\gamma = \rho \frac{d\varepsilon}{d\rho}$

ε = dielectric constant

ρ = density

In cgs gaussian units, γ is of the order of unity[14] (for most materials). We have tabulated (Table 4-1) the strain that would be induced in several available single crystals as a function of optical field strengths. The elastic modulus that has been used in these calculations is the bulk modulus. In particular scattering experiments, it would, of course, be more appropriate to use elastic constants associated with a particular crystallographic direction. Our purpose here, however, is to provide an estimate of the strain levels that can be achieved using electrostriction.

The smallest strain that would be of value in shuttering experiments is probably of the order of 10^{-6}. As can be seen from Table 4-1,

MATERIAL	FIELD STRENGTH (VOLTS/cm)	FLUX DENSITY (WATTS/cm^2)	STRAIN
SILICON	10^4	10^6	$6x10^{-10}$
	10^5	10^8	$6x10^{-8}$
	10^6	10^{10}	$6x10^{-6}$
	10^7	10^{12}	$6x10^{-4}$
KCL	10^4	10^6	$3.9x10^{-9}$
	10^5	10^8	$3.9x10^{-7}$
	10^6	10^{10}	$3.9x10^{-5}$
	10^7	10^{12}	$3.9x10^{-3}$
LiF	10^4	10^6	$8.7x10^{-10}$
	10^5	10^8	$8.7x10^{-8}$
	10^6	10^{10}	$8.7x10^{-6}$
	10^7	10^{12}	$8.7x10^{-4}$

Table 4-1. Stimulated Brillouin Scattering.

very high flux levels are required to approach this level with electrostriction. The damage level for most optical materials is below 10^{10} WATT/cm^2. A more detailed discussion of optical damage levels is given in the latter part of this section.

The second question that must be answered in relation to the use of SBS for production of lattice perturbations involves the speed with which the acoustic waves can be excited. Chiao, et al.[14] have noted that if frequencies at both the primary and shifted (ω light + Ω acoustic) are present in the input beam, a resonant shock is applied to the solid. They estimate that the strain builds up to a very significant level in the reciprocal of an acoustic cycle. Since acoustic frequencies in typical SBS experiments are around 20 GhZ, we would expect a rise time of the acoustic fields to potentially as fast as a few tens of picoseconds.

Stimulated Raman experiments (in which optical branch lattice vibrations are excited) have been performed in a variety of solids.[6] The frequencies bandwidths are much larger (as much as an order of magnitude greater than acoustic branch) than the SBS case. The rise times that are potentially available, thus, start to approach a few picoseconds.

In addition to higher frequencies, SRS also offers the advantage of potentially more efficient coupling of optical energy into vibration (compared to SBS). The sequence of processes that lead to stimulated Raman scattering is the following. A strong input optical wave is scattered by a particular thermally excited optical vibration mode.

The scattered wave which is shifted in frequency beats with the input. This beat frequency modulation can in turn directly couple into and drive the vibrational mode in a type of feedback process. If the input is strong enough, a net amplification can occur, thus, leading to very large vibration and high conversion efficiency of input to scattered light.

In parametric processes such as SBS and SRS, the coupling efficiency of optical into vibrational energy is limited by the phase matching conditions implied by the Manley Rowe relations[14] (or, in other words, by the ratio of optical to acoustic frequencies). Going to the higher frequencies allowed by Raman scattering should, thus, permit greater efficiency of transfer of energy to the vibrations.

In the experiment performed by Giordmaine and Kaiser[9] in calcite, they estimated that the displacement of the oxygen atoms (in the stretch mode of the CO_3^{2-} ion) to be 2×10^{-6} Å for a power density of 10^7 WATTS/cm^2. Although the type of motion occurring in this experiment would not be appropriate for controlling x-ray scattering (most of the x-ray scattering power is primarily concentrated in the calcium atoms, for example, for (211) reflection f_{Ca}~15, f_C~3.4, f_O~6), it gives one a good idea of the magnitude of vibration amplitude that could be reasonably excited.

Stimulated Raman scattering would, thus, seem to be both more efficient and have a potentially faster rise time (2-10 times) than stimulated Brillouin processes.

The flux levels required to excite SBS and SRS are near the damage level for most materials. In fact, SBS and SRS are often cited as possible mechanisms producing optical damage.[15]

Since little information seems to be available on optical damage levels in semiconductors[16][17] (silicon being of prime interest in this study), an experimental test of laser damage thresholds was performed as part of the present study. The experimental configuration used is shown in Figure 4-3. A single 100-200 p.s. pulse from a mode locked Nd glass laser was focused onto the surface of a silicon sample. The energy varied between 5-40 millijoules. The damage was evaluated primarily by investigation of the sample under a microscope. Observation of the uniformity of transmitted light (from a CW Yag laser) through the sample was also used.[18] The threshold for damage seemed to occur at the relatively high level of 5×10^9 WATTS/cm^2. For SBS, we see from Table 4-1 that this flux level corresponds to the relatively low strain magnitude of 6×10^{-7}.

In closing this section on stimulated scattering processes, we note that laser damage studies on glass and some crystals[15] indicate that the damage was primarily due to acoustic phonons of frequency toward the higher end of the acoustic phonon spectrum.

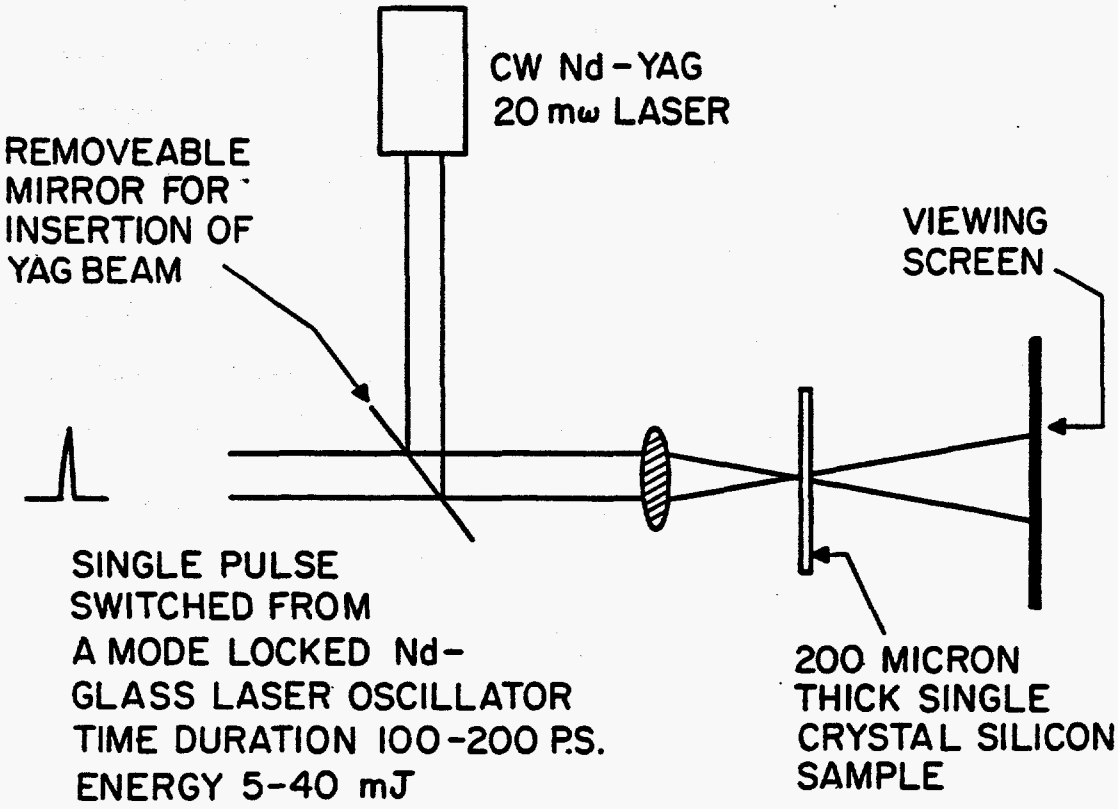

Figure 4-3. Experimental configuration used to determine the optical damage thresnold in silicon single crystals.

4.1-2(b) PIEZOELECTRIC EFFECTS

By far, the most common way of exciting acoustic perturbations in solids is the use of the piezoelectric effect. By reason of their symmetry, many crystalline solids can have a strain induced in them through direct application of an electric field. As contrasted with electrostriction, piezoelectricity is linear in the applied field. The following equation is traditionally written to describe the piezoelectric effect.[19][20]

$$T_x = C_{xx} \nabla u - e_{xx} E_x \qquad (4\text{-}2)$$

T = stress, ∇u = strain, E = electric field.

The constant quantities C and e in 4-2 are, in general, tensor quantities. We write 4-2 for the simple case where an E field applied along the x direction results in a strain along the same axis. When no externally applied stress is present, the quantity d=e/c relates the piezoelectrically induced strain to the applied field. A typical value for d in quartz[19] is 3×10^{-2} cm/volt. (Many materials have much higher d values, $BaTiNO_3$ being two orders higher.) A field strength of 10^4 v/cm would, thus, produce a substantial strain of 3×10^{-6}. (The field strength of 10^4 v/cm is equivalent to an optical flux density of 10^6 WATTS/cm^2.)

Unfortunately, it is not possible to couple optical energy (with $\nu \approx 5 \times 10^{14}$) directly into piezoelectric strain efficiently. Optical

frequencies are far above any lattice resonances, and, thus, can only cause slight perturbations. Several methods exist[21][22], however, for rectifying subnanosecond optical pulses. Subnanosecond electrical pulses can also be produced by optically induced switching techniques[23]. One that is of particular interest[21] uses the pyroelectric effect (which is quite similar to the piezoelectric effect). A polarization is produced due to the heating of the lattice, caused by the input subnanosecond optical pulse. Given that it is possible to produce intense subnanosecond rise time electrical pulses, the question that does not seem to have been considered is: How fast can such a pulse excite piezoelectric strains in a solid?

The answer to the question of piezoelectric strain rise times lies in an analysis given by Jacobsen.[20] In this paper, he analyzes the spatial location of the sources of acoustic waves in a piezoelectric solid perturbed by an electrical pulse. He has rewritten the elastic wave equation in a form that shows clearly the nature of the driving term.

$$\nabla_x^2 u - 1/v^2 \frac{\partial^2 u}{\partial t^2} = \nabla_x \left[d_{xx} E_x (t) \right] \qquad (4\text{-}3)$$

From 4-3, we see that it is the spatial gradient of (d E) (piezoelectric stress) that is the source of acoustically induced strain. Normally, when an electrical pulse is applied to a solid, the strongest gradient in the stress is at the surface, where an approximately discontinuous change in the stress occurs. Jacobsen was primarily

considering the case of a tone burst (of microwave power) applied to the solid. In this case, he showed that in order to have any other acoustic source comparable in strength to the surface effect, the spatial gradient (of the envelope), the field would have to be of the order of the acoustic wavelength.

We are interested in non-modulated bursts of the order of 10^{-10} sec. For such a pulse, an effective acoustic wavelength would be of the order of 7000 Å. At any instant of time, the spatial extent of 10^{-10} sec electrical pulse is 3 cm, which clearly produces no significant spatial field gradient.

A 10^{-10} second laser induced electrical pulse applied to a piezoelectric solid would, thus, produce the following effects. As the electrical pulse passes by any particular point on the solid surface, a sharp shock is applied to a very thin layer near the surface. A region of the order of the acoustic wavelength is, thus, affected almost instantaneously. Thereafter, the acoustic disturbance propagates into the interior of the solid at the acoustic velocity.

One would like to know if the surface effect represents the fundamental limitation on pulsed excitation of piezoelectric strain.

The limitation of surface generation could be removed if strong internal field gradients could be produced. A suggestion for the production of large field gradients is proposed as part of this study. The fundamental nature of the idea is indicated in Figure 4-4. The beam from a mode locked, frequency doubled Nd laser would be split in two and recombined inside the crystal to form an inter-

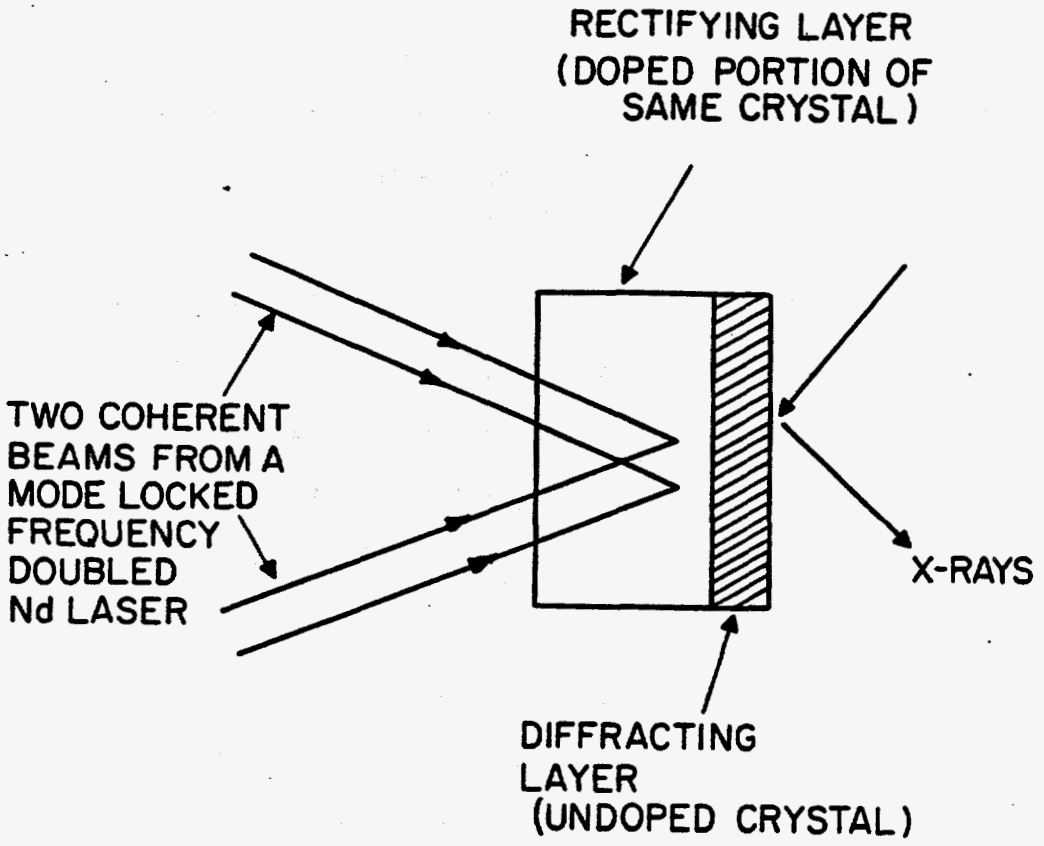

Figure 4-4. Illustration of a method for the production of bulk acoustic perturbations by a piezo-electric interaction.

ference pattern.The rectifying layer is separated from the diffracting portion since most of the schemes for producing optical rectification require a doping of the crystal that would probably interfere with the x-ray diffraction process. The interference pattern would lead to a large spatial gradient in field (over a few thousand angstroms) and, thus, bulk generation of acoustic waves. The volume over which interference occurs would be located very close to the undoped diffracting layer for two reasons. The close proximity would prevent a significant spreading of the electrical field pattern (and, thus, avoid averaging out of the spatial gradient). This will also prevent any significant dispersion broadening of the pulse.

Another method for establishing large field gradients would be to establish an internal grating-like structure of charge carriers. Such an experiment has been performed by Shiren[24] and others. Such structures are produced initially by acoustic waves and the resultant charge separation caused by propagation in a piezoelectric medium. The structure, once established, will remain for long periods if the solid is cooled to liquid He temperatures by acoustic waves. It has been demonstrated (although on a much slower time scale than that which is of interest in our proposed x-ray switching applications) that such a structure will produce bulk acoustic generation when an r-f burst is applied. Since the process involves the conduction electrons of the solid, it would probably not significantly affect the x-ray scattering properties.In addition bulk waves have been demonstrated in several crystals that can easily be grown

with adequate perfection for x-ray diffraction work (for example, GaA, which has the same diamond cubic structure as silicon and gemanium). A particular drawback to the use of this method, however, is the need to keep the crystal at liquid helium temperature.

4.1-2(c) THERMAL HEATING OF DIFFRACTING LATTICE STRUCTURES

In this section, we present calculations that characterize the limitations on the control of x-ray propagation through heating of the lattice. The transfer of heat energy by absorption of a laser pulse could, for example, take place on a very fast time scale. It has been experimentally shown that absorbed laser energy could be transferred to lattice energy in a time interval on the order of 20 picoseconds.[22]

As a control mechanism itself, however, lattice heating would usually be too inefficient to be practical. A study of the processes is, however, a crucial step in understanding the limitations on x-ray switching and shuttering processes.

Calculations in the present section are based on the Debye-Waller factor[1], as shown in Equation 2-60. Experimental[26] and theoretical[25] results indicate that this factor is only an approximation to the behavior of x-ray diffraction in real solids. In a complete analysis, two corrections to the Debye-Waller factor must be considered[26]. First, the exponent in the Debye-Waller factor must be multiplied by a weakly temperature dependent correction factor. Secondly, a correction factor that accounts for multiple reflection (dynamical) effects must be considered. However, the normal (kinematical) Debye-Waller calculation is sufficient to estimate the performance limitations of thermal processes in modifying the x-ray diffraction from a crystal.

Consider the diffracting geometry illustrated in Figure 4-5.

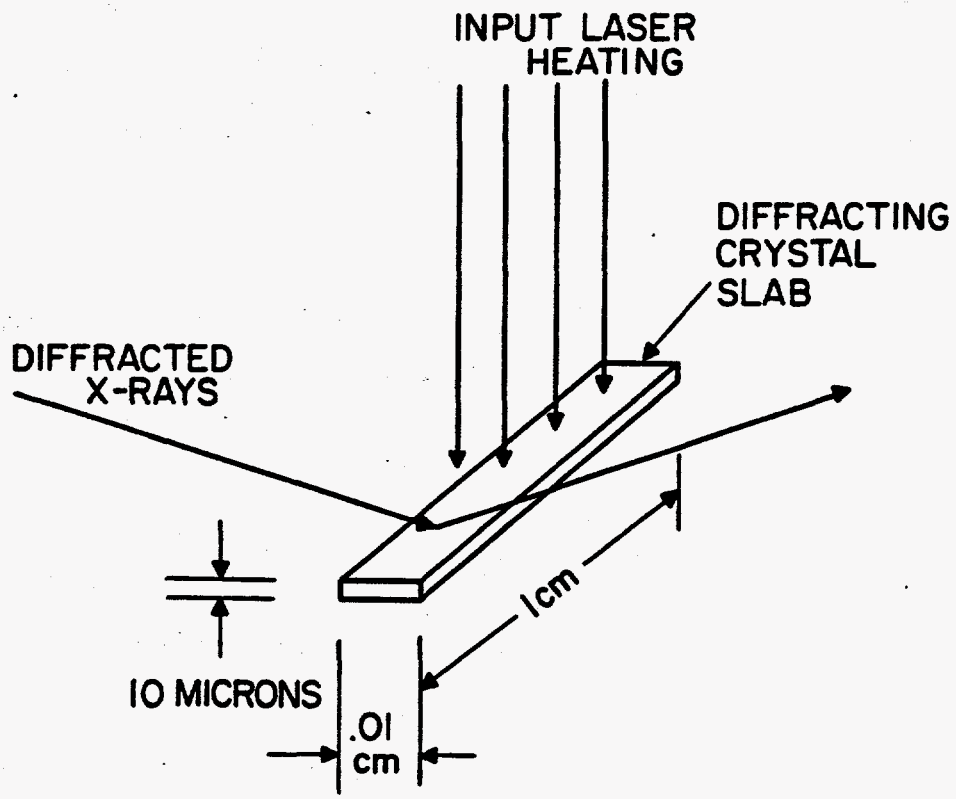

Figure 4-5. Thermal Heating of Diffracting Crystalline Material.

A crystal slab 1 cm x 10^{-2} cm x 10^{-3} cm is shown diffracting in the Bragg geometry. This represents a typical useable diffracting volume, such as one might encounter in an x-ray spectrometer.[27]

To calculate the required temperature rise for given reduction in diffracted intensity, values for the Debye-Waller factor tabulated in the International X-ray Crystallography Tables[28] were used. The required heat depostion for the volume of crystal shown in Figure 4-5 was calculated using known specific heats. Table 4-3 shows the results of these calculations for silicon and NaCl. As expected, the reduction in diffraction becomes larger for atomic planes with small 2d spacings (i.e., reflections with large values of sin θ/λ).

It is possible to deposit 10^{-2} joules in the 10^{-5} cm^3 on a subnanosecond time scale. Such an experiment requires, however, a large pulsed laser system. The large amount of energy needed could, thus, not be thought of as a switching beam (i.e., auxiliary to other laser heating experiments). X-ray diffraction from a laser heated medium could, however, have other useful applications, which will be discussed in Chapter 5.

Our primary interest here is in the magnitudes of perturbation, shown in Table 4-2. The magnitudes of rms atomic displacement were calculated from experimental data for silicon[28] and NaCl[1]. We define the following quantity, which, in some textbooks[5] on solid state, is referred to as an effective "strain".

MATERIAL	REFLECTION	TEMP./HEAT RISE DEPOSITED TO REDUCE DIFFRACTED INTENSITY BY 1/2 (°C / Joules)	RMS EXCURSION OF ATOM (PERPENDICULAR TO LATTICE PLANES) ABOUT LATTICE POINT AT ELEVATED TEMP. (Å)	"STRAIN", e, CAUSED BY ATOMIC MOTION
SILICON	220	5800°/ .10	.340	6.9×10^{-2}
	440	920°/1.6×10^{-2}	.17	5×10^{-2}
	444	430°/7.5×10^{-3}	.13	4×10^{-2}
NaCl	400	1550° /3×10^{-2}	*.175	4.3×10^{-2}
	800	850°/1.65×10^{-2}	*.133	8×10^{-2}

*Average of Na and Cl movement.

Table 4-2. Effect of elevated temperature on diffraction.

$$e = \frac{d(T) - d(300)}{2d}$$

where $d(T) = \left[\begin{array}{l}\text{Rms atomic displacement} \\ \text{at elevated temperature} \\ T\end{array}\right]$

$$d(300) = \left[\begin{array}{l}\text{Rms atomic dis-} \\ \text{placement at} \\ 300^{o}\ K\end{array}\right]$$

$$2d = \left[\begin{array}{l}\text{2d spacing of particular} \\ \text{reflection involved}\end{array}\right]$$

The quantity e is a useful parameter that can be compared with the genuine strain induced by narrow bandwidth acoustic waves.

A large rms vibration of the atoms is, of course, always present at room temperature. As can be seen from the last column of Table 4-2, however, even the change in rms amplitude due to elevated temperatures results in effective strains (compared to ordinary acoustically induced strains).

The reason for the small effect on x-ray scattering is essentially one of coherence. First, a large part of the thermal energy goes into motion that has no effect on any particular reflection (such as in plane motion of the atoms). Even taking this into account, however, the rms displacement normal to the lattice planes is still very large. The random displacement of the scattering centers leads to an averaging out of any disruption of the x-ray interference. The situation is analogous to a random array of diffracting apertures, which still leads to a sharp Fraunhofer diffraction peak.

We, thus, see that the highly random motion that is induced by thermal heating is not as effective in reducing diffracted x-ray intensity as monochromatic strain. We have seen earlier that monochromatic strains of the order of 10^{-5} can reduce diffracted intensity by about .5. The atomic motion in such a case is, thus, far less than the thermally induced atomic displacements shown in Table 43.

The thermal process involves excitation of the full vibrational spectrum of the solid, and, thus, represents the largest bandwidth excitation mechanism possible. Thus, in evaluating a method of lattice perturbation, an important consideration is the number of modes that would be excited by the process.

4.1-2(d) LASER INDUCED SHOCK WAVES AND SHOCK INDUCED SURFACE EFFECTS

Recently, several papers have been published[29],[30] describing the use of high power lasers for exciting intense shock waves in solids. When a high power laser pulse is absorbed in a thin layer near the surface of a solid, a large thermal gradient can be created. This results in a strong shock wave being propagated into the unheated solid material. With subnanosecond pulsed lasers, it is possible to deposit energy in very short periods of time, thus producing temporally very sharp shocks. Shocks with subnanosecond rise times have been produced in this way[29]. Laser induced shock waves provide a possible method for fast switching of x-ray radiation.

The potential rise times of solid shock waves are limited by the impulse response of the solid, described earlier in this chapter. Excitation of a large number of modes of the solid lattice (as will happen with a thermally induced shock) is not a severe limitation (in terms of x-ray effects) in this case. Large (multi-kilobar) pressure gradients can be established[29] which would provide strain in any specified direction. One expects shock rise times of at least 100 p.s. to be attainable.

Even though temporally sharp shock waves can be excited, the time required to affect a region that is diffracting or scattering x-rays is still essentially limited by the acoustic velocity. As shown in previous sections, however, the dimensions of such regions can (in many cases) be quite small. Limitations imposed by acoustic transit times will be discussed in Section 4-2.

A special method for producing laser induced shock waves has been described by Auth[31]. He proposes interfering two optical beams on the surface of a solid or liquid. The preferential heating caused by the interference pattern will induce very large thermal gradients that will relax into acoustic waves. We propose here a use of the same experimental configuration for a somewhat different purpose.

Consider the two laser heating schemes, shown in Figure 4-6. In Figure 4-6a, the laser radiation is absorbed over a substantial volume of the solid. The regions of high thermal absorption (high field) expand, beginning the process that leads to acoustic wave propagation. We are interested here only in the initial stages of the first cycle of this process. Formation of sine wave pattern will require one transit (at acoustic velocity) of the acoustic wavelength Λ. This transit time interval represents a delay with respect to the exciting laser pulse, and not the rise time of the process.

As was shown in Chapter 1, surface perturbations of the order of a few hundred angstroms are useful in diffracting x-rays. At this point, let us consider typical orders of magnitude. With a frequency doubled Nd laser (λ=.56μ), one should be able to produce fringe spacings of about 0.4μ. For typical acoustic velocities, this implies a frequency of about 12.5 GhZ. The acoustic rise time for a 200 Å perturbation would be about:

$$t_r = \frac{2\times10^{-6}\ \text{cm}}{5\times10^{+5}\ \text{cm/sec}}$$

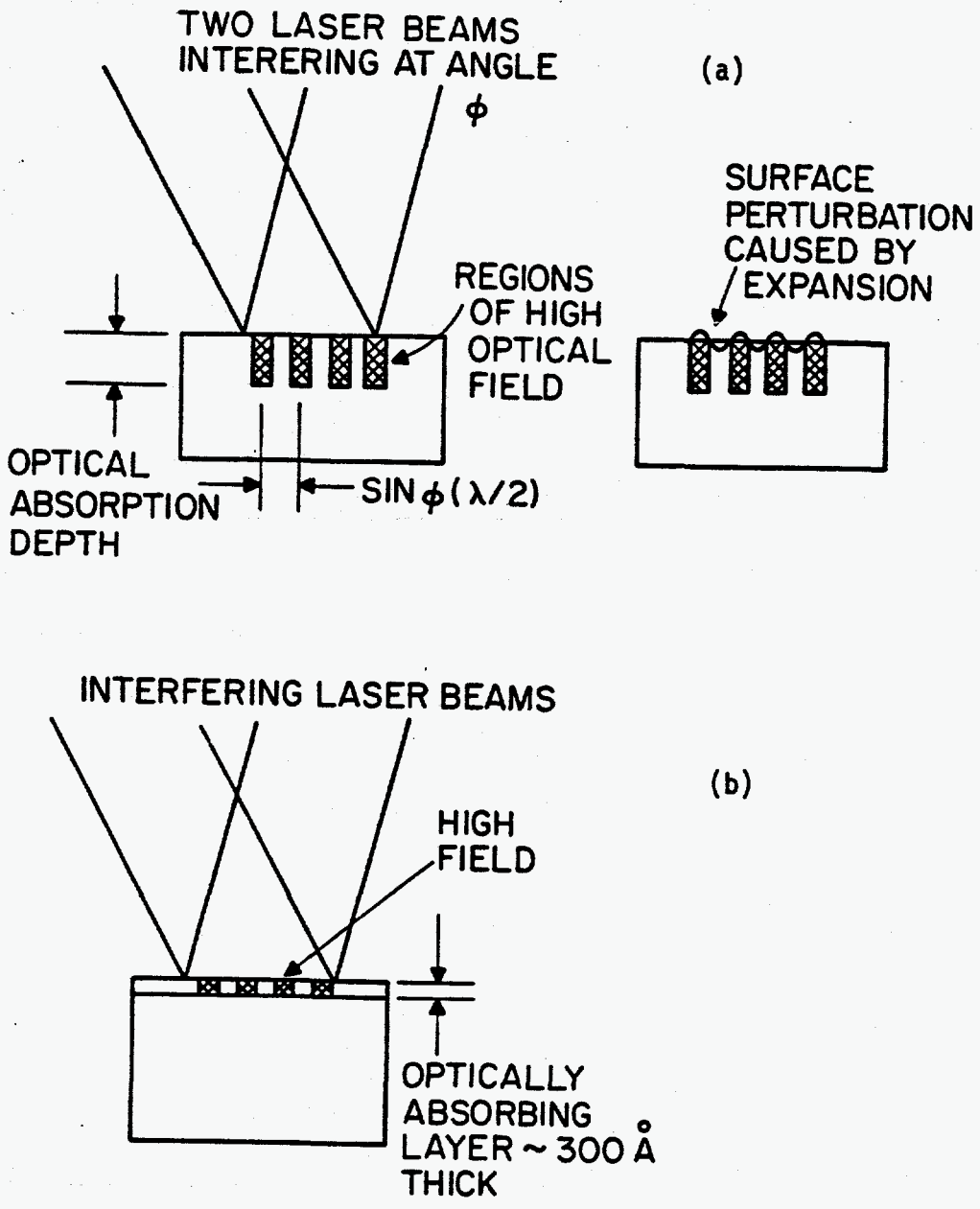

Figure 4-6. Surface perturbations resulting from laser induced shocks. (a) bulk absorption (b) surface absorption

$t_r \simeq 4$ p.s.

The second method for producing acoustic waves is illustrated in Figure 4-6b. Here, the optical absorption is confined to a thin layer by coating the solid with a film specially prepared to enhance optical absorption. With a thickness of only a few hundred angstroms, the film could be made to negligibly absorb x-rays. In the regions of high field, micro shocks will be applied to the surface. In this situation, no delay time would be involved.

4.1-3 STEADY STATE AND PULSED MICROWAVE ULTRASONICS

In the experimental part of this thesis, tests were described that employed cw acoustic waves of frequency up to 60 MhZ. With techniques that have been developed over the past ten years, this frequency can be increased to about 5 GhZ[32] without great difficulty. The most common method employs a block of piezoelectric material cut to be an integral part of a microwave cavity.[20] The field and piezoelectric stress gradient across the free surface of the material forms the source of sound.

Such techniques provide the methods needed for ultra high frequency modulation of x-rays, as will be described later in this chapter. The basic limitation to increasing the frequency is the larger acoustic absorption encountered at higher frequencies[32]. Nevertheless, there are materials that exhibit low loss (the most widely studied are $LiNbO_3$ and $LiTaO_3$[32]) at frequencies up to 5 GhZ, and can be grown with a

reasonable degree of crystalline perfection. Operation at frequencies higher than 5 GhZ generally requires cooling the material to cyrogenic temperatures.

Keeping in mind the application of acoustic wave diffraction of x-rays, we show in Table 4-3 the acoustic wavelength for longitudinal propagation in various materials. We see that frequencies between one and five GhZ are required to obtain periodic perturbations with wavelengths of the order of a micron.

Table 4-3. Acoustic wavelengths at 1 GhZ.

MATERIAL	ACOUSTIC WAVELENGTH at 1 GhZ (MICRONS)
$LiNbO_3$ [11-20]	6.57
Fused Quartz	5.95
Silicon [110]	8.90
$LiTaO_3$	6.19

We next consider the magnitude of steady state strain amplitudes one could reasonably expect to excite. Consider the geometry shown in Figure 4-7. Assume the $LiNbO_3$ to be oriented so that the input electrical field excites pure longitudinal waves along the $\hat{x}$ axis, as shown. The rms strain can be simply related to the acoustic power density[19].

$$\varepsilon = \sqrt{2I/\rho v_i^3} \qquad (4\text{-}4)$$

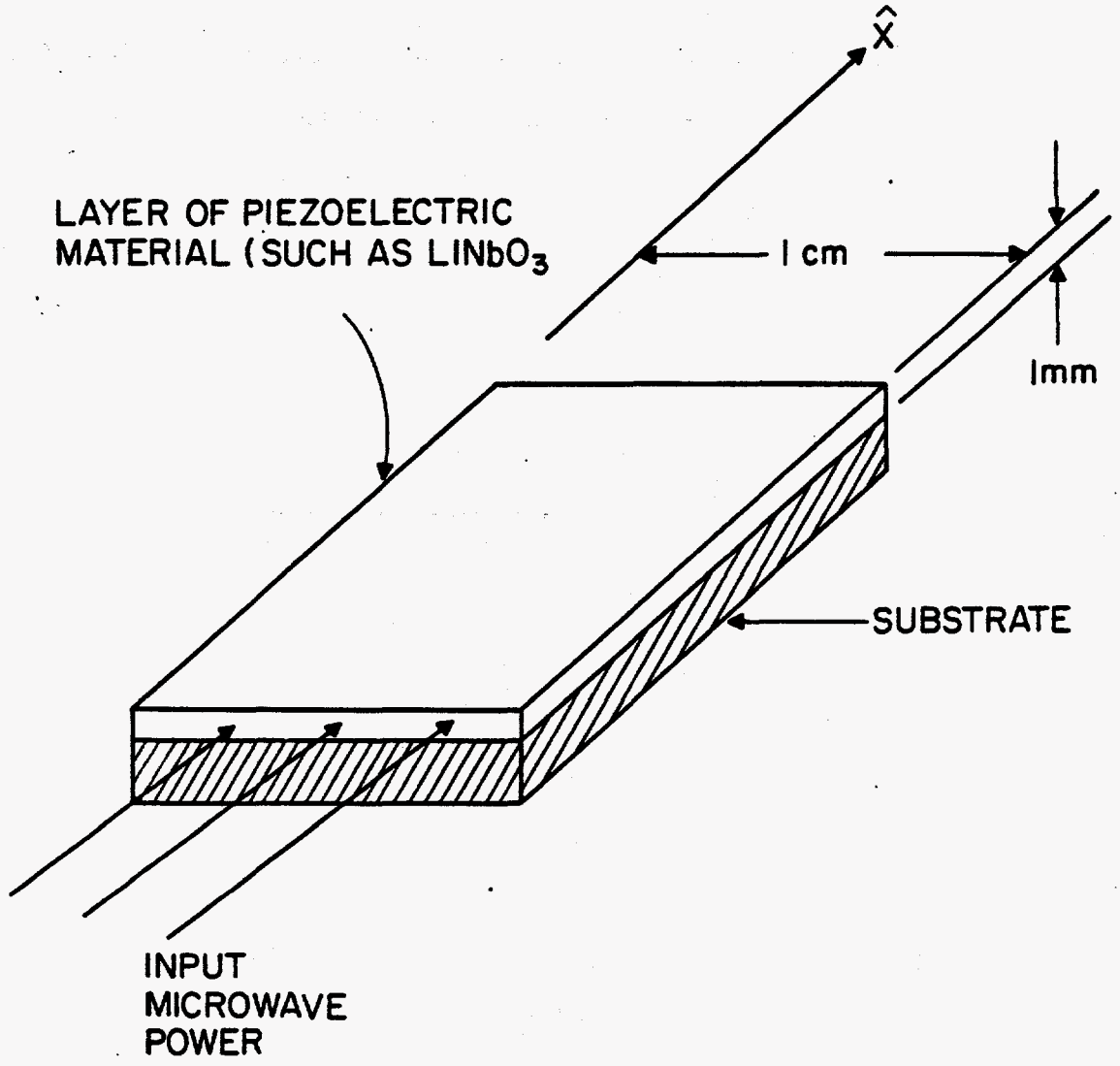

Figure 4-7. Production of x-ray diffracting surface perturbations through the use of microwave ultrasonic techniques.

ρ = density

v_t = acoustic velocity.

For a strain of the order of 5×10^{-5}, an input(acoustic)power of about 20 watts for a travelling wave (the input power can be considerably reduced by establishing a standing wave). Assuming a poisson ratio of 0.3, the surface perturbation would have an amplitude of about 150 Å. On a quasi CW (long tone burst) basis, the micro wave power requirements are, thus, rather modest.

SUMMARY OF LATTICE EXCITATION METHODS

We can conclude from the analysis of Section 4.1 that subnanosecond switching or shuttering of x-rays will probably have to be a surface effect. The magnitude of optical field strengths needed to produce useable amplitude lattice vibrations were seen to be 10^8 - 10^9 WATTS/cm^2. Such large fields can only be produced in a limited spatial volume. The methods utilizing total external reflection are by their nature surface effects.

Very high frequency (steady state) modulation effects can involve more of the bulk of the solid. At room temperature, acoustic losses and limitations on microwave power generation would seem to limit the frequency to about 5 GhZ.

4.2 X-RAY DIFFRACTION CONSTRAINTS ON DEVICE PARAMETERS

The basic principles involved in the use of x-ray diffraction for modulation and shuttering have been studied theoretically in Chapter 2 and experimentally in Chapter 3.In the present section,this information will be used to formulate the general principles that govern the design of diffraction devices to control x-ray propagation.In addition, the basic limitations on device parameters will be outlined.

4.2-1 CRYSTALLINE PARAMETERS AND THEIR RELATION TO DEVICE DESIGN

In Chapters 2 and 3,the sensitivity of x-ray diffraction to lattice perturbations was shown to be governed by the width of the diffraction curve. We will refer to the sensitivity of the diffraction process to lattice perturbations as diffraction sensitivity. Experimentally, in the Borrmann case(where diffraction curve width depends strongly on absorption, as shown in 2-34), strains of the order of 10^{-5} were found to be needed to reduce the diffracted intensity by factors of.1 to .5. The diffraction sensitivity in the Bragg geometry is shown by formula 2-14 to be directly proportional to F_H.Thus, in both the Bragg and Laue (Borrmann) geometries,the diffraction sensitivity is inversely related to the diffraction efficiency. These are the kinds of tradeoffs that must be considered in designing x-ray modulating and shuttering devices for any particular application. Table 4-4 lists the various crystal parameters that are at the disposal of a designer.

Table 4-4 . Effect of crystal properties on modulator design.

CRYSTALLINE PROPERTY	BASIC NATURE	RELATION TO MODULATOR DESIGN
(1) Diffraction Curve Width, $\Delta\theta$	(a) Proportional to $F_h\lambda^2/\sin\theta_B$ in the Bragg geometry (b) Proportional to $\left[\frac{1}{\mu t - 1}\right]^{1/2} F_h\lambda^2/\sin\theta_B$ in Borrmann mode.	Diffraction sensitivity is directly proportional to this quantity.
(2) Diffraction Efficiency	Inversely proportional to $\Delta\theta$.	This quantity (plus absorption in the Borrmann mode) governs "insertion loss" of a modulator or shutter.
(3) Extinction Distance, d_{ext}	Proportional to λF (thus, becomes larger as $\Delta\theta$ becomes larger).	Governs characteristic distance over which diffracted field is established.
(4) Absorption Distance, $d_{abs.}$	Roughly proportional to Z (Atomic number) of crystal. In Borrmann mode, diffraction sensitivity directly related to $d_{abs.}$	In fast shuttering applications, this quantity governs the important depth over which fields are absorbed.
(5) Lattice Spacing, 2d	Since $\frac{\lambda}{\sin\theta} = 2d$, as 2d increases, $\Delta\theta$ also increases.	λ must be < 2d and convenient configurations have $\lambda \lesssim 0.8(2d)$.

We will now investigate the behavior of the fundamental parameters in Table 4-4 in typical situations. In the present section, we will emphasize the Bragg geometry.

The crystals that are most commonly available in highly perfect form are a family of semiconductor materials with diamond cubic structure.We will use three of these,Ge,Si,Insb,to illustrate the behavior of the parameters in Table 4-5.(Another very familiar member of this group, GaAs, has almost identical x-ray scattering properties to Ge because of nearly identical lattice constant and atomic weight).

Table 4-5 . Typical diffraction parameters.

MATERIAL	REFLECTION	2d SPACING o (A)	$\Delta\theta$ DIFFRACTION CURVE WIDTH (RADS)	EXTINCTION DISTANCE (MICRONS)	ABSORPTION DISTANCE (MICRONS)
SILICON	111	6.26	3.2×10^{-5}	4.8	69.0
	220	3.82	2.2×10^{-5}	4.1	"
	440	1.91	$.74\times10^{-5}$	6.1	"
GERMANIUM	111	6.52	8.2×10^{-5}	1.7	27.4
	220	4.00	6.3×10^{-5}	1.4	"
	440	2.00	2.2×10^{-5}	2.1	"
InSb	111	7.50	8.8×10^{-5}	12.1	6.5
	220	4.57	6.6×10^{-5}	10.8	"
	440	2.29	2.5×10^{-5}	17.5	"

All calculations for CuK_α (λ = 1.54 Å) & Bragg geometry.

In examining Table 4-6, we see first that in order to increase the diffraction sensitivity (decrease $\Delta\theta$), we can use higher index diffracting planes. The diffraction efficiency (which is directly proportional to $\Delta\theta$ for an uncollimated incident beam) is proportionally reduced. In addition, higher index planes will only accommodate harder radiation (since λ must be $< 2d$).

The extinction distance will gradually increase with higher index planes, although not monotonically (see Table 4-6). Thus, by increasing the diffraction sensitivity (through going to higher index planes), the region of the crystal that must be perturbed (i.e., perturbation volume) is increased. The exact requirements on the perturbation volume depend on the particular acoustic field configuration employed.

4.2-1(a) FAST SHUTTERING

Very fast shuttering methods were shown to be limited to surface effects. The implications of this requirement in the Bragg geometry are illustrated in Figure 4-8(a).

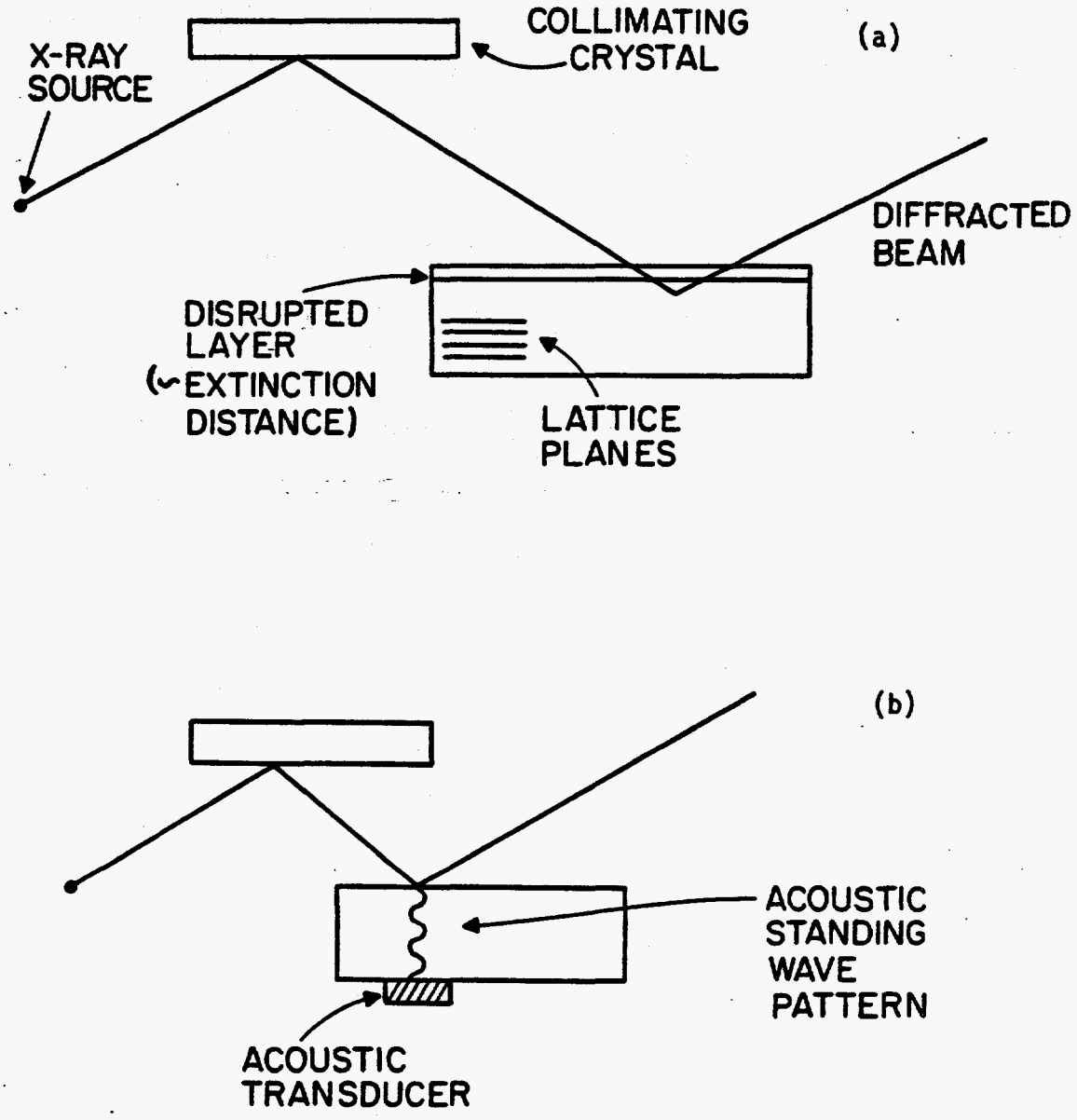

Figure 4-8. Fast shuttering configurations utilizing Bragg geometry x-ray diffraction.

If a layer near the surface is disrupted(e.g.2d spacing changed) the radiation merely penetrates this layer (suffering absorption) and is diffracted from the undisturbed layers below.Only if a region with a depth of the dimension of an absorption distance were disrupted would a significant decrease in diffracted intensity occur.If acoustic transit times are the fundamental limitation,an absorption depth can be addressed in a time period of the order of 10 nanoseconds.Thus, in order to have subnanosecond switching effects utilizing crystal diffraction, the effective participating layer must be limited to a region of the dimension of an extinction distance. One method of accomplishing this would be the use of thin single crystal films.Techniques have been demonstrated[34] for growing highly oriented thin films on a substrate.

Another method for limiting the diffraction to a thin layer near the surface is shown in Figure 4-8(b).A high frequency acoustic standing wave is excited, as shown. Only the regions of the crystal near the nodes will have an undisturbed 2d spacing. Suppose, for example, the strain amplitude is 10^{-4} and the acoustic wavelength 40 microns(an acoustic frequency of about 100 MhZ).The strain will rise to 10^{-5}(greater than a typical diffraction curve width) in a distance within one micron of the surface. Thus, effective diffraction will be limited to a thin surface layer. The acoustic pattern could be maintained essentially stationary with respect to any subnanosecond events.

A region lying at the first node away from the entrance surface will also diffract effectively. The radiation will, however, have to pass through 40 microns of absorbing material. If the diffracting

crystal is InSb, (and λ = 1.54 Å), a ray diffracted from the region of the second node suffers absorption which reduces it to 5% of its input value. Therefore, in this case, the effective contrast ratio (or modulation depth) is limited by the acoustic field configuration and crystal properties to about 95%.

It would be difficult to apply the Borrmann mode to surface effect techniques. High modulation depth relies on a ray passing through sufficient (≃ .5 mm) material in order to suffer a large integrated absorption.

4.2-1(b) HIGH FREQUENCY MODULATION

While surface perturbations in the Bragg geometry are most useful for transient modulation (i.e., shuttering) applications, continuous wave high frequency modulation is best suited to the Laue (Borrmann) geometry.

In the Bragg geometry, the modulation depth is governed by the steepness of the strain gradient at the entrance surface of the crystal. For very small extinction distances, rather large strain gradients would be required.

In the Borrmann mode, the fundamental limitation on modulation depth is also the acoustic strain gradient. However, the important consideration is the magnitude of the strain gradient in relation to the spread of rays within the Borrmann fan. In the Borrmann mode, the entire acoustic field is utilized, not just a portion of it near the surface.

4.2-2 CONTROL OF DIFFRACTION SENSITIVITY

In this section, we address the general question of the basic potential (other than those based on crystal properties) for increasing diffraction sensitivity. An increase in diffraction sensitivity will lead to greater modulation depth for a given strain gradient.

In Table 4-6, we list diffraction configurations (not involving crystalline parameters) and their relation to modulator design.

Table 4-6. Characteristics of various diffraction configurations.

DIFFRACTION CONFIGURATION	BASIC PROPERTIES	RELATION TO MODULATOR DESIGN
(1) Asymmetric Bragg Diffraction	Decrease $\Delta\theta$ by cutting entrance surface at an angle with respect to lattice planes.	Can be used to enhance diffraction sensitivity.
(2) Multiple Crystal/X-ray Interferometers	Multiple X-ray reflections in both Laue or Bragg geometries.	Can significantly increase fall off in tails of diffraction curve. Can, thus, (with properly chosen operating point) create greater diffraction sensitivity.
(3) Single Crystal Multiple Reflection	Two or more sets of lattice planes participating in reflection.	Same advantages as multiple crystal arrangements.

We will now discuss in detail the first two methods in Table 4-6., beginning with multiple crystals and x-ray interferometers.

The experiemntal work in Chapter 3 showed that the use of a double crystal Borrmann configuration increased the sensitivity. The use of two crystals has long been recognized as a method of achieving greater resolving power in x-ray spectrometers. A major breakthrough, however, occurred when Bonse and Hart[34] fabricated a device where several x-ray reflections could be achieved within one monolithic block of crystalline material. This effectively opened up the new field of x-ray interometry.

The first arrangement use by Bonse and Hart was essentially the same as that used in the experimental part of this thesis and shown in Figure 3-23. The only difference in the Bonse-Hart case is that lattice planes parallel to the interferometer arms are now employed.The situation is illustrated in Figure 4-9.

The basic effect of the multiple reflections is to greatly decrease the energy in the wings of the (Darwin) diffraction curve.The result is that the edges of the diffraction curves become very steep.In the case of five reflections (for 220 planes in Silicon),a change of 3 orders of magnitude in intensity can occur for an angular change of one arc second (4.8×10^{-6} RAD). As was shown in our experiments(Chapter 3)one can adjust the operating point on the diffraction curve by applying a mechanical prestress to the interferometer. This can also be accomplished by a DC bias when the interferometer is constructed out of piezoelectric material. Once an operating point on the steep portions of the diffraction curve has been established, further perturbation by acoustic waves can lead to very large changes in diffracted intensity.

It should be noted that the multiple reflection phenomena can be achieved without the use of multiple crystals or interferometers. For example, double reflection involves two separate sets of lattice planes (with different Miller indices). The phenomena is usually referred to as Umweganregung[1].Diffraction sensitivites comparable to those possible with Bonse Hart type devices have been achieved.[35]

As can be seen from Figure 4-9, the multiple reflection process tends to greatly increase the fall off in the wings of the diffraction

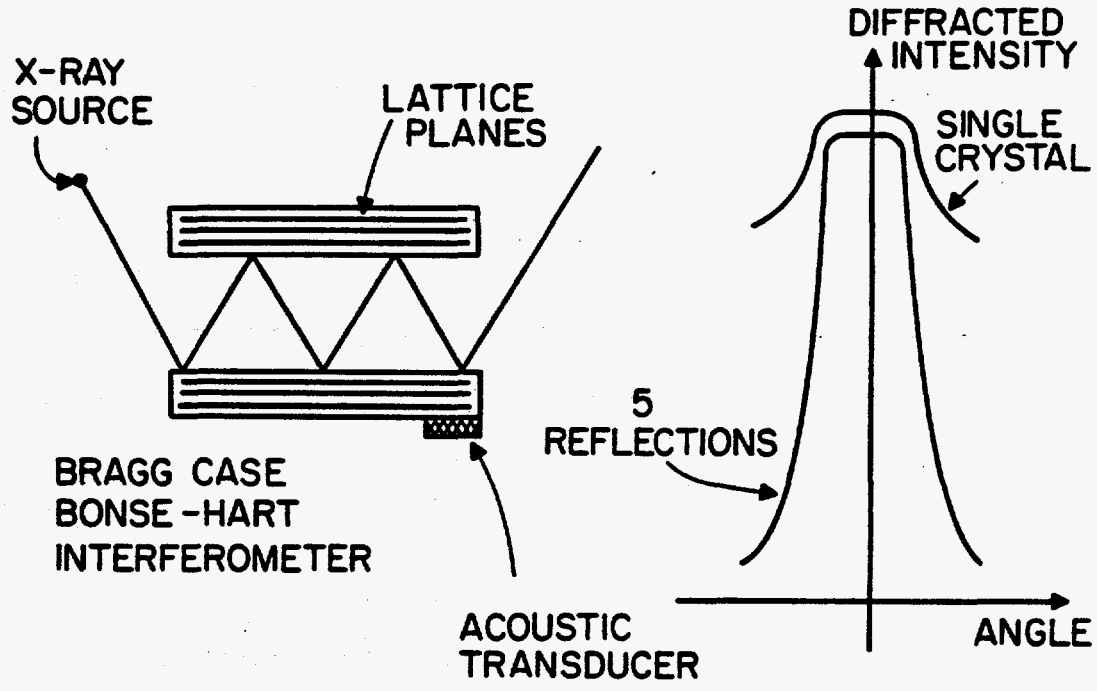

Figure 4-9. Use of a Bragg case x-ray interferometer for x-ray modulation.

curve while leaving its width about the same. A narrowing of the width of the diffraction curve can be accomplished through the use of asymmetric reflection, which occurs when the entrance surface of the crystal is cut at an angle with respect to the diffracting lattice planes. The effect can easily be seen in the Bragg case by referring to the dispersion surface diagram, as shown in Figure 4-10. In the left hand portion of the figure, the entrance surface of the crystal is normal to the diffracting planes. In the Bragg case, the angular width is proportional to the distance AB, corresponding to tie points T_1 and T_2 on different branches of the dispersion surface. The right hand portion of Figure 4-10 displays the situation when the entrance surface is cut at an angle with respect to the lattice planes (as shown in the bottom of the figure). Once again the distance AB corresponds to the angular width of the reflection, which is clearly less than for the left hand diagram. It can be shown[2] that the width of the diffraction curve is given by:

$$W = W_o \left[\frac{\sin(\theta_B-\alpha)}{\sin(\theta_B+\alpha)}\right]^{1/2}$$

where W_o = width of the diffraction curve for an entrance surface normal to diffracting planes

α = angle of the entrance surface with respect to the lattice planes.

Cutting the entrance surface of the crystal in this manner is, thus, another technique available for increasing the diffraction sensitivity.

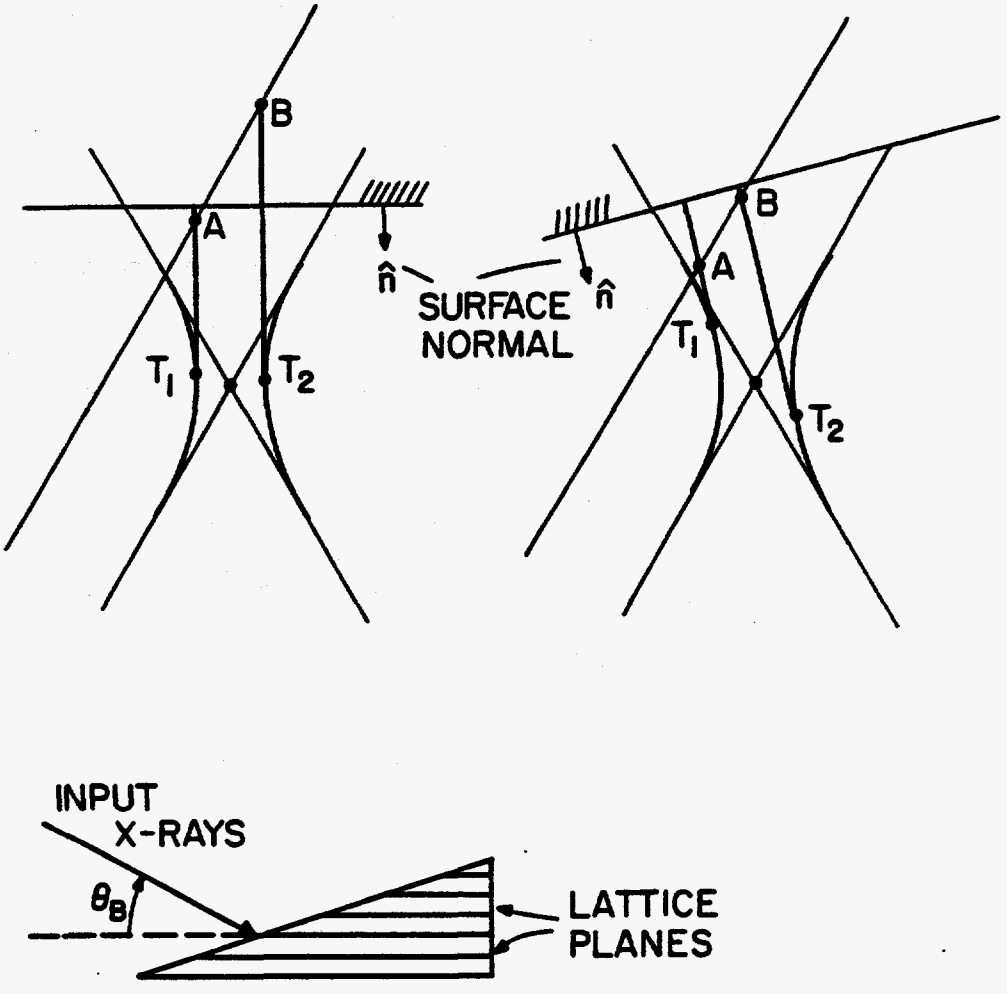

Figure 4-10. Illustration of the narrowing of the diffraction curve through the use of an asymmetrically cut entrance surface.

4.3 TYPICAL MODULATOR DESIGN

In this section, we will outline the design of a specific x-ray modulator. The design will utilize the general procedures and criterion developed in section 4.2. To illustrate as broad a range of design problems as possible, a compound device utilizing both the Bragg and Laue geometries is presented.

The basic configuration is shown in Figure 4-11 Bragg reflection precedes and follows Borrmann transmission through the central element. Acoustic perturbation can be applied to either the Bragg sections or the Borrmann element. The multiple reflections will result in a sharp fall off in the wings of the diffraction curve similar to the pure Bragg case discussed above. The operating point on the diffraction curve can be selected through "tuning" the central element by applying a force, as shown in Figure 4-11. If even greater diffraction sensitivity is desired, the device can be cut so that the final Bragg reflection is asymmetric.

To illustrate the general behavior of the diffraction sensitivity of the compound device, we will base our considerations (for the moment) on a uniform change in 2d spacing (uniform compression or tension across the whole crystal) of the lattice planes. The diffraction sensitivity is calculated by multiplying the two Darwin diffraction curves (characterizing the Bragg reflections) by the Borrmann diffraction relation given by Equation 2-38. An example of this calculation, for the case of the 220 planes in silicon, is illustrated in Figure 4-12. The thickness of the Borrmann transmitting element is such that $\mu t = 25$.

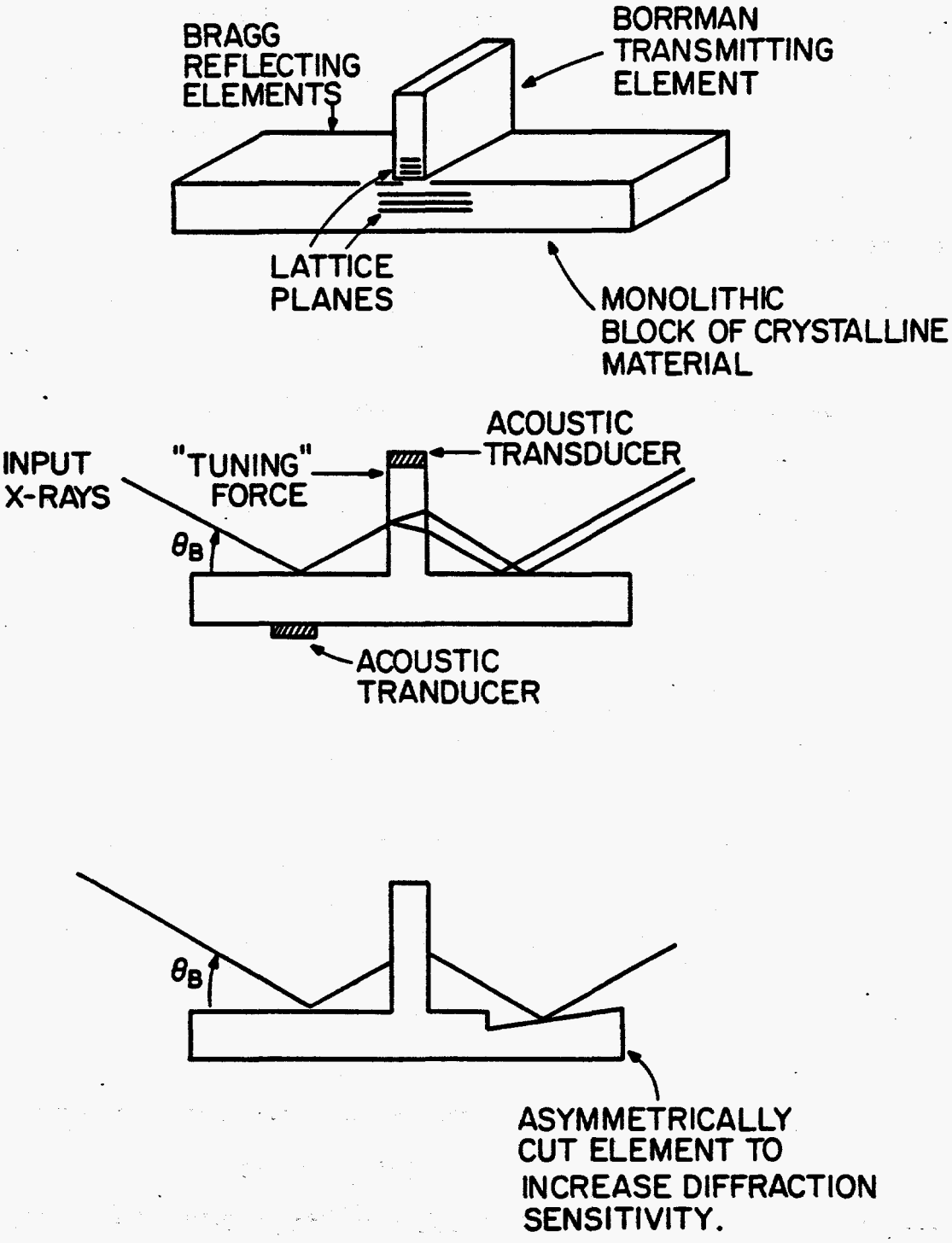

Figure 4-11. X-ray modulator configuration.

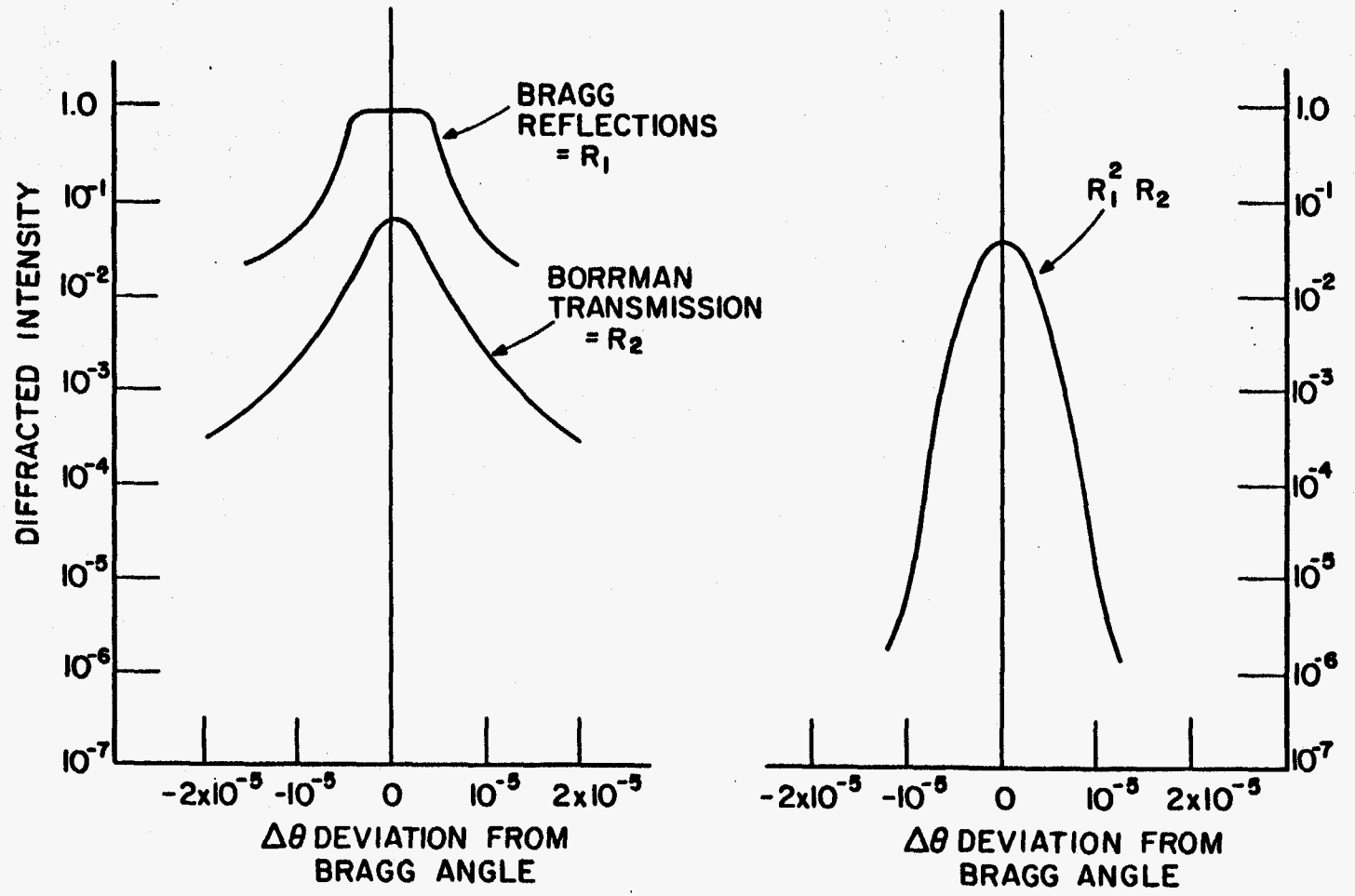

Figure 4-12. Diffraction curves characterizing the operation of the x-ray modulator (illustrated in Figure 4-11.

Several interesting characteristics of the behavior of this structure as a modulator can be seen from the curves in 4-12.The sharp fall off in the wings of the compound curve ($R_1^2R_2$) can easily be seen. For example, in going from $\Delta\theta=4x10^{-6}$ to $\Delta\theta=10^{-5}$ the diffracted intensity falls by 3 orders of magnitude. The curve $R_1^2R_2$ is, thus, used to establish the contrast ratio (or modulation depth) for a given amplitude of acoustic perturbation.

We also note, from Figure 4-12 that the unperturbed diffraction ($\Delta\theta = 0$) is considerably greater for Bragg reflection than for Borrmann transmission. This is, of course, due to the fact that x-rays passing through the crystal (in the Laue geometry) always suffer some absorption, even when there is no perturbation to the lattice (as can be seen from Equation 2-38).

The Borrmann mode, however, offers two advantages.First,the Laue geometry provides the convenience of transverse acoustic perturbation as the modulating mechanism. The surface to which the acoustic transducer is bonded (see Figure 4-11) and the acoustically reflecting surface can be carefully polished by optical techniques.In the Bragg case, the x-ray diffraction occurs from the acoustic reflection surface. This necessitates the use of complicated chemical polishing techniques that will maintain the surface flatness (for acoustic reflection)and lattice perfection (for x-ray diffraction). The second advantage of the Borrmann mode is a more rapid fall off in the wings. The rate of fall off can be increased by increasing the μt of the crystal. Thus, the Borrmann mode, in general, offers a greater potential contrast ratio(relative to

brass reflection) at the expense of a higher insertion loss.

The operating point on the diffraction curve can, to a small degree, be selected by tilting the Borrmann diffracting element. The structure must, however, be cut so that this process does not introduce significant strains into the region where Bragg diffraction is occurring.

When using the Borrmann element as the "control" element, different design procedures will be required depending on the acoustic wavelength. At very low frequencies, the strain field will be essentially constant over the extent of the Borrmann fan (see Figure 4-11). For the 220 planes of silicon and a frequency of 1MhZ, the acoustic wavelength is about 1cm, which would satisfy this requirement. In this case, the curves in Figure 4-12 can be used directly to predict the modulation depth for given acoustic amplitude.

At higher frequencies, there will be strain variation within the Borrmann fan. In this case, the more detailed ray trace calculations (used in Chapter 3) must be applied. These calculations will produce correction factors to the dependence shown in 4-12. The basic behavior of the diffraction sensitivity is, however, still described by the graph in Figure 4-12.

The rise time of the device is essentially limited by the spatial extent of the Borrmann fan. The acoustic time of transit through the Borrmann fan represents the shortest interval over which the x-ray field in the crystal can be perturbed.

From Equation 2-41, we may write the average width of the Borrmann fan as:

$$W = (t/2)\tan^{-1}\left\{\left[\frac{2\ln 2}{\mu_o \varepsilon t - 1}\right]^{1/2} \tan(2\theta_B)\right\} \qquad (4\text{-}4)$$

where t = thickness of crystal.

We can now write an expression for the rise time.

$$t_r = W/v_t \qquad (4\text{-}5)$$

where v_t = acoustic velocity.

For the 220 planes in silicon, $v_t = 8.9 \times 10^5$ cm/sec and

$$t_r \simeq 15 \text{ n.s.}$$

When perturbation of the Bragg reflections is used, the rise time is given by:

$$t_r \simeq d_{ext}/\, v_t$$

In the case of 220 reflection in silicon

$$t_r \simeq 4.5 \text{ n.s.}$$

When used as a free running shutter (or chopper), much higher frequency operation is possible. In the steady state, the local strain at

at any point in the solid is varying at the acoustic frequency. The x-ray transmission is, thus, also modulated at the acoustic frequency.

The rise time of one cycle of such a device could be extremely fast. As an example, let us use the diffraction sensitivity given in Figure 4-12. A strain of approximately 10^{-5} would be required to change the device from an "on" (diffracting) state to an "off" state. If the strain amplitude of the acoustic wave were 10^{-4} at a frequency of 1 GhZ, the device would be turned "off" in 100 p.s.

CHAPTER 4 REFERENCES & FOOTNOTES

1. James, R.W., Optical Principles of the Diffraction of X-Rays, Cornell University Press, (1948).

2. Warren, B.W., X-Ray Diffracting, Wiley, (1966).

3. Maraududin, A., Montroll, E.W., and Weiss, G.H., Theory of Lattice Dynamics in the Harmonic Approximation, Academic Press, (1963).

4. Ziman, J.M., Principles of the Theory of Solids, 2nd ed., Cambridge, (1972).

5. Kittel, C., Introduction to Solid State Physics, 3rd ed., Wiley, (1966).

6. Pantell, R.E., and Puthoff, H.E., Fundamentals of Quantum Electronics,

7. Woods, A.D.B., et al., "Lattice Dynamics of Alkali Halide Crystals", Phys. Rev., 131, 102, (1963).

8. Eckhardt, G., "Selection of Raman Laser Materials", IEEE J. Quant. Elec., QE-2, (1), p. 1, (1966).

9. Giordmaine, J.A., and Kaiser, W., "Light Scattering by Coherently Driven Lattice Vibrations", Phys. Rev., 144, (2), p. 676, (1966).

10. Krishnan, R.S., Proc. Indian Acad. Sci., A22, p. 182, (1945).

11. Cochran, W., "Lattice Vibrations", RPTS on Prog. in Physcis, vol. XXVI, p. 1, (1963).

12. Brillouin, L., Wave Propagation in Periodic Structures, Dover, (1946).

13. Page, L., and Adams, N.I., Principles of Electricity, D. Van Nostrand, (1949).

14. Chiao, R.Y., Garmire, E., and Townes, C.H., "Raman and Phonon Masers" in Proceedings of the International School of Physics, Enrico Fermi, Quantum Electronics and Coherent Light, Academic, New York, p. 326, (1964).

15. Giuliano, G.R., "Laser Induced Damage to Transparent Dielectric Materials", Appl. Physics Lett., 5, (7), (1964).

16. Krokhin, O., "Intensity Dependence of Optical Absorption in Semiconductors", in Proceedings of the International School of Physics, Enrico Fermi, Quantum Electronics and Coherent Light, (1963), Academic, New York, p. 273, (1964).

17. Ryvkin, S.M., "Thermal Radiation from Silicon Illuminated by a Laser Beam", Soviet Physics - Solid State, 10, (4), p. 807, (1968).

18. A very useful follow on to the present experiment would be an investigation of the laser induced damage, using x-ray topography. As outlined in Chapter 3, x-ray topography provides a very sensitive method for observing small amounts of damage in crystal structures. To the author's knowledge, topography has not been previously employed in laser damage studies and could provide a sensitive tool for evaluating damage mechanisms.

19. Blitz, J., Fundamentals of Ultrasonics , Butterworths, (1963).

20. Jacobsen, E.H., "Sources of Sound in Piezoelectric Crystals", J. Acoustical Soc. Am., 32, (6), p. 949, (1960).

21. Auston, D.H., and Glass, A.M., "Optical Generation of Intense Picosecond Electrical Pulses", Appl. Phys. Lett., 20, (10), (1972).

22. Auston, D.H., "Optical Rectification by Impurities in Polar Crystals", Phys. Rev. Lett., 28, (14), p. 897, (1972).

23. Johnson, A.M., and Auston, D.H., "Microwave Switching by Picosecond Photoconductivity, IEEE J. Quan. Elec., Qe-11, (6), p. 283, (1975).

24. Shiren, N.S., et al., Phys. Rev. Lett., 24, 819, (1973).

25. Afanasev, A.M., and Kagen, Y., "The Role of Lattice Vibrations in Dynamical Theory of X-Rays", Acta. Cryst., A24, p. 163, (1967).

26. Batterman, B.W., "Effect of Thermal Vibrations on Diffraction from Perfect Crystals", Phys. Rev., 126, p. 1461, (1962).

27. For example, x-ray spectrometers used in laser plasma diagnostics typically have line widths of a few tenths of a millimeter on the film plane (depending on the crystal and spectrometer geometry). Ten microns is a typical extinction distance.

28. International Tables for X-Ray Crystallography, vol. II, Kynoch Press, (1968).

29. Peercy, P.S., et al., "Ultrafast Rise Time Laser Induced Stress Waves", Appl. Phys. Lett., 16, (3), p. 120, (1970).

30. Fox, J.A., "Production of Stress Waves with Nanosecond Laser Pulses", Appl. Optics, 13, (8), p. 1760, (1974)

31. Auth, D.C., "New High Power Source of Coherent Microwave Phonons", Appl. Phys. Lett., 16, (12), (1970).

32. Spencer, E.G., et al., "Dielectric Materials for Electrooptic, Elastooptic, and Ultrasonic Device Applications", Proc. IEEE, 55, p. 2074, (1967).

33. Fancombe, M., and Sato, H., (Ed.), Single Crystal Films, MacMillan, (1964).

34. Bonse, U., and Hart, M., "Tailless X-Ray Single Crystal Reflection Curves Obtained by Multiple Reflection", Appl. Phys. Lett., 7, p. 238, (1965).

35. Kottiwitz, D.A., "High Resolution Monochromatization of Neutrons and X-Rays by Multiple Bragg Reflection", Acta. Cryst., A24, p. 117, (1968).

CHAPTER 5

CONCLUSIONS & SUMMARY

The contributions presented in this thesis can be placed in one of two broad categories:

1) The investigation of techniques for the modulation and control of x-ray propagation through acoustic perturbation of solids.

2) The use of x-ray diffraction and x-ray optical techniques for the study of acoustic propagation and atomic motion.

The primary emphasis was placed on the first category of investigation.

Through the analysis in Chapter 1, we have established the general direction that investigation of x-ray modulation and control techniques must take.

The control of x-ray propagation through perturbation of the electronic structure of scattering atoms was shown to be quite difficult. It was, however, shown that in special circumstances, it would be possible to produce detectable changes in the imaginary part of the x-ray index.

Significant changes in x-ray propagation can be effected by acoustic perturbation of such processes as crystal diffraction and total external reflection. The analysis in Chapter 1 established that practical methods for the control of x-ray propagation must involve changes in the spatial configuration of x-ray scatterers.

In Chapter 2, the basic theoretical framework for the study of x-ray propagation in acoustically perturbed crystals was derived.

With respect to the Bragg geometry, a new technique (matrix) was presented for solving the fundamental (Darwin) equations of propagation.

The solutions obtained by this technique were then used to demonstrate important characteristics of x-ray diffraction. The phenomenon of extinction was shown to limit the depth of penetration of x-ray fields into the crystal (in the Bragg case). The extinction distance was, thus, seen to be the characteristic spatial interval over which the diffracted field is established. The extinction distance, thus, establishes the region of the crystal that must be perturbed in order to significantly change the diffracted intensity.

The solutions to the Darwin equations were also used to analyze the diffraction sensitivity (which was defined as the variation of diffracted intensity as a function of lattice perturbation).

Numerical methods were developed that predict the detailed characteristics of x-ray propagation in acoustically perturbed crystals. In developing these methods, special emphasis was placed on Borrmann transmission in thick crystals. In particular, (in the case of small strain gradients), these techniques were used to calculate both the trajectory and attenuation of rays propagating in a crystal containing an acoustically produced sinusoidal strain gradient.

Finally, a general analysis of x-ray diffraction in the presence of crystal lattice vibrations was presented. This analysis presented a derivation of the effect of thermal (quasi random) and monochromatic lattice vibrations in one unified treatment.

Chapter 3 presents experimental demonstration of x-ray modulation and shuttering. This represents the first use of crystal diffraction techniques for the modulation and control of x-rays[1]. The primary thrust of Chapter 3 was a basic quantitative investigation of the x-ray-acoustic interactions that were used to produce modulation and shuttering.

Special experimental techniques were developed for the measurement of high frequency (acoustically induced) strain that should be of general value in acoustooptic investigations.

In the case of single crystal Borrmann transmission, it was found that for longitudinal acoustic plane waves, propagating perpendicular to the diffracting lattice planes, a time average strain amplitude of about 10^{-5} (at 5 and 10 MhZ) was needed to produce a measurable decrease in diffracted x-ray intensity. The measured decrease in diffracted intensity agrees with the theoretically predicted values to within experimental error.

It was found that at higher values of strain gradient (approximately $3x10^{-5}$ amplitude at 22 MhZ), the decrease in diffracted intensity for a given strain amplitude shows a divergence from the theoretically predicted values. This departure is due to the phenomena of interbranch scattering.

The diffraction sensitivity of a two crystal x-ray interferometer was also investigated. It was shown that this configuration had a greater sensitivity to acoustic perturbation than the single crystal case. Experiments were performed with one arm of the interferometer intentionally misaligned (through the use of a special mount). This

experiment demonstrated that the operating point on the diffraction curve can be selected at will.

Through the use of specially designed electronic circuitry, shuttering of x-ray transmission on a microsecond time scale was demonstrated.

The technique of Borrmann topography was shown to be useful in the detailed study of acoustic fields in solids. A quantitative evaluation of the structure of a longitudinal standing wave was performed in this way.

Chapter 4 presents an analytical investigation of the basic potential and limitations of x-ray modulation and control devices. It was shown that subnanosecond x-ray switching processes would have to be limited to surface effects. The spectrum of crystal lattice vibrations was demonstrated to limit x-ray switching to rise times of greater than 10^{-12} sec.

Chapter 4 also presented a formulation of the basic design criteria for x-ray modulation devices. Special examples of the application of these criteria to practical devices were presented.

CHAPTER 5 REFERENCE

1. Hauer, A., U.S. Patent, "Methods for the Control and Measurement of X-Rays", Serial No. 594846 (issued 11/19/76).

APPENDIX

FURTHER APPLICATIONS

This basic study of x-ray acoustic interactions provides the basis for several practical applications. Chapter 4 emphasized applications involving the control of x-ray propagation. In the present appendix, we will briefly review applications which are not directly related to x-ray modulation and shuttering.

A-1 ACOUSTIC FIELDS IN SOLIDS

In Chapter 3, it was demonstrated that Borrmann topography can be used to study the detail of high frequency acoustic fields in solids. The Borrmann method has a particular adavantage (over thin crystal diffraction techniques)in that it works with thick crystals that are closer to structures of most interest in solid mechanics. With refinement of the numerical contrast analysis techniques (developed in Chapter 2), it will be possible to very accurately map the strain fields present in an acoustic standing wave pattern.

More complicated three dimentional fields can also be analyzed by this method. By using different sets of diffracting planes, one can probe the field along numerous different directions in analogy with x-ray tomography.[1] For example, the 220 silicon planes (used in the Borrmann work in Chapter 3) are but one of six identical sets of planes rotated by 30^{o} around the 6 fold (111) axis of symmetry, as illustrated in Figure 5-1.

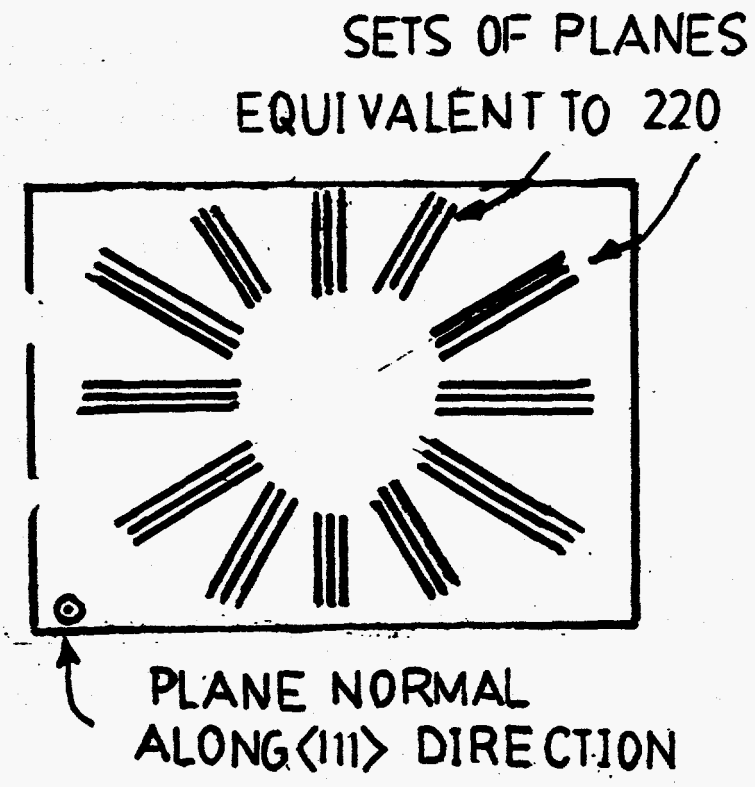

Figure A-1. X-ray topography of acoustic fields.

By using each of these sets of planes, one may probe the acoustic standing wave at 60^{o} intervals over a full 360^{o}. In addition to using different crystal planes, one can also change the angle of diffraction by using different wavelength x-rays. There is, thus, a great deal of flexibility available in the quantitative topographic probing of acoustic fields.

The utilization of reduction in Borrmann transmission, originally proposed as part of this study, has recently been applied to the study of very intense phonon fields produced by acousto-electric amplification.

X-ray techniques developed in this study should also be useful

in the study of surface acoustic waves. Surface or Rayleigh wave propagation usually results in surface perturbations that are somewhat lower in amplitude than would be useful for shuttering or modulation. For example, White[3] has estimated that a 15 Å surface protrusion resulted in a typical Rayleigh wave experiment. Rayleigh waves tend to have lower propagation velocities than bulk modes. A 1 GhZ surface wave in quartz has an acoustic wavelength of about 3 microns. At an amplitude of 15 Å, this would lead to a change in the angle of incidence of about 2^{o}. This could lead to several per cent change in x-ray reflectance. Although such a change would not be very practical as a shuttering method, it could be useful as a surface probe technique.

Pulsed x-ray sources (such as a laser produced plasma) also make possible the study of transient acoustic phenomena. Very short duration (100 p.s. or less) x-ray pulses can be produced by laser plasmas. Since the x-ray pulse is produced by laser irradiation of a target, it can be conveniently synchronized with other laser matter interaction experiments.

Transient x-ray diffraction analysis can be used to study the generation and propagation of very high pressure laser induced shock waves. A strong shock wave propagating in a crystal would create an instantaneous perturbation similar to a naturally occurring fault plane. The Takagi method for analysis of x-ray propagation in distorted crystals has been applied to this case.[4]

The very high pressures produced in laser initiated shocks can be expected to induce phase changes in solids. Phase changes

can also be expected when large amounts of heat are deposited in solids. An example would be a ferroelectric crystal (such as $BaTiO_3$) heated above its Curie temperature. Transient x-ray diffraction techniques offer the possibility of time resolved study of such processes.

Transient x-ray diffraction could also be used to study other types of optically induced solid perturbations. Stimulated scattering processes (such as SBS and SRS) have been shown to produce lattice perturbations that are potentially observable by x-ray diffraction (see Chapter 4). The natural extension of such studies would be in the investigation of optically induced damage mechanisms.

There is also an interest in the interaction of acoustic waves with naturally occurring defects in solids.[5] X-ray topographic visualization of the interaction of acoustic standing wave and a dislocation was demonstrated in Chapter 3. Such a technique is equally applicable to transient interaction in the case of a travelling acoustic wave. The high pressures available in laser induced stress waves could be applied to the study of acoustic perturbation of dislocations. Kittel[6] estimates that certain dislocations can be moved by an applied stress of less than 10^5 dynes/cm^2. From the analysis in Chapter 2, we can see that such a stress can easily be produced by SBS.

A-2 PLASMA DIAGNOSTICS

X-ray diffraction could be a useful diagnostic of the initial stages of laser heating of solids. Laser heating of a solid target is primarily due to electron avalanche ionization followed by inverse bremsstrahlung. The initial deposition of energy is, thus, into the electrons. A finite time period is required before energy is transferred to the ions (lattice). During this period, the regular arrangements of ions (that characterized the original crystal lattice) might continue to diffract x-rays. Such a situation has, in fact, been proposed as a possible feed-back mechanism for an x-ray laser.[7]

In order to analyze the behavior of the diffracted x-ray signal, theories of x-ray propagation in distorted crystal structures (such as those discussed in Chapter 2) will be needed.

APPENDIX REFERENCES

1. Gordon, Richard, "Image Reconstruction from Projections", Sci. Am., 233, (4), p. 45, (1975).

2. LeRoux, S.D., and Colella, R.L., "Effects of Acoustoelectric Phonons on Anamalous Transmission of X-Rays", 37, (16), p. 1956, (1976).

3. White, R.M., "Surface Elastic Waves", Proc. IEEE, 58, (8), p. 1238, (1970).

4. Indenbom, V.L., and Chukovski, F.N., "Problem of Image Formation in X-Ray Optics", Soviet Phys. Uspk., 15, (3), p. 298, (1972).

5. Beyer, R.T., and Letcher, S.V., Physical Ultrasonics, Academic Press, (1969).

6. Kittel, C., Introduction to Solid State Physics, 3rd ed., Wiley, (1966).

7. Horvath, G., Fizikai Szemle (Hungarian), 167, p. 169, (1974).

United States Patent [19]

Hauer

[11] **3,991,309**

[45] **Nov. 9, 1976**

[54] **METHODS AND APPARATUS FOR THE CONTROL AND ANALYSIS OF X-RAYS**

[75] Inventor: **Allan Hauer**, Rochester, N.Y.

[73] Assignee: **University of Rochester**, Rochester, N.Y.

[22] Filed: **July 9, 1975**

[21] Appl. No.: **594,846**

[52] U.S. Cl. 250/272; 250/273; 250/505; 250/514

[51] Int. Cl.² G01N 23/20

[58] Field of Search 250/272, 273, 274, 275, 250/277, 505, 514

[56] **References Cited**

UNITED STATES PATENTS

3,376,415	4/1968	Krogstad	250/274
3,381,127	4/1968	Spielberg	250/272
3,591,803	7/1971	Spielberg	250/273
3,769,507	10/1973	Kenney	250/272

Primary Examiner—Craig E. Church
Attorney, Agent, or Firm—Martin Lukacher

[57] **ABSTRACT**

Fast X-ray excitation processes such as occur during nuclear fusion reactions where high energy laser pulses hit a target, as for the purpose of stimulating atomic emission, may be analyzed by interposing a crystal in the path of the X-rays. The X-rays are transmitted through this crystal by means of the anomalous transmission or Bormann effect. A periodic strain field is established in the crystal to enable or inhibit anomalous transmission. The transmitted radiation is received by a measurement system which is operated in synchronism with the strain field. A solid state shuttering mechanism is obtained which rapidly interrupts the X-rays so that they can be measured even when produced by fast X-ray excitation processes. Various methods and apparatus for producing the periodic strain field are described, particularly electrostrictive techniques, piezoelectric techniques using separate transducers mounted on the crystal or the piezoelectric properties of the crystal itself and techniques for stimulating acoustic vibration by means of an optical beam.

41 Claims, 9 Drawing Figures

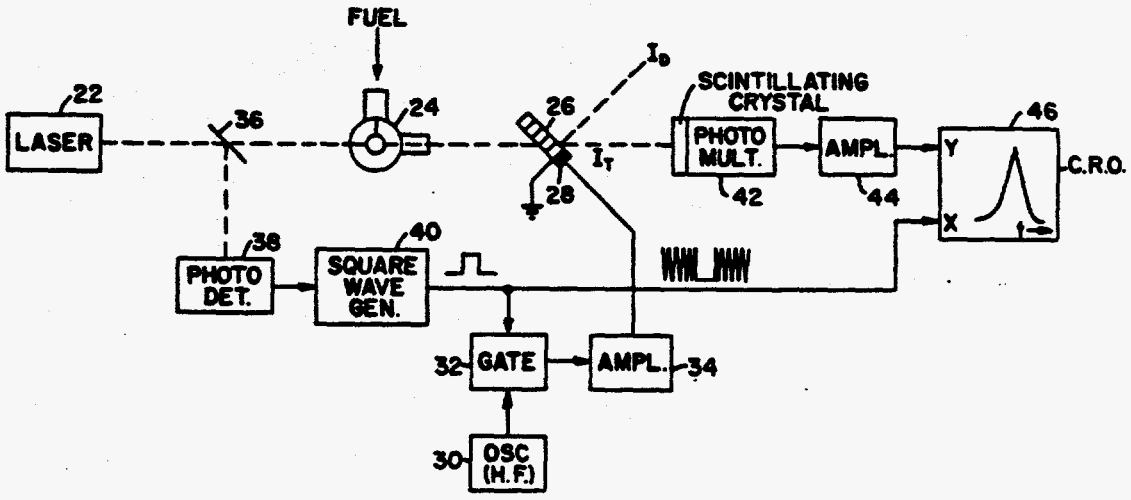

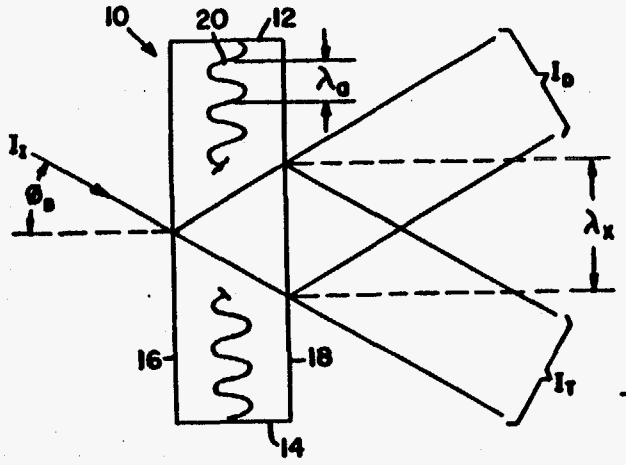

FIG.1.

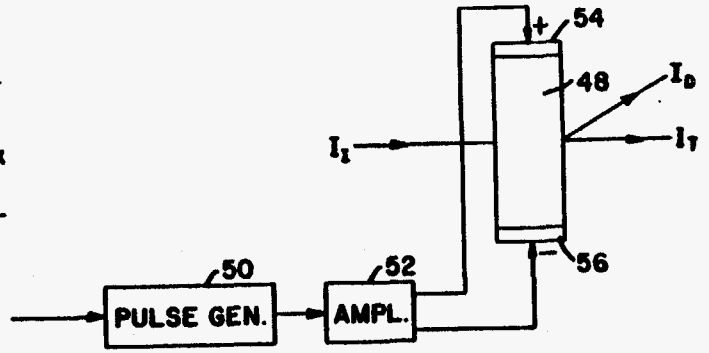

FIG.3.

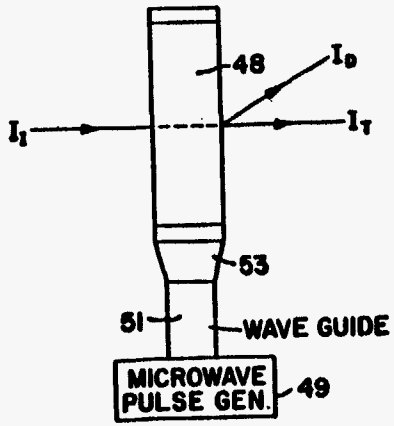

FIG.3A.

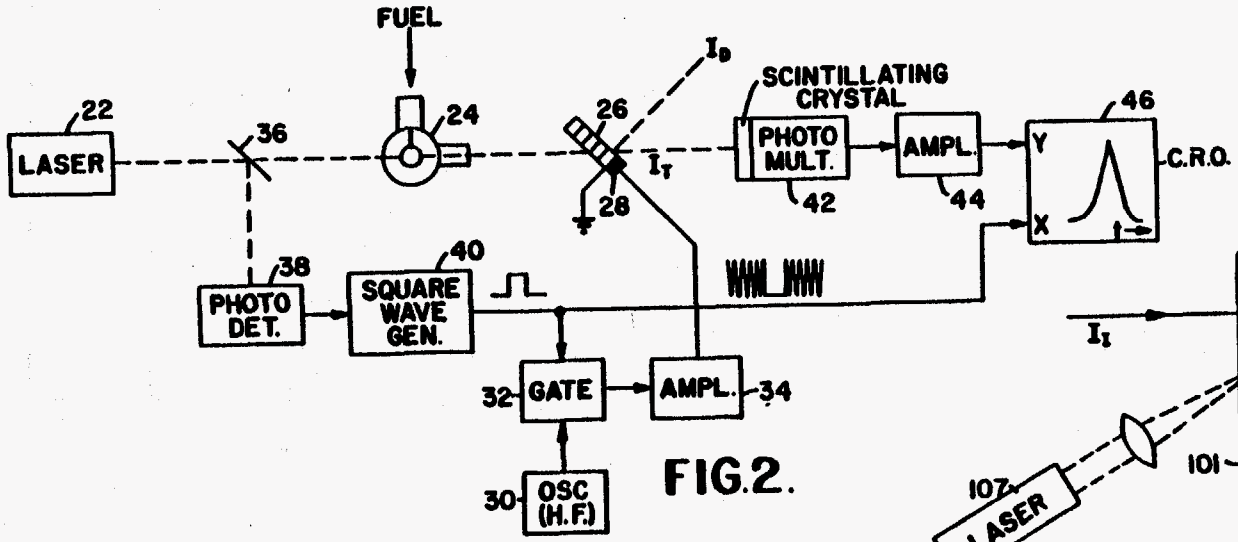

FIG.2.

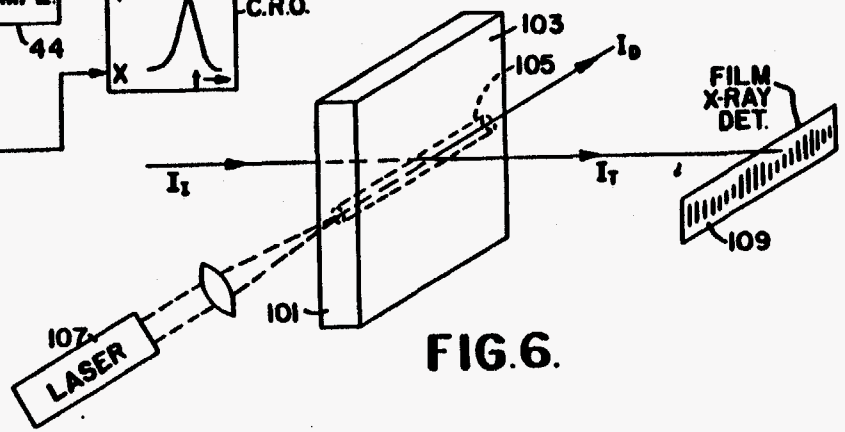

FIG.6.

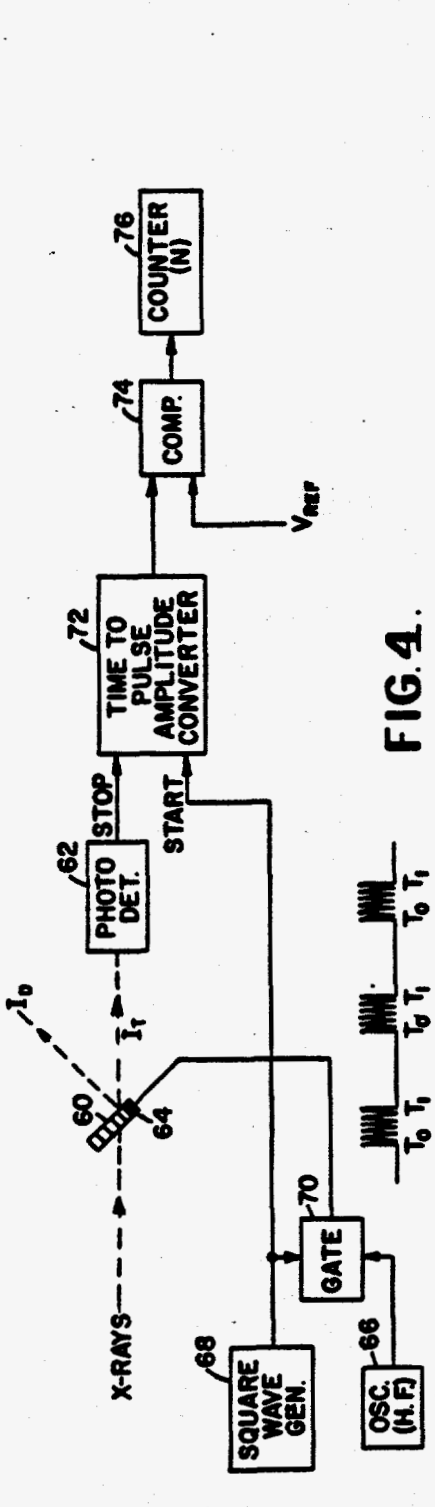
COUNTER (N)
76
COMP.
74
V_{REF}
TIME TO PULSE AMPLITUDE CONVERTER
72
STOP
START
PHOTO DET.
62
I_0
I_T
60
64
X-RAYS
GATE
70
SQUARE WAVE GEN.
68
OSC. (H.F.)
66
T_0 T_1

FIG. 4.

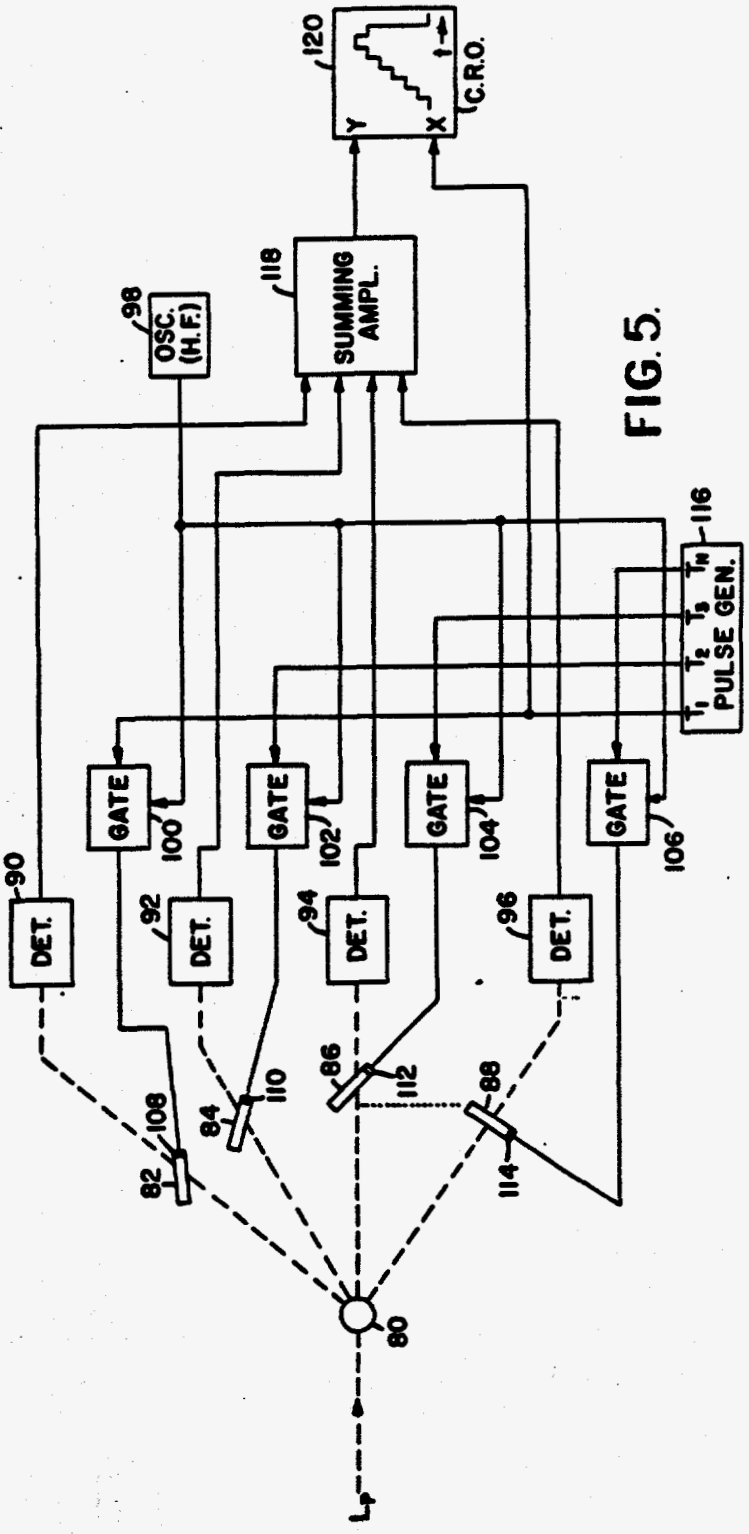
120
C.R.O.
Y
X
t
118
SUMMING AMPL.
98
OSC. (H.F.)
116
T_1 T_2 T_3 T_N
PULSE GEN.
GATE
100
GATE
102
GATE
104
GATE
106
DET.
90
DET.
92
DET.
94
DET.
96
82
84
86
88
108
110
112
114
80
L_P

FIG. 5.

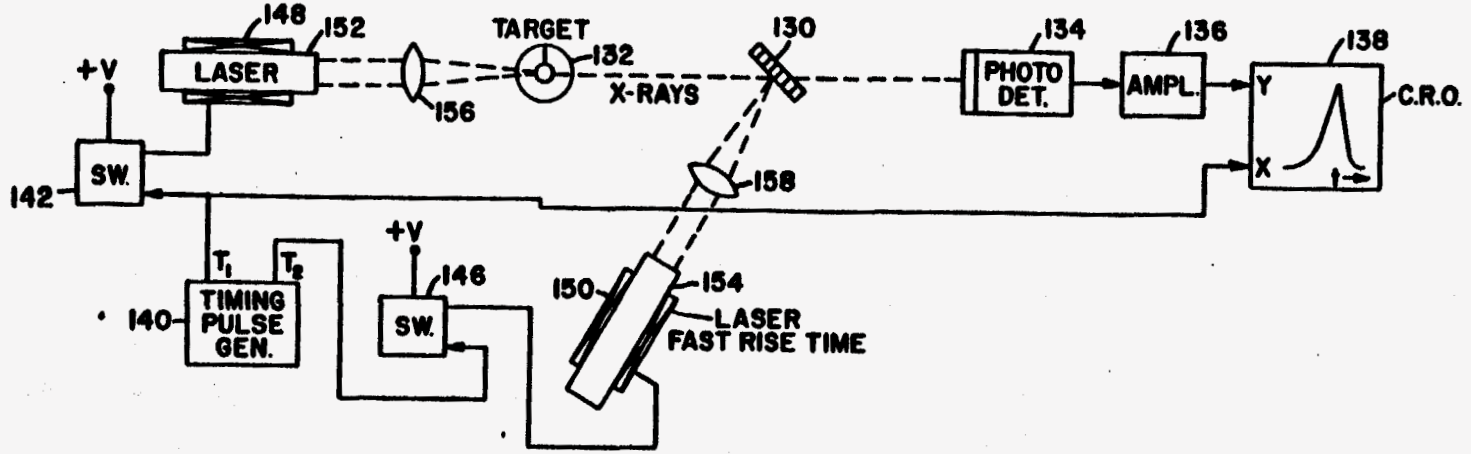
148
152
TARGET
130
134
136
138
+V
LASER
132
X-RAYS
PHOTO DET.
AMPL.
Y
C.R.O.
156
SW.
158
X
142
+V
T_1
T_2
146
150
154
TIMING PULSE GEN.
SW.
LASER FAST RISE TIME
140

FIG. 7.

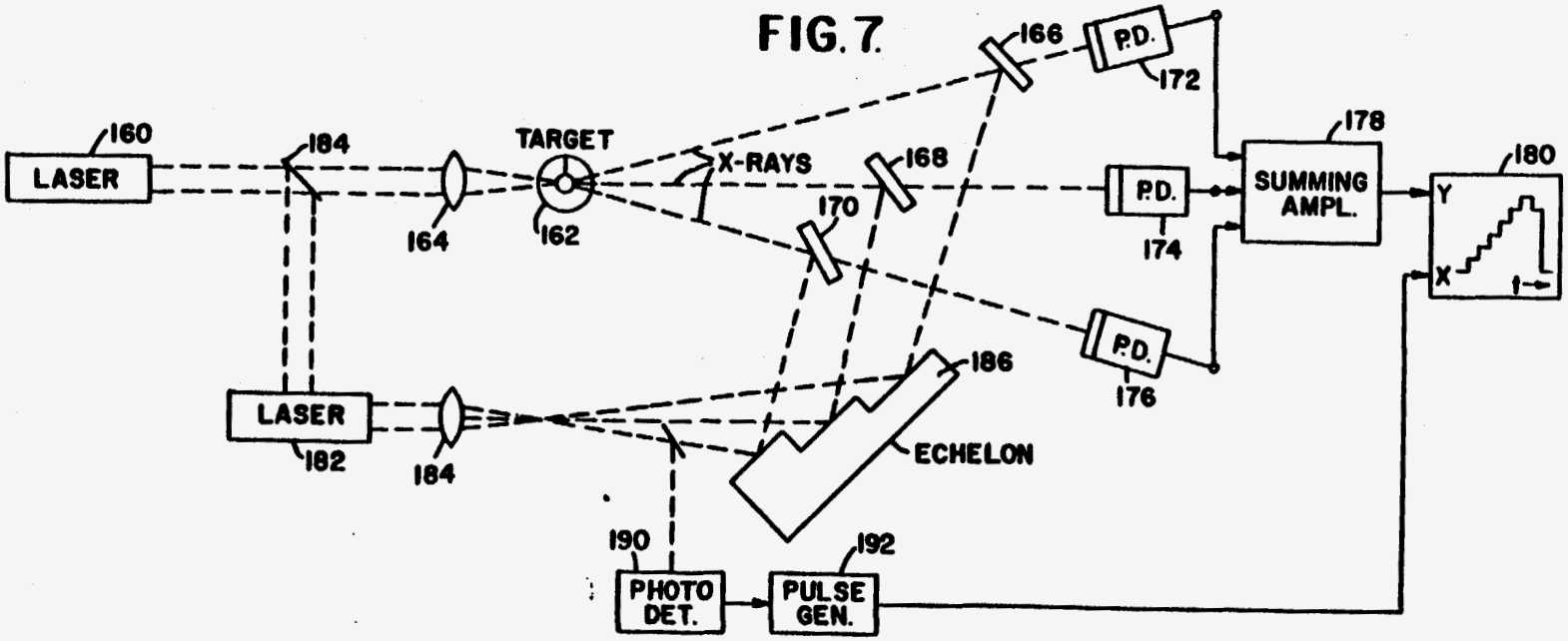
166
P.D.
172
160
184
TARGET
X-RAYS
168
178
180
LASER
164
162
170
P.D.
SUMMING AMPL.
Y
174
X
P.D.
186
LASER
176
182
184
ECHELON
190
192
PHOTO DET.
PULSE GEN.

FIG. 8.

METHODS AND APPARATUS FOR THE CONTROL AND ANALYSIS OF X-RAYS

The present invention relates to methods and apparatus for the control and analysis of x-ray radiation and particularly to improved methods and apparatus for providing x-ray shutter and modulation mechanisms.

The invention is especially suitable for use in the control and analysis of x-rays produced by very fast x-ray excitation processes. Such processes occur in a laser produced plasma resulting when a high intensity laser pulse strikes a target of material of moderate atomic number (e.g., deuterium or tritium). The invention is also applicable for the control and analysis of X-ray emission from other X-ray sources, and particularly when an understanding of the temporal characteristics of the X-ray radiation is desired.

The analysis of very fast excitation processes has presented a challenge both in the field of plasma physics and optical physics. X-ray emission characteristics may enable laser plasma mechanisms to be better understood. For example, the temporal profile of the intensity of X-ray radiation may be related to the absorption of laser power in the thermonuclear fuel element used in a laser fusion reaction. The X-rays emanating from a laser produced plasma occur in fast bursts and their measurement must take place in correspondingly short periods of time. The devices which have been suggested for the purpose of making measurement of these fast and short lifetime X-ray emissions are principally of the type known as "streak" cameras. These are complex electro-optical devices available only as costly laboratory instruments. Further information respecting streak cameras may be had by reference to an article appearing in the *Review of Science Instruments*, Vol. 43, No. 12, December, 1972, pps. 18–19, by M. Y. Scheleb, M. C. Richardson, and H. A. Alcock, entitled "Operation of a Grid-Shuttered Image Converter Tube in the Picosecond Region". Electromechanical X-ray shutters (see, e.g., U.S. Pat. No. 3,643,095) are too slow to follow fast X-ray excitation processes.

Certain effects on X-ray radiation have been observed in crystal structure. For example, the control of X-ray transmission by diffraction effects has been suggested (see U.S. Pat. No. 2,853,617). Optical energy has been modulated by means of changing the internal structure of a crystal (see U.S. Pat. Nos. 3,365,581; 3,509,489; 3,665,255; and 3,869,197). It has also been observed that anomalous or Bormann transmission of X-rays through a crystal is affected by strains and elevated temperatures within the crystal. Reference may be had to an article by P. P. Ewald, entitled "Crystal Optics for Visible Light and X-rays", appearing in *Reviews of Modern Physics, Vol.* 37, No. 1, January, 1965, p. 46, for a detailed discussion of the Bormann Effect. An article by L. P. Hunter entitled "X-Ray Measurement of Microstrains in Germanium Single Crystals", appearing in the *Journal of Applied Physics*, Vol. 30, No. 6, June, 1959, discusses the effect of strain on Bormann or anomalous transmission in crystals. An article by B. W. Batterman entitled "Effect of Thermal Vibrations on Diffraction From Perfect Crystals, I. The Case of Anomalous Transmission", appearing in the *Physical Review*, Vol. 126, p.1, May, 1962 discusses the effects of temperature on anomalous or Bormann Transmission.

It has been discovered, in accordance with the invention that where the strains are introduced temporarily in a crystal, and particularly where the strains are periodic in nature as in the form of acoustic waves, very fast switching or shuttering of anomalous or Bormann transmission of X-rays can be obtained. The periodic waves may be piezoelectrically excited acoustic waves (say shear or compressional waves) having a displacement in a direction perpendicular to the diffracting lattice planes in the crystal. The periodicity of the strain field which is stimulated in the crystal is preferably less than the extent of spreading of an X-ray as it passes through the crystal. The requisite periodicity may be obtained by exciting extremely high frequency vibrations in the crystal; for example, of the order of 1 MHz to 1 GHz, thus providing a wavelength of the vibration such that the lattice planes of the crystal shift and do not remain at the nodes of a standing wave pattern produced in the crystal by the incident X-rays. The atoms of the lattice planes are then capable of absorbing the X-rays. It should be understood of course, that this invention is not limited to any theory of operation such as the theory set forth above whereby anomalous transmission and the Bormann effect is explained by reason of a critical match between a standing wave electric field and an extended path of perfect periodicity in the crystal, when X-rays incident to the lattice planes of the crystal form the Bragg angle with the lattice planes.

In accordance with the invention the periodic strain field may be established by means of a transducer mounted on the crystal which launches an acoustic wave in the crystal. By acoustic wave, it is meant a vibrating condition in the crystal at any frequency including, but not limited, to frequencies in the audible range. Thus a suitable acoustic wave may be introduced by applying high frequency electric signals, say of the order of 10 MHz, to the transducer. Alternatively, acoustic waves may be launched in the crystal by applying microwave pulse energy to an end face of the crystal or by applying a high voltage pulse across the crystal in a direction perpendicular to the lattice planes; the crystal having piezoelectric properties. It is desirable when extremely fast rise time acoustic waves are needed, to excite such waves by means of a high intensity optical beam which is incident on the crystal in the same region as the X-rays.

The anomalous transmission of X-rays through the crystal may be measured synchronously with the launching of the acoustic wave. Alternatively, the acoustic waves may be launched and measurement of the anomalous transmission made synchronously with the generation of the X-rays as by, or simultaneously with the output of a laser which excites the emission of the X-rays as by means of a laser produced plasma.

A temporal profile of the intensity of the X-ray emission may be obtained by means of a plurality of crystals disposed to receive X-rays which emanate from a target in different ones of a plurality of directions. Acoustic waves are launched in these crystals sequentially so as to interrupt anomalous transmission through different ones of the crystals in sequential order. X-ray detectors responsive to the X-ray transmitted through each crystal provide signals which vary in amplitude in accordance with the variation in intensity of the radiation emanating from the target with time.

It is therefore an object of the present invention to provide improved methods of and apparatus for controlling the transmission of X-ray radiation.

It is another object of the present invention to provide improved methods of and apparatus for shuttering and/or modulating X-ray radiation.

It is a further object of the present invention to provide improved methods of and apparatus for the analysis of X-rays, particularly X-rays produced by fast excitation processes.

It is a still further object of the present invention to provide improved methods of and apparatus for analysis of X-ray radiation from plasmas produced as a result of laser irradiation of targets.

It is a still further object of the present invention to provide improved methods in apparatus for switching X-rays on and off.

It is a still further object of the present invention to provide improved X-ray shutter apparatus.

It is a still further object of the present invention to provide improved methods of and apparatus for controlling Bormann transmission to provide an X-ray shuttering mechanism.

It is a still further object of the present invention to provide an improved method of and apparatus for electromagnetic excitation of crystals in a manner to control X-ray transmission of the anomalous or Bormann type whereby to provide a fast X-ray shuttering mechanism.

The foregoing and other objects and advantages of the present invention will become more apparent from a reading of the following description in connection with the accompanying drawings in which:

FIG. 1 is a schematic diagram illustrating an X-ray shuttering mechanism provided in accordance with the invention;

FIG. 2 is a block diagram of apparatus provided in accordance with the invention for the analysis of X-rays produced by a laser produced thermonuclear reaction;

FIGS. 3 and 3A are schematic diagrams of solid state X-ray shutters in accordance with embodiments of the invention wherein acoustic waves are produced by piezoelectrically exciting the crystal itself with voltage pulses and with microwaves;

FIG. 4 is a block diagram illustrating apparatus for interrupting anomalous or Bormann transmission through a crystal and measuring such transmission, all in accordance with the invention;

FIG. 5 is a block diagram illustrating apparatus for measuring the temporal profile of X-ray transmitted from a target;

FIG. 6 is a schematic diagram illustrating an X-ray shuttering mechanism which makes use of an optical beam, in accordance with another embodiment of the invention;

FIG. 7 is a block diagram illustrating apparatus in accordance with the invention for controlling and measuring X-rays emanating from a laser produced plasma wherein the X-rays are controlled electro-optically; and

FIG. 8 is a block diagram schematically illustrating apparatus for measuring the temporal profile of X-rays emitted from a target on which laser pulse energy is incident.

Referring more particularly to FIG. 1, there is shown a crystal 10 suitable for use in X-ray control and analysis apparatus, which apparatus embodies the invention. This crystal may suitably be a rectangular body of silicon. The crystal may be grown from a melt through the use of the Szolchalski process. The crystal is pulled from the melt while rotating the pulling device. This results in a cylindrical body. The body is cut along planes perpendicular to its axis to provide the opposite ends 12 and 14 of the crystal. Cuts are made parallel to the longitudinal axis of the cylindrical body so that the 2, 2, 0 lattice planes are perpendicular to the front face 16 and rear face 18 of the crystal. The crystal is oriented for diffraction in the Lave geometry, so that incoming X-rays I_i arrive at the Bragg angle, ϕ_B, to the 2, 2, 0 planes. The dimensions of the crystal are selected such that the bending of the lattice planes is small. Suitable dimensions are 5 centimeters in length, 1.2 centimeters in width and 2 millimeters in thickness. The thickness dimension is shown in FIG. 1 as being the dimension between the front and rear faces 16 and 18. The length dimension is the dimension between the ends 12 and 14.

Due to multiple reflections from the planes, energy from a single ray will spread in a direction perpendicular to the planes as this X-ray energy travels through the crystal between the faces 16 and 18. In other words, the energy spread is in a direction between the ends 12 and 14 of the crystal. The dimension of the energy spread is indicated in FIG. 1 as λ_E. As shown in the drawing, the X-rays pass through the crystal and are transmitted and diffracted; the transmitted rays being indicated as I_T and the diffracted rays as I_D. Transmission and diffraction takes place through the crystal in accordance with the Bormann effect and is also known as anomalous transmission. The mechanism of such transmission is described in the above referenced publications, particularly the article by Professor P. P. Ewald. In accordance with the invention, a periodic strain field is introduced into the crystal and has a displacement in a direction perpendicular to the lattice planes (i.e., in a direction between the ends 12 and 14 of the crystal). This periodic strain field is illustrated as a sine wave 20. In accordance with the invention the periodicity or wave length, λ_s, is comparable to or less than the distance λ_E of the energy spread of the X-rays.

This periodic strain field is an acoustic field, which is meant that vibrations are established in the crystal having the desired periodicity or wavelength. The use of the term acoustic should not be taken as restricting such vibrations to audible frequencies. A suitable acoustic frequency, for example, is 10 MHz which affords a wavelength of about 0.8 mm (viz., $\lambda_s = 0.8$ mm). This wavelength is obtained considering the velocity of propagation of acoustic energy in the crystal to be 10^6cm/sec. Inasmuch as the energy spread of the X-ray radiation is greater than the wavelength of the acoustic strain field, the lattice planes in the crystal are displaced such that Bragg's law is no longer satisfied when the acoustic strain field is present. Theoretically, it is believed that the lattice planes are displaced such that they do not remain at the nodes of a standing X-ray wave pattern. Absorption of the X-ray energy can then take place in the atoms of the crystal which are located at the lattice planes.

By exciting the acoustic strain field in the crystal, there is provided a shuttering mechanism for controlling X-ray radiation. By means of the crystal, the X-ray radiation may be controlled quickly, such that fast X-ray excitation processes may be analyzed through the measurement of X-rays which are transmitted

through the crystal, either before or after the acoustic strain field is applied. Means provided by the invention for establishing and applying the acoustic strain field and for the measurement and analysis of the X-ray radiation transmitted through the crystal are discussed hereinafter.

Referring now to FIG. 2, there is shown a system for measuring and analyzing X-ray emission from a laser produced plasma which results from a thermonuclear or laser fusion reaction. A high power pulse laser 22 produces a high energy laser pulse which is incident upon a target of moderate atomic number material, such as deuterium or tritium, in a target chamber 24. For further information respecting high energy pulse lasers and appparatus for providing a laser fusion reaction, reference may be had to U.S. Pat. No. 3,723,246 issued to Dr. M. J. Lubin on Mar. 27, 1973. X-rays emanating from the laser produced plasma are incident upon a crystal 26 which is oriented for Bormann or anomalous transmission. Such transmission is indicated as I_T emanating from the rear face of the crystal 26. The crystal 26 may be of the same type as described in connection with FIG. 1. Acoustic waves are launched by means of a transducer 28 and propagate through the crystal in a displacement direction perpendicular to the lattice planes. This transducer is a body of piezoelectric material, such as PZT, which is bonded to an end of the crystal (either the upper end 12 or the lower end 14, as illustrated in FIG. 1).

An oscillator 30 affords a source of high frequency sinusoidal signals. Thus the transducer 28 is excited with the continuous wave A.C. signals. The oscillator 30 is connected to a gate 32 which is normally enabled. The output of the gate 32 is amplified in an amplifier 34 and drives the transducer 28. A continuous wave acoustic signal having a frequency of 10 MHz is therefore launched and exists in the crystal. Bormann or anomalous transmission through the crystal is therefore normally cut off.

When the laser pulse is generated, a portion of that pulse is diverted by means of a dichroic mirror 36 to a photo detector 38. The photo detector triggers a square wave generator 40, such as a one-shot. The output pulse from the square wave generator 40 inhibits the gate 32 and cuts off the continuous wave excitation of the crystal 26 for the period of the pulse from the square wave generator 40. As shown by the waveform adjacent to the output line from the amplifier 34, the driving signal applied to the transducer is a continuous wave, say of 10 MHz, interrupted during the period of the pulse from the square wave generator 40. This period is initiated by the laser pulse (viz., in synchronism therewith) and permits Bormann or anomalous transmission through the crystal 26 for the duration of this pulse.

The X-rays due to the anomalous transmission through the crystal, are applied to an X-ray detector 42 which may consist of a scintillating crystal and a photo multiplier. The signals from the X-ray detector 42 are amplified in an amplifier 44 and are applied to deflect the beam in a Cathode Ray Oscilloscope (CRO) 46. The time base on the oscilloscope is initiated by the leading edge of the square wave pulse from the square wave generator 40. Since the amount of deflection is a function of the intensity of the X-ray radiation anomalously transmitted through the crystal, the display on the oscilloscope is a temporal profile of the X-ray pulse envelope.

Referring to FIGS. 3 and 3A, there are illustrated other crystals 48 similar to the crystal 10 described in connection with FIG. 1 and the crystal 26 described in connection with FIG. 2, except that the crystal 48 is of piezoelectric material, suitably quartz. A periodic wave may be launched in the crystals 48 by exciting the crystal with a high voltage pulse of short duration as shown in FIG. 3 or with microwave pulses as shown in FIG. 3A. The pulse may be intermittent or repetitive, as when repetitive shuttering action is desired. In FIG. 3, excitation of the crystal is implemented by a pulse generator 50 which produces pulses either when triggered or repetitively at a certain rate, say 1000 pulses/sec. These pulses enable a voltage amplifier 52 which may be a tube-type amplifier of the type used in television cathode-ray tube deflection circuits and which generates a high voltage pulse. This high voltage pulse is applied between electrodes 54 and 56 bonded to opposite ends of the crystal 48 (viz., ends which are parallel to the lattice planes in the crystal). In FIG. 3A the pulse is obtained from a microwave pulse generator 49, e.g., a pulsed magnetron and coupled to an end face of the crystal by a wave guide 51 and matching horn 53. An acoustic wave is launched due to the contraction and expansion of the crystal at the leading edge and trailing edge of the high voltage pulse or by the microwave pulse. This acoustic wave operates to disrupt Bormann or anomalous transmission through the crystals 48.

Referring to FIG. 4, there is shown apparatus for measuring anomalous transmission of X-rays through a crystal 60 during the intervals that such transmission is switched off by means of an acoustic strain wave which propagates through the crystal. The crystal is oriented for Laue diffraction such that anomalous transmission of X-rays, I_T, through the crystal is incident on a photo detector 62. The photo detector 62 may be similar to the detector 42 described in connection with FIG. 2. The acoustic waves are launched in the crystal 60 by a piezoelectric transducer 64 mounted on one end thereof A high frequency oscillator 66 generates a continuous wave, suitably at 10 MHz. A square wave generator 68 produces a repetitive pulse train having a repetition rate, say of 1 KHz. A gate 70 is enabled by the pulses from the square wave generator 68, such that a repetitive train of bursts of high frequency signals each of duration T_0 to T_1 is applied to the transducer 64. Anomalous transmission to the crystal is terminated or at least substantially reduced for the duration of each burst.

The leading edge of each pulse from the square wave generator triggers the start input of a time-to-pulse amplitude converter. The output of the photo detector 62, when it reaches a certain level of voltage which corresponds to a certain X-ray intensity, is applied to the stop input of the converter 72. The photo detector output level which provides a stop trigger to the converter 72, may be suitably a level equal to twice the level of the photo detector output under conditions when the acoustic wave is established in the crystal 60. The time-to-pulse amplitude converter 72 may be a commercial instrument which provides an output pulse of amplitude corresponding to the interval between the start and stop trigger pulses which are applied thereto. A suitable instrument may be procured from Ortec, Inc., of Oak Ridge, Tennessee, their Model 457. The output of the converter 72 is applied to one input of a comparator 74. A reference voltage, which may be

adjustable, is applied to the other input of the comparator. When the amplitude of the converter output pulse equals the reference voltage amplitude, a pulse is produced by the comparator 74 which is counted in a counter 76. The count registered in the counter is a factor related to the probability that an X-ray photon is transmitted through the crystal 60 by the anomalous transmission mechanism during the intervals T_o to T_1 when the acoustic strain field is established in the crystal 60, and is therefore a measure of the shuttering efficiency of the crystal 60.

Consider that the acoustic wave requires a finite time to propagate through the crystal, for example, an acoustic wave propagating at a velocity of 10^4cm/sec requires about 50 nano seconds to cut off anomalous transmission to the crystal. During the period from T_o until a time thereafter when anomalous transmission is cut off, the X-ray shutter provided by the crystal is open. Thereafter the shutter is closed. The propagation time may be reduced or substantially eliminated by the use of optical means for stimulating the acoustic wave, as will be described hereinafter in connection with FIGS. 6 to 8.

A temporal profile of the X-ray radiation, as when a laser pulse L_p strikes a target 80 may be obtained by the apparatus shown in FIG. 5. A plurality of crystals 82, 84, 86 and 88 are disposed about the target, each for transmitting X-rays emanating from the target in a different direction. While four crystals 82 to 88 are shown, a larger number as indicated by the dash lines in FIG. 5, may be provided to obtain a higher resolution in measurements of the X-ray transmission characteristics. Each of the crystals 82 to 88 is oriented for Laue diffraction of X-rays in a different direction. The X-rays which are anomalously transmitted by each crystal are detected by separate detectors 90, 92, 94 and 96, which may be scintillating crystal photo multiplier detectors of the type described above in connection with FIG. 2. A source of high frequency, say 10 MHz oscillations, such as an oscillator 98, is connected through separate gates 100, 102, 104 and 106 to drive separate transducers 108, 110, 112 and 114 on one end of the crystals 82 to 88. The gates 100 to 106 are enabled by pulses produced by a timing pulse generator 116. The leading edge of these pulses occur after successive periods of time. The leading edge of the first pulse occurs at time T_1, the second at time T_2, the third at time T_3 and the last at time T_n. The pulses are overlapping such that even the first occurring pulse T_1 does not terminate until after the termination of the last pulse T_n. The last pulse T_n terminates at the end of the measurement interval. The first pulse T_1 is applied to the gate 100 so that an acoustic wave is launched first in the crystal 82. The next occurring pulse T_2 enables the gate 102 so that the high frequency driving signal is next applied to transducer 110 of the second crystal 84. Each of the crystals successively receives the high frequency driving signals at its transducer and the anomalous transmissions of X-rays through the crystals are successively cut off.

The outputs of the photo detectors 90 to 96 are applied to a summing junction of a summing amplifier 118. This summing amplifier also integrates the signals applied thereto. For example, it may be an operational amplifier having a capacitor connected in feedback relationship therewith. The integrated output is applied to the Y deflection input of a cathode ray oscilloscope 120. The time base of the oscilloscope 120 is triggered at T_1 by the leading edge of the first pulse from the pulse generator 116. The crystals 82 to 88 are each open for anomalous transmission for short, successive periods of time. Each crystal transmits the X-ray radiation from the target 80 during each such successive intervals of time. Since the X-ray radiation is sampled successively by each of the crystals, the total radiation which is measured and displayed on the oscilloscope 120 is a temporal profile of the X-ray intensity variations of the X-rays produced when the laser pulse L_p strikes the target 80.

A faster shuttering action may be obtained through the use of the radiation pressure to directly excite acoustic fields locally in a crystal in a region where the X-rays are incident. Such radiation pressure may be produced by an intense electromagnetic beam, such as a light beam produced by a laser which is incident on the crystal in the region where the X-rays are incident. FIG. 6 illustrates an embodiment where the light beam is incident on an edge 101 of a crystal 103 so as to excite an acoustic field 105 in a region transverse to X-rays which are incident on a front face of the crystal. FIGS. 7 and 8 illustrate embodiments where the light beam and X-rays are both incident in the same area of the front face of a crystal. The crystals are oriented for anomalous transmission of X-rays which are incident upon the face of the crystal in the same region as the light beam. It is believed, without inferring or implying any limitation to any particular theory, that acoustic fields of fast rise time, since they are not dependent upon acoustic propagation, occurs due to a stimulated Brillouin effect, by means of which the optical beam creates an acoustic wave in the crystal by locally generated electrostriction. Such acoustic fields may build up very rapidly and be of extremely small wavelength, such acoustic frequencies may be greater than 10 GHz.

The apparatus shown in FIG. 6 is operative in the streak mode. A laser 107 produces an optical pulse having a fast rise time and relatively long duration, suitably several microseconds, as by holding the flashlamps on for that period of time. A strip of X-ray sensitive film 109 or an array of X-ray detectors detects the anomalous transmission I_T through the crystal as it is cut off by the optical pulse. The pattern or the film 109 is a streak in the direction between the edges of the crystal which follows the progressive cut-off of anomalous transmission during the optical pulse period.

Alternatively the crystal 103 may be oriented with respect to the incident X-rays, I_i, at an angle which differs slightly from the Bragg angle. When the optical pulse, which is preferably a short pulse, say less than one microsecond duration, but having fast use time, is incident upon the crystal edge 101, an aperture for anomalous transmission through the crystal is opened which moves in the direction between the edges of the crystal thereby exposing a streak on the film 109.

FIG. 7 illustrates X-ray control and analysis apparatus which uses a laser beam to launch an acoustic wave in a crystal 130 which is oriented in the path of X-rays from a laser target in a chamber 132 so as to interrupt the anomalous transmission of these X-rays. A photo detector 134 opposite the rear face of the crystal 130 detects and measures the intensity of the anomalously transmitted X-rays. The output of the photo detector is amplified in an amplifier 36 and applied to the Y deflection input of a cathode ray oscilloscope 138.

A timing generator 140 uses two successive timing pulses at successive times T_1 and T_2. These pulses en-

able switches 142 and 146 which apply a voltage to the pumping means 148 and 150 of a main laser 152 and a control laser 154. These pumping means may consist of flash lamps which receive voltages from capacitor banks (the voltages being indicated at +V) so as to flash the lamps.

Upon occurrence of the first flash at time T_1, the main laser 152 is pumped and a laser pulse, focused by a lens 156, hits a laser fuel material in target chamber 132. X-rays are then produced. Shortly thereafter at time T_2, the switch 146 is operated and laser 154 is pumped so as to provide an optical beam. This beam is focused by a lens 158 on the front face of the crystal 130 in the location where the X-rays from the target 132 are incident. Acoustic waves are then launched in the crystal as by means of the stimulated Brillouin effect mentioned above. The anomalous transmission of X-rays through the crystal is cut off with extreme rapidity. During the period between T_1 and T_2, the X-rays which are anomalously transmitted are displayed on the oscilloscope 138. The time base of the oscilloscope commences at the time T_1 since it is triggered by the first timing pulse at time T_1. Accordingly, a temporal display of the X-ray emission characteristics, resulting from the laser plasma produced at the target by the pulse from the main laser 152, is displayed and may be measured.

Referring to FIG. 8, a laser 160 provides a pulse of high intensity optical energy which is focused and made incident on a target 162 by a lens 164 so as to produce a laser atomic particle emission reaction which generates X-rays. These X-rays emanate from the target in different directions. A plurality of crystals, only three crystals 166, 168 and 170 being shown to simplify the illustration, are disposed along different ray paths and oriented for anomalous X-ray transmission to photo detectors 172, 174 and 176. The outputs of these photo detectors 172, 174 and 176 are applied to an integrating summing amplifier 178 which operates a cathode ray oscilloscope display 180 in the same manner as the summing amplifier 178 and the cathode ray oscilloscope 120 described in connection with FIG. 5.

Anomalous transmission through the crystals 166, 168 and 170 is interrupted by beams from an auxiliary laser 182 which is pumped by optical energy from the main laser 160. Such energy is diverted to the laser 182 by means of a dichroic mirror 184. Accordingly, immediately after the laser 160 produces its pulse, the laser 182 is pumped. An optical pulse produced by the laser 182 is split into a plurality of beams which are incident on the front face of the crystals 166, 168 and 170 by a lens 184 and echelon 186 arrangement. The lens 184 and echelon 186 are disposed to provide ray paths of successively longer length to successive ones of the crystals 166, 168 and 170. The ray paths to the crystal 170 is shortest. The path to the crystal 168 is longer and the path to the crystal 166 is longest. The beams from the auxiliary laser 182 serve to launch acoustic waves in the crystals in the vicinity where the X-rays from the target 162 are incident thereon; thus interrupting anomalous transmission through the crystals. Since the ray paths to the crystals 166, 168 and 170 are successively longer, the X-ray transmission will be interrupted at successive periods of time. Accordingly, the X-rays from the target 162 will be successively sampled so that, when these rays are translated into electrical signals by the photo detectors 172, 174 and 176, and summed and integrated in the amplifier 178, a display corresponding to the temporal profile of the X-ray pulse envelope generated by the laser fusion reaction of the target 162 will be generated on the oscilloscope 180.

The oscilloscope 180 is synchronized by the beam to the earliest operating one of the crystals 170 by means of a photo detector 190 which receives a portion of the laser beam which is incident on the crystal 170. The crystal 170 is the first of the crystals in which anomalous transmission is interrupted. Immediately prior to the interruption of X-ray transmission through the crystal 170, the photo detector 190 generates a signal. This signal triggers a pulse generator 192, which may be a one-shot, the output pulse from the one-shot is applied to trigger the time base (or X axis sweep) of the oscilloscope display.

From the foregoing description it will be apparent that there has been provided improved methods of and apparatus for controlling, analyzing and measuring X-ray radiation, and particularly X-ray radiation which results from fast X-ray excitation processes such as can occur in a laser produced plasma as may result from a laser fusion reaction. While various embodiments of the methods and apparatus provided by the invention have been disclosed, it will be appreciated that variations and modifications thereof within the scope of the invention will undoubtedly suggest themselves to those skilled in the art. Accordingly, the foregoing description should be taken merely as illustrative and not in any limiting sense.

What is claimed is:

1. The method of analysis of X-ray radiation which comprises the steps of

orienting a crystal in the path of said radiation to enable anomalous transmission therethrough in accordance with the Bormann effect,

introducing temporarily different conditions of strain in a direction transverse to the lattice planes of said crystal whereby to enable and inhibit the anomalous transmission through said crystal, and

measuring the X-ray radiation transmitted through said crystal.

2. The invention as set forth in claim 1 wherein said step of introducing different conditions of strain is carried out by transmitting acoustic waves through said crystal in said direction.

3. The invention as set forth in claim 2 wherein the wavelength of said acoustic waves does not exceed the distance in said direction over which X-rays from a point source incident on one face of said crystal spread as said X-rays pass through said crystal to the face thereof opposite to said one face.

4. The invention as set forth in claim 1 wherein said step of introducing said different conditions of strain is carried out by temporarily applying strain to said crystal in said direction for a certain period of time which is short relative to the period when said strain is removed.

5. The invention as set forth in claim 1 wherein said step of introducing said different conditions of strain is carried out by continuously applying strain in said direction, and removing said strain for a period of time which is short relative to the period when said strain is applied.

6. The invention as set forth in claim 3 wherein said step of transmitting acoustic waves is carried out by periodically applying bursts of acoustic waves to said crystal.

7. The invention as set forth in claim 3 wherein said step of transmitting acoustic waves is carried out by continuously applying acoustic waves to said crystal, and periodically cutting off the application of said acoustic waves.

8. The invention as set forth in claim 3 wherein said step of applying acoustic waves is carried out by piezoelectrically exciting said crystal with electrical signals.

9. The invention as set forth in claim 8 wherein said electric signals have a frequency in a range much higher than the upper end of the acoustic frequency range.

10. The invention as set forth in claim 3 wherein said crystal is of piezoelectric material and said step of applying acoustic waves is carried out by applying and removing a high voltage electric field extending between opposite ends of said crystal, which ends are substantially coplanar with said lattice planes.

11. The invention as set forth in claim 3 wherein said crystal is of piezoelectric material and said step of applying acoustic waves is carried out by applying bursts of microwave energy upon an end of said crystal which is substantially coplanar with said lattice planes.

12. The invention as set forth in claim 3 wherein said step of applying acoustic waves is carried out by directing a beam of optical energy upon said crystal in a region thereof adjacent where said X-rays are incident.

13. The invention as set forth in claim 12 wherein said optical energy is directed to be incident upon an edge of said crystal at a location which is in approximately the same plane as the X-rays which are incident upon a face of said crystal.

14. The invention as set forth in claim 3 wherein said step of applying acoustic waves is carried out by directing a beam of optical energy to be incident upon a face of said crystal in approximately the same location on said face where said X-rays are incident.

15. The invention as set forth in claim 12 wherein said optical energy beam is in the form of a burst.

16. The invention as set forth in claim 3 wherein the step of transmitting acoustic waves through said crystal in said direction is carried out with the aid of an electrostrictive transducer mounted on an end of said crystal which is substantially perpendicular to said direction, and including the step of applying periodic signals to said transducer.

17. The invention as set forth in claim 16 wherein said step of applying periodic signals includes the step of applying said signals in a burst.

18. The invention as set forth in claim 16 wherein the frequency of said signals is of the order of 10 MHz.

19. The invention as set forth in claim 18 wherein said signals are applied to said transducer in bursts, which bursts occur repetitively.

20. The invention as set forth in claim 1 wherein said X-rays emanate from a target, and wherein said orienting step consists of the step of orienting a plurality of crystals in locations spaced from each other about said target to enable anomalous transmission of X-rays which emanate from said target in a plurality of directions, the X-rays emanating in different directions being incident upon different ones of said plurality of crystals.

said strain introducing step consists of the steps of sequentially introducing a like change in the condition of strain in different ones of said crystals, the changed condition of strain existing for successive periods of time, and

said measuring step includes measuring the anomalous X-ray radiation transmitted through each of said crystals.

21. The invention as set forth in claim 20 wherein said strain introducing step is carried out by the step of launching acoustic waves through each of said crystals in a direction perpendicular to the lattice planes thereof.

22. The invention as set forth in claim 21 wherein said acoustic waves are launched by generating a periodic signal having a wavelength in said crystals less than the distance, in a direction perpendicular to the lattice planes thereof, which said X-rays spread in passing through said crystal in a direction parallel to said planes, and electrostrictively exciting different ones of said crystals separately with different successively occurring ones of said bursts.

23. The invention as set forth in claim 21 wherein said acoustic waves are launched by generating a plurality of light beams, different ones of which occur at successive intervals of time, and directing different ones of said light beams so that they are incident upon different ones of said crystals in approximately the same location on said crystals as where said X-rays are incident.

24. Apparatus for the control of X-ray radiation which comprises

a crystal having lattice planes spaced from each other from one end of said crystal to an opposite end thereof,

said crystal being disposed in the path of said X-ray radiation so that said X-rays are incident on one face of said crystal at angle to said lattice planes to enable anomalous transmission through said crystal from said one face to the face thereof opposite to said one face in accordance with the Bormann effect, and

means for exciting a strain field in a direction between said ends of said crystal for selectively inhibiting and enabling said anomalous transmission whereby to control said X-ray radiation.

25. The invention as set forth in claim 24 wherein said crystal consists of piezoelectric material and said exciting means comprises means for generating a high voltage electric pulse, and means responsive to said pulse for generating an electric field in a direction between said ends of said crystal for exciting acoustic vibration in said crystal.

26. The invention as set forth in claim 24 wherein said means for exciting said strain field comprises means for launching an acoustic strain field in said crystal having a wavelength in said direction less than the distance in said direction which X-ray radiation spreads as it passes between said faces of said crystal.

27. The invention as set forth in claim 26 wherein said launching means comprises means for exciting said transducer into acoustic vibration at a frequency of at least 10 MHz.

28. The invention as set forth in claim 24 wherein said exciting means comprises an electroacoustic transducer mounted on said one end of said crystal, and means for applying periodic electric signals to said transducer.

29. The invention as set forth in claim 28 wherein said applying means includes means for generating bursts of high frequency electric signals which occur repetitively.

30. The invention as set forth in claim 28 wherein said applying means includes means for generating a continuous wave high frequency signal, and means for inhibiting said signal for a predetermined period of time.

31. The invention as set forth in claim 30 wherein said X-rays are generated when a target is illuminated by a high energy pulse of laser energy, and said applying means includes means for detecting said laser pulse, means for producing a control pulse having duration equal to said predetermined period of time when said laser pulse is detected, and means for applying said control pulse to said inhibiting means.

32. The invention as set forth in claim 24 wherein said exciting means comprises means for generating a pulse of optical energy which is incident on said crystal in about the same region thereof as said X-rays.

33. The invention as set forth in claim 32 wherein said exciting means includes means for generating a beam of said optical energy which is incident upon an edge of said crystal, the location of incidence of said beam and X-rays being in the same plane mutually perpendicular to said edge and said one face.

34. The invention as set forth in claim 32 wherein said optical energy provided by said exciting means is a beam, said beam being incident on said one face in about the same location as said X-rays.

35. The invention as set forth in claim 34 wherein said X-rays are provided by a first laser which produces a pulse of high intensity light which is incident on a target, said first laser having pumping means operative when enabled to provide said high intensity pulse, said exciting means comprising a second laser having pumping means operative when enabled to cause said second laser to produce said pulse of optical energy which is incident on said one face of said crystal, means for successively operating said first laser pumping means, and said second laser pumping means, and means for measuring the anomalous X-ray transmission through said crystal during a period commencing when said first laser pumping means is operated.

36. The invention as set forth in claim 24 wherein a plurality of said crystals are provided each for receiving X-rays emanating in a different direction from a source thereof, said exciting means includes means for exciting different ones of said crystals successively, and means responsive to anomalous X-rays transmission through said crystals for providing an output signal representing the intensity of said X-ray radiation from said source.

37. The invention as set forth in claim 36 wherein said exciting means comprises a plurality of electrostrictive transducers mounted on a different one of said plurality of transducers at said one end thereof, a source of high frequency oscillations, and means for successively connecting said source to different ones of said transducers.

38. The invention as set forth in claim 36 wherein said exciting means comprises a laser which produces a high intensity pulse of light, and means for splitting said laster pulse into a plurality of beams, along paths of different length, each incident upon a different one of said crystals in the same region thereof where said X-rays are incident thereon.

39. The invention as set forth in claim 38 wherein said splitting means includes an echelon disposed in the path of illumination from said laser.

40. The invention as set forth in claim 24 including means for measuring the anomalous X-ray radiation transmitted through said crystal so that the temporal characteristics of said radiation can be analyzed.

41. The invention as set forth in claim 40 wherein said exciting means comprises a piezoelectric transducer mounted on said one end of said crystal, a source of pulses having a certain repetition rate, a high frequency oscillator providing A.C. signals of frequency much higher than said repetition rate, gate means operated by said pulses for applying said A.C. signals to said transducer for the duration of said pulses, and wherein said measuring means includes an X-ray detector disposed in the path of anomalous X-ray transmission through said crystal and providing an output in response to said anomalously transmitted X-rays, means for converting the intervals of time between the onset of each of said pulses and said outputs into output pulses having amplitudes corresponding to the duration of said intervals of time, and means for counting each of said pulses which exceed a certain amplitude.

* * * * *